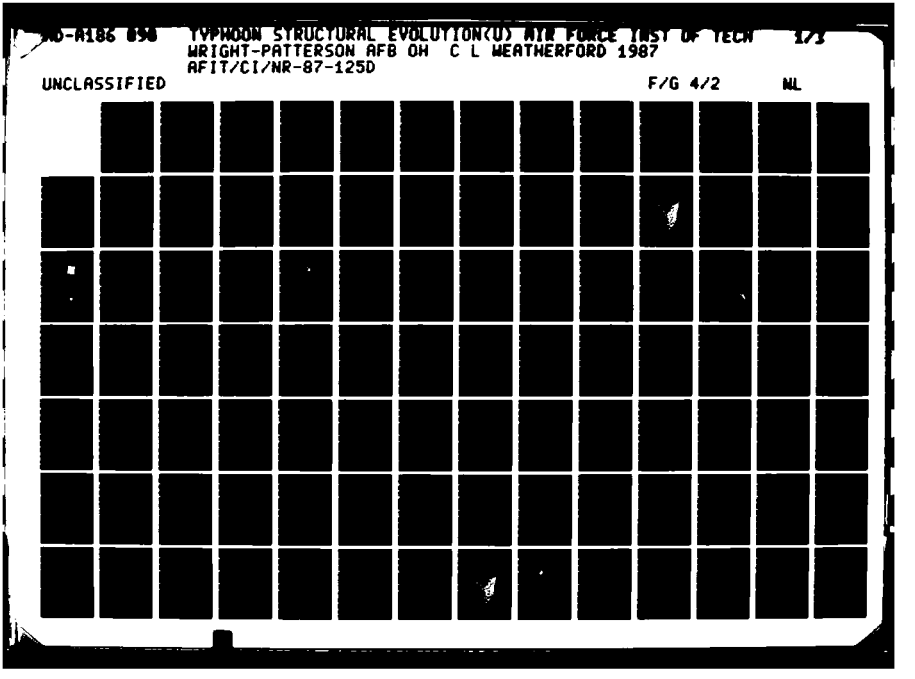
AD-A186 850 TYPHOON STRUCTURAL EVOLUTION(U) AIR FORCE INST OF TECH 1/3
WRIGHT-PATTERSON AFB OH C L WEATHERFORD 1987
AFIT/CI/NR-87-125D
UNCLASSIFIED
F/G 4/2
NL

[illegible]

[illegible]

[illegible] There are expanding eyes with [illegible] [illegible] disappearance [illegible] on average [illegible] pressure [illegible] mb. Concentric eyes are observed nearly as often in the deepening as in the filling stage for central pressures below 945 mb.

By removing the symmetric portion of the tangential wind field of the vortex and the cyclone motion vector, the residual asymmetric wind flow in the cyclone's interior

[illegible] Weatherford
Department of Mathematics
[illegible] State University
Fort [illegible]
[illegible]

DISSERTATION

[illegible]

[illegible]

[illegible]

[illegible]

[illegible]

[illegible]

Colorado State University

Fort Collins, Colorado

[illegible]

A1

ACKNOWLEDGEMENTS

[illegible] Grant Number AFM8810110

TABLE OF CONTENTS

LIST OF FIGURES

LIST OF TABLES

LIST OF SYMBOLS AND ACRONYMS

CYCLONE Tropical cyclone of intensities ranging from tropical depression to super-typhoon.

MSLP Minimum Sea-Level Pressure measured at the surface by dropsonde equipment or at 700 mb by aircraft equipment.

OCS Outer Core Wind Strength Area-weighted average tangential wind speed relative to the moving cyclone per four-radial leg mission for the region of the outer core from 1° to 2.5° radius.

INTERIOR REGION Cyclone center to 2.5° latitude radius.

INNER CORE The region of the tropical cyclone from the center to 1° radius.

OUTER CORE The region of the tropical cyclone from 1° to 2.5° radius.

NAT [illegible]

MOTROT [illegible]

MOTROT VORT [illegible]

[illegible]

VORT [illegible]

V_T **(MOTROT-VORT)** : V_T (MOTROT) - V_T (VORT)= V_T (asym.). The asymmetric tangential wind vector in the cyclone-relative coordinate system that results after the mean vortex has been removed.

V_R : Radial wind speed.

RESIDUAL WIND : V_T (MOTROT-VORT) + V_R (MOTROT)= V_T (asym.) + V_R (MOTROT).

RMW : Radius of Maximum Wind speed.

JTWC : Joint Typhoon Warning Center (US Air Force and Navy) based on Guam.

Chapter 1

INTRODUCTION

Tropical cyclones account for nearly 65% of worldwide deaths resulting from natural disasters (see Anthes, 1982 for more detail). But for all its destruction, the damaging winds of a tropical cyclone have yet to be accurately observed and forecasted. Research aircraft have flown into tropical cyclones since 1947 for the express purpose of obtaining information on the inner 1° radius wind structure (primarily the maximum wind region) but have not described in detail the manner in which these inner-core winds change throughout a cyclone's life cycle. Larger scale structural studies (beyond 2° radius), accomplished primarily through rawinsonde composites, have not been able to properly relate the core region wind changes with those of the outer- region wind changes. As a result, the wind field changes which occur during the cyclone's lifetime are poorly documented and understood. This study will focus on the evolution of the tropical cyclone's 700 mb level wind field by analyzing aircraft data of cyclones from development to decay.

An adequate forecast must not only specify the expected changes in the wind profile, but also where the entire vortex will move in time. The question of motion is as crucial to the forecaster as the question of structural change. For example, the average growth of a typhoon's radius of damaging winds (25 ms^{-1}) is 80 km per day (Weatherford and Gray 1987b). And yet, the cyclone's expected position usually differs from the forecast position by 230 km over the same 24-hour period (Matsumoto 1984). The underlying reason for this forecast discrepancy is that the current which steers the cyclone is inadequately measured. Knowledge of this background wind field can shed light not only on future cyclone track changes but the manner in which the environment interacts with the cyclone during its life cycle. This study provides more insight into the steering current of the

tropical cyclone within its 2.5° radius region and how this interior steering current differs from the actual cyclone motion.

1.1 Background on the Tropical Cyclone's Wind Structure

Over the last 30 years, the inner-core portion (1° radius) of Atlantic tropical cyclones' wind field has been investigated by operational and research aircraft. Most of what has been learned from aircraft research is due to case studies of various Atlantic hurricanes

Daisy and Helene (Riehl and Malkus, 1961; Colon et al., 1961, 1964), Cleo (LaSeur and Hawkins, 1963); Ella, Janice and Dora (Sheets, 1967, 1968); Debbie and Hilda (Hawkins and Rubsam, 1968a,b, 1971); and Allen, David, Anita and Frederic (Jorgensen, 1984a,b). Shea and Gray (1973), Gray and Shea (1973), and Gray (1962, 1965, 1967) combined many of these cases studies in order to obtain a more general view of the inner-core hurricane wind structure and its variability from storm to storm.

However, because of the sparseness of outer radius (> 1° radius) reconnaissance information, little has been done relating the cyclone's inner core region with its adjoining outer core (1 to 2.5° radius). Although Merrill (1984) showed that Atlantic cyclones are typically smaller than Pacific cyclones, cases have been observed in the Pacific to be as small as those found in the Atlantic (Arakawa, 1950). For this reason Pacific cyclones classified according to size, are felt to adequately match the wind field of cyclones found in any tropical ocean basin.

Outer-core structural studies using reconnaissance aircraft data are few. First to study the cyclone's 1 to 4° region was Hughes (1952). His important and much quoted study on the average wind profiles of 13 late 1940's large and mature typhoons presented the first aircraft information on the low level wind profile of the mean typhoon. His [illegible] of the typhoon's suspected strong boundary layer inflow had great impact [illegible] [illegible]

Since Hughes' study, Weatherford and Gray (1987) undertook the task of relating the cyclone's inner-core (0-1° radius) and outer-core (1-2.5° radius) winds using far more accurate wind-measuring equipment. They found a high degree of variability between the cyclone's inner core maximum winds and the radius of gale force winds found in the outer core. They were able to show that the smaller the size of the eye, the smaller the radius of gale-force winds and the weaker the winds through the outer core. For the first time, the entire wind profile from the radius of maximum winds to the radius of gale force winds was depicted for cyclones of different intensities and eye sizes

In the late 1970's till the present the goal of Atlantic hurricane research flights has been to study the hurricane's finer-scale convective processes. Studies such as those done by Willoughby, et al. (1982), Barnes, et al. (1983), Jorgensen (1984), Frank (1984), Marks and Houze (1986), and Barnes and Stossmeister (1986) have uncovered much about the convective and mesoscale processes of the hurricane. Although these later studies moved away from the snapshot depictions of the wind field that were common in the 1950's to 1970's and followed the changes on a mesoscale time frame (generally less than an hour to a few hours), still lacking was a depiction of the tropical cyclone's wind field through its outer core (1-2.5° radius) for periods beyond a day.

The question of wind structural evolution on a time scale beyond a day was attempted by Dunn (1951), who suggested four stages of cyclone development: 1) formative, 2) immaturity, 3) maturity, and 4) decay. Colon in 1963 further verified what forecasters have known for years that individual cyclone wind profiles differ considerably from case to case. On this premise he classified the tropical cyclone's wind evolution into two types: a small inner-core "Dassy" type of wind evolution and a large "Helene" type of wind evolution. The [illegible] with his depictions was his data sample which [illegible] did not extend beyond the inner core and thus did not sample the radius of gale-force winds. Weatherford and Gray's data sample of 9 hurricanes, most of which were sensed for one day or more, [illegible] for which four days of data were analyzed. The typical lifetime of a tropical cyclone is about a maximum of about 10 days. Therefore, [illegible] for investigating [illegible] a [illegible] of the [illegible] of tropical cyclones.

These early life cycle studies provided good general wind field patterns given a limited data sample. Yet the question typically raised from limited data studies remains: can a handful of cases adequately describe all cyclones? It is felt that a large *number* of randomly selected cases each individually followed throughout their lifetimes might provide a more complete description of the cyclone's wind field. Only then can different cyclones be sorted and compared for similarities.

This study attempts to fill in the present gap of knowledge about the tropical cyclone's wind evolution by focusing on the 700 mb winds from the center to 3° and occasionally to 4° radius, thereby capturing the wind field from its maximum value to its gale- force strength throughout the life cycle of the cyclone. Additionally, once the mean vortex is removed and all cyclones are oriented to a common directional heading, the resulting background wind field can be examined for indications of steering current and cyclone motion differences.

1.2 Focus of this Study

Ideal for such a study are the operational reconnaissance flight data of the northwestern Pacific Ocean basin in which aircraft missions are routinely flown from the center to 4° radius every 12 hours on nearly all cyclones from genesis to decay. All five years of flight observations during the 1980-84 period were processed and analyzed. This represents an analysis of 750 aircraft missions into 101 tropical cyclones. This study explores the 700 mb [illegible] wind field changes evident in both the mean vortex and its 700 mb steering current of the tropical cyclone from just past genesis until cyclone decay.

Chapter 2 discusses the data used and the manner in which they were processed. Chapter 3 examines the basic steady-state structure of the tropical cyclone by intensity and [illegible] wind classes. Chapter 4 provides information on how the background wind [illegible] and mean vortex removed) steers the cyclone. The effects of differing [illegible] are depicted. Chapter 5 discusses the changing wind profile of the [illegible] genesis to maximum intensity through decay. The changing [illegible] are documented. Chapter 6 describes the typical

role of the cyclone's eye on the life cycle. Finally in Chapter 7, the tropical cyclone is portrayed through its 'typical' life cycle. The influence of the outer core region (1-2.5° radius) on cyclone intensity change and motion is discussed as well. Two appendices have been added to further enhance this report. Appendix A describes a detailed account of the data reduction. Appendix B depicts the manner in which 47 different tropical storms and typhoons central pressures, outer core winds, eye diameters, and eye temperatures changed throughout their lifetimes.

Chapter 2

DATA REDUCTION PROCEDURES

The primary goal of this research is to describe the 700 mb wind structure of the tropical cyclone as it evolves throughout its life cycle. In departing from the usual portrayal of the mean cyclone's snapshot view, the cyclone will be described as it changes its structure with time. To achieve this goal a large number of tropical cyclones must be observed through their full life cycles. Thus the data used for this study encompassed over 750 flight missions into 101 named tropical cyclones that traversed the northwestern Pacific ocean basin for the 5- year period of 1980 to 1984. Figure 2.1 depicts the tracks of the cyclones in this five year data set.

2.1 Scope of the Flight Missions

Because these missions were designed to track and measure cyclones from genesis to decay, a wide range of intensities, latitudes and headings were sampled. In order to draw comparable and consistent results, only the 700 mb data were processed. Thus the boundary level missions (designed to fly below cloud base, generally at 300 m), flown during the development stage of the vortex, are not included. Once past genesis then, no attempt was made to sample one cyclone intensity class over another. Because all categories of cyclones were sampled as they naturally occurred, an ideal data set for study of the cyclone's life cycle was available.

The limitations imposed upon these operationally-designed flights prohibited missions over land, within 100 nautical miles of the People's Republic of China or Vietnam, or north of 35° latitude. However, these restrictions did not limit a complete analysis of the typical life cycle of the cyclone. Because flights were taken nearly every 12 hours on nearly all

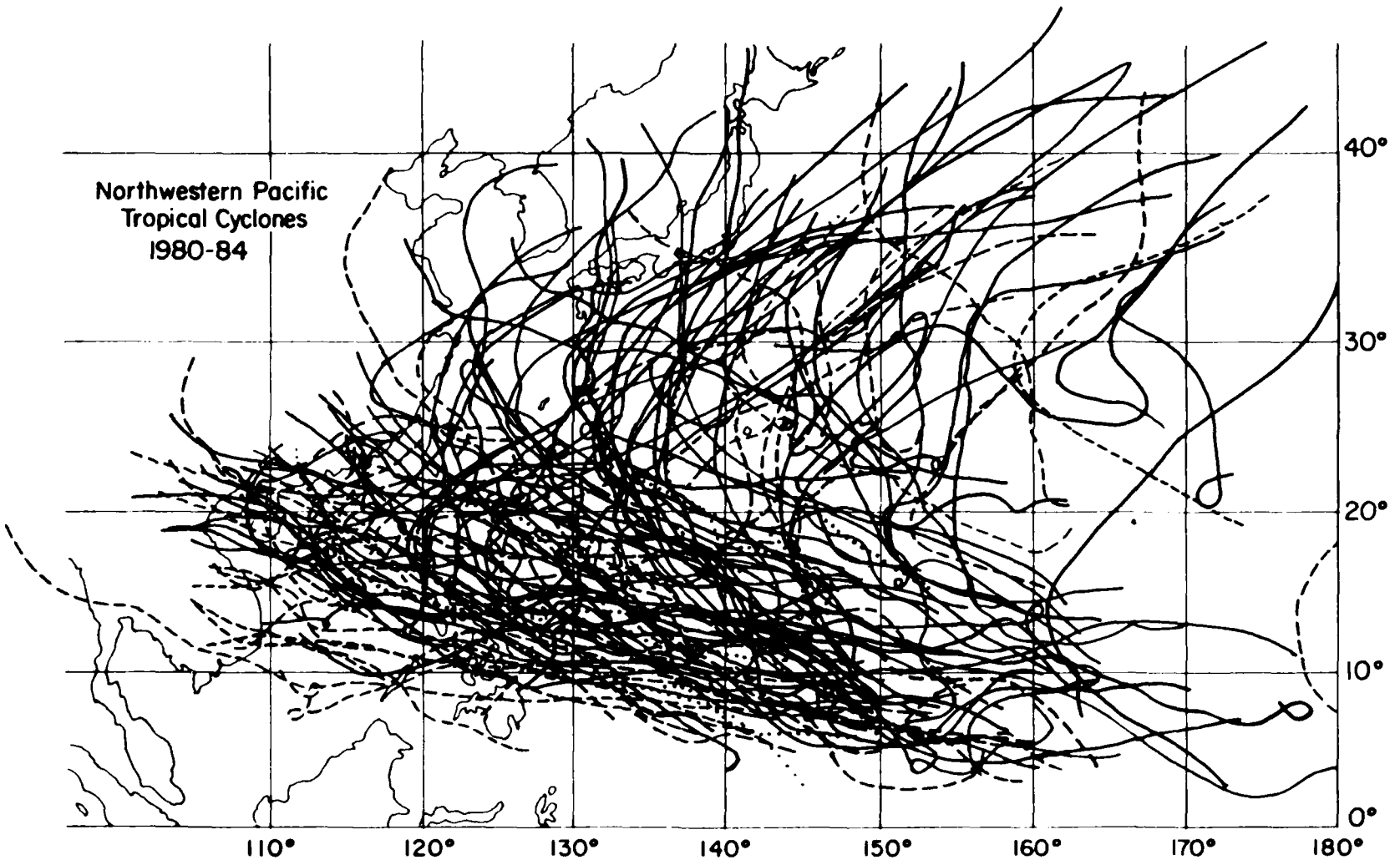

Figure 2.1: Northwestern Pacific tropical cyclone tracks for the 101 cases of 1980-84 used in the present study. Solid lines are the paths of the cyclone while a typhoon and dashed lines denote the tracks of the cyclones' tropical storm stage.

cyclones of the northwest Pacific, very extensive data were available. Data extended out to 450 km (most often beyond the radius of gale-force winds) throughout the natural life cycle of the cyclone.

In order to continuously monitor the development of the tropical cyclone, missions were flown into the center of the cyclone 4 times a day. Typical flight tracks consisted of 4-quadrant radial leg passes from the center to 2.5 degrees latitude and 2-quadrant entry and exit passes to 4 degrees at 700 mb twice a day (Fig. 2.2). This provided information every .5° radius inside 2.5° along each radial leg. In order to provide the forecaster with information on the cyclone prior to the forecast times of 00 and 12 GMT, flight data sampling within 4° of the center typically spanned a four-hour period clustering about 9 and 21 GMT (often 18 and 6 local time, respectively), although total flight time lasted 10-12 hours per mission.

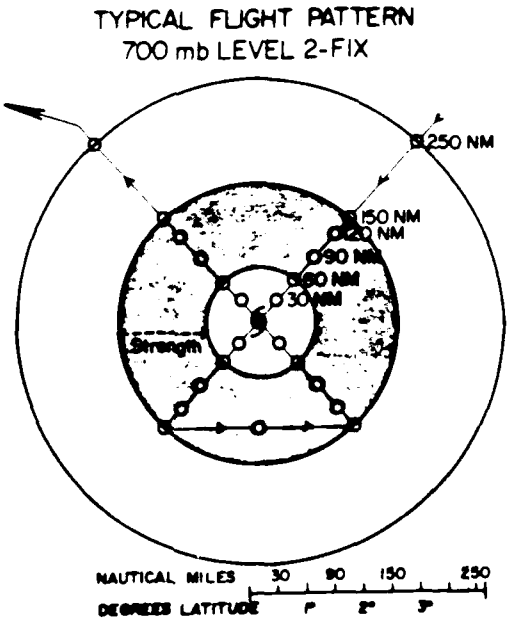

Figure 2.2: Typical 700 mb flight pattern for a single mission into a tropical cyclone. Circles denote required observation positions taken every .5° (55 km), with four additional observations taken at the radius of maximum wind. The shaded region marks the outer core (1° to 2.5° radial band) while the unshaded inner core is defined as the region inside 1° radius.

Two-thirds of all the cyclones studied here developed into typhoons. The average life of a tropical cyclone which developed into a typhoon was 7.5 days while that of a tropical

storm was 4.5 days. The longest lived cyclone of this data set was Typhoon Pamela of 1982 which traversed the Pacific for 16 days. These flight missions afforded a substantial tropical cyclone data set with which to study the life cycle of these systems. Figure 2.3 depicts the natural frequency of cyclone intensity.

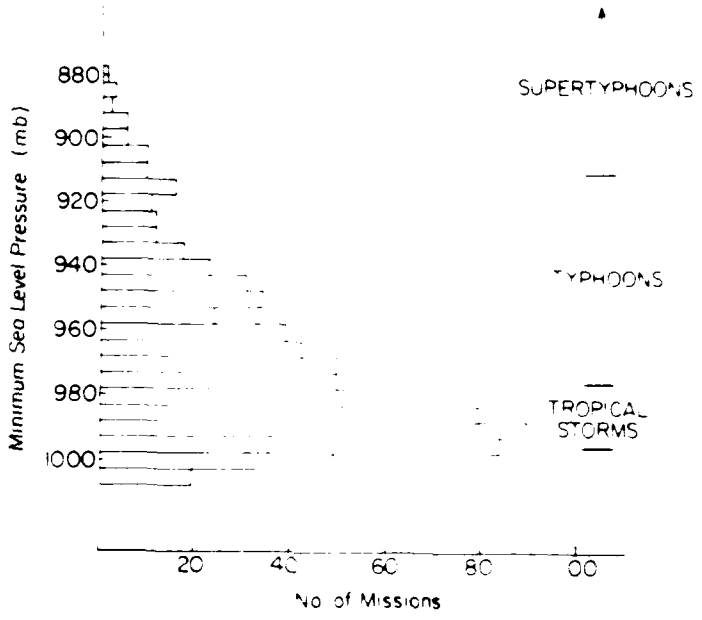

Figure 2.3: Histogram showing the aircraft observed frequency of MSLP (Minimum Sea Level Pressure) for overwater tropical cyclones of the northwestern Pacific from 1980 to 1984.

2.2 Data Navigation

Depending on its use, all data were positioned to the center of the cyclone either in the earth-relative (natural—here termed NAT) or cyclone motion and direction relative (here termed MOTROT—MOT for MOTion and ROT designating that all cyclones were ROTated to a common heading) coordinate systems. The advantage of the earth-relative coordinate system was that, once the vortex flow was removed, the flow pattern of the environment could be examined. This is also the coordinate system in which the forecaster views the cyclone. In the cyclone-relative coordinate system one can detect the environment which the cyclone senses as it moves through the 700 mb stream. Therefore

the process of navigating each observation to either a stationary or moving cyclone center was important. Basically this involved using the Best Track center positions provided by the Joint Typhoon Warning Center (JTWC) and interpolating them through time to result in a smooth track. Aircraft observations were then fixed relative to the cyclone center. Details of the data navigation are explained in full by Weatherford (1985) and Weatherford and Gray (1987a).

2.3 Compositing Method

This data set was an expansion of the author's previous analysis of 3 years of flight data. An extra two years (1983, 1984) of data was processed in order to obtain a more representative sample of the typical changes occurring during the typhoon's lifetime. This 5-year data sample (101 cyclones) allowed composite stratifications to be made with full data coverage at all octants of the cyclone. Notice from Fig. 2.4 how full the data coverage is from the center to beyond 4° when like cases of cyclones have been composited together as in this example of cyclones with medium-sized eyes. The stratification with the least amount of observations was that of missions into cyclones undergoing rapid deepening (defined as an MSLP drop of 42 mb/day)—see Fig. 2.5. Even in this minimal data stratification, a relatively large number of observations are available. An ample supply of observations was thus available for all stratifications.

The design of the composite grid shown in Fig. 2.6 was based on the frequency of data. Observations were typically taken every 0.5° or 55 km out to 275 km and then sharply tapered off to 460 km. Figure 2.7 shows a larger grid encompassing 4° (440 km) of radius from the center with the total data count for all missions portrayed in each grid box. Notice how the frequency of data drops off significantly beyond 2.5° (275 km). The grid used in the analysis will thus extend only as far as 2.5° as shown in Fig. 2.8 for a composite example of the tangential wind of extreme typhoons.

Although there were typically not enough data points for a plan view depiction of a subset beyond 2.5°, azimuthally-averaged composites allowed radial depictions of wind, moisture and vorticity fields to extend out to 4° radius.

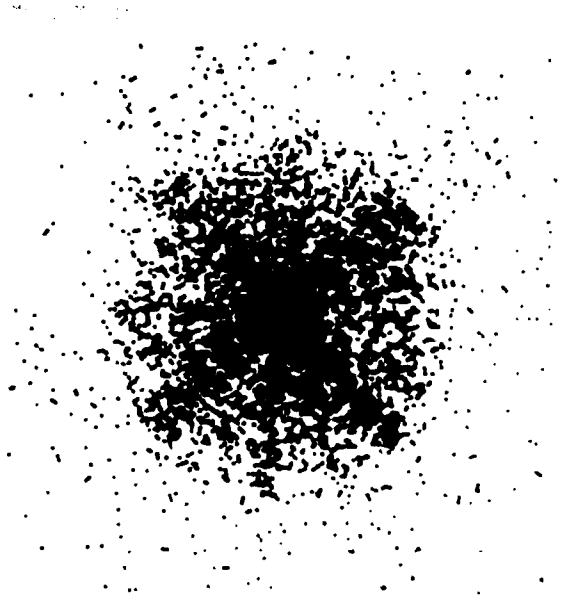

Figure 2.4: Data points of a composite of all aircraft missions flown into tropical cyclones with medium eyes (diameters ranging from 28 to 55 km)

Figure 2.5: Data point spread for a composite of all flight missions into cyclones undergoing a rapid deepening of MSLP ($\geq$ 42 mb per day)

[illegible] data averaging [illegible] were averaged and assigned [illegible] This is the technique for providing spatially [illegible] averages [illegible] were scattered evenly throughout each box [illegible] distances between forecast and actual locations. Note [illegible] of the radial flight tracks were for all missions flown into the single [illegible] as will be discussed in Chapter 3. Those data points that lay inside 28 km from the [illegible] were rejected because they fell in the region of rapidly changing fields and did [illegible] represent the maximum wind. Obviously averaging maximum wind speeds [illegible] and variable center winds would result in misrepresentative values. Thus the [illegible] was limited from 25 - 28 km to 2.5 radius (278 km) with all data failing [illegible] box being averaged. This avoided the light and variable winds [illegible] and usually the maximum wind value as well. Maximum wind speeds were [illegible] for purposes of comparison as will be discussed later in this chapter but [illegible] was not included in the plan views. Throughout this paper this composite [illegible] used in both the NAT and MOTROT coordinate systems. This allows one to [illegible] the asymmetries in both earth-relative and the cyclone-relative coordinates.

2.4 Definitions

[illegible] definitions and abbreviations used in the previous study will be used here [illegible]

MSLP Maximum Sea Level Pressure. This intensity measure was obtained directly by [illegible] or was extrapolated from the 700 mb flight level. This more [illegible] intensity measure was used in lieu of the maximum wind speed.

OCS Outer Core Wind Strength. An area-weighted average tangential wind speed from [illegible] 2.5 degrees radius per mission. This allowed a conservative measure of the outer [illegible] related to the inner core MSLP. As was shown by Weatherford and Gray [1987], the OCS correlates highly [illegible] with the radius of gale-force winds.

RMW Radius of Maximum Wind speed.

Figure 2.9: Flight paths for all missions flown into Wynne of 1980

2.5 Vortex-Averaged Maximum Wind Estimate

It is vital to reliably estimate the vortex-averaged maximum wind speed. For a study of the wind profile, this would be superior to surface estimates which are affected by gust factors, the cyclone's speed of motion and azimuthal differences. As was explained in Weatherford and Gray (1987a), the doppler wind equipment used on board the WC-130 aircraft occasionally attenuated in the heavy rain that accompanied the convection within the eyewall. Therefore some doubt was cast on the reliability of the maximum wind and the radius of maximum wind measurements in cases with well developed eye walls. And yet it is the value of this maximum wind speed that is most crucial to any tropical cyclone damage forecast. This necessitated the estimation of maximum winds using an analytical approach given flight observations of the pressure profile or outer wind speeds, both of which were reliably measured.

The first attempt to find an accurate estimate of the cyclone's maximum wind involved solving the modified Rankine vortex equation (Depperman 1947)

$$V R^{x} = V_{max} R_{max}^{x} \qquad 2.1$$

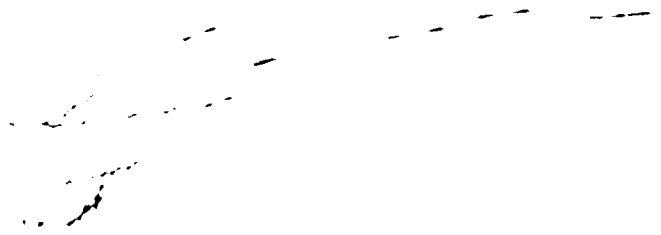

[illegible] Assessment [illegible] differing 7.6 mb height [illegible]

[illegible] Hurricane Debbie a study was first made [illegible] data set [illegible] were already available [illegible] Shea and Gray [illegible] [illegible] [illegible] Atlantic hurricanes in 1965 [illegible] Gray and [illegible] All of these missions used Doppler wind equipment. There was a [illegible] difference between these missions and the missions that comprised the 1956-1961 [illegible] Each data were taken every 55km (0.5) along each radial pass with [illegible] measure at the radius of maximum wind. If the Doppler attenuated this [illegible] In the Atlantic however wind reports were provided and automatically [illegible] later averaged to every 2.5 n mi (4.6 km). For Shea and Gray's [illegible] or attenuation was thus easily identified and missions in error were sorted [illegible] missions flown at 7.6mb were used in order to closely match the 7.6 mb [illegible] western Pacific data set used here. In addition data from hurricanes Anita [illegible] and Alma 1970 in which the Inertial Navigation System (INS) was used in lieu of [illegible] were tested. All height data for each hurricane were best fitted [illegible] in a least squares manner from which a cyclostrophic wind was

[illegible] radially averaged observed [illegible] wind [illegible] It was then decided that this scheme [illegible] averaged maximum wind.

[illegible] this scheme Holland's equation

$$[illegible]$$ (2.2)

was used [illegible] scaling parameters A and B by use of a sum of squares [illegible] the height of the environment [illegible] the height at the center, and [illegible] the [illegible] International Mathematics and Statistical Library (IMSL) routine [illegible] Levenberg-Marquardt algorithm [illegible] as described in Brown and Dennis (1972), Levenberg (1944) and Marquardt [illegible] lists the hurricanes used in the test and compares the observed [illegible] maximum wind speeds along with the RMW [illegible] Holland's [illegible] Note that the hurricane with the greatest error was Allen (1980) as its MSLP reached a most unusually low 899 mb central pressure. Figure 2.11 shows a [illegible] observed versus the calculated height profiles for Allen. In this most extreme case [illegible] calculated profile, a slight error can produce errors in the maximum wind estimate when the pressure profile is unusually steep. Also, the radial accelerations may [illegible] negligible.

For the environmental height, a climatological average was chosen. Overall, though, the study showed how reliable Holland's scheme was when carefully applied to height data. Finally, gradient winds were compared with cyclostrophic winds with little significant observed difference. As a result, the simpler cyclostrophic estimate was applied to the 1980-1984 northwestern Pacific data set as it was for the Atlantic data. Figures 2.12 and 2.13 show how well Holland's scheme best approximated the height profiles of the 1980-1984 Pacific data set for Supertyphoon Wynne and Typhoon Owen.

Once the Holland maximum wind estimate was tested and found to provide very representative values, it was applied to the 1980-84 data set. The value used for the height of the northwestern Pacific environment was 3130 meters. This was derived from

Table 2.1 Comparison of observed quadrant averaged maximum wind speeds and their radii with the Holland estimate for 19 test cases of Atlantic hurricanes.

Hurricane	Date	Radius of Max (km)		Maximum Wind ($m\ s^{-1}$)	
Name	(Yr-Mo-Da)	Observed	Holland Estimate	Observed	Holland Estimate
HANNAH	591001	46	37	40	37
HANNAH	591002	35	39	33	44
ANNA	610721	41	19	33	34
CARLA	610908	74	61	38	40
CARLA	610909	70	46	42	45
FLORA	631003	19	19	57	54
FLORA	631010	113	80	31	36
DORA	640905	54	56	43	39
DORA	640907	67	80	35	34
DORA	640908	89	80	31	36
DORA	640909	72	93	32	34
GLADYS	640917	35	28	46	41
GLADYS	640917	46	28	48	52
HILDA	641002	54	65	43	43
ISBELL	641014	24	19	30	38
DONNA	600907	33	37	55	55
ANITA	770901	24	24	68	64
ALLEN	800807	17	15	67	79
ALLEN	800808	19	17	56	56

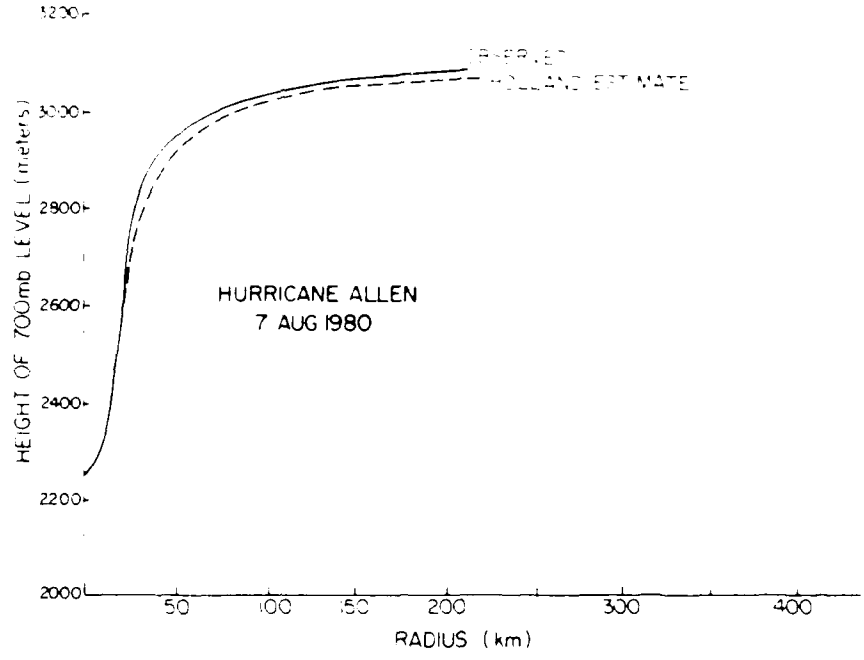

Figure 2.11: 700 mb height vs radius profiles for the observed and Holland-estimated shapes.

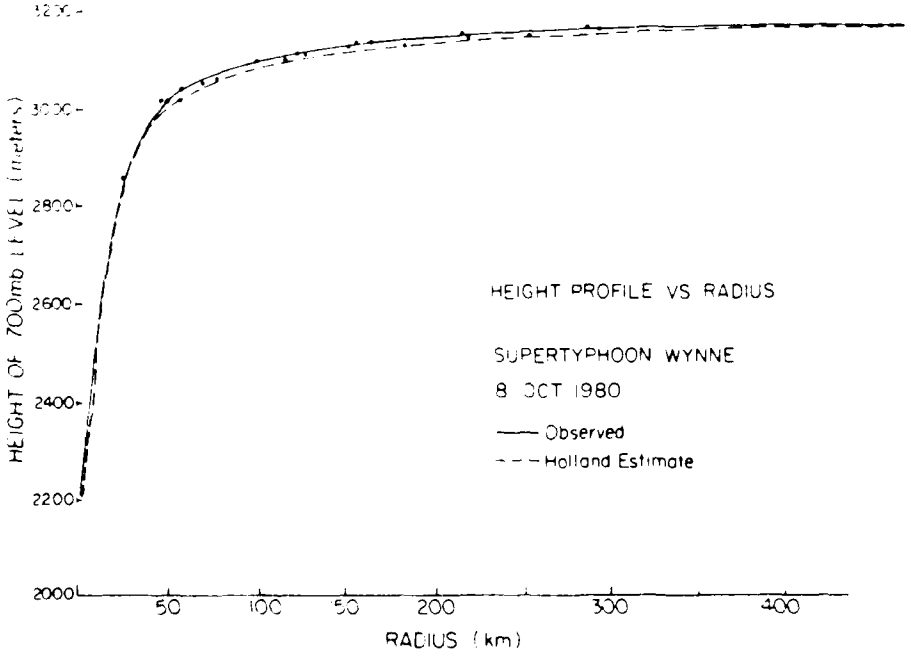

Figure 2.12: 700 mb height vs. radius profiles for the observed curve (actual data points shown) and the Holland-estimate for Supertyphoon Wynne.

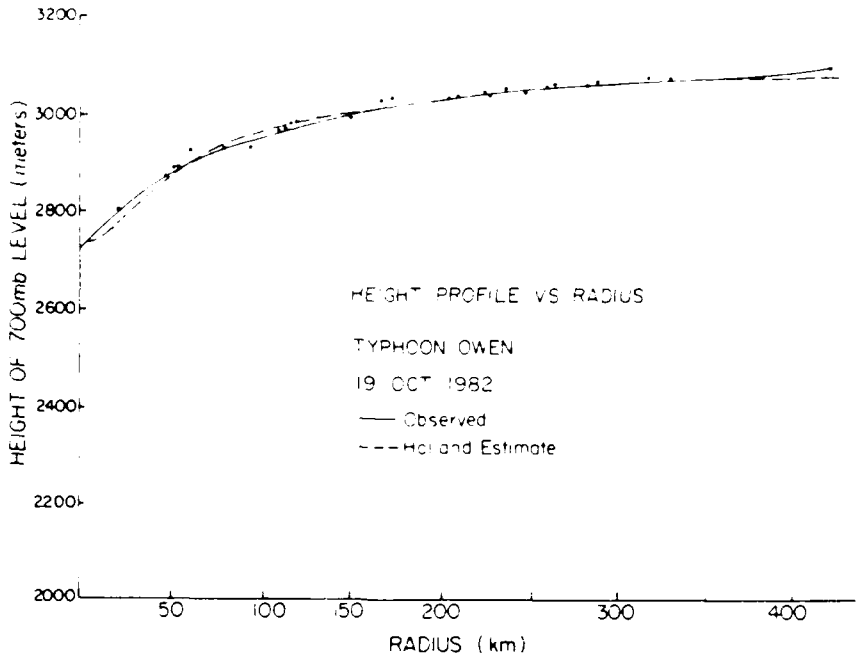

Figure 2.13: 700 mb height vs. radius profiles for the observed curve (actual data points shown) and the Holland-estimate for Typhoon Owen.

an average of the 700 mb height observations located 6° to 8° radius from the center. The tropical cyclones of this study varied in MSLP from 1007 mb to 878 mb and in 700 mb estimated maximum wind speed from 5 to 76 ms^{-1}. Table 2.2 lists the average, median, standard deviation and range of values found for the scaling parameters A and b, and the calculated maximum wind speed and RMW once Holland's scheme was applied to the 5- year data set used here. Figure 2.14 shows a good correlation of the estimate to the observed MSLP (.93) implying that even though the pressure gradient can play a major role in determining the maximum wind speed, the minimum pressure value dominates. When the observed maximum winds were compared with the MSLP the correlation coefficient was .88 (Weatherford and Gray 1987a).

It is vital to both forecaster and researcher to have an objective method of estimation of the maximum wind speed of a tropical cyclone. The attempt here was to provide a consistently objective method of estimating an azimuthally averaged 700 mb maximum wind speed. Adjustments would have to be made for a surface wind estimate, cyclone motion, and wind asymmetry in the natural coordinate system. This method relied on

Table 2.2: Statistics on the Holland derived scaling paramenters A and b that best fit height data to a logarithmic hyperbola and the resultant estimates of Radius of Maximum Wind speed (RMW) and maximum wind speed as applied to the 780 missions of the northwestern Pacific data set.

PARAMETER	AVERAGE	STANDARD DEVIATION	MEDIAN	RANGE
A (km)	118	± 243	44	1 - 2081
b	.99	± .29	.97	.1 - 2.1
RMW (km)	61	± 50	48	7 - 330
MAX WIND (ms-1)	32	± 13	30	5 - 76

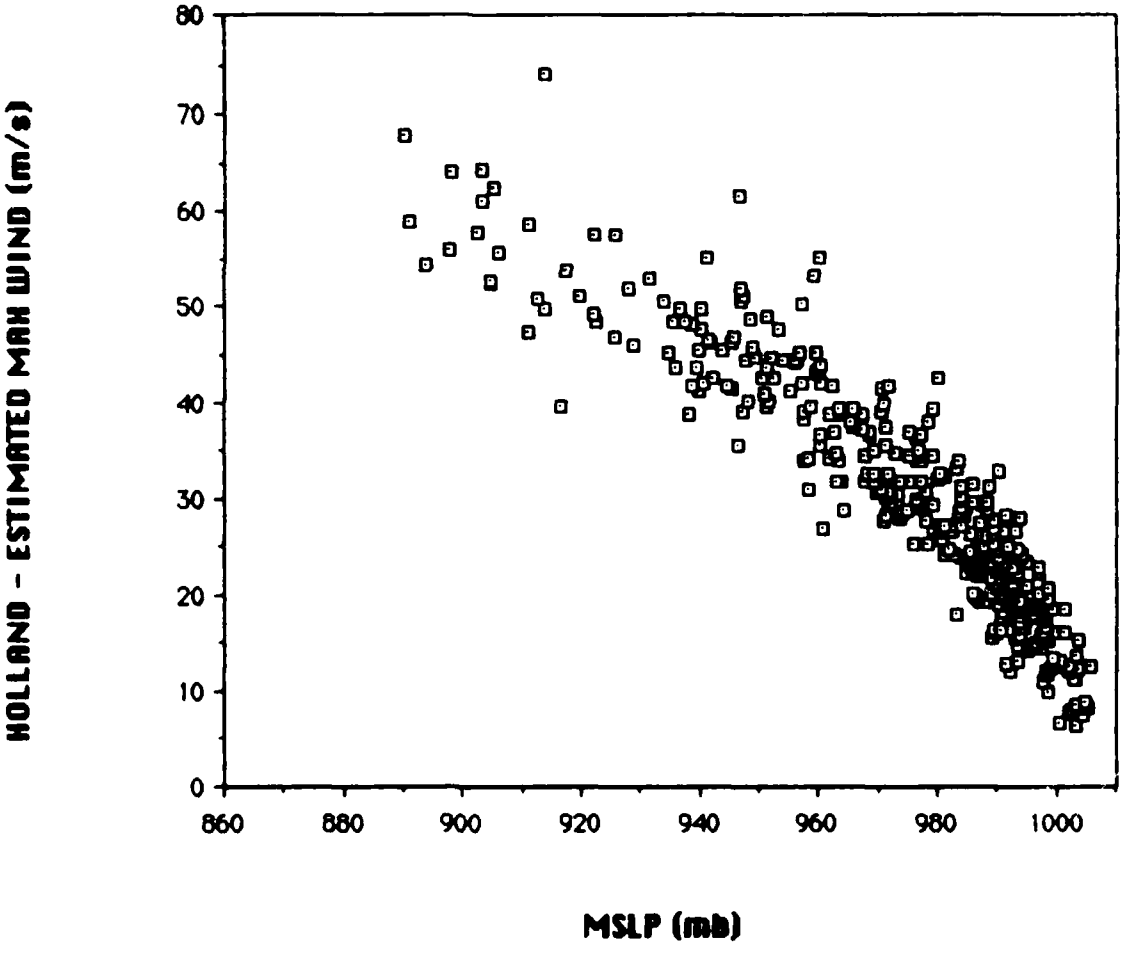

Figure 2.14: Scatter plot of the Holland method estimated maximum wind speeds versus the accompanying MSLP for all cyclones used in the present study.

the shape of the height profile unique to each flight mission not to a particular surface gust factors.

2.6 The Normalized Wind Profile

When modelling the wind profile of the tropical cyclone, it would be most convenient to normalize the tangential wind field. Theoretically, as the maximum wind changes, the entire wind field would change accordingly. The most straightforward way to approach this scaling method would be to normalize the wind profile to the radius of maximum wind speed (RMW) given the value of the wind speed there. This accounts for variations in both the maximum wind speed and its position relative to the center. Then, as the RMW contracts while the cyclone intensifies and then expands as the MSLP fills, the normalized wind profile should remain the same. The potential use for this method is great in that often the maximum winds can be obtained, either directly by aircraft measurement or indirectly from satellite analysis (Dvorak, 1975) and then applied to regions beyond the RMW. Since the results in this paper will show considerable changes in the outer core as well as the inner core, the question must be addressed whether the changes in the OCS (which is fixed in space to a region of 1° to 2.5° radius) are due merely to the changes in the value and radius of the maximum wind. Can the wind profile be simplified when normalized to the RMW?

We proceeded to test this theory of normalizing the wind field by applying the theory to observed wind profiles for the 101 cyclones of this data set. The procedure used to scale the wind profile relied on the observed RMW and the Holland-estimate of the maximum wind speed. The RMW was not accurately measured when the Doppler wind equipment attenuated so in those cases the diameter of the eyewall was employed. Using the data from the hurricane flights of the late 1950's through 1970's, in which the Doppler wind equipment did not attenuate, a regression equation was derived which best fit the RMW given the MSLP and eyewall diameter. The result which explained 73% of the variance was:

$$RMW = -133 + .1468(MSLP) + .967(\text{ eye radius}) \tag{2.3}$$

where the RMW and eye radius are in nautical miles and MSLP in millibars.

Figure 2.15 depicts seven different wind profiles by their actual values of radius and speed. Figure 2.16 depicts these same profiles in the normalized radius which extends to multiples of RMW and normalizes the wind speed by the maximum wind speed as such:

$$V_t/V_{t-max} = \text{ the normalized wind speed.} \tag{2.4}$$

Notice how little the variability was reduced when compared with the unnormalized profiles. We suspected that this method would not simplify the wind profiles as was hoped. One reason is that wind profiles in nature are generally not smooth and are inherently difficult to approximate.

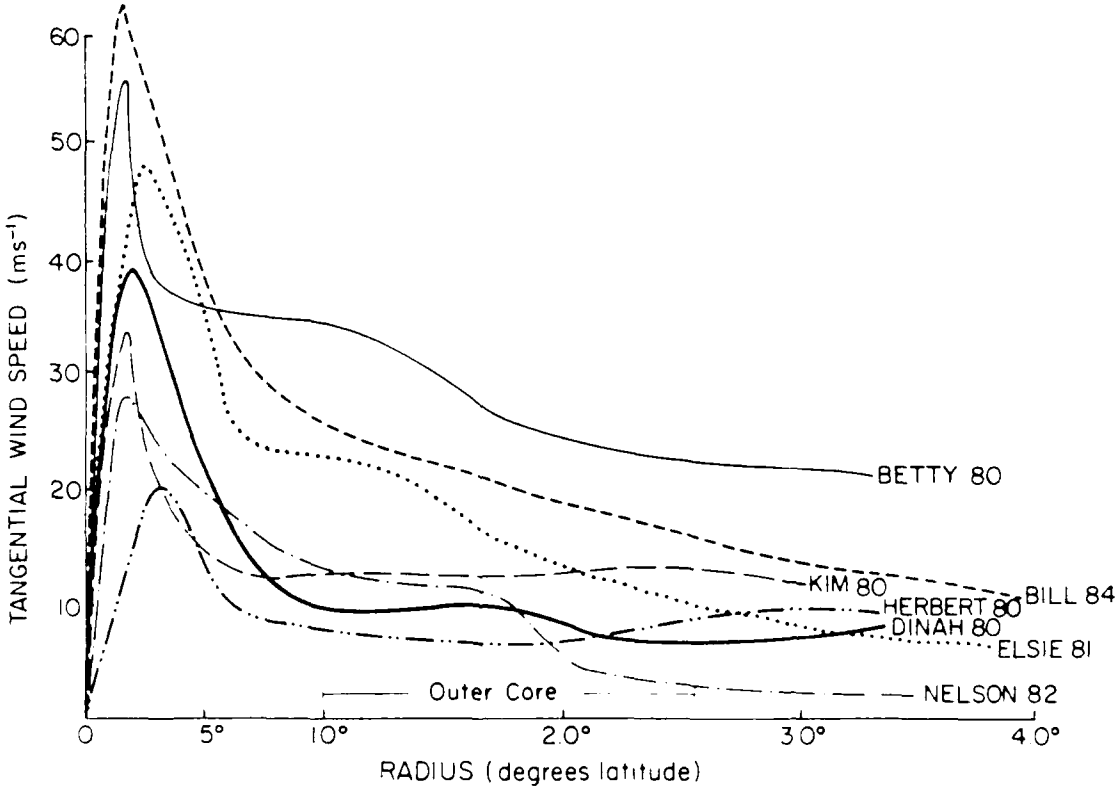

Figure 2.15: Actual tangential wind profiles for seven tropical cyclones. The outer core extends from $1°to2.5°$ radius.

In an attempt to reduce the variability between the inner and outer cores, a normalized outer core wind strength, NORM-OCS, was calculated. The actual OCS was fixed in space,

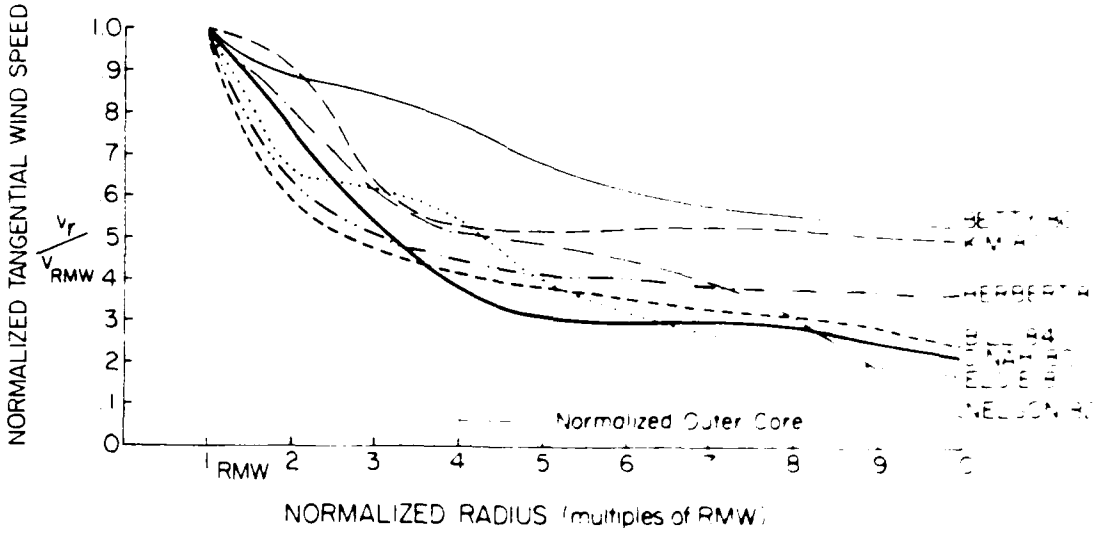

Figure 2.16: Normalized tangential wind profiles in which radius varies as multiples of RMW and wind speed values are a fraction of the maximum wind value. A comparable outer core extends from 4 to 10 times the RMW.

as shown in Fig. 2.15, from 1° to 2.5° radius while the RMW varied with each mission. On average, the outer core resided in a region from 4 to 10 times the RMW. Thus to match an appropriate normalized-OCS, the RMW was fixed and the outer core now varied from 4 to 10 times the RMW. The normalized-OCS, an area-weighted value from 4 to 10 times the RMW was then calculated. Comparisons were made using the ratio of the maximum wind/normalized-OCS versus the ratio of the max wind OCS, in order to see if the normalized method would reduce the observed variability between inner and outer core winds. Notice from Fig. 2.17 that for all cases, the actual OCS (Fig. 2.18) correlated much better to the maximum wind (-.42) than the normalized scatter plot (-.02 seen in Fig 2.18). When only intensifying cases were compared, as shown in Fig. 2.19, the actual plot correlated even better (-.67) than the normalized plot (-.09) seen in Fig. 2.20. This implies that the higher the maximum wind speed, in the intensifying phase, the smaller the ratio of inner core to outer core speeds for the un-normalized cases. The normalized cases show, surprisingly, no relationship, whatsoever.

The method employed here had a flaw due to the range of observations provided by the aircraft. When the RMW was located inside or near the average (28 km), it was

Figure 2.17 Scatter diagram of the maximum wind speed vs the ratio of the SCS maximum wind speed for a random number of cyclones

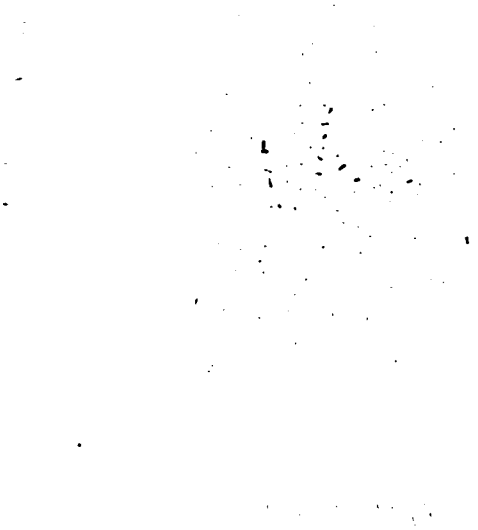

Figure 2.18 Scatter diagram of the maximum wind speed vs the ratio of the normalized SCS maximum wind speed for the same cyclones as in Fig. 2.17

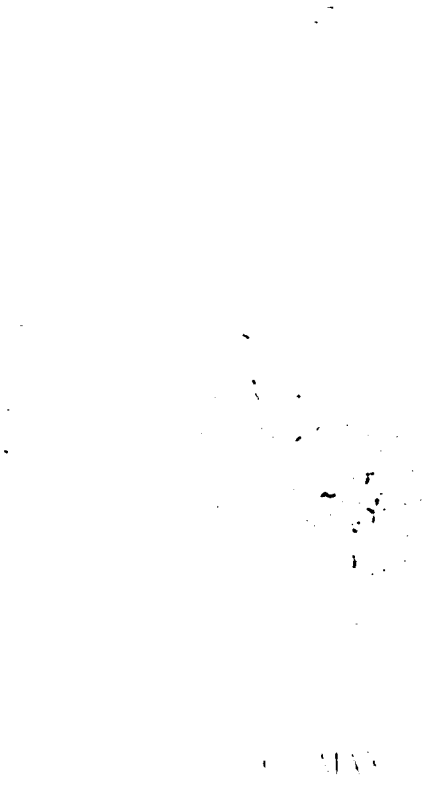

Figure 2.19: Scatter diagram of the maximum wind speed vs. the ratio of OCS maximum wind speed for intensifying cyclones

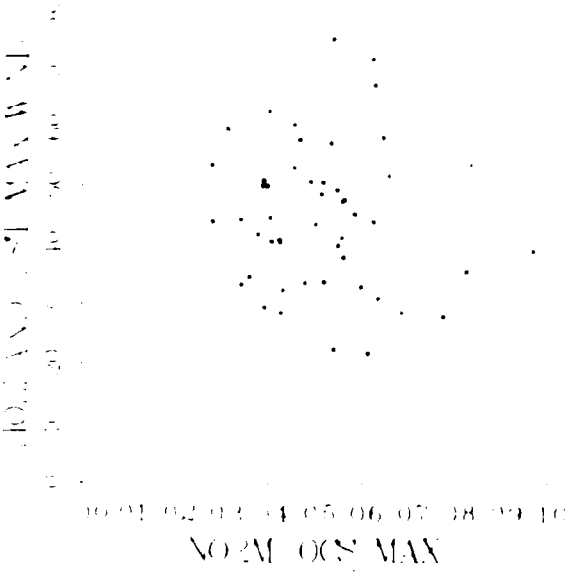

Figure 2.20: Scatter diagram of the maximum wind speed vs. the ratio of the normalized OCS maximum wind speed for the same cyclones as in Fig. 2.19.

extrapolation to that wind at a radius of 1.5 times this because most storms are symmetric beyond the RMW. However, for an RMW much beyond 28 km, winds at a radius of 1.5 times this just were not available. Thus this scheme is weighted towards smaller storms.

It would seem that the normalizing of the wind field was not a process seen in nature, at least not by the method utilized here. It would be more appropriate to use actual wind radii.

Chapter 3

THE MEAN BASIC STATE WIND STRUCTURE OF THE TROPICAL CYCLONE

Before life cycle changes can be described, we must first portray the mean basic state of the cyclone's structural features. We begin by portraying the mean typhoon. But even the mean typhoon is a broad class ranging in actually measured maximum wind speeds from 33 ms^{-1} to 80 ms^{-1}. For this reason we will break this into three typhoon sub-classes along with the mean tropical depression and tropical storm to depict the various intensity classes the tropical cyclone can develop into. In addition, the cyclone is stratified into *three outer core strength classes*.

3.1 The Mean Typhoon

The mean typhoon is positioned at approximately 20 N latitude and 135 E longitude. It moves at an average speed of 5 ms^{-1} towards the NNW (330 degrees) with an MSLP of 945 mb and *OCS* of 22 ms^{-1}. Figure 3.1 depicts the azimuthally-averaged tangential and radial wind field of the mean typhoon showing the inflow that exists within 150 km at the 700 mb level. (Note that data inside 28 km is not averaged resulting in a data void region near the center. The average maximum wind speed shown is the Holland-estimate placed at the Holland-derived RMW.) Notice how the 700 mb inflow is concentrated in the cyclone's inner core region where convection is densely packed.

Asymmetric features appear in the plan view of the mean typhoon for which all 358 typhoon missions were composited. In the natural coordinate system (NAT), one sees that the 700 mb portion of the environmental steering flow in which the cyclone is embedded (Fig. 3.2) is from South to North. This implies that the average typhoon lies about even

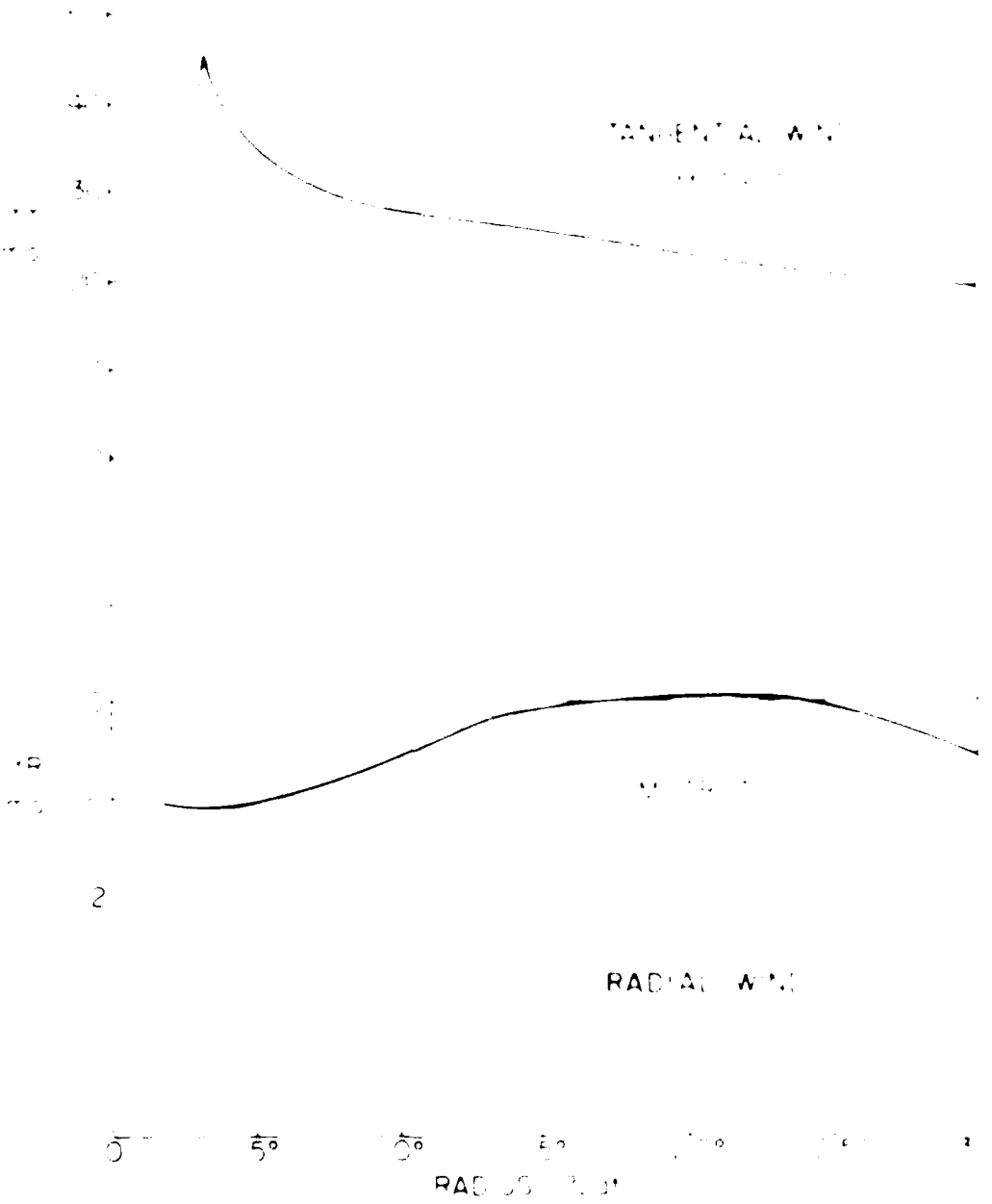

Figure 3.1 Azimuthally-averaged tangential (V_t) and radial (V_r) wind fields for the [illegible] typhoon at 700 mb. All values are in ms^{-1} with positive radial wind denoting [illegible] w

[illegible] Frank (1977a) showed this to be the case for the [illegible] on a much larger scale as indicated by composited [illegible] The 700 mb current seen here is generally flowing at 4 ms^{-1} and yet [illegible] through the 700 mb stream at a faster speed of 5 ms^{-1}. Notice [illegible] moves at a heading of 330° while the 700 mb current is heading [illegible]

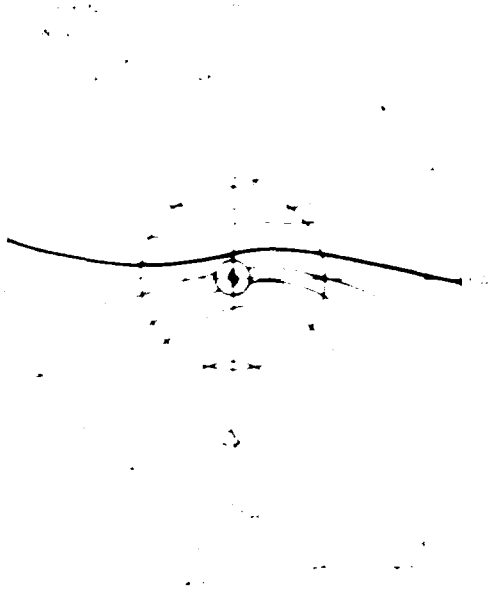

[illegible] depiction of the mean typhoon's 700 mb radial wind speed in NAT. [illegible] cyclones are shown by arrows in the rim. Solid curves [illegible] dashed curves outflow.

[illegible] up to 2.5° the mean typhoon moves faster and to the left. Its [illegible] in quite a similar fashion as it does from radii of 3-7° as determined [illegible] superposing of Frank and Gray (1977) and Chan and Gray (1982). This [illegible] that the inner 2.5° radius belt also reflects the cyclone's steering current. The [illegible] the motion question will be dealt with in greater detail in the next [illegible]

Moving [illegible] the storm relative coordinate system (MOT) in which the cyclone's speed and the mean vortex (VORT) have been subtracted from all winds and the cyclone heading has been rotated (ROT) to a common forward direction (MOTROT = VORT). The

resulting background wind asymmetries are isolated and portrayed as in Fig. 3.3. There is a slight maximum on the left-rear quadrant and a minimum in the right front quadrant. This and all plan views portray the .25-2.5° radius region which is usually outside the maximum wind zone. In these composites for which all data points are averaged in a grid box, maximum winds that do lie in the .25-2.5° region are smoothed with other winds lying in the same grid box. For this reason these results do not deal with maximum wind asymmetries.

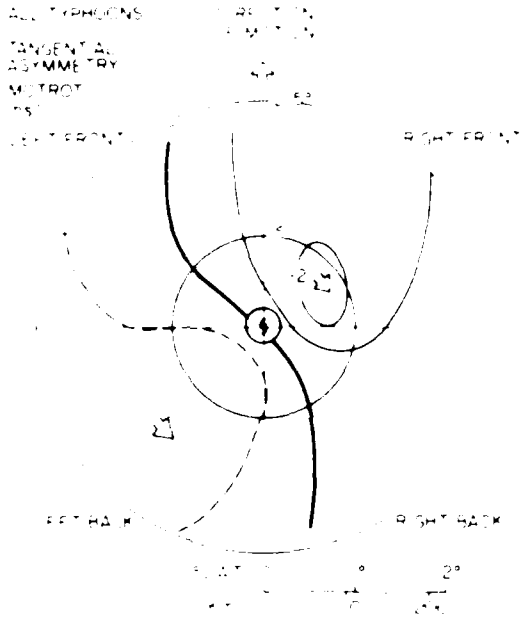

Figure 3.3. Plan-view depiction of the asymmetrical structure of the tangential wind field at 700 mb for the mean typhoon in MOTROT-VORT (both the mean motion and cyclone vortex have been removed). Solid curves denote tangential wind decrease, while dashed curves increase.

3.2 Methodology of the MOTROT-VORT Depiction of Asymmetries

The MOTROT-VORT coordinate system is calculated in order to reveal cyclone asymmetries. All wind vectors are placed in a cyclone-relative coordinate system (MOTROT) with the mean VORTex removed. To remove the mean VORTex, an symmetrically-averaged tangential wind speed is calculated at each radial band and then subtracted from the tangential wind speed located in each grid box. Thus the mean vortex

is removed to reveal the asymmetric structure of the background wind field by itself. The following definitions are used:

TANGENTIAL WINDS

$$\vec{V}_T\ (MOTROT\ -\ VORTex) = \vec{V}_{T_{MOTROT}} - \vec{V}_{T_{VORT}}$$

$$\vec{V}_T\ (asym.) = \vec{V}_T\ (asymmetry)$$

RADIAL WINDS

$$\vec{V}_R\ (MOTROT) = \vec{V}_{R_{MOTROT}}$$

TOTAL WINDS

$$Residual\ Wind\ (Res.) = \vec{V}_T\ (asym.) + \vec{V}_{R_{MOTROT}}$$

$$V_{Res} = \vec{V}_{T_{MOTROT\ -\ VORT}} + \vec{V}_{R_{MOTROT}}$$

The radial wind field is portrayed in Fig. 3.4 in the MOTROT system. Easily observed is the general radial wind flowthrough from left-front to right-rear. When these MOTROT radial winds are vectorially combined with the tangential wind asymmetry field for which the cyclone motion and mean vortex vectors have been subtracted from all winds, one obtains the total residual wind field as portrayed in Fig. 3.5. This residual 700 mb current is observed to flow through both the inner and outer core regions of the typhoon.

The average typhoon thus moves left of and faster than the 700 mb environmental wind in which it is embedded. Because the cyclone's speed of motion exceeds the 700 mb flow, there is a natural maximum wind region on the left and a weaker wind field on the right at this level.

3.3 Intensity Classes

One great advantage with the large number of missions flown during the five-year period of 1980-84 is that the mean typhoon could be broken down into various intensity classes to isolate differences due to the intensity of the vortex. Not only were missions

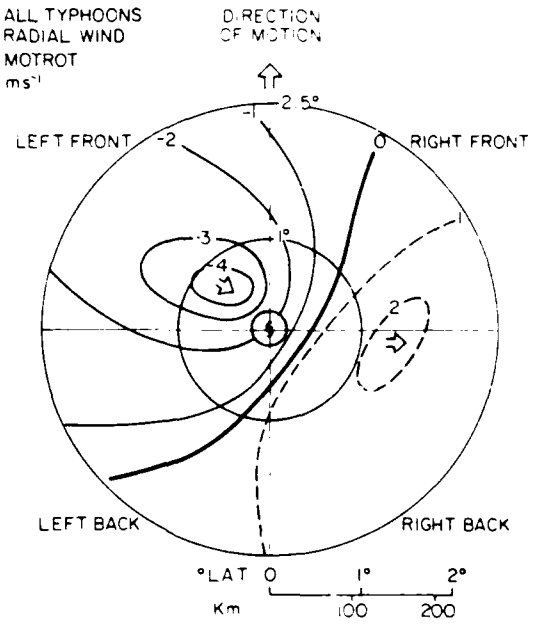

Figure 3.4: Plan-view depictic of the 700 mb radial wind field in the cyclone-relative coordinates (MOTROT) for the mean typhoon. Solid curves denote inflow and dashed curves outflow.

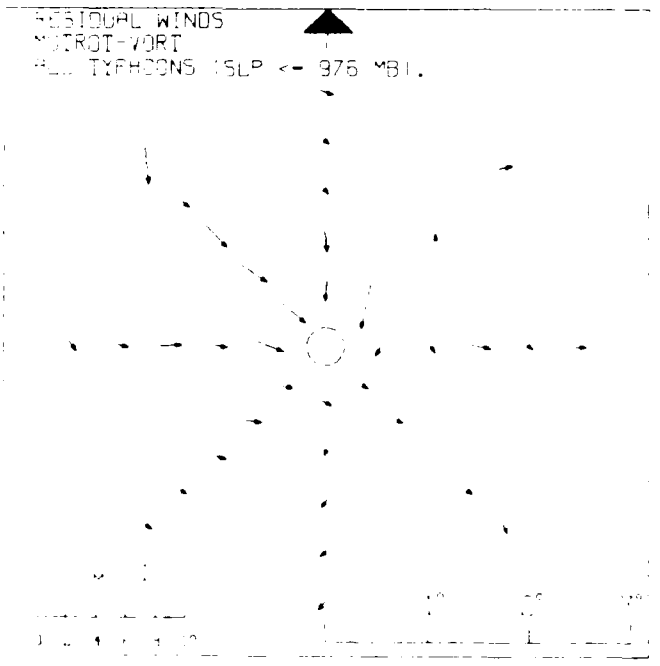

Figure 3.5: Plan view depiction of the 700 mb residual wind field for the mean typhoon which incorporates both the radial and asymmetrical tangential wind vectors in MOTROT-VORT (both motion and the mean vortex have been removed). The bold arrow marks the cyclone's heading of motion. Vector lengths denote speed as shown in the lower left corner.

flown into typhoons, but also into many tropical storms and tropical depressions. These are included in the data sample. The number of missions for each intensity class is indicative of the natural frequency with which these intensity classes occurred. The one exception to this is the much weaker class of the tropical depression which were usually flown at levels below 700 mb level (roughly 950 mb) in its formative stages. This data set does not include the low-level missions into early-stage depressions. Additionally, all depression missions included here developed into tropical storms at the very least thus we are not dealing with the genesis question. Missions into developed depressions which were later flown at 700 mb are, however, included, and as such do not reflect the natural frequency at which tropical depressions occur. A description of the various intensity classes are defined as follows:

EXTREME TYPHOON MSLP $\leq$ 920 mb 59 MISSIONS

INTERMEDIATE TYPHOON MSLP 920-950 mb 113 MISSIONS

MINIMAL TYPHOON MSLP 950-976 mb 205 MISSIONS

TROPICAL STORM MSLP 976-996 mb 329 MISSIONS

TROPICAL DEPRESSION MSLP $\geq$ 996 mb 91 MISSIONS

Table 3.1 depicts the average statistics of these various intensity classes of cyclone. All typhoon classes were situated at similar positions, heading toward the same approximate direction with the same speed. Apparently, each typhoon subclass was embedded in the same average steering current. Tropical storms and depressions were situated at lower latitudes and headed in a more westward direction than the typhoon cases. Because the tropical depressions included in this data set were well developed, their MSLP was near 998 mb with their average maximum wind speed of 13 ms^{-1}.

Classifying the tropical cyclone by its intensity allows for greater detail of the symmetrical wind fields than was provided by the mean typhoon alone. The tangential wind field of Fig. 3.6 shows quite a flat field for the tropical depression but as the intensity

Table 3.1: Average statistics for cyclones of different intensity class by latitude (°N), longitude (°E), speed of motion (ms^{-1}), cyclone heading (degrees), MSLP (mb), Outer Core Wind Strength (OCS 1-2 1/2° radius ms^{-1}), and maximum wind speed (Holland estimate ms^{-1}).

INTENSITY CLASS	LAT	LONG	SPEED	HEADING	MSLP	OCS	MAX WIND
EXTREME TYPHOON	19°	133°	5	325	892	25	56
INTERMEDIATE TYPHOON	20°	135°	5	330	938	23	48
MINIMAL TYPHOON	21°	137°	6	327	964	21	37
TROPICAL STORM	17°	137°	5	310	988	14	23
TROPICAL DEPRESSION	15°	139°	6	290	998	9	13

increased, the wind increased as well, albeit much more rapidly near the center than in the outer core. (The Holland-estimated maximum wind value was used here at the Holland-derived RMW.) Notice also that the RMW contracts with intensity thereby concentrating momentum in the inner core. Notice how the tangential wind was nearly the same at 3° radius for the extreme, intermediate, and minimal typhoons, but considerably different in the inner core region. The tropical storm showed the least 700 mb inflow of all intensity classes with the intermediate typhoon exhibiting the most inflow. The depression was observed to have outflow at this 700 mb level likely reflecting the undeveloped nature of this early stage. Such inflow appears to build up as the cyclone intensifies. Aside from the tropical depression, the 700 mb inflow appears to concentrate in the inner core. The relative vorticity fields of Fig. 3.7 bear out this inner core wind concentration of tangential wind. Note how much the vorticity increases at the inner core as opposed to the outer core. This follows from the simplified tangential equation of motion:

$$\delta v/\delta t = -u(\varsigma + f) \tag{3.1}$$

If the tangential winds are increasing in time either inflow or vorticity must increase. For these intensity classes, they both do. As shown in Fig. 3.8, this concentration in intensity is well reflected in the change in the 700 mb divergence field.

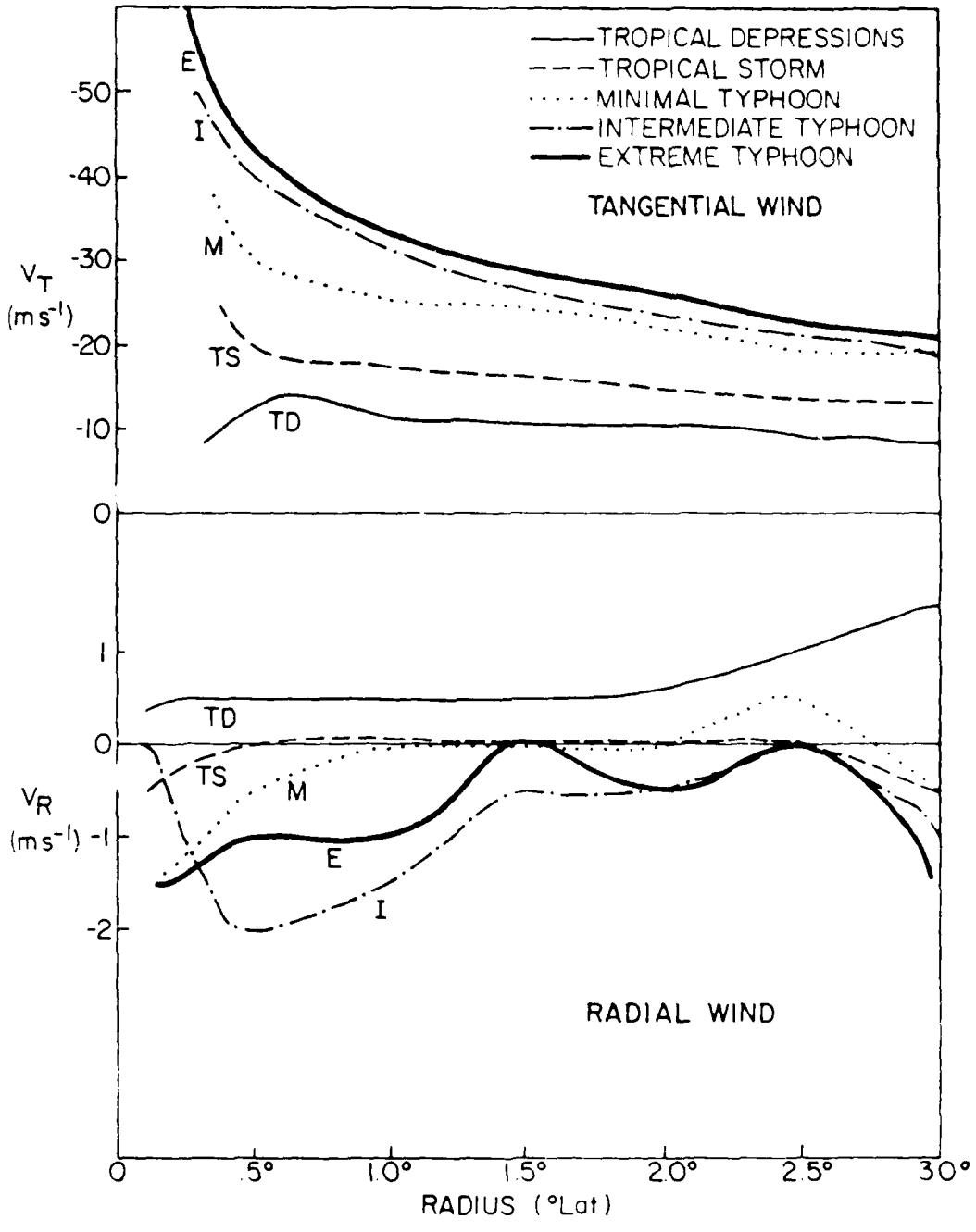

Figure 3.6: Azimuthally-averaged 700 mb tangential (V_t) and radial (V_r) wind fields for the five classes of tropical cyclone as defined in the text.

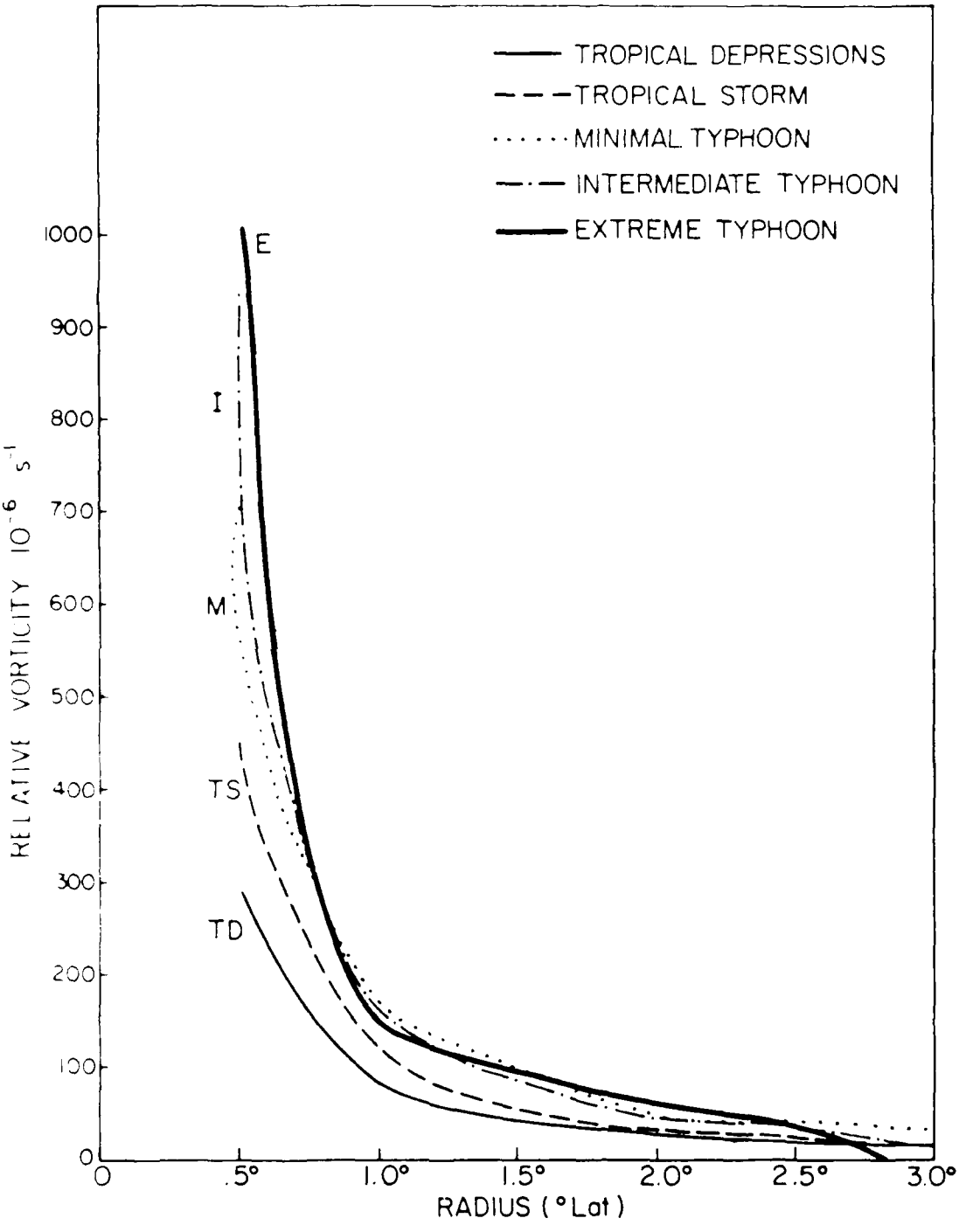

Figure 3.7: Azimuthally-averaged relative vorticity fields for the five classes of tropical cyclone at 700 mb.

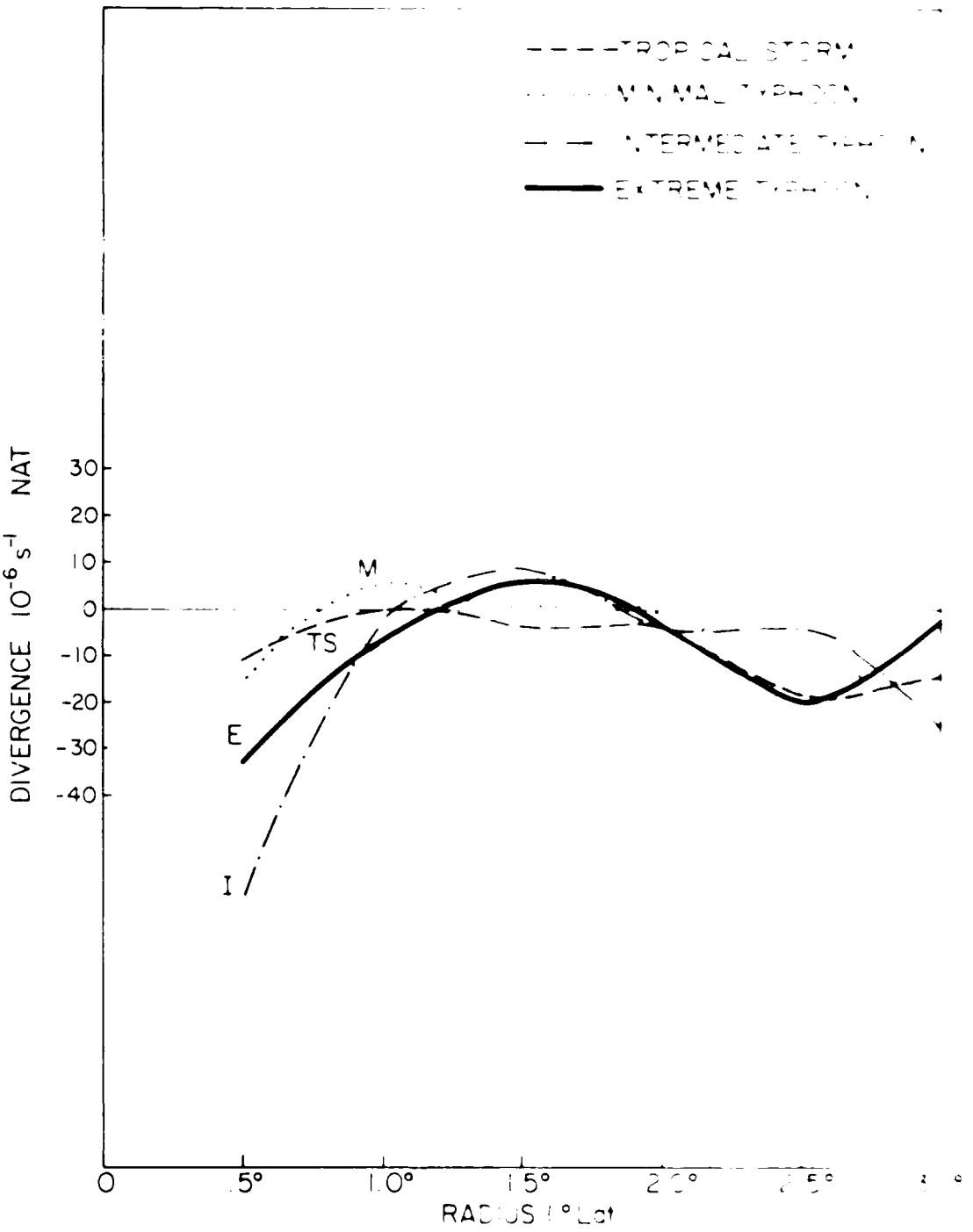

Figure 3.8: Azimuthally-averaged divergence fields for different tropical cyclone intensity classes at 700 mb.

The two soundings of Fig. 2 show significantly rising 700 mb moisture for increasing intensity. This is generally a reflection of the higher θ_e content and greater convection in the more intense cyclones. Although the pressure falls throughout the inner 3° of the [illegible] intensities generally only 1-2°C to the moisture increase. Relative humidity (not shown) also increases as well with intensity implying a greater surface flux of moisture to the T.C. circulation by means of more vigorous convection.

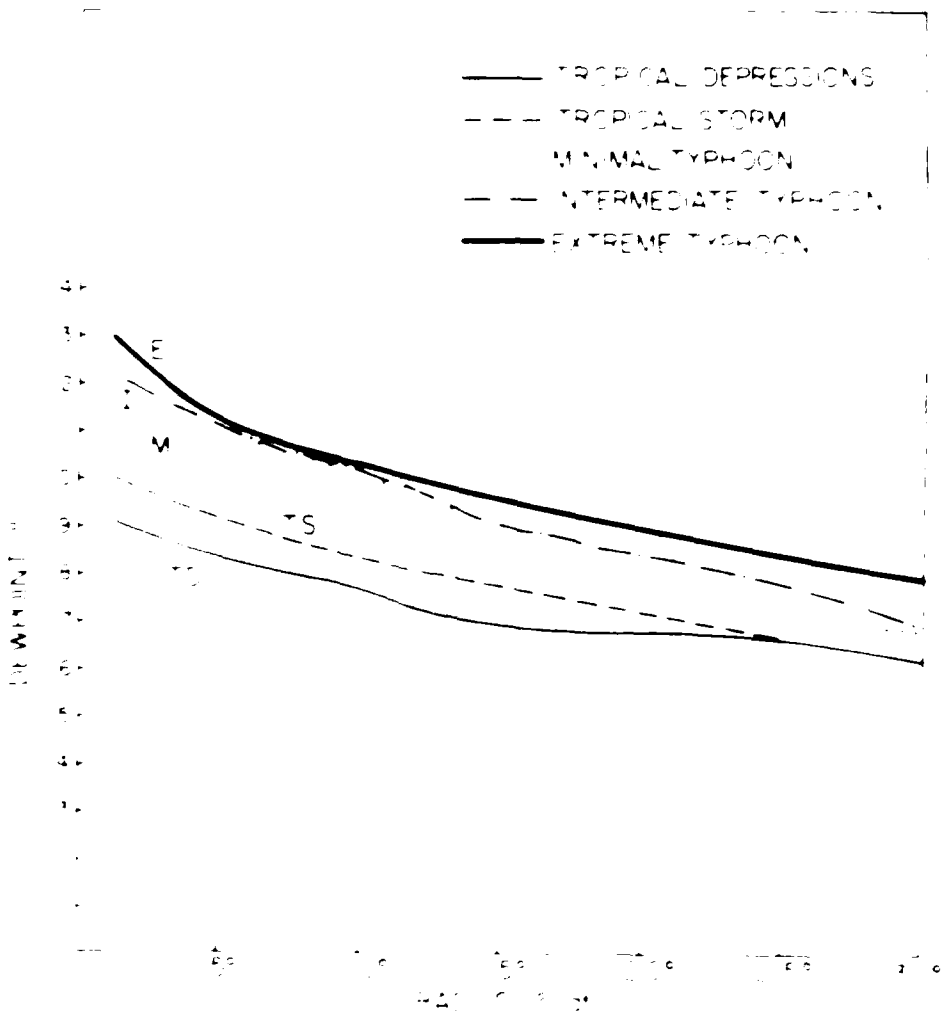

average latitude of each center for the simplified gradient form of the radial equation of motion:

$$< v^2 > /r + < v >< f >= g\delta < z > /\delta r \tag{3.2}$$

All individual tangential wind measurements were squared before averaging. Figure 3.10 shows the ratio of wind ($V_T^2/R + fV_T$) to pressure gradient g (dh/dr). Pressure accelerations were observed to be significantly greater than the wind accelerations. The extreme typhoon exhibited only about half the wind acceleration at 0.5° radius than the pressure gradient would dictate. Evidently cumulus convective momentum transports contribute significant terms to the symmetric radial equation of motion:

$$\delta u/\delta t + u\delta u/\delta r + w\delta u/\delta z - v^2/r - fv = -g\delta h/\delta r \tag{3.3}$$

We can see the likely effect of cumulus momentum transfer more readily when each wind is divided into its time averaged mean ($< v >$) and deviation from the mean (v'). The instantaneous tangential wind speed is then:

$$v =< v > +v' \tag{3.4}$$

With the aid of the continuity equation, the radial equation of motion becomes:

$$\delta u\ \delta t + < u > \delta < u > /\delta r + < w > \delta < u > /\delta z - < v >^2 /r - f < v >= -g\delta < h > /\delta r$$

$$A \qquad B \qquad C \qquad D \qquad E \qquad F \tag{3.5}$$

$$< v'v' > \ r - 1\ \rho\delta\ \delta r(< \rho u'u' > - 1\ \rho\delta/\delta z(< \rho u'w' >)$$

$$G \qquad H \qquad I$$

Let's look at the relative importance of each term to locate which one is of the same order of magnitude as terms D or F which dominate near the center of an extreme typhoon (generally $10^{-3} ms^2$). Averaging all extreme typhoons, some of which are intensifying others filling, would cancel out term A, thus a steady state assumption is valid here. Term B is at most 10^{-5} with u = -1 ms^{-1} on average at 700 mb and thus negligible

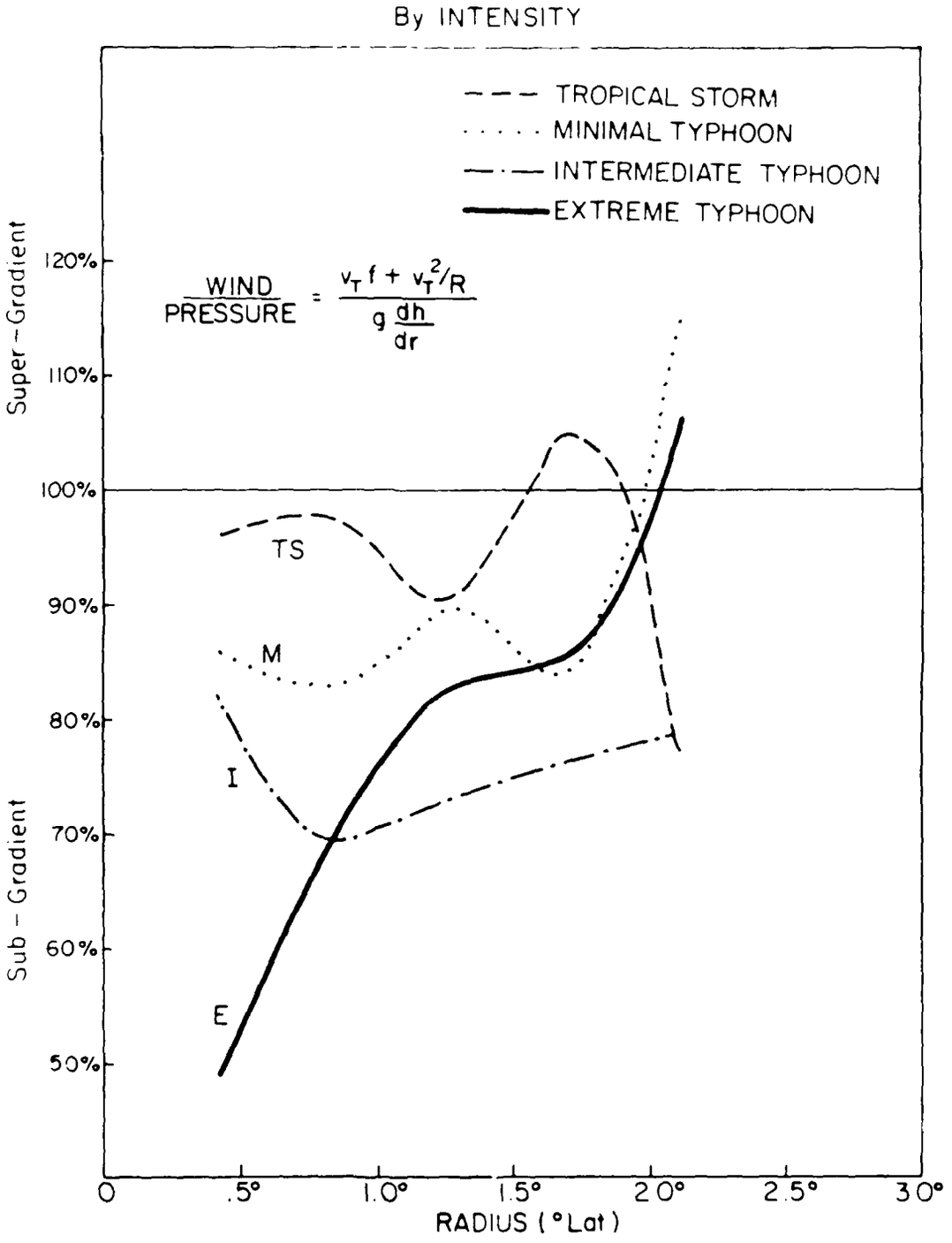

Figure 3.10: Azimuthally-averaged ratio of 700 mb wind to pressure gradient fields (Coriolis + centrifugal forces/pressure gradient) for different tropical cyclone intensity classes.

Term C is also negligible on average (10^{-5} at most). Terms D and G combine to closely approximate $< v^2 > , r$ which was calculated in Fig. 3.10.

An example would clarify the v^2/r term better. What was calculated was $< v^2 > /r$ but:

$$< v^2 > /r \textit{ is greater than } < v >^2 /r + < v'v' > /r \tag{3.6}$$

Although the calculated centrifugal term slightly exceeds the mean plus eddy terms it doesn't exceed it by much. For instance, let:

$$v_1 = 5, v_2 = 3 \text{ and } r = 1$$

$$\text{then, } < v >= 4, v_1' = 1 \text{ and } v_2' = -1$$

$$< v^2 > /r = (25 + 9)/2/1 = 18$$

$$\text{but } < v >^2 /r = 4^2/1 = 16$$

$$\text{plus } < v'v' > /r = 1/1 = 1$$

$$\text{and } < v >^2 /r + < v'v' > /r = 17$$

Thus, our calculated centrifugal term slightly overestimates the mean plus eddy terms combined making the sub-gradient result even more valid.

In other words, breaking the centrifugal term into mean and eddy terms does not account for the sub-gradient result shown in Fig. 3.10. Therefore, let's look at the contributions from the cumulus transport terms.

Term H can, in a region of vigorous convection, provide a significant contribution to the radial equation of motion. As was observed in the extreme Hurricane Allen in 1980 (and documented by Jorgenson, 1984b) u reached values of -25 ms^{-1} beneath the eyewall convection in the boundary layer. If these values are brought up to the 700 mb level where u is generally 1 ms^{-1}, then term H can easily reach values of $10^{-3} ms^{-2}$ competing with the pressure gradient term. Thus, in a region of intense convection, as is typical of extreme typhoons, cumulus transport of strong boundary layer inflow can provide the outward force necessary to balance the observed sub-gradient fields. Recall that in term

H: $-1/\rho\delta/\delta r(< \rho u'u' >)$ although u' is negative, it is squared thus providing a positive value. The radial gradient outside the eyewall is negative as one moves away from the region of dense convection. The result is a positive term and as such provides an outward force on air parcels which when added to the Coriolis and centrifugal terms likely balances the pressure gradient as such:

$$g\delta h/\delta r = < v >^2 /r + < v'v' > /r - 1/\rho\delta/\delta r(< \rho u'u' >) \qquad (3.7)$$

Thus, Fig. 3.10 implies that the more intense the typhoon the more vigorous the convection which acts to provide a stronger outward force on air parcels. This is a form of cumulus friction acting at the 700 mb level and likely above it as well. Lee (1984) discussed the effect of cumulus-driven momentum transports from the tangential equation of motion. What is shown here is a similar effect on the radial equation of motion which appears to drive the gradient equation more and more sub-gradient, the more intense the cyclone.

Term I was considered to play a negligible role in the equation of motion. Although $u'w'$ is generally negative in value (updrafts generally bring up the associated inflow from the boundary layer while downdrafts are associated with outflow), the vertical gradient of the product is small. Above the level of free convection, w' would increase with height while u' would decrease with height, thus cancelling out.

3.4 700 mb Flow as Related to Differing Cyclone Intensity

We next investigate the asymmetric winds associated with cyclones of different intensity classes. Plan views of the radial winds in the earth-relative (or NAT) coordinate system are shown in Figs. 3.11, diagrams a through e. It appears that the tropical cyclone moves through the 700 mb environment at a relatively slower speed as the intensity of the cyclone becomes greater. (Recall that the absolute speed changes little with intensity.) The most intense cyclones move at about the same velocity as the 0-2.5° radius current. This implies that the more intense the typhoon, the more nearly it moves with the 700 mb steering flow. Presumably, this has to do with the character of the steering current

which lies above the 700 mb level, for which core data is not available. Although the vertical wind structure is unknown, this implies that the relative movement is less for intense cyclones because they are in an environment with less vertical shear. This same information can be portrayed in the MOTROT system as in Fig. 3.12 showing that the more intense the tropical cyclone, the more the resultant environmental flowthrough is only from left to right. It seems the more intense the cyclone, the better the 700 mb level was in approximating the forward or parallel component (Fig. 3.13) but the less it resolves the environment-cyclone 700 mb left to right or perpendicular component as shown in Fig. 3.14. The extreme typhoon reflects only a 700 mb leftward drift.

Also notable from these MOTROT radial wind plan views is the inner-core convergence seen in the typhoon but not evident in the tropical storm or depression. For the weaker systems the flowthrough did not appear to be absorbed into the inner core as much as in the more intense systems. Evidently the stronger the cyclone intensity, the more the vortex converges in its near environment inward.

The total asymmetric wind field in the MOTROT-VORT coordinates is shown in Figs. 3.15a-e. The tropical depression, tropical storm and minimal typhoon show that this flowthrough added a tangential speed component to the lower-left quadrant and took away a tangential component on the front-right of the cyclone. Since the contribution to the steering current near the surface is very likely even less than at 700 mb, this tangential asymmetry is probably more pronounced near the surface. Thus, surface winds likely have a natural maximum on the lower-left quadrant of greater magnitude than shows here for the 700 mb level, when the cyclone's motion has been removed. However, the more intense the cyclone the less noticeable this asymmetry pattern. Note how nearly symmetric the intermediate and extreme typhoon classes are. It appears that the cyclone is more resistant to 0-2.5° parallel wind flowthrough the more intense it becomes. This is also evidenced in the residual wind fields of Fig. 3.16a-e. Note how this flowthrough is oriented from front to back in the depression but from left to right in the more intense typhoons.

Another important feature relates to intensity differences. The environment is drawn into the cyclone's inner regions and becomes more symmetric as the intensity increases.

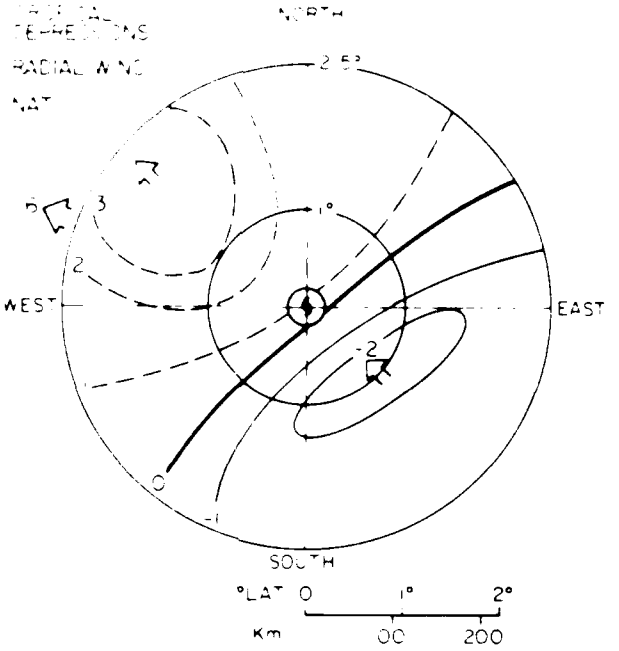

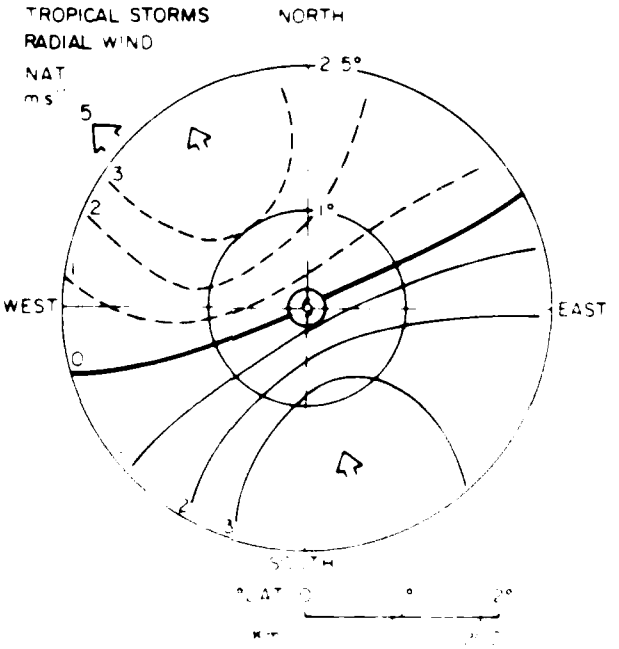

Figure 3.11 a-e Plan-view depictions of the radial wind field in NAT for a) tropical depressions, b) tropical storms, c) minimal typhoons, d) intermediate typhoons, and e) extreme typhoons. Mean motion and speed (ms^{-1}) shown by arrow on the rim.

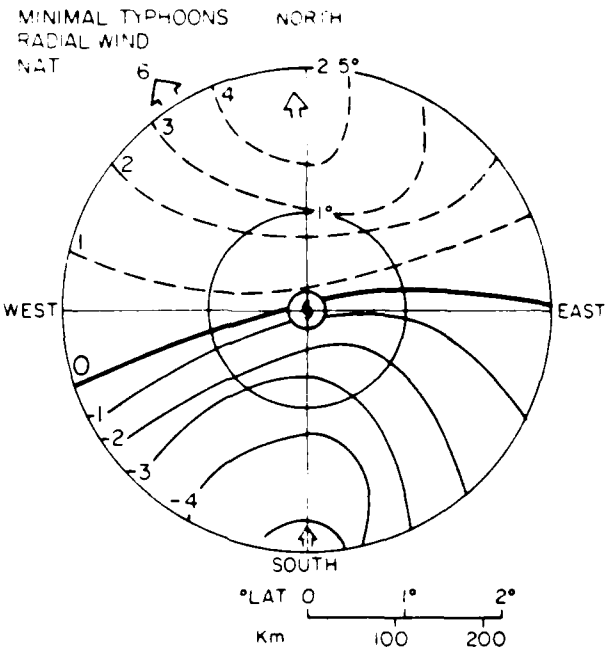

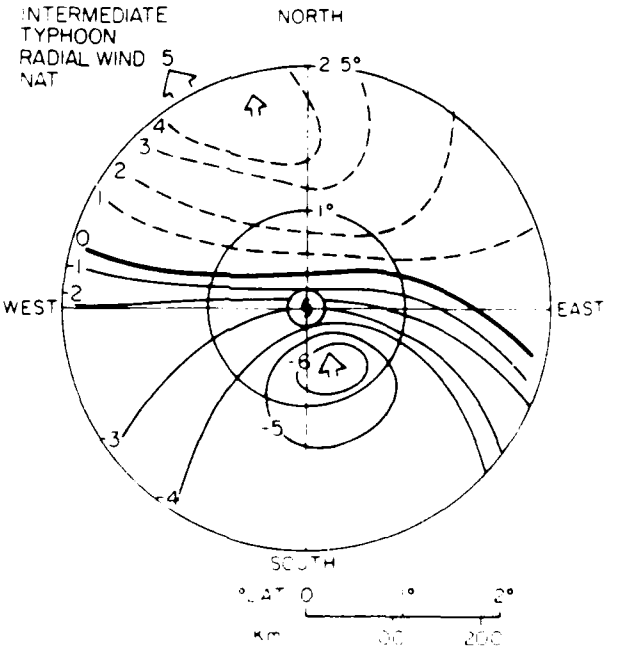

Figure 3.11: a-e. Continued.

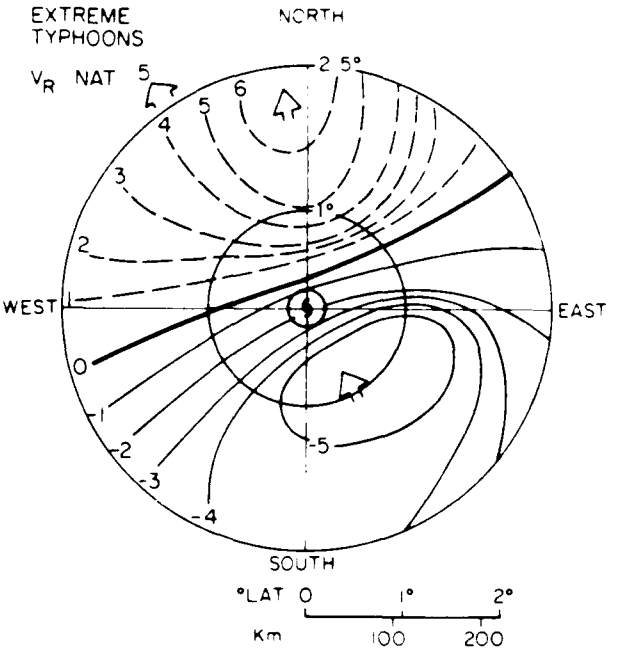

Figure 3.11: a-e. Continued.

This is presumably due to the more vigorous convection characteristic of the more intense cyclones. Notice how the 700 mb environment seemed to be flowing through the region of the depression seemingly unaware that a cyclone exists. This is in sharp contrast to the intermediate typhoon which is drawing 700 mb air into the inner core from all quadrants. Once again it is easy to see that the predominant 700 mb flowthrough decreased with increasing intensity. It is important to understand that we are discussing the structure of the basic 700 mb wind patterns as related to cyclone intensity class and are not directly treating the question of the intensity change process here. This will be discussed in Chapter 5.

3.5 Outer Core Wind Strength (OCS)

Often, a tropical forecaster will not have information on the center of an approaching tropical cyclone but will obtain bits and pieces of data in outer regions. Particularly when the cyclone is bearing down on land, it is the outer core which causes the initial damage to structures and disrupts the normal societal activities. The strongest OCS observed in

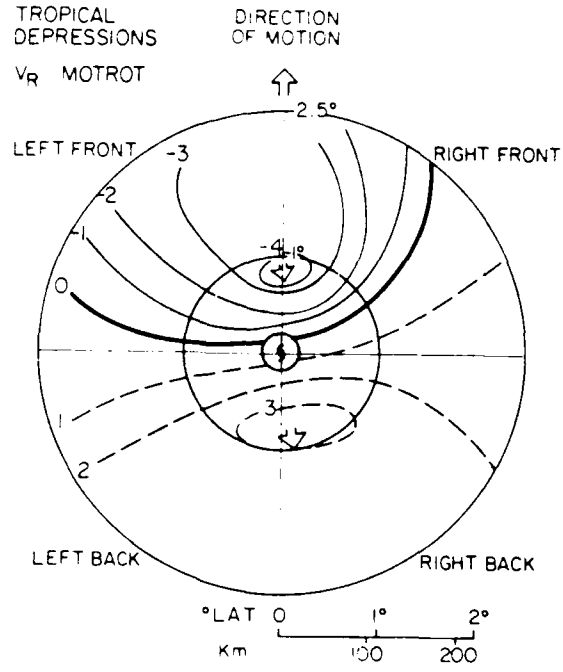

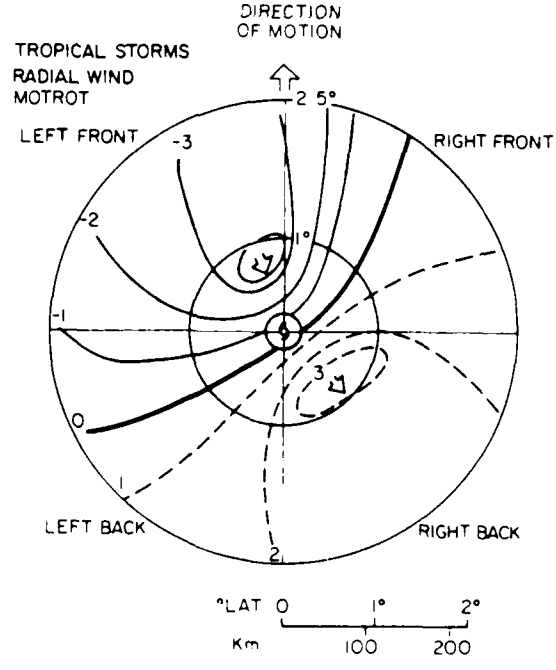

Figure 3.12: a-e. Plan-view depictions of the radial wind field (ms^{-1}) in MOTROT for a) tropical depressions, b) tropical storms, c) minimal typhoons, d) intermediate typhoons, and e) extreme typhoons.

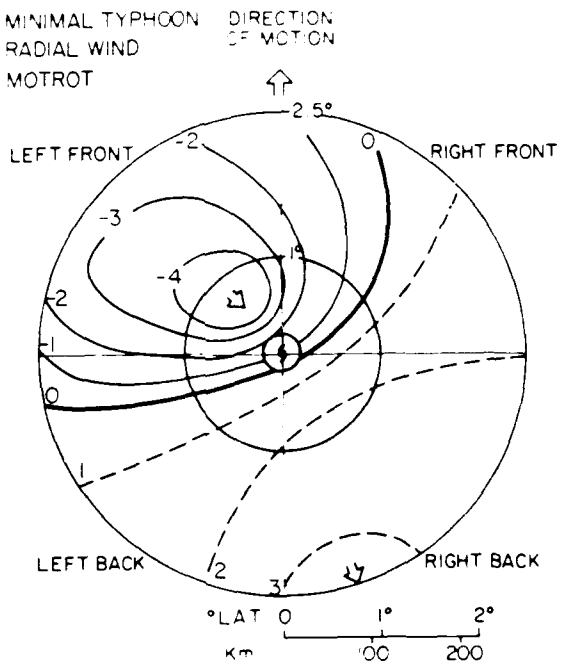

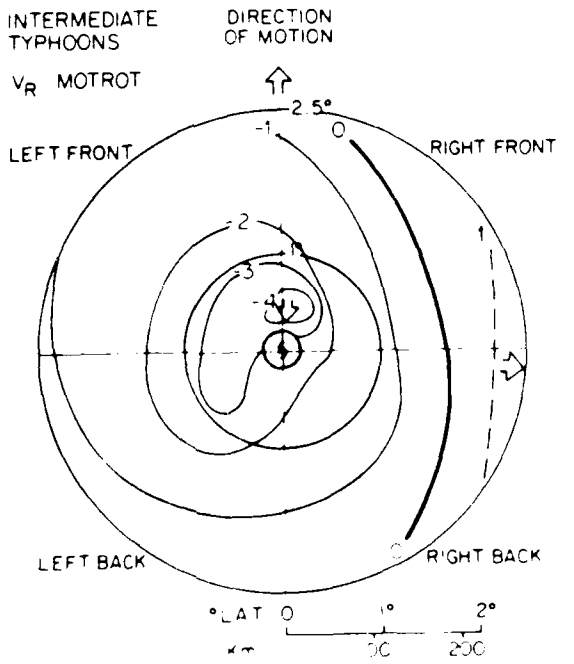

Figure 3.12: a-e. Continued.

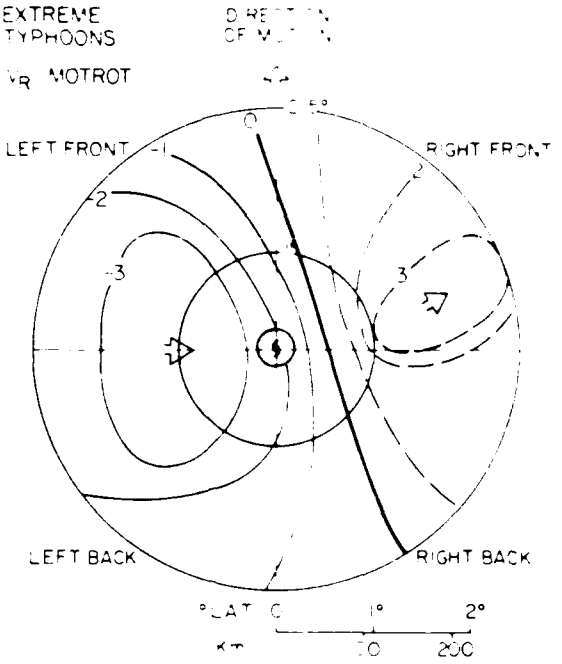

Figure 3.12: a-e. Continued.

the five-year period of 1980-84 was 37 ms^{-1}, for Supertyphoon Forrest of 1983, surpassing typhoon force winds throughout the 0- 2.5° region. Weak, medium, and strong outer core winds are thus stratified irrespective of the intensity of the inner core in order to focus on this outer core alone. As was discussed in a previous paper (Weatherford and Gray, 1987b) MSLP and OCS are not necessarily related. OCS classes are defined as follows:

WEAK OUTER CORE WIND 0 TO 13 ms^{-1} 407 MISSIONS

MEDIUM OUTER CORE WIND 13 TO 23 ms^{-1} 260 MISSIONS

STRONG OUTER CORE WIND OVER 23 ms^{-1} 135 MISSIONS

Table 3.2 depicts the averages of position, motion, MSLP, OCS, and maximum wind speed for each OCS wind class. Notice that, in general, the average wind strength of the outer core is half of the maximum wind speed. However, this must be treated carefully, for as was shown in Weatherford and Gray (1987b), there was much variability in the ratio of inner to outer core wind speeds. All OCS classes moved at the same average speed

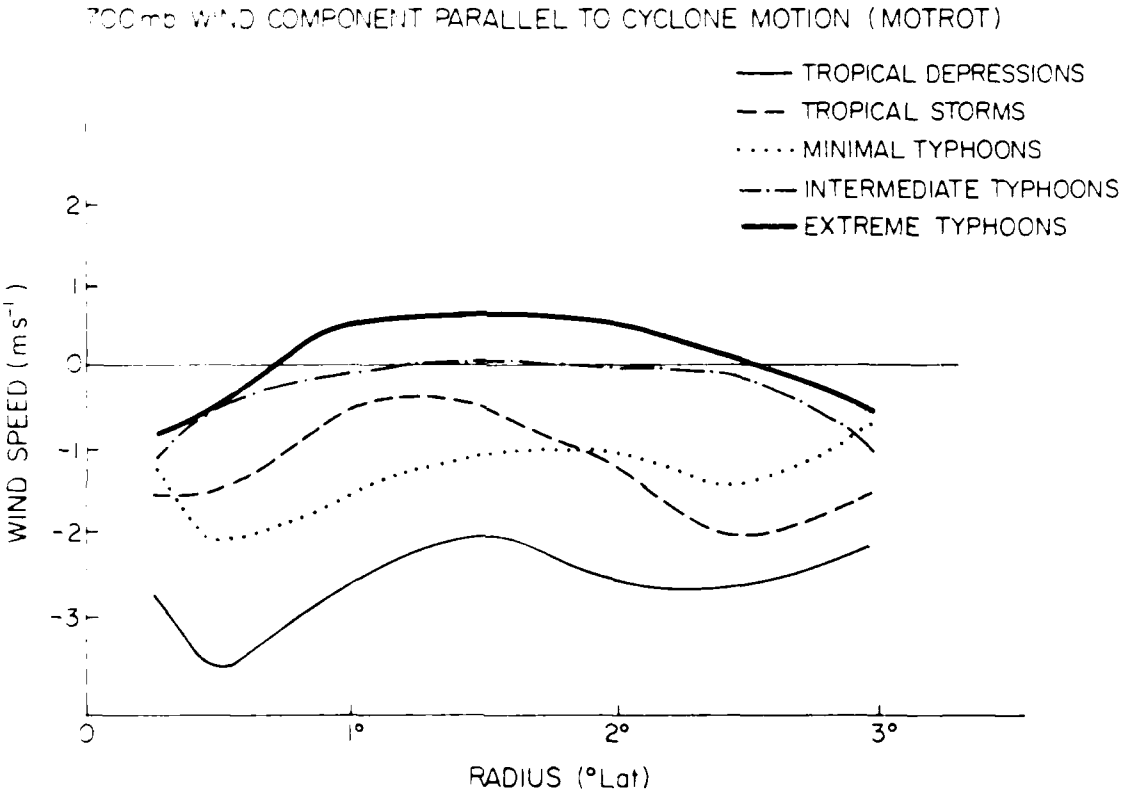

Figure 3.13: Azimuthally-averaged component of the 700 mb wind current which is parallel to the cyclone's direction of motion for: tropical depressions, tropical storms, minimal typhoons, intermediate typhoons, and extreme typhoons. Negative values (ms^{-1}) imply the cyclone is moving faster than the 700 mb stream.

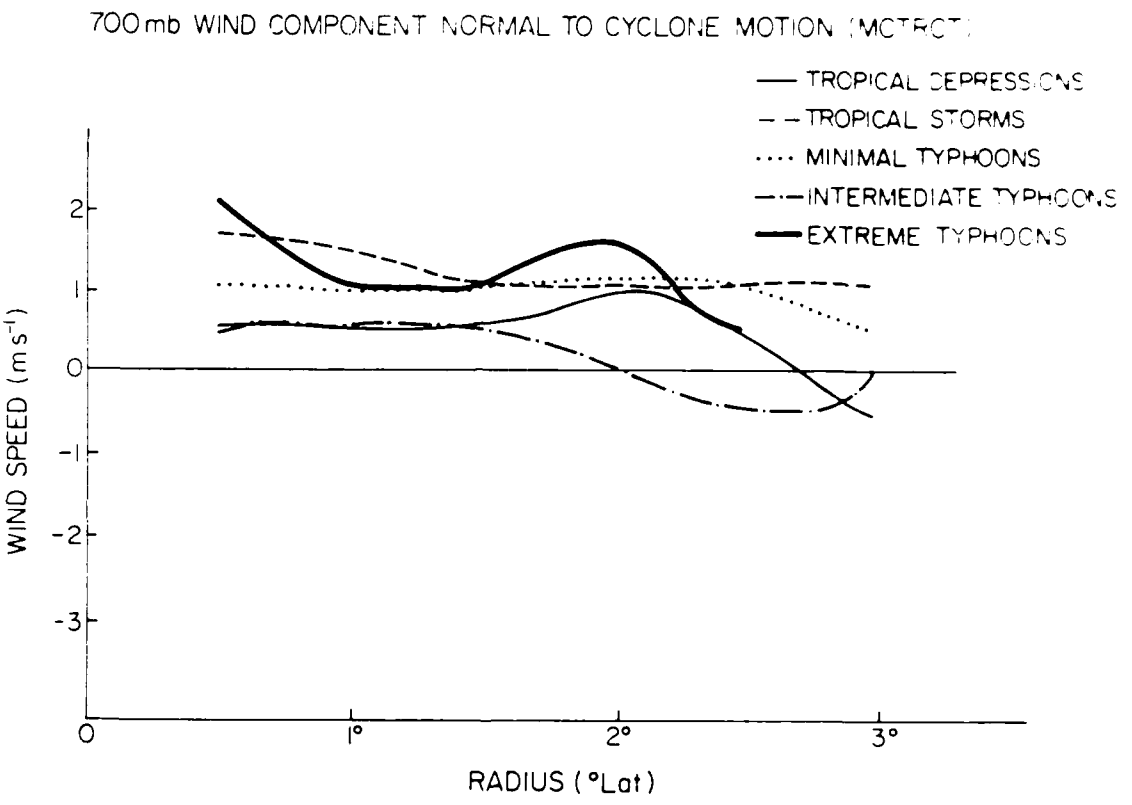

Figure 3.14: Azimuthally-averaged component of the 700 mb wind current which is normal to the cyclone's direction of motion for: tropical depressions, tropical storms, minimal typhoons, intermediate typhoons, and extreme typhoons. Positive values (ms^{-1}) imply the cyclone is moving left of the 700 mb stream.

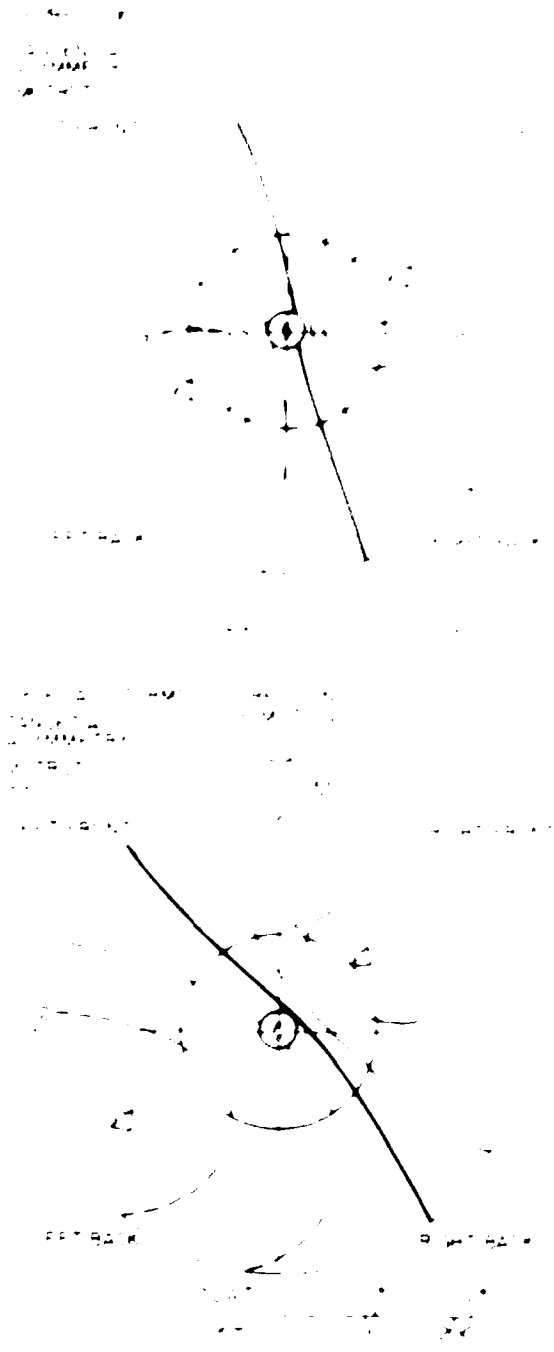

Figure 3.15: a-e. Plan-view depiction of the tangential asymmetries of the tangential wind field at 700 mb for a) tropical depressions, b) tropical storms, c) minimal typhoons, d) intermediate typhoons, and e) extreme typhoons in MOTROT-VORT (both the mean motion and cyclone vortex have been removed). Solid curves denote values lower than the mean while dashed curves, higher. Values in ms^{-1}

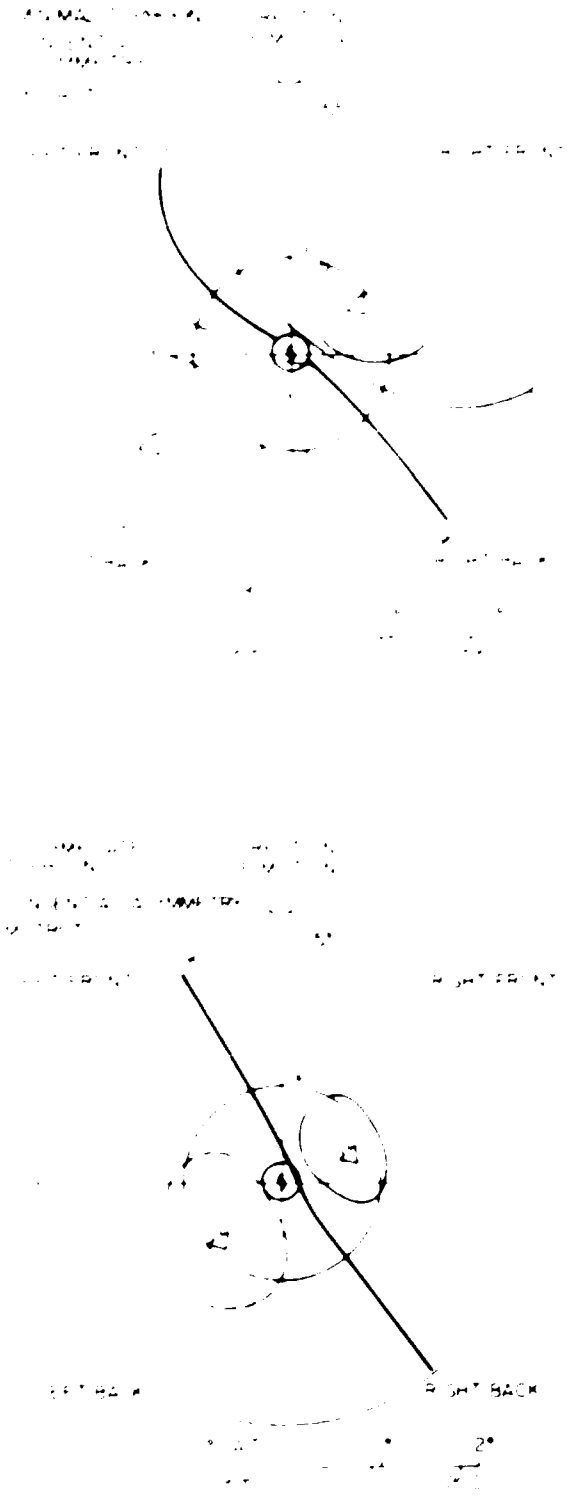

Figure 3.15 a-e Continued

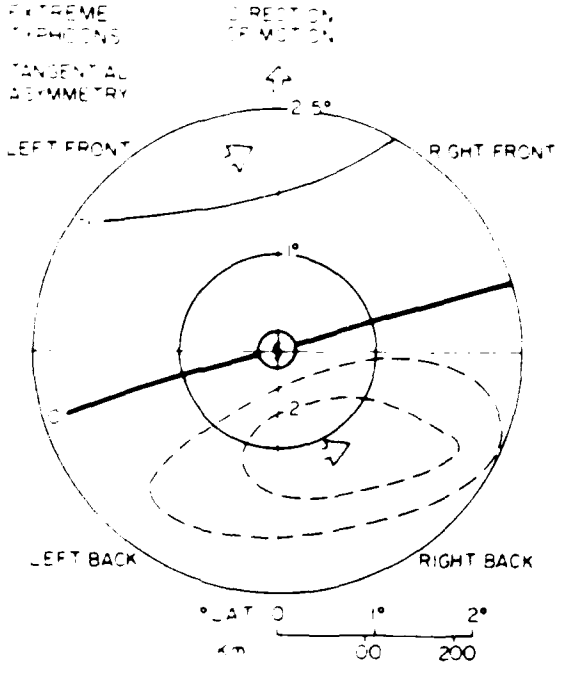

Figure 3.15: a-e. Continued.

Table 3.2 Average values of position, motion, intensity, and OCS for each OCS class.

OCS CLASS	LAT.	LONG.	HEADING	SPEED (ms^{-1})	MSLP (mb)	MAX WIND (ms^{-1})	OCS (ms^{-1})
WEAK	17°	137°	310°	5	980	20	10
MEDIUM	18°	136°	315°	5	964	35	18
STRONG	23°	134°	345°	5	941	45	27

Damage potential is closely related to the kinetic energy of the cyclone which, for a given mass, is merely the square of the wind speed. Therefore, although the average OCS of the strong cyclone is 2.7 times the average for the weak cyclone, the damage potential is 7.3 times greater in the strong system than for the weak OCS, on average, and up to 14 times greater for the strongest case in this data set.

The biggest difference between outer core strength values, aside from the OCS, is the moisture. Figure 3.17 shows that the dewpoint temperature of the strong OCS cases significantly exceeds the other cases. Figure 3.18 depicts the mixing ratio difference revealing 10% to 30% more moisture at the 700 mb level in the strong than in the weak

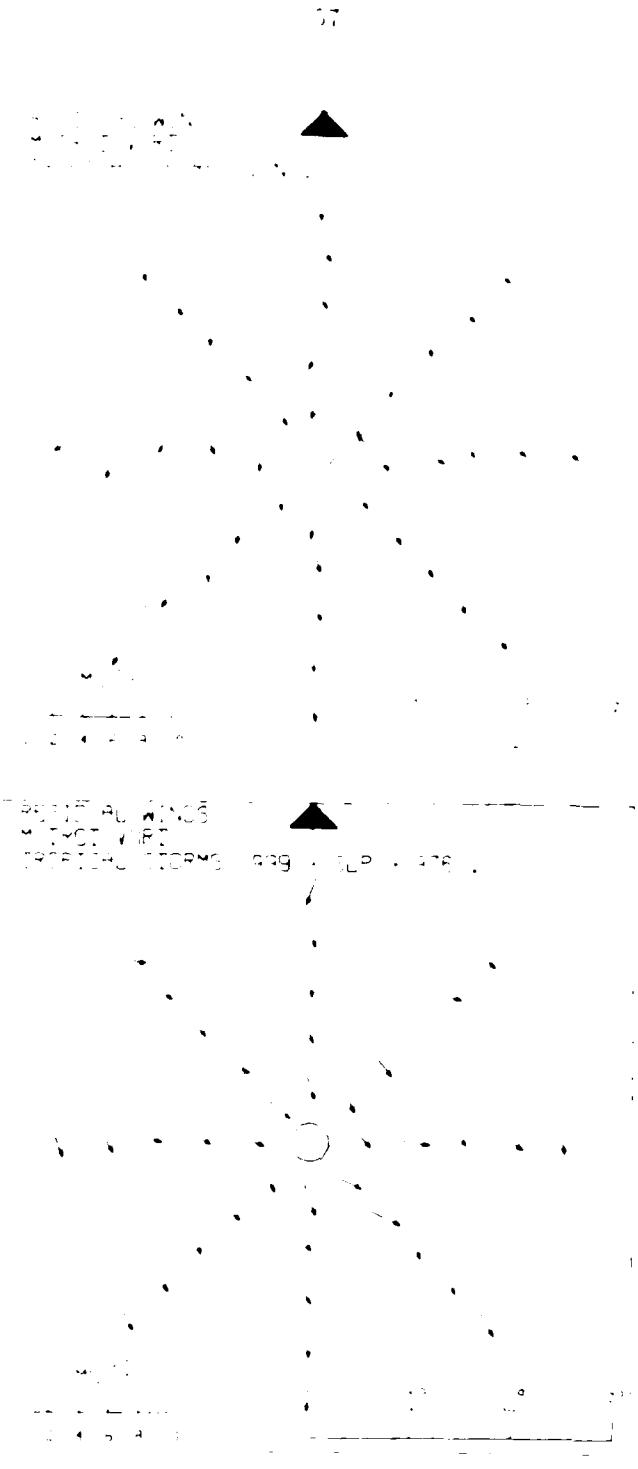

Figure 3.16: a-e. Plan-view depiction of the 700 mb residual wind field for a) Tropical Depressions, b) Tropical Storms, c) Minimal Typhoons, d) Intermediate Typhoons and e) Extreme Typhoons which incorporates both the radial and asymmetrical tangential wind vectors in MOTROT-VORT (both motion and the mean vortex have been removed). The bold arrow marks the cyclone's heading of motion. Vector lengths imply speed as shown in the lower left.

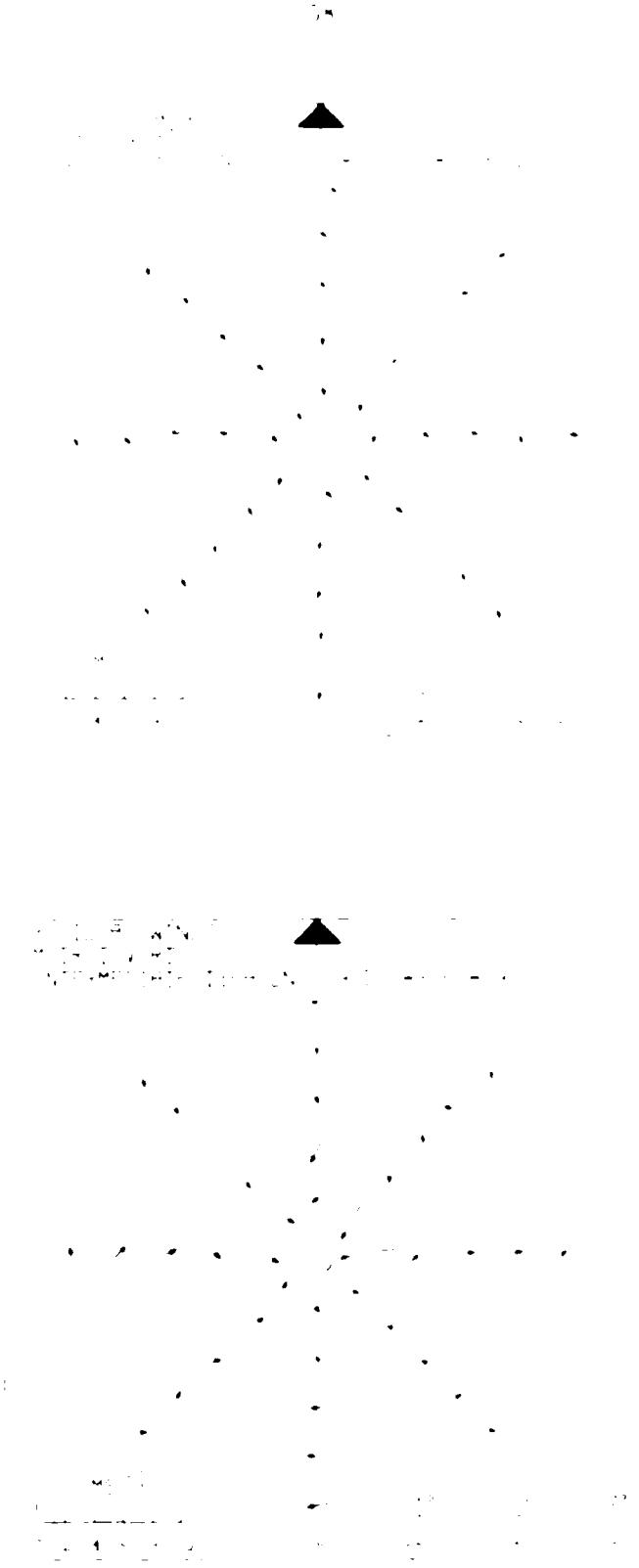

Figure 3.16: a-e. Continued.

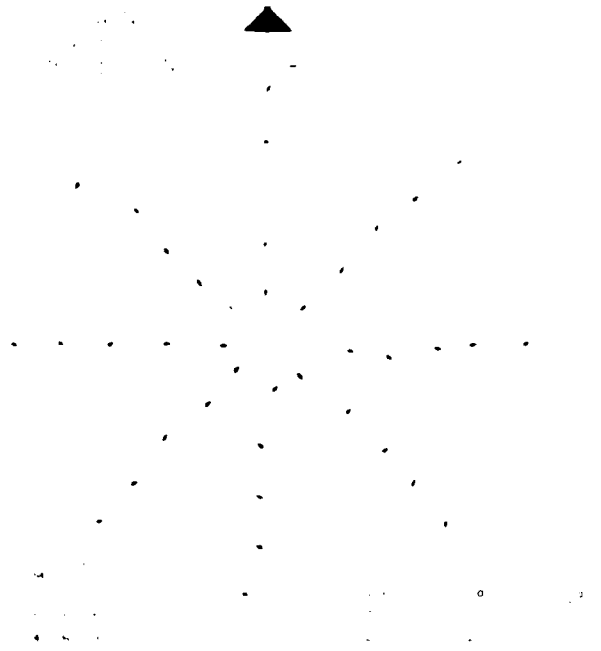

Figure 3.16: a-e. Continued.

OCS systems. (Relative humidity increases generally 10% throughout this region as well for the stronger outer core wind cyclones.) Larger differences occur as one moves closer to the cyclone center. Two possibilities can raise the mixing ratio at the 700 mb level. One, the higher the OCS the lower the height field through the 1° to 2.5° region will for the same SST values can account for the higher mixing ratio. This effect accounts for roughly only 10% of the mixing ratio increase and is therefore considered to be minor. Secondly and more importantly, the higher boundary layer winds induce more vigorous acquisition of surface energy and moisture which can be brought up through the 700 mb level within the convective cells. Such an increase of moisture at 700 mb cannot be due to horizontal advection from outside the vortex because the environment simply does not have these high values of moisture. This additional moisture increase out to 3° radius with the cyclones of greater outer core circulation is likely due to increased convection in the stronger outer core areas. This implies heavier rainfall and more cumulus cloudiness. Thus a land- falling cyclone with a strong OCS could potentially cause greater flood problems regardless of its MSLP or its maximum inner core winds.

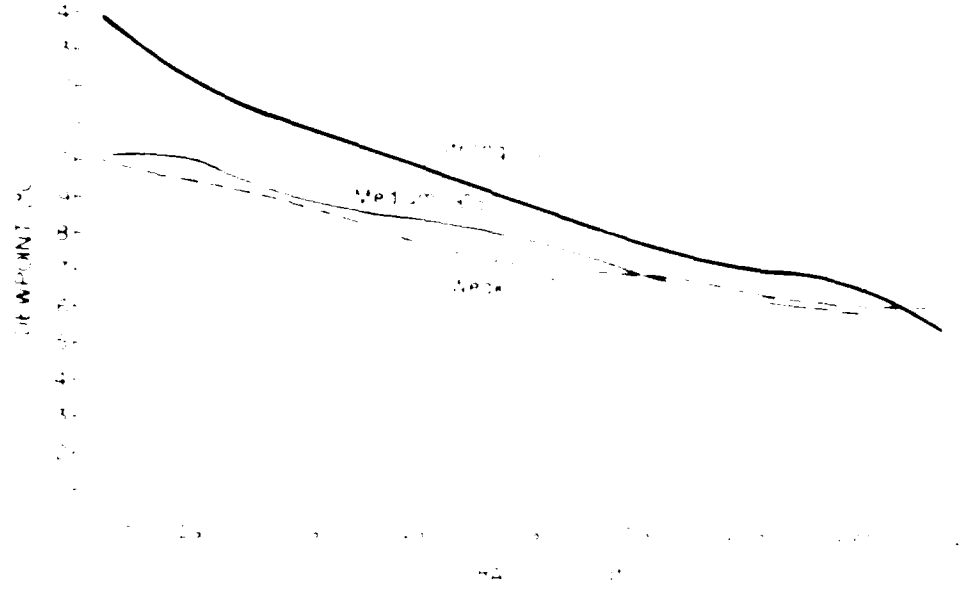

Figure 3.17 Azimuthally-averaged dew-point temperature fields for the three classes of OCS at the 700 mb level

Looking at the plan views, the 700 mb environment appeared to flow slightly faster the stronger the OCS in earth-relative coordinates but with very little converging into the inner core (see Figs. 3.19a-c). An interesting phenomenon is the greater the OCS, the greater the leftward drift exerted on the vortex. Inspection of Figs. 3.19a-c shows that the environment flowed towards 330° for weak OCS systems, 340° for medium systems, and 23° for the strong OCS systems. When the cyclones' average headings and motion were subtracted from this, the resulting leftward drift angles were 20° for weak, 25° for medium, and 38° for strong OCS systems. This supports the theory that the beta-effect causes a more pronounced drift with systems encompassing a larger area (De Maria, 1985). Apparently the stronger winds advect more earth-vorticity via the vorticity equation term

$$v \partial f / \partial y \qquad (3.8)$$

The radial wind field seen in cyclone-relative coordinates in Figs. 3.20a-c reveal inflowing and converging environmental air in the medium and strong OCS cyclones but not in

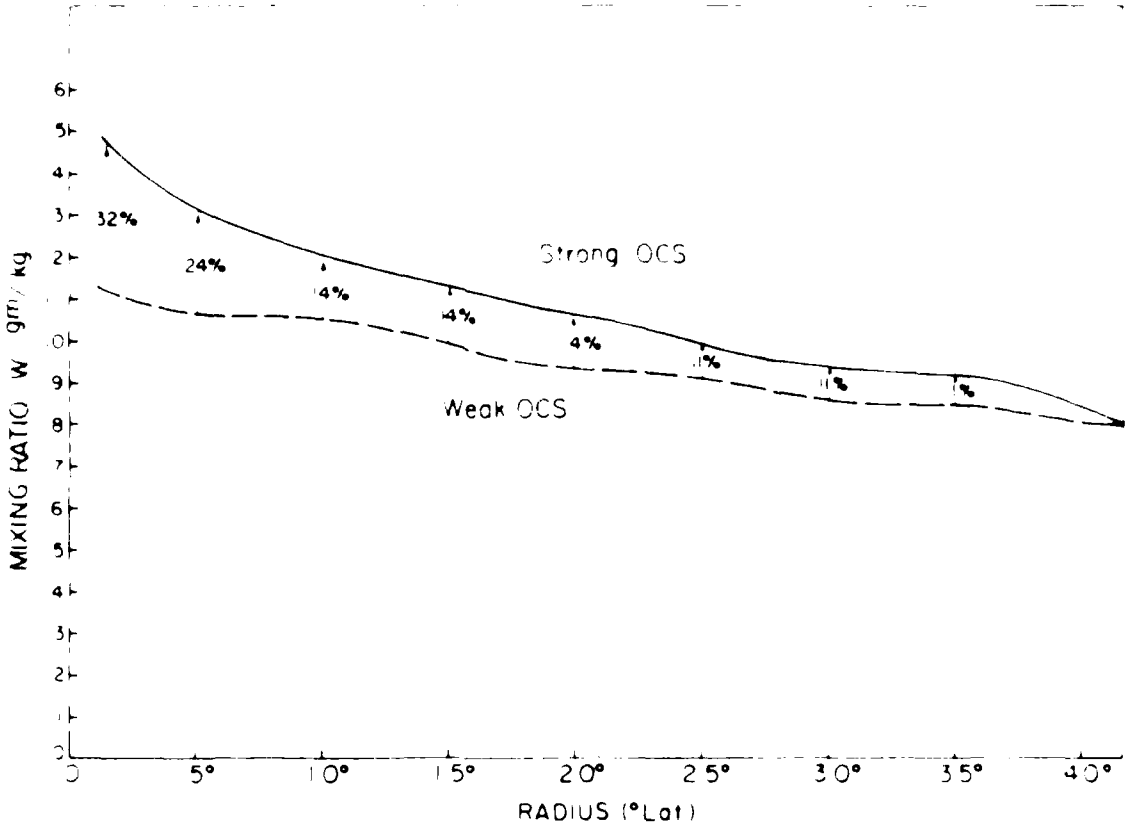

Figure 3.18: Azimuthally-averaged mixing ratio fields for the three classes of OCS at the 700 mb level.

the weak case. Notice there are higher values of inflow than outflow for the medium and strong OCS cases but equal values of inflow and outflow for weak cyclones. This implies that strong outer core systems advect environmental air in at 700 mb and up through the convection near the core to a higher level as proposed by Willoughby, et al. 1984, unlike that of weak systems. Cyclones with weak OCS' were generally weaker in intensity as well (mostly tropical storms which do not show significant inflow at 700 mb).

When the symmetric tangential wind was removed (MOTROT-VORT) coordinates as in Figs. 3.21a-c, the flowthrough became less apparent the stronger the OCS. The stronger the OCS the more symmetric the tangential wind field and the more detached or shielded the inner-core circulation appears to become. This is evident in the residual flowthrough seen in Figs. 3.22a-c. The weaker the OCS, the stronger the wind field on the lower left of the cyclone and the weaker it is on the upper right. The medium outer core composite appears to accept more environmental air from the left-front than it allowed to pass through it to the opposite side. And finally, the strongest outer core composite allowed the least outer-core air from entering the inner core. This strong case provided the sturdiest shield against environmental effects.

Thus, it appears that the stronger the outer core, the more it is influenced by the beta-effect. Also, the higher the moisture content of the 700 mb air. One of the new and fundamental points to be noted is that the cyclone's basic steering current is quite evident in the inner core circulation. Evidently the concept an inner gyre unaffected by its environment is not quite accurate. The shielding effect appears gradually with strength of winds but not completely. Residual winds still appear although much lessened. The 700 mb steering current is flowing through the cyclone in all cases but this flowthrough is progressively less apparent the stronger the outer core. Once again, this does not address the changes which are occurring in the inner core nor the different environments in which these cyclones are embedded, only what the basic structure is like. The effects on a cyclone of differing environments is covered in the next chapter.

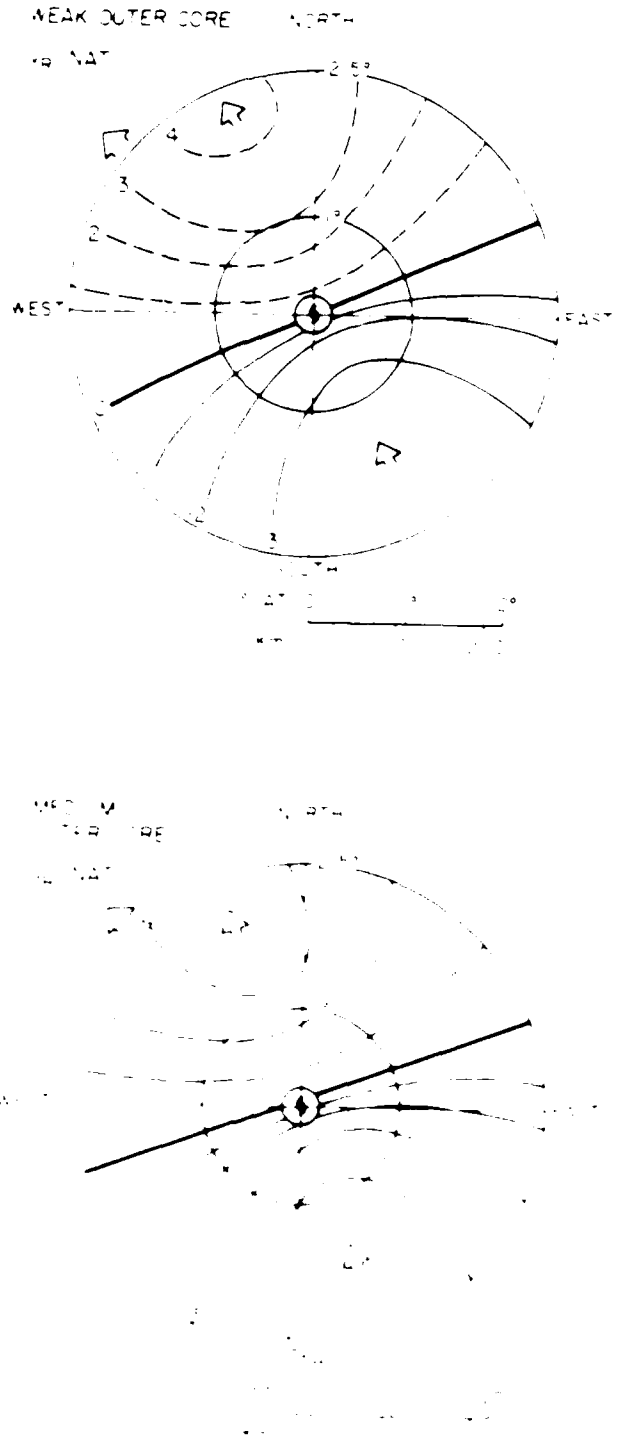

Figure 3.19 (a-c) Plan-view depictions of the radial wind in NAT for a) weak OCS, b) medium OCS, and c) strong OCS. Mean motion and speed (ms^{-1}) shown by arrow on the rim.

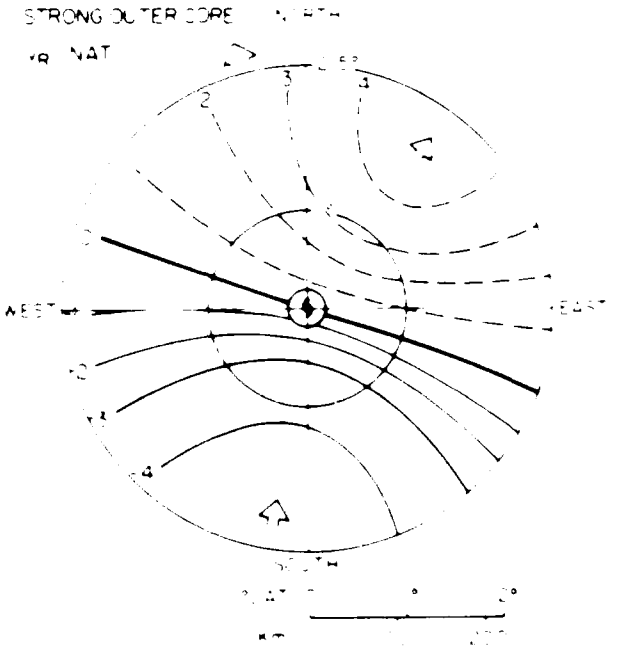

Figure 3 19 a-c Continued

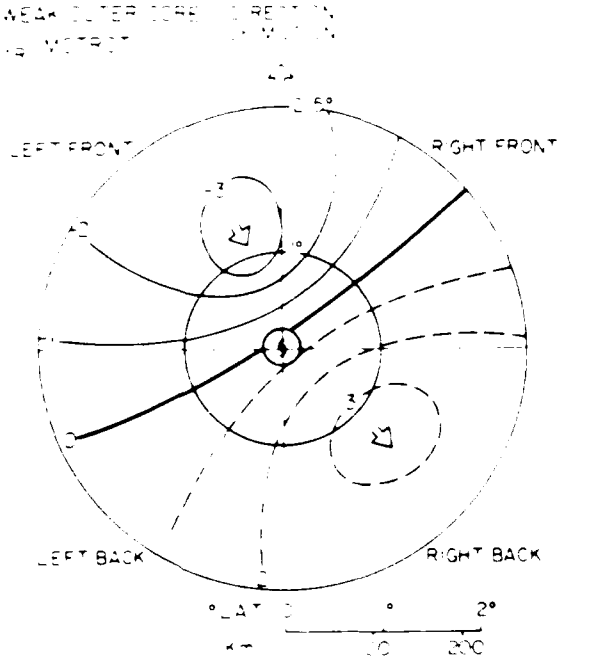

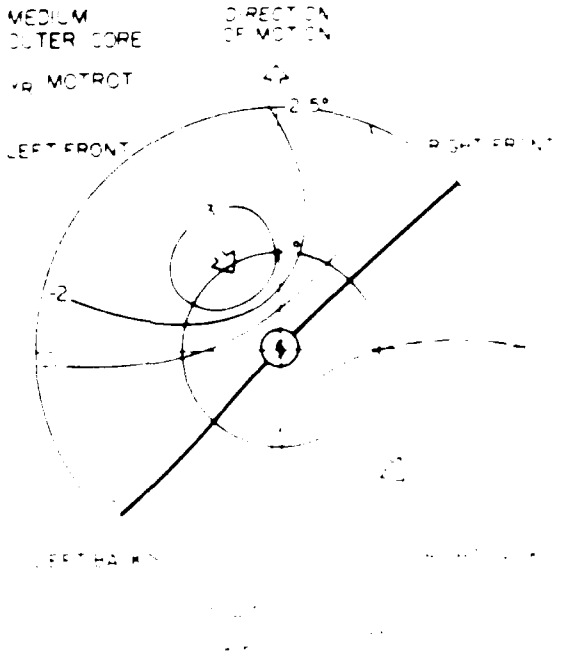

Figure 3.20 (a-c) Plan-view depictions of the radial wind in Model B for (a) weak OCS, b) medium OCS, and c) strong OCS. Values are in m/s.

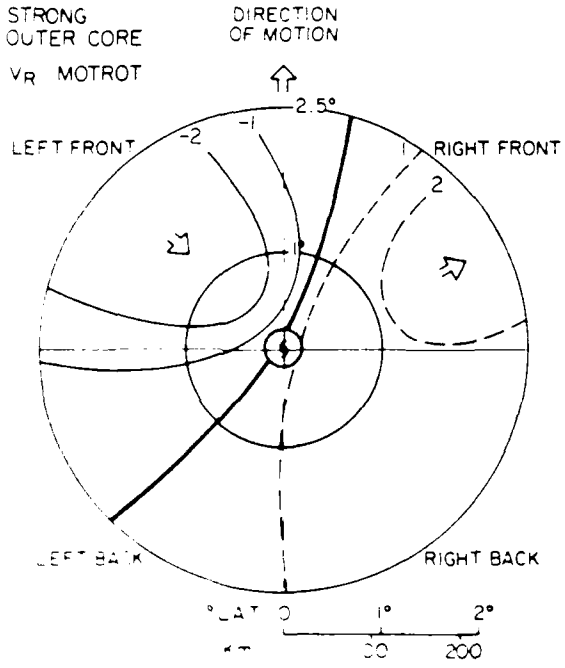

Figure 3.20: a-c. Continued.

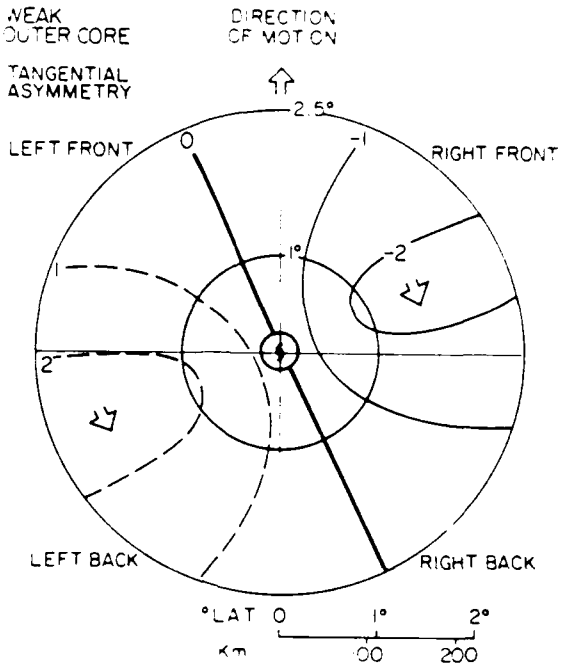
WEAK
OUTER CORE
TANGENTIAL
ASYMMETRY
DIRECTION
OF MOTION
2.5°
LEFT FRONT
0
-1
RIGHT FRONT
1°
1
-2
2
LEFT BACK
RIGHT BACK
°LAT 0
1°
2°
Km
00
200

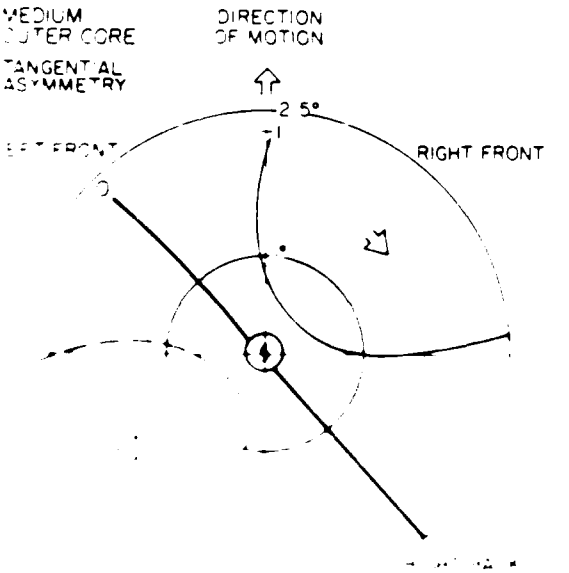
MEDIUM
OUTER CORE
TANGENTIAL
ASYMMETRY
DIRECTION
OF MOTION
2.5°
-1
RIGHT FRONT

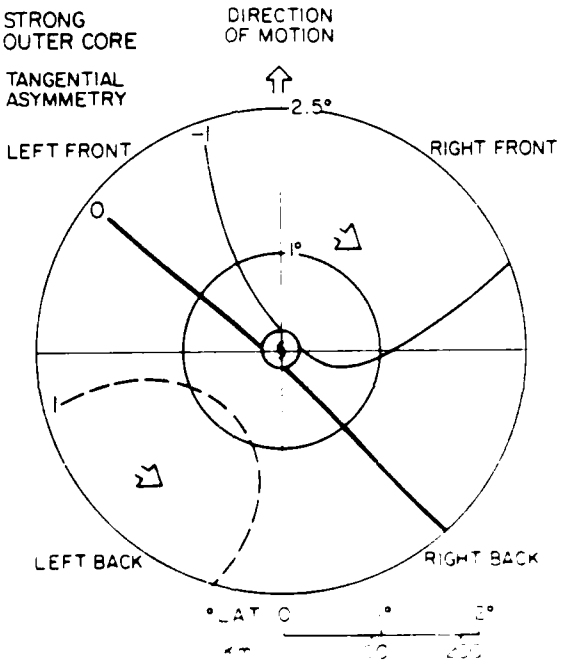

Figure 3 21 a-c Continued

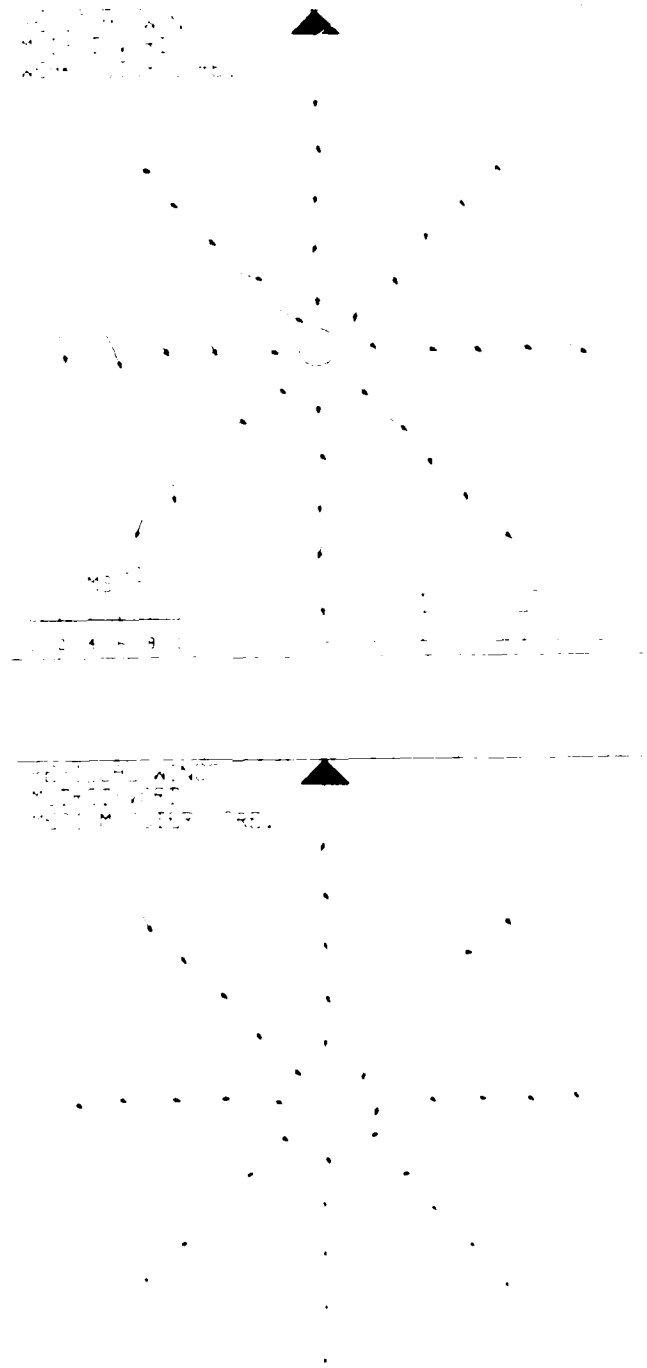

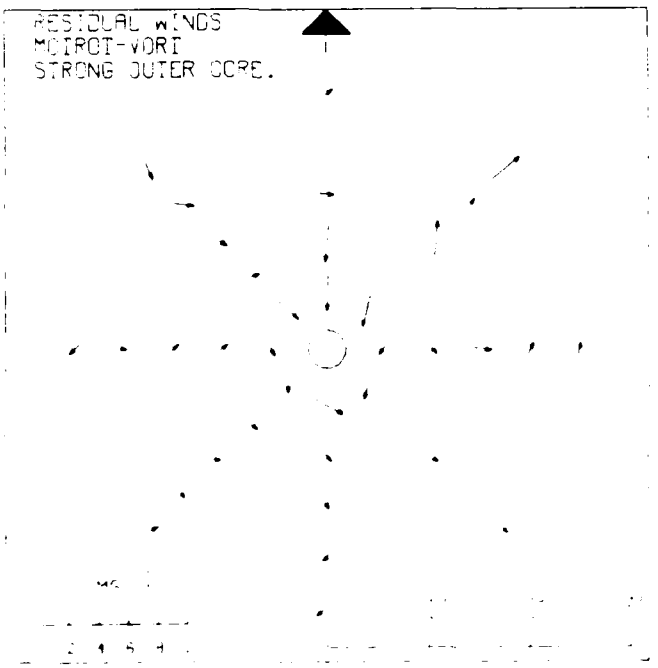

Figure 3.22. a-c. Continued.

Chapter 4

THE 700 MB INTERIOR STEERING CURRENT

Tropical cyclones are in large part moved by the environmental steering current in which they are embedded. While the large scale flow pattern is easily detected on a day-to-day basis, small scale meanders are not and pose some of the tropical cyclone forecasters' top questions: when is the cyclone going to recurve, when will it loop around a minor circle while remaining on the same general course, and is a change in course of 12 hours indicative of the changes it will make over the next few days? It is the portion of the steering current that comes close to the cyclone itself that is not detectable on the synoptic observational network because so much of these winds are due to the vortex. By removing the mean cyclone vortex, this interior background wind field can be examined to reveal the nature of the steering current. This residual wind field reflects both the 700 mb interior (.25 to 2.5° radius) steering current and its interaction with the central vortex. We analyze variations in this vortex subtracted wind field as a function of cyclone heading, speed, and latitude.

4.1 The Steering Current

An important question to address is the relationship of the tropical cyclone's motion to the interior 700 mb wind field. (This interior region will be shown from .25° to 2.5° radius. Recall from the data chapter that the region inside and including the average maximum wind zone (0 to .25° radius) is not depicted in the plan-view composites.) Although the deep layer 850 to 300 mb steering current is superior to the single level of 700 mb, 700 mb is known to adequately describe the deep-layer mean flow (George, 1975, and George and Gray, 1976). Chan and Gray (1982) found that at the 5-7° radius region the 700-500 mb [illegible] correlated with cyclone motion. Can this 700 mb interior region data

be used for cyclone steering or is this region shielded from the environment which moves it?

During the storm season, which is most active from July until November, the dominant flow pattern steers the cyclone around the middle-level subtropical ridge. Cyclones south of the ridge move westward as Fig. 4.1 shows for the typical zonal tropospheric flow. (These tropospheric mean winds were obtained from 21 years of rawinsonde observations composited out to 15° radius for the environment one year before a position of tropical cyclone genesis as described in Lee, 1986.) Note that easterly winds typically increase with height and that the mean 850-300 mb layer near zonal steering current is larger than the 700 mb component. The mean layer current thus steers the cyclone vortex faster than the 700 mb winds would indicate. Thus a moving vortex experiences flow from front to back across the tropical cyclone at the 700 mb level when south of the subtropical ridge. Cyclones north of the ridge typically have a significant eastward component as Fig. 4.2 shows.

Note again that an 850 to 300 mb mean zonal steering current is greater than the zonal wind at 700 mb. One should also expect cyclones north of the subtropical ridge would experience an environmental flow through at 700 mb from front to rear.

4.2 Tropical Cyclone Stratified by Latitude

The tropical cyclones of the northwestern Pacific generally exist in a latitude belt from 5° to 40° North latitude. Figure 4.3 shows the tracks of all the cyclones of this 1980-84 data set. Within this latitude belt, cyclones reside south, even and north of the ridge axis during their typical lifetime. As inferred by Fig. 4.4, the most intense tropical cyclones reached maximum intensities in the latitude belts from 15° to 25°, and typically fill north of 25°. We stratify cyclones in the various latitude belts of 5-15°, 15-25°, and north of 25° to provide a general separation of cyclone position into zones which are south, even with, and north of the middle-level ridge axis.

LOW-TROPICAL LATITUDES 5 15° NORTH 275 MISSIONS

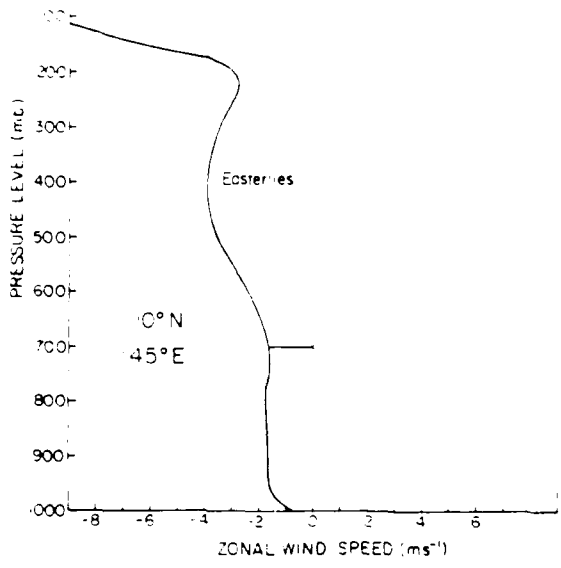

Figure 4.1: Mean zonal wind profile for the tropical troposphere located at 10° north, 145° east, derived from 21 years of rawinsonde composites. Values in ms^{-1}.

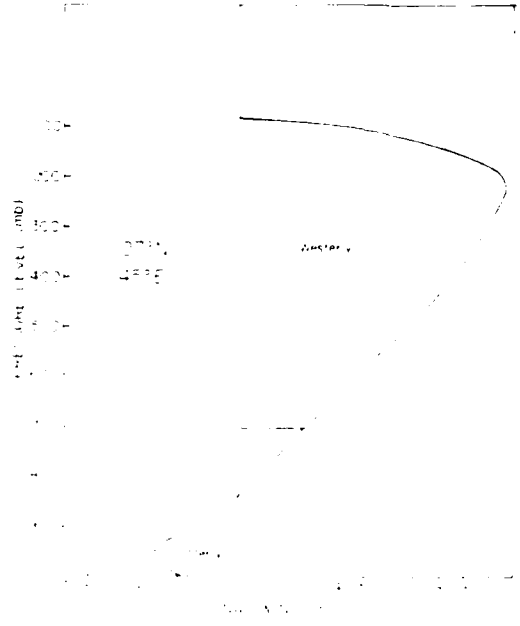

Figure 4.2: Mean zonal wind profile for the tropical troposphere located at 27° north, and 145° east, derived from 21 years of rawinsonde composites. Values in ms^{-1}

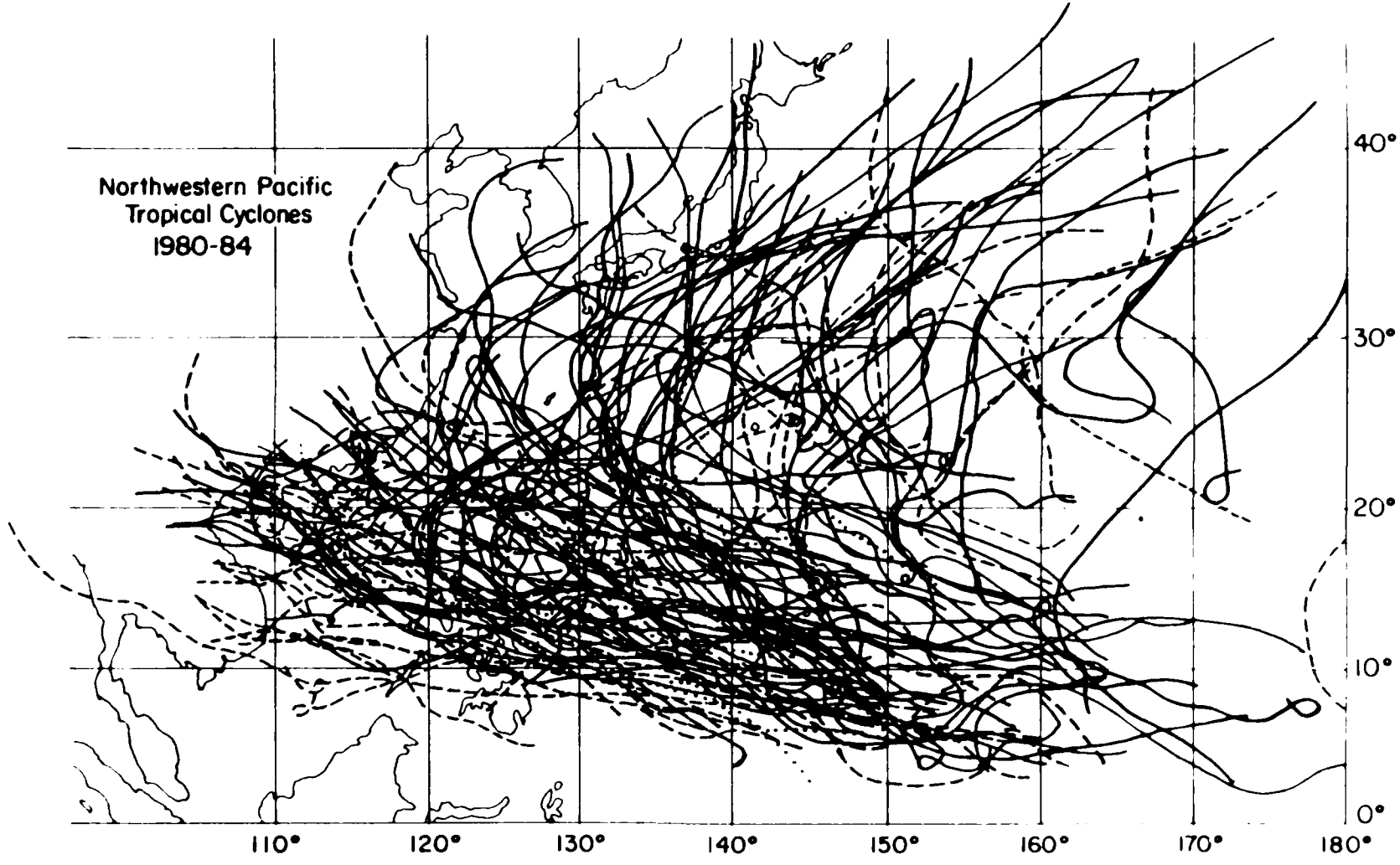

Figure 4.3: Cyclone tracks of the 101 cyclones used in this study for the 5 year period of 1980-84

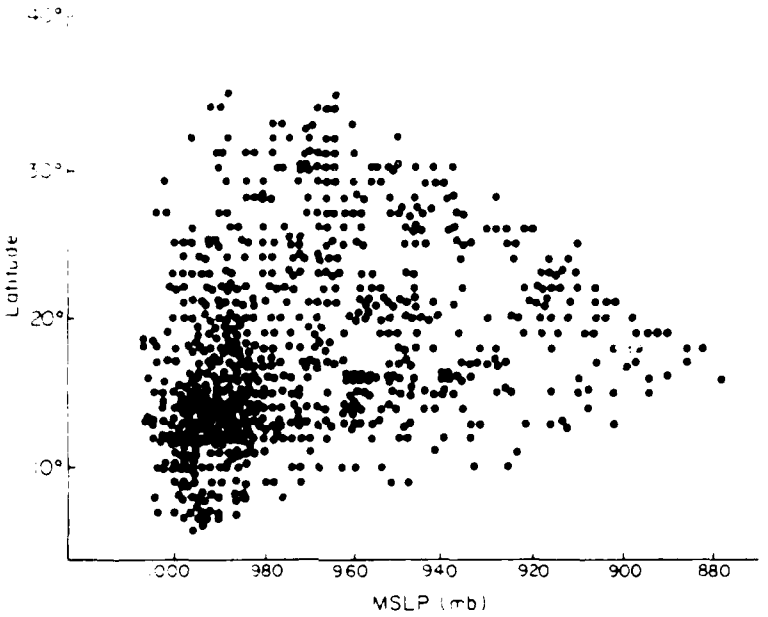

Figure 4.4: Scatter diagram of cyclone center latitudes versus MSLP for the 750 missions of this data set.

MID-TROPICAL LATITUDES 15 – 25° NORTH 388 MISSIONS

HIGH-TROPICAL LATITUDES 25 – 35° NORTH 134 MISSIONS

While a number of cyclones tracked north of 35° latitude, reconnaissance aircraft did not. This limited the aircraft data sample to 35°N yet adequately describes cyclones north of the subtropical ridge. Table 4.1 depicts the averages of position, motion, intensity and OCS for each latitude stratification. Those systems in the lower-latitude belt (5-15°) were generally weaker in both their inner and outer cores. Systems in the mid (15-25°) and higher tropics (> 25°) had similar average maximum winds but very different outer core wind strengths. This reflects the fact that cyclones generally reached maximum intensity when even with the ridge axis but did not attain their strongest outer core speeds until reaching the higher-tropical latitudes.

The plan view depictions by latitude belt reflect the 700 mb steering current. In earth-relative coordinates (NAT system), Figs. 4.5a-c display the 700 mb cyclone interior radial wind flow for these three latitude classes of cyclones south, even with, and north

Table 4.1: Averages of position, heading and speed of motion, MSLP, maximum wind speed (Holland estimate), and OCS.

LATITUDE CLASS	LAT.	LONG.	HEADING	SPEED (ms^{-1})	MAX WIND (ms^{-1})	MSLP (mb)	OCS (ms^{-1})
LOW-TROPICS	12°	138°	295°	5	27	979	15
MID-TROPICS	20°	133°	320°	5	35	961	19
HIGH-TROPICS	29°	141°	360°	7	35	963	24

of the subtropical ridge. It is easy to see the 700 mb current flowing to the northwest, north and northeast, respectively. What is not apparent in these figures is a reflection of the Solitary Eddy Solution (SES) as described by Flierl et al., (1980) for which the environmental flow moves around the vortex but not through. All three latitude classes show that the cyclone is not only moving faster than the 700 mb interior flow but nearly 30° to the left as well. This question of why cyclones move left of the mean steering current is largely attributed to the Beta effect (Hubert, 1959; George and Gray, 1976; Anthes, 1982; and Holland, 1983).

Figures 4.6a-c give the perspective which the cyclone experiences as it moves through the 700 mb stream in the MOTROT coordinate system. These show the 0 to 2.5° interior radial winds blowing from the left front to the right rear directly across the cyclone. Given this front to back flow-through in the MOTROT coordinate system, one would expect a weaker tangential wind asymmetry on the right and stronger on the left. This was observed in all cases (shown in Figs. 4.7a-c).

Combining both radial and tangential components of the background wind field, as in Figs. 4.8a-c, shows the greatest inner-core convergence in the lower-tropics, some convergence of environmental air in the mid tropics and divergence at higher-tropical latitudes. The higher-tropical inner-core cyclone vortex readily accepts 700 mb environmental air and allows it to pass directly through it. This is counter to the concept of the typhoon as a spinning top embedded in a stream which moves through stream momentum impingement on the edges. This data indicates that the cyclone's steering current extends to near the radius of maximum winds. Whether this current penetrates the Stationary Band

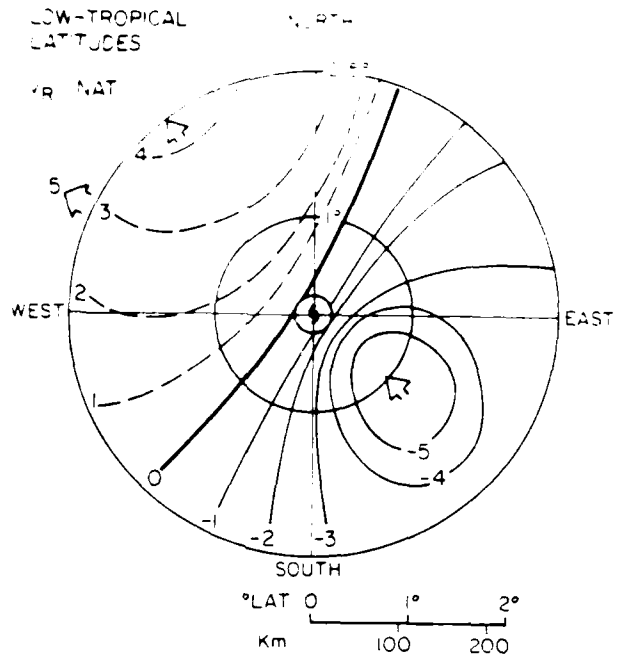

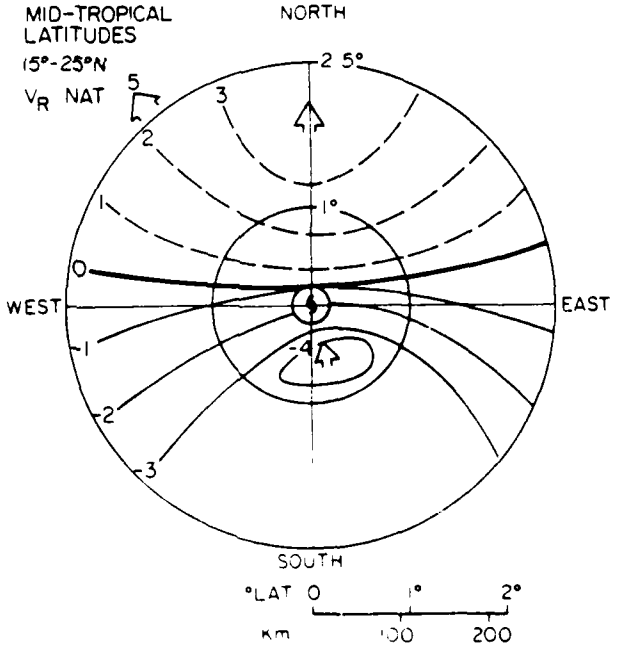

Figure 4.5: a-c. Plan-view depictions of the 700 mb radial wind field (V_r) in ms^{-1} and in earth-relative coordinates (NAT) for the three classes of a) low-tropical latitudes, b) mid-tropical latitudes, and c) high-tropical latitudes. Arrow on the rim depicts mean cyclone motion

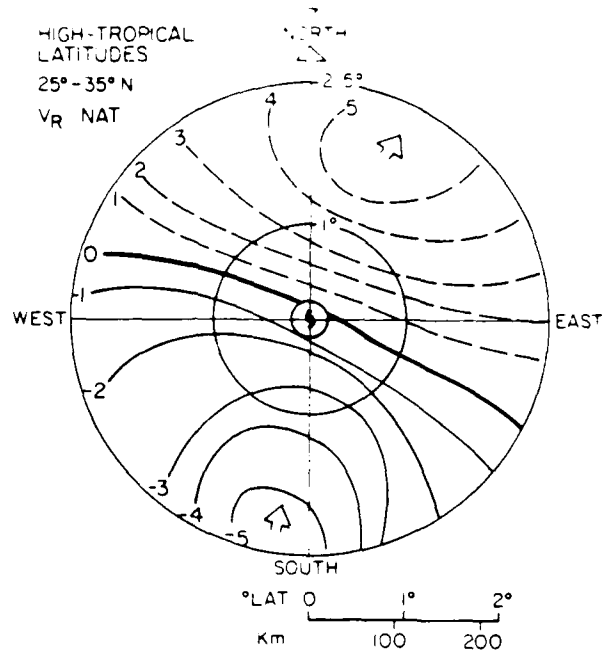

Figure 4.5: a-c. Continued.

Complex, SBC, (Willoughby, et al.) cannot be resolved with certainty here due to the fact that information on feeder bands were not recorded. However, Willoughby, et al.'s study showed that the SBC resided from 80 to 120 km from the center. their main contention was that inside the SBC, environmental air did not penetrate and a 'spinning top' regime existed which was shielded from environmental air. Figures 4.8a-c show that inside 80 to 120 km environmental air does indeed pass through. If this region were shielded from outside air these figures would show either no flow or light and variable flow inside 80 to 120 km.

4.3 Cyclone Heading

While classification by latitude band depicts the general heading classes, smaller scale changes to the mean flow exist. To classify most precisely by heading the following stratifications are used:

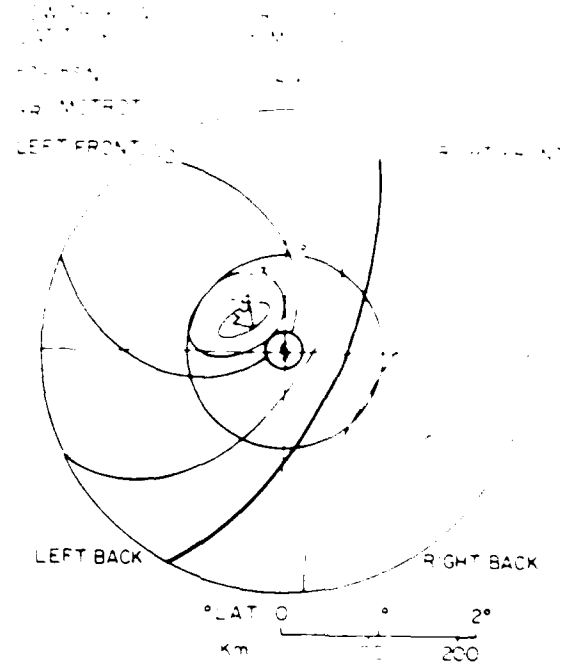

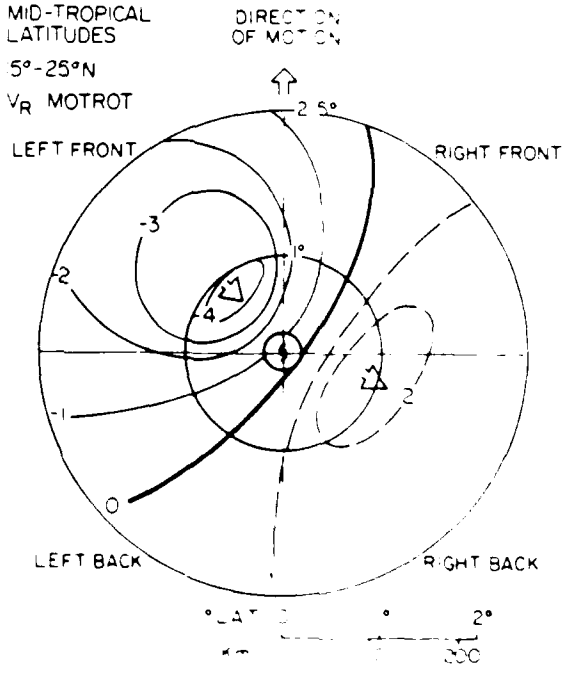

Figure 4.6 a-c. Plan-view depictions of the 700 mb radial wind field (V_r) in ms^{-1} in storm-relative coordinates (MOTROT) for the three classes of a) low-tropical latitudes, b) mid-tropical latitudes and c) high-tropical latitudes.

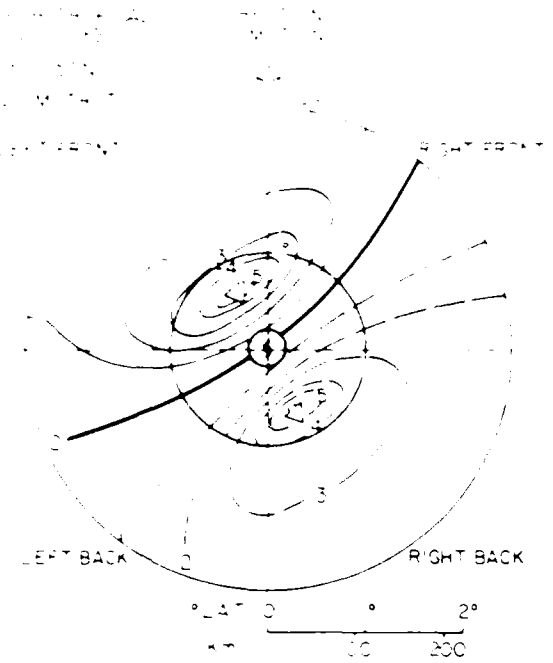

Figure 4.6: a-c. Continued.

HEADING CLASS	RANGE	NO. OF MISSIONS
SOUTHWEST	180° – 265°	66
WEST ←	250° – 290°	207
NORTH ↑	330° – 30°	176
EAST →	30° – 120°	87

Notice there are a significant number of cyclones moving to the southwest. Southwest heading cyclones are atypical in that they move the slowest and characteristically move in a more erratic path as seen for Typhoon Faye in Fig. 4.9. We include this class to further study the Beta effect. Table 4.2 gives the average position, motion, intensity and OCS values for each class. Cyclones moving north appear to slow down under the influence of a reduced steering current and then speed up again when north of the ridge and moving east. Eastward-moving cyclones have a slightly stronger OCS but a weaker intensity than their northward-moving counterpart.

Plan-view depictions of the radial wind in earth-relative or NAT coordinates are shown in Figs. 4.10a-d. Once again, it can be seen that each cyclone class moved left of the mean 700 mb steering current. Holland (1983) attributed this leftward drift to the

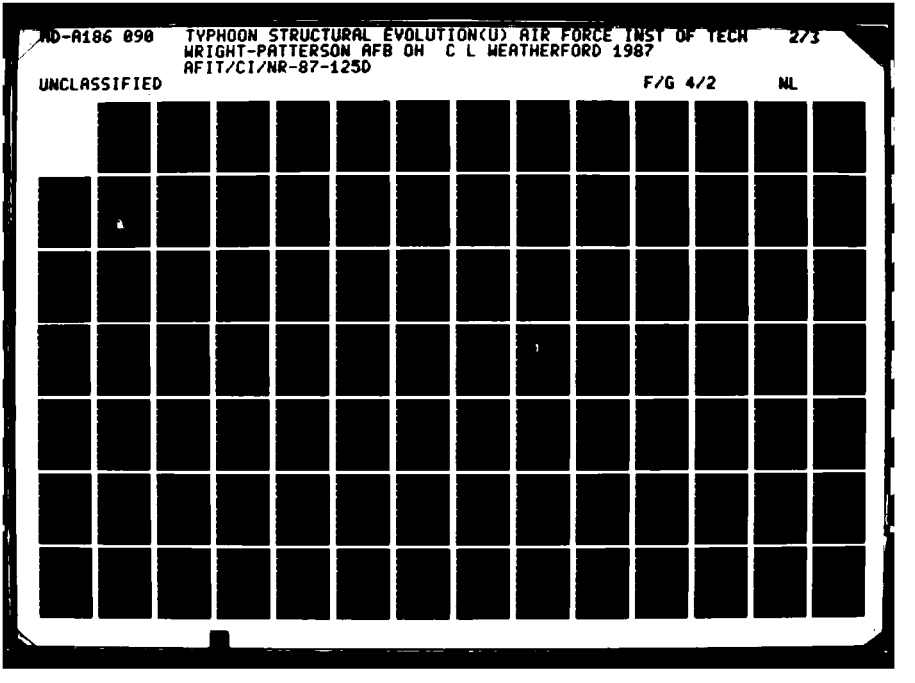
AD-A186 090 TYPHOON STRUCTURAL EVOLUTION(U) AIR FORCE INST OF TECH 2/3
WRIGHT-PATTERSON AFB OH C L WEATHERFORD 1987
AFIT/CI/NR-87-125D
UNCLASSIFIED
F/G 4/2
NL

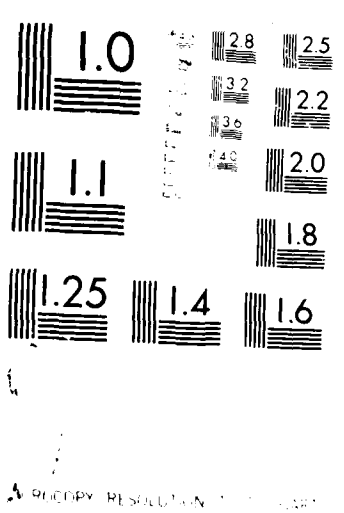
1.0
1.1
1.25
1.4
1.6
1.8
2.0
2.2
2.5
2.8
3.2
3.6
4.0

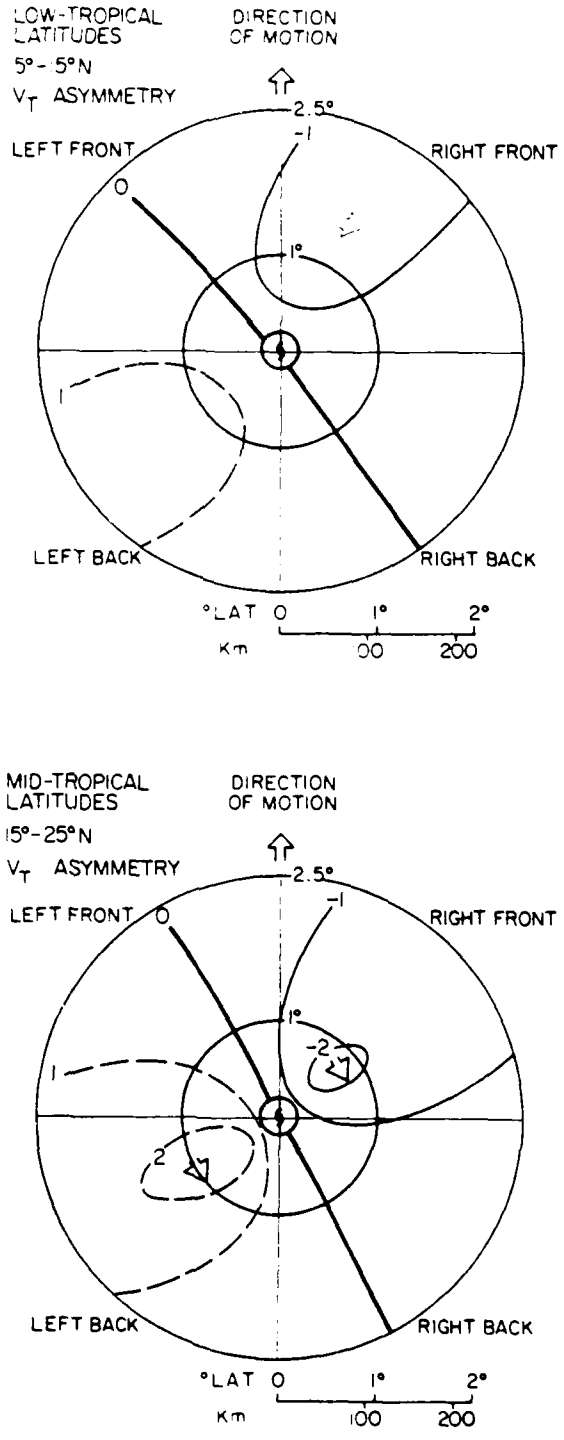

Figure 4.7: a-c. Plan-view depictions of the 700 mb tangential asymmetry pattern in ms^{-1} and in cyclone-relative coordinates (MOTROT-VORT) in which the mean vortex has been removed for the three classes of a) low-tropical latitudes, b) mid-tropical latitudes, and c) high-tropical latitudes.

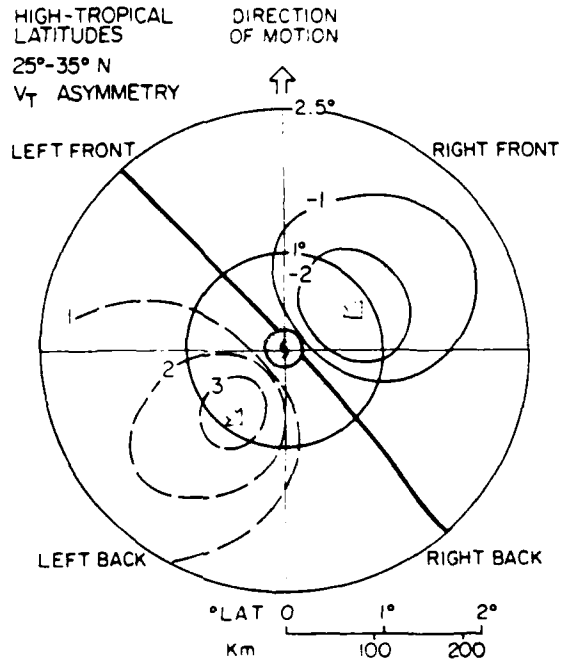

Figure 4.7: a-c. Continued.

Table 4.2: Average values of position, heading, speed of motion, maximum wind speed (Holland estimate), MSLP, and OCS for each cyclone heading of motion class.

HEAD	LAT.	LONG.	HEAD	SPEED (ms^{-1})	MAX WIND (ms^{-1})	MSLP (mb)	MSLP CHANGE (mb/d)	OCS (ms^{-1})
Southwest	17°	138°	240°	4	27	980	0	14
West	15°	136°	275°	6	28	975	- 10	15
North	22°	138°	360°	5	36	959	0	21
East	24°	136°	45°	6	34	966	+ 5	22

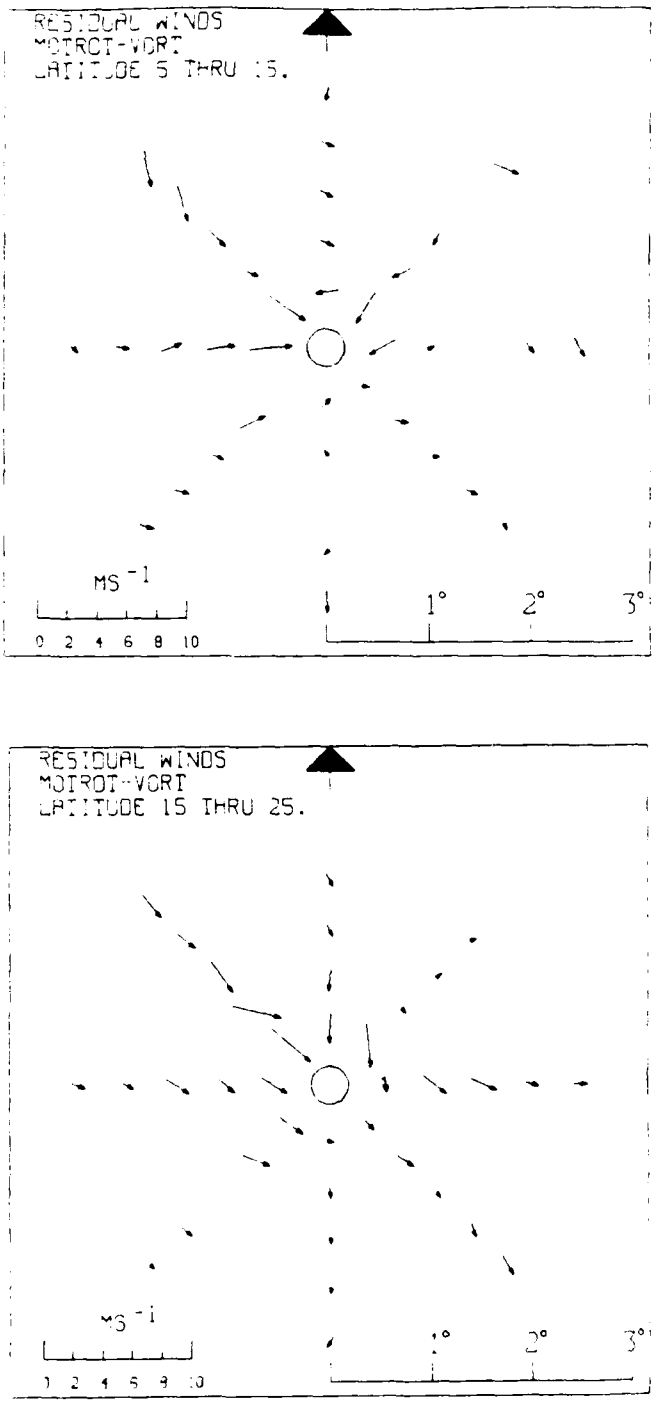

Figure 4.8: a-c. Plan-view depictions of the 700 mb residual wind field flow-through pattern in cyclone-relative coordinates (MOTROT-VORT) with the bold arrow denoting the cyclone heading of motion. Values are in ms^{-1} with arrow length implying speed as shown in the lower left corner. The classes are: a) low-tropical latitudes, b) mid-tropical latitudes, and c) high-tropical latitudes.

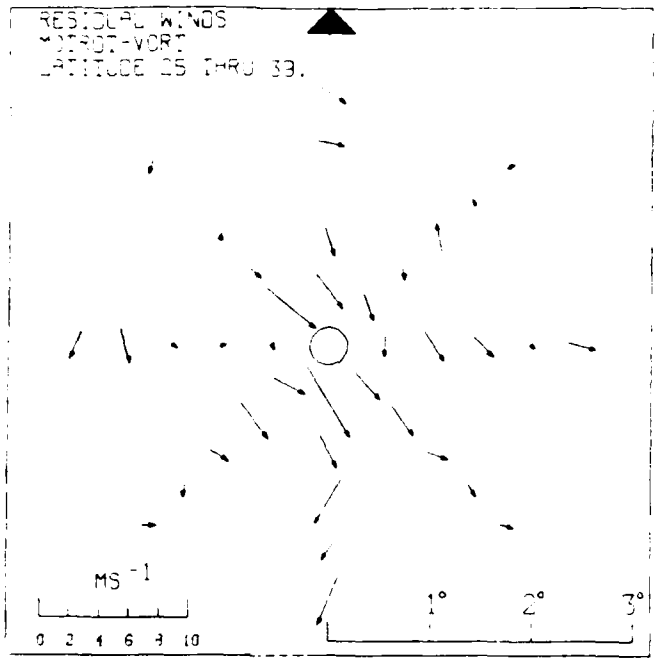

Figure 4.8: a-c. Continued.

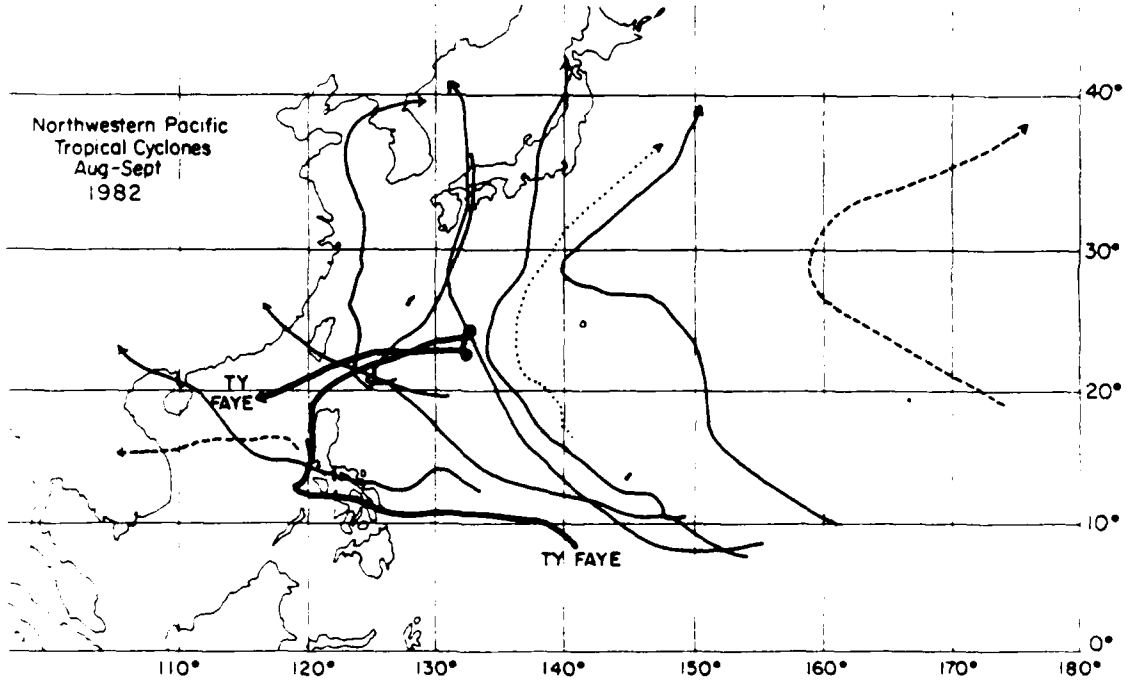

Figure 4.9: Tropical cyclone paths for the northwestern Pacific cyclones of August and September 1982.

Beta effect. A cyclonically rotating vortex on the large scale typical of typhoons would advect higher earth-vorticity (the Beta effect) on the cyclone's west side while low earth-vorticity would advect up the cyclone's east side. Assuming the vortex moves towards the region of maximum vorticity advection, the cyclone would appear to move left of its steering current. However, this left-drift effect should work only for cyclones embedded in an environment flowing north of an east-west axis. Those in an environmental current flowing south of an east-west axis should be deflected right of the steering flow. It was hoped that the 66 cases of southwest heading cyclones would provide some new insight on this latter case. However, as Fig. 4.10a shows, those cyclones moving towards the southwest were embedded in an environment moving westnorthwest, thus still in a left-drift regime. Right-drift motion was not measured with the composited cyclones of 1980-84. (The few cases which headed southeast or south were undergoing a looping pattern and thus are not considered to be under the influence of a dominant steering current.) What is interesting about these southwest movers is that they are in a markedly slower environment and yet appear to drift leftward the most (nearly 85°). This is likely due to the more dominant role of earth-vorticity advection, as opposed to relative vorticity advection, for these slow-moving cyclones.

When viewed in the cyclone-relative coordinate system (Figs. 4.11a-d), all cases moved faster than the 700 mb environment. Thus, the cyclones were being fed by the 700 mb environment they moved into. One interesting partial deviation to this was the case of eastward moving cyclones. Notice in Fig. 4.11d that the flow-through that normally entered from the left-front and exited the right-back prevailed on only the lower left half of the figure with a different regime on the upper right of the figure. This peculiar pattern is more clearly understood from the tangential asymmetry pattern.

The one-wave asymmetry pattern observed in cyclones embedded in a left- drift environment shows up well for cyclones heading southwest, west, and north when viewed in the MOTROT-VORT system (Figs. 4.12a-c). East- heading cyclones, however, deviated from the one-wave asymmetry pattern and revealed a two-wave pattern clearly dominating the residual tangential wind field. What appears to be happening is that the 700 mb current

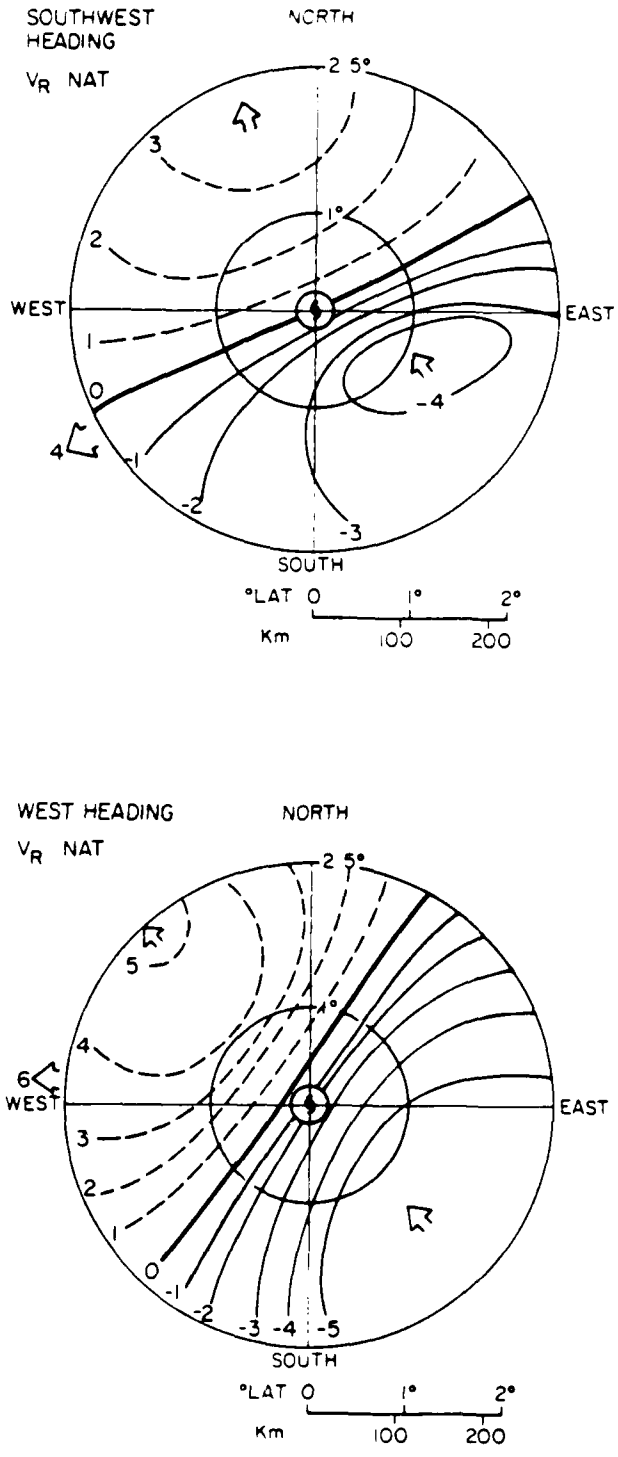

Figure 4.10: a-d. Plan-view depictions of the 700 mb radial wind field (V_r) in ms^{-1} and in earth-relative coordinates (NAT) for the four cyclone headings of a) southwest, b) west, c) north, and d) east. Arrow on rim denotes cyclone motion.

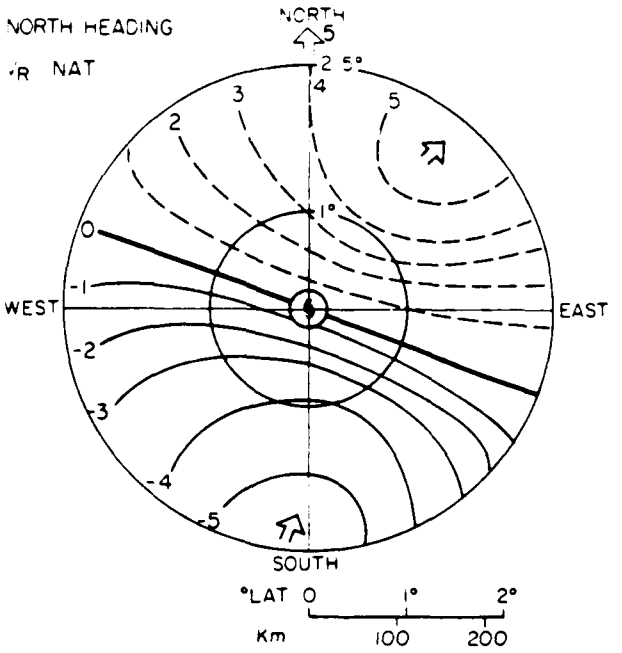

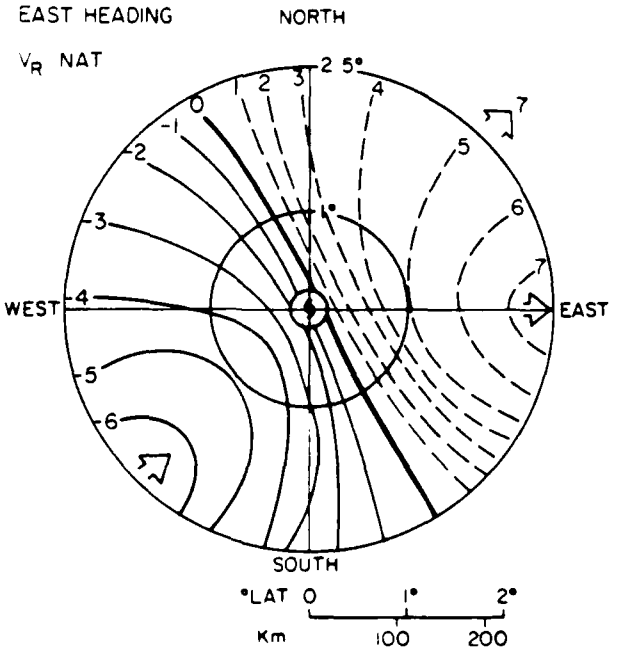

Figure 4.10: a-d. Continued.

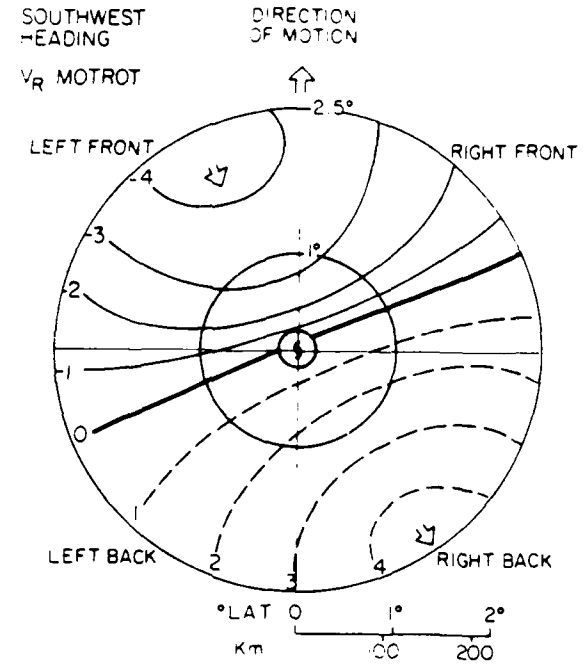

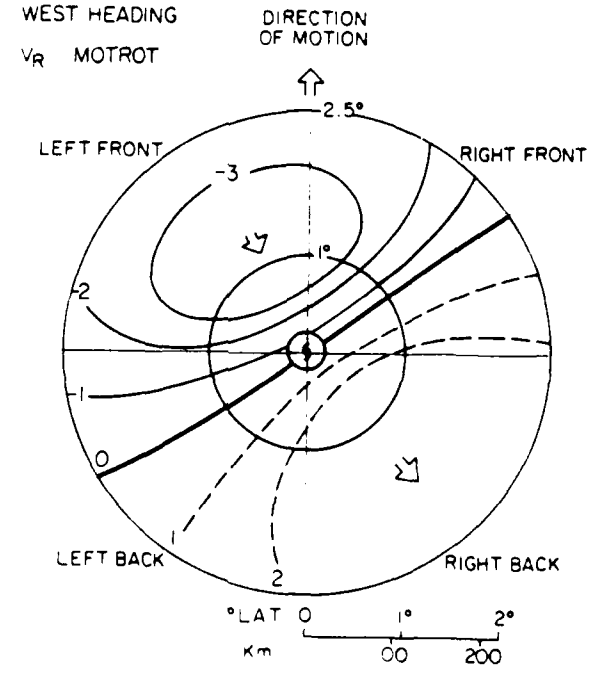

Figure 4.11: a-d. Plan-view depictions of the 700 mb radial wind field (V_r) in ms^{-1} and in cyclone-relative coordinates (MOTROT) for the four cyclone headings of a) southwest, b) west, c) north, and d) east.

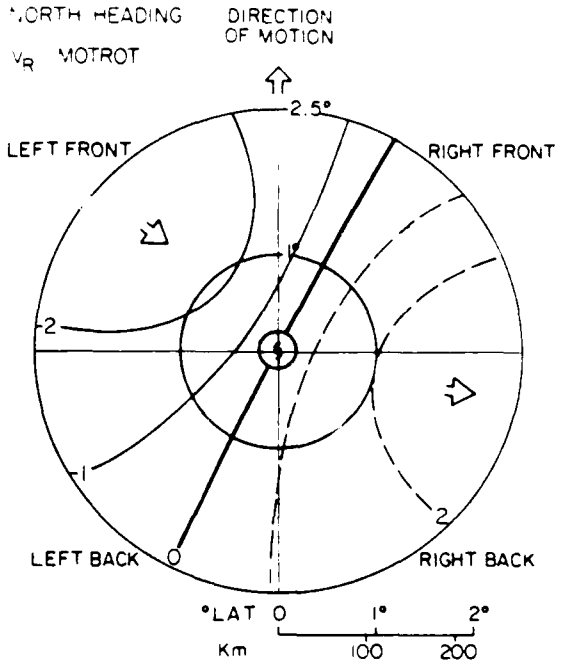

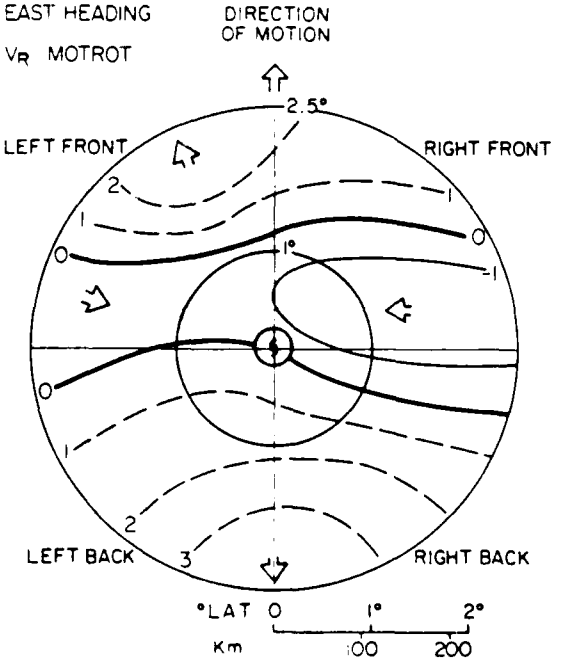

Figure 4.11: a-d. Continued.

enters into the cyclone from the left-front but only affects the lower left portion, indicative of cyclones which are moving faster and left of the 700 mb environmental stream. The upper right half of the cyclone, however, exhibits a flow-through which enters from the right, as shown in the schematic of Fig. 4.13. Apparently, these east-heading cyclones are, on average, situated on a bend in the 700 mb current as the stream curves around the ridge, with the lower portion on the current moving northeast while the upper portion in the current is moving due eastward, as shown in Fig. 4.14. The cyclone is encountering increasing westerly shear when rounding the bend with the 700 mb wind field becoming stronger and more westerly towards the north. Since the cyclone's heading is an average center movement, the lower portion lies in a slower, less westerly 700 mb current while the upper portion lies in an increasingly stronger current veering more and more right of the average heading and the cyclone appears to move right of the mean flow (Fig. 4.15). This induces the observed flow-through from right to left.

Evidently, the atypical flow pattern seen in the upper right of Fig. 4.11d is due entirely to the horizontal shear at 700 mb as the cyclone approaches increasing westerlies to the north. Superimposed on the tangential asymmetry field, what appears to be a two-wave eddy shown in Fig. 4.12d is a reflection of the sheared environment. This resulting horizontal shearing pattern clearly takes its toll on the cyclone since these eastward moving cyclones are filling at a rate of 5 mb/d.

4.4 Cyclone Speed of Motion

In addition to depicting the cyclone by its latitude and heading of motion, it is important to contrast cyclones by their differing speeds. The average speed of motion for a tropical cyclone was 5 ms^{-1} but this varied from 0 to 26 ms^{-1} for this data set, as seen in Fig. 4.16. Therefore, the final strictly environmental influence to be looked at is the difference between cyclones moving rapidly and those moving slowly. The intent is to study those cases which are much different from the average and are classified as follows:

SPEED CLASS	RANGE OF SPEEDS	NO. OF MISSIONS
FAST MOVERS	$\geq 7.5ms^{-1}$	137
SLOW MOVERS	$\leq 2.5ms^{-1}$	154

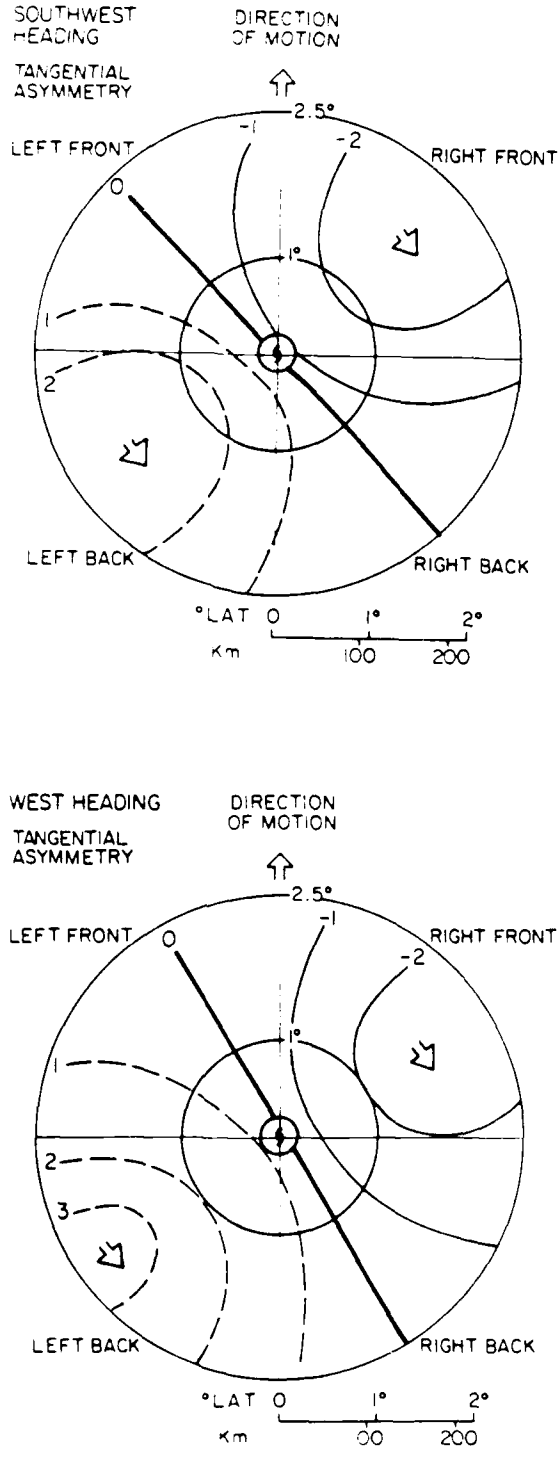

Figure 4.12: a-d. Plan-view depictions of the 700 mb tangential asymmetry pattern in ms^{-1} and in cyclone-relative coordinates (MOTROT-VORT) for the four cyclone headings of a) southwest, b) west, c) north, and d) east.

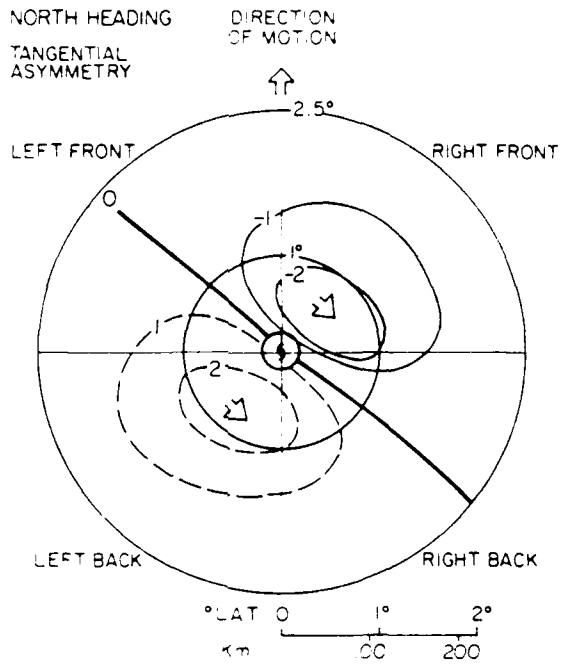

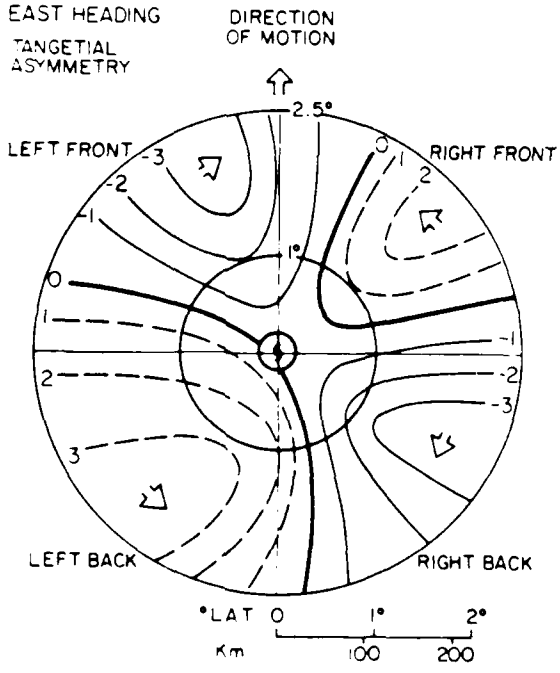

Figure 4.12: a-d. Continued.

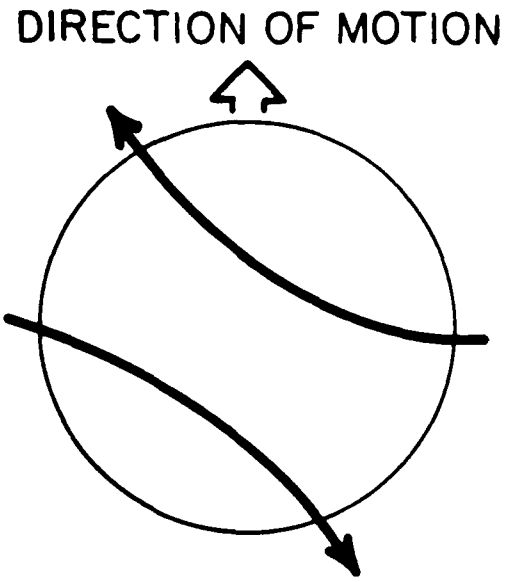

Figure 4.13: Schematic diagram of the environmental flow through pattern evident in eastward-moving cyclones in the MOTROT-VORT system.

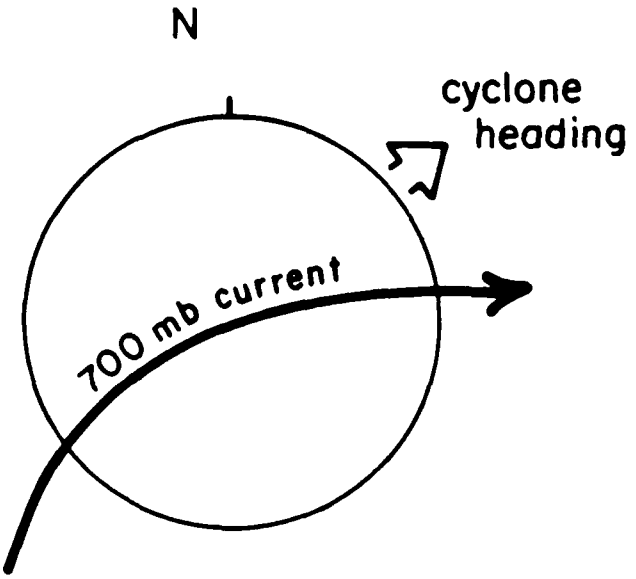

Figure 4.14: Schematic of the manner in which the environment bends as it passes through eastward heading cyclones in the natural coordinate system.

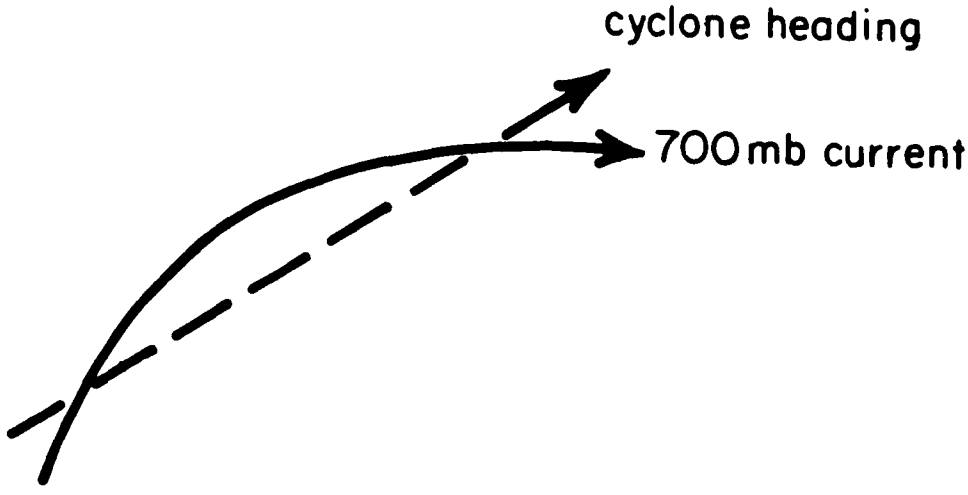

Figure 4.15: Schematic depiction of the cyclone's motion vector superimposed on the curving environmental current.

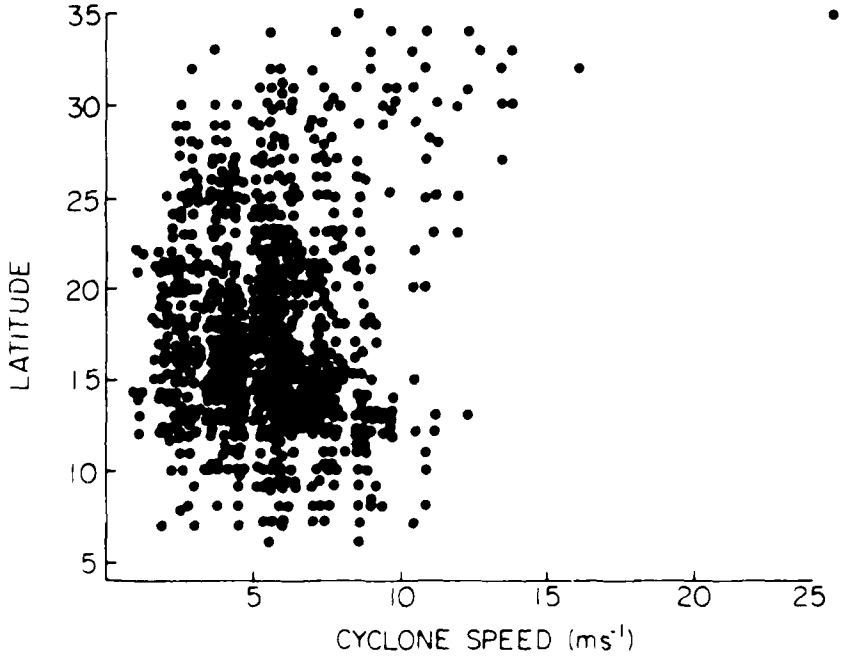

Figure 4.16: Scatter diagram of cyclone latitude versus speed of motion.

Both those cases moving significantly faster than the mean and those moving significantly slower have roughly the same inner and outer core wind structure and are minimal typhoons, as shown in Table 4.3, thus differences between the two do not reside within their basic structure. The fast movers are farther north and east than the slow movers but heading in roughly the same direction. It is somewhat surprising that the latitude separation is so small. One might expect that the significantly faster moving cyclones would be those caught up in the westerly jetstream that lies north of 30°, but since these quickly transform into extra-tropical cyclones, they are of a different breed and beyond the scope of this study. Thus it appears that some cyclones move much faster than others at relatively similar latitudes but within obviously different steering currents.

Table 4.3: Average positions, motion, MSLP, maximum wind speeds, and OCS values for the speed classes of fast and slow.

SPEED CLASS	LAT.	LONG.	HEAD	SPEED (ms^{-1})	MSLP (mb)	MAX WIND (ms^{-1})	OCS (ms^{-1})
FAST MOVERS	20°	139°	330°	9	972	30	19
SLOW MOVERS	18°	134°	320°	2	969	32	18

The 700 mb environmental current is observed to be superimposed on the mean vortex as in the plan-view depictions of Figs. 4.17a-b. Although the 700 mb current is flowing faster for the fast movers, it is not enough to account for the four-fold difference between the cyclone's speed and the 700 mb stream. The 700 mb current is only twice the speed of the slow movers, therefore the environment that lies above the 700 mb level must be faster still in order to move the cyclone so rapidly. It does appear, in these earth-relative plan-views, that the fast-moving cyclones lie even with the ridge axis as evidenced by the northward heading 700 mb flow. The slow-moving cyclones whose 700 mb flow is moving northeastward lie slightly north of the ridge it even though they are at lower latitudes, indicative of early and late season cyclones when the ridge axis lies farther south. Once again, the cyclone moves left of its 700 mb current. Notice how much more the slow-moving cyclones drifted left of the mean 700 mb current than fast-moving cyclones (70° versus

30°). This lends further support to Beta-effect arguments that contend the cyclone will move towards the region of greatest vorticity advection. The slower the steering current, the greater the role of planetary vorticity advection as is borne out here.

When viewed in the cyclone-relative coordinate system, as in Figs. 4.18a-b, it appears that the flow-through was drastically more reduced for the slow movers than for the fast movers. This implies that the 700 mb advection was consequently much less for the slow movers. These slow movers are, on average, not changing their intensity (no MSLP change of either the past 12-hour period nor the next 12 hours). The fast movers, on the other hand, are deepening slightly at a rate of 3 mb/d. This flow-through manifests itself in both cases as a one-wave asymmetry pattern resulting in higher winds on the left-back quadrant although the fast movers show this asymmetry much farther out from the inner core than the slow movers (Figs. 4.19a-b). This increased flow-through shows up in the residual wind field in MOTROT-VORT as in Figs. 4.20a-b. Although both classes are minimal typhoons, the slow movers reflect very little flow-through due to the fact that there is apparently very little environmental current flowing at 700 mb. The flow-through pattern of the fast movers, though, seemed to pass right through the center with little being absorbed in the inner core.

The cyclone speed most conducive to intensity increase is an average speed of 5 ms^{-1} (Weatherford and Gray, 1987a). Neither significantly slower nor faster speeds appear to enhance the deepening process. This question of intensity change, although intimately connected with the environment, is addressed directly in the next chapter as cyclones are separated by their life cycle stage of development.

4.5 Discussion

The steering current is observed to flow directly through the tropical cyclone vortex. This is counter to the concept of a stiff inner vortex moving as a spinning top embedded in a stream which impinges on only the vortex' outer edges. Apparently, the steering grips the vortex from not only its fringes but near the center as well, thereby moving it through the stream. Our concept of cyclone motion must include steering of the eyewall as well

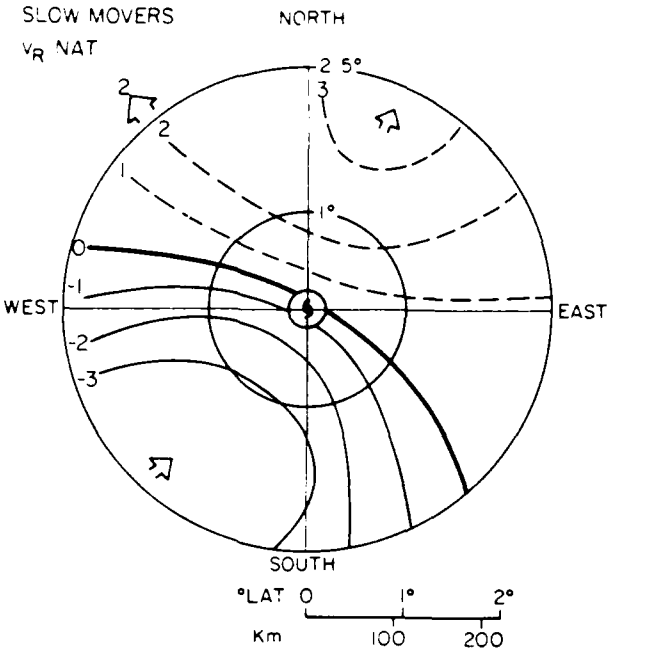

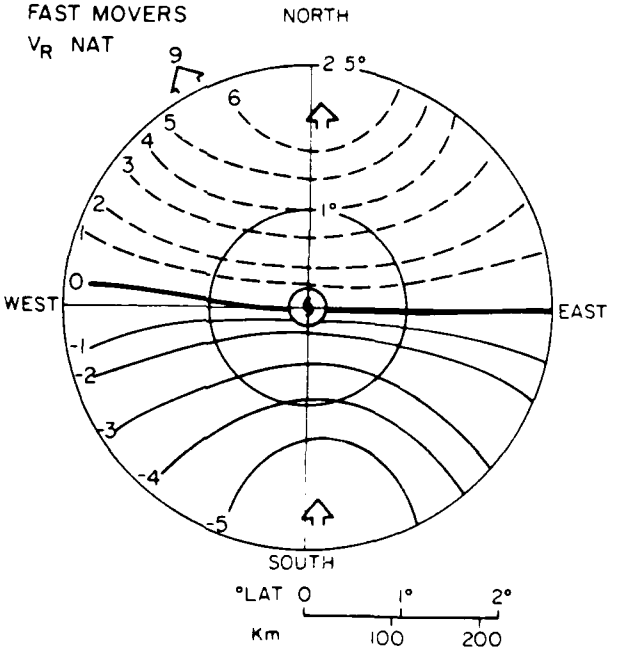

Figure 4.17: a-b. Plan-view depictions of the 700 mb radial wind field (V_r) in ms^{-1} and in earth-relative coordinates (NAT) for the classes of slow moving cyclones (less than 2.5 ms^{-1}) and fast moving cyclones (speed greater than 7.5 ms^{-1}). Arrow on rim denotes mean cyclone motion.

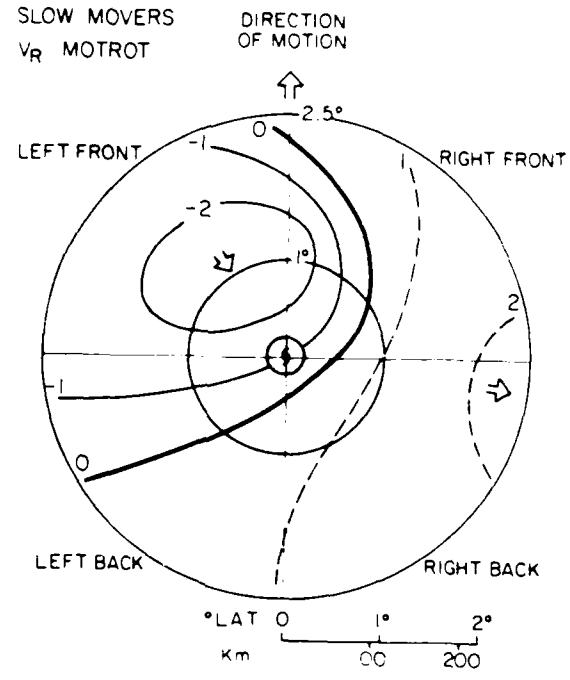

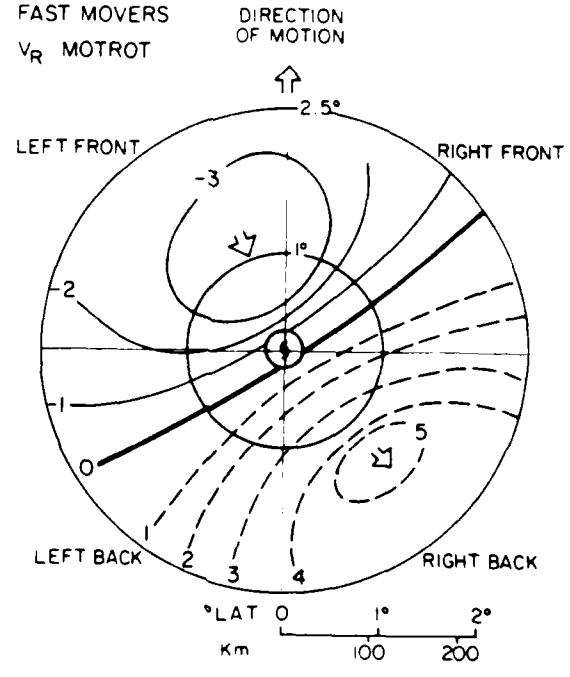

Figure 4.18: a-b. Plan-view depictions of the 700 mb radial wind field (V_r) in ms^{-1} and in cyclone-relative coordinates (MOTROT) for the classes of slow moving cyclones (less than 2.5 ms^{-1}) and fast moving cyclones (speed greater than 7.5 ms^{-1}).

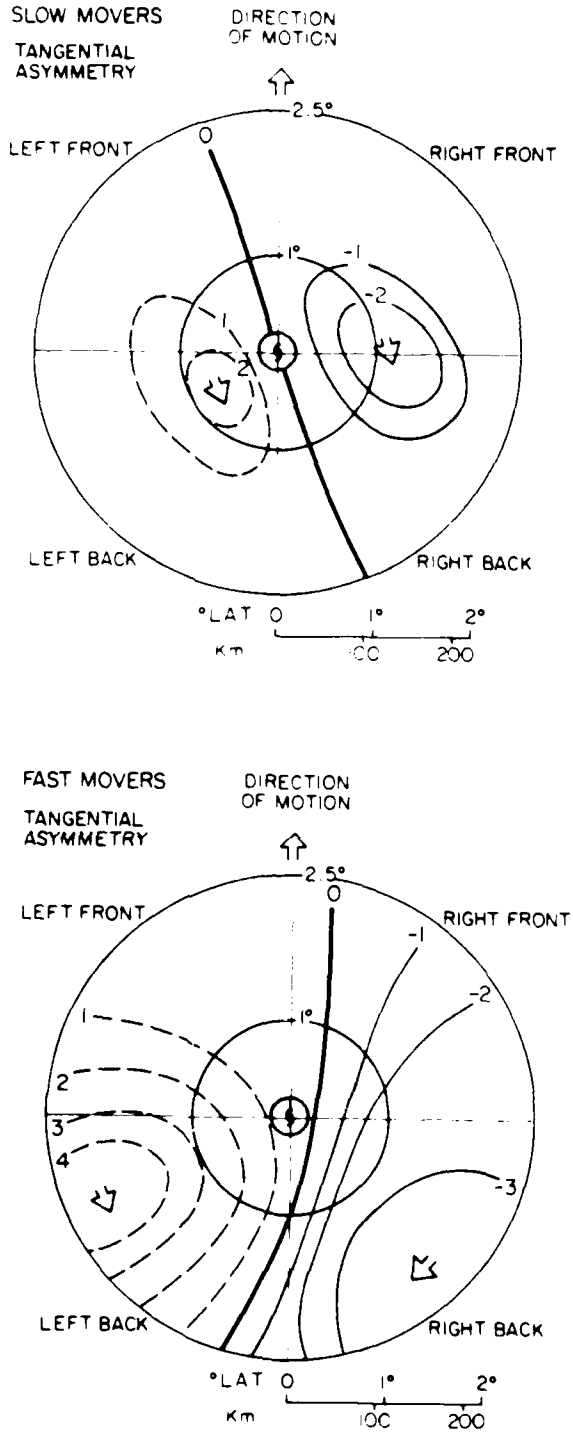

Figure 4.19: a-b. Plan-view depictions of the tangential asymmetry pattern in ms^{-1} and in MOTROT-VORT for the classes of slow moving cyclones (less than 2.5 ms^{-1}) and fast moving cyclones (speed greater than 7.5 ms^{-1}).

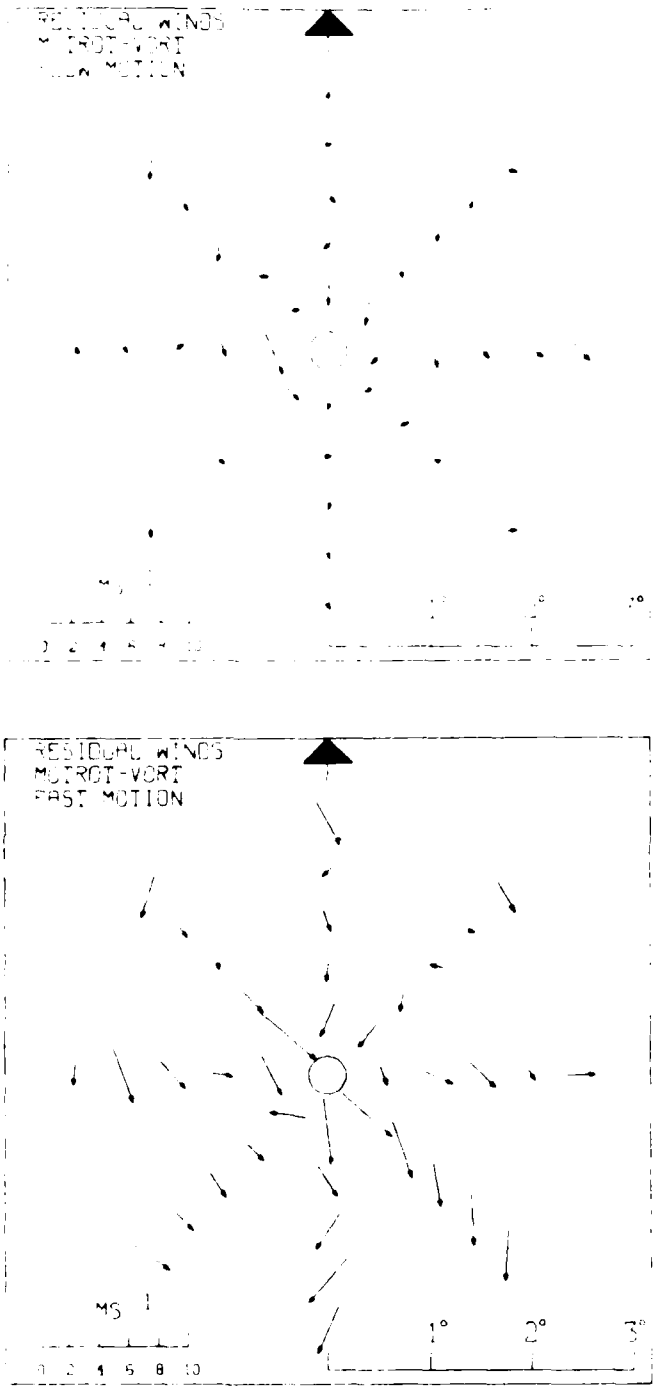

Figure 4.20: a-b. Plan-view depictions of the 700 mb residual wind field in MOTROT-VORT with the bold arrow denoting the mean cyclone heading of motion. Values are in ms^{-1} with arrow length implying speed as shown in the lower left corner. The classes are a) slow moving cyclones (speed less than 2.5 ms^{-1}) and b) fast moving cyclones (speed greater than 7.5 ms^{-1}).

as the outer regions. This makes inner core flight data capable not only of describing the wind field but its steering current as well. Once the mean vortex is removed, much of the residual wind field comprises the steering current itself. The remaining portion of the residual wind field reveals the vortex-environmental interaction. Recall from the previous chapter that the more intense the cyclone, the more environmental air was drawn into the center of the vortex. Although this steering current is seen to penetrate into the cyclone's inner core region, the stronger the vortex the more the cyclone shields the center from environmental air because the steering current contributes a smaller portion of the total wind field. However, this shielding effect is not total but increases gradually with intensity and strength.

One important question that arises from this new concept is that a vortex not shielded from the steering current of the environment is consequently not shielded from the lower potential temperatures characteristic of the outer regions. Indeed, environmental air passes through the vortex unimpeded. This continual washing-effect implies that the composition of the environment into which the environment is moving is intimately related to its future intensity potential.

The Beta-effect appears in all substratifications of the environment adhering well to the Beta drift theory (Adem, 1956; Holland, 1983; DeMaria, 1985; Chan and Williams, 1987). Additionally, the slower the vortex moves the more it drifts leftward due to the larger role of the Beta effect. Further evidence was revealed in the previous chapter showing that the larger the vortex, the greater the leftward drift as first proposed by DeMaria, 1985.

Tangential asymmetry patterns appear for all cases. By far the most common is a one-wave asymmetry pattern resulting from the fact that the cyclone moves through the 700 mb level faster than the 700 mb stream, inducing stronger winds on the left-back portion and weaker winds on the upper-right quadrant. When significant horizontal shearing is encountered, as for the case of east-heading cyclones nearing the westerly jetstream, this shear induces a two-wave asymmetry pattern in the tangential wind field. These asymmetry patterns are not believed to be due to impulses radiating from the cyclone itself but rather are presumed to be a result of the environment itself.

Chapter 5

THE LIFE CYCLE OF THE TROPICAL CYCLONE

Tropical cyclones go through characteristic life cycles. Because they spend most of their lifetime changing, a steady state depiction is incomplete. In order to adequately understand and forecast these changes, the tropical cyclone's typical progression must be fully described. How far out will the gale-force winds extend? How strong will the winds be at large radius? When will damaging wind speeds first make landfall?

Although changes occur more quickly near the tropical cyclone's center (within this data set, Supertyphoon Forrest, 1983, exhibited the greatest MSLP drop of 92 mb in one day!) changes well away from the center can be important as well. As was shown in the study by Weatherford and Gray (1987b), damaging wind radii for Typhoon Owen (25 ms^{-1}) expanded 188 km in a twelve-hour period. However, if the tropical cyclone is followed throughout its life cycle, distinct patterns are observed. It is these patterns of change which may assist the forecaster in predicting the tropical cyclone's future wind field. Therefore the focus here will be to describe typical tropical cyclone behavior so that its changing wind field can be better understood and forecast.

The tropical cyclone's life cycle is traditionally viewed by following its changing central pressure. Typically the central pressure falls slowly in the depression and storm stages and intensify more rapidly through the typhoon stage. Steady state periods have been observed to occur at any time through the deepening and filling process but are more likely to occur in weaker cyclones. Of the nearly 800 missions in this data set, 44% were into intensifying cyclones, 33% into steady state systems, and 22% into filling systems. The intensification period was typically prolonged while the filling process was often swift as the cyclone struck land or took on extra tropical characteristics.

Typhoons could undergo intensity changes in many different ways. Some intensify slowly while others do so incredibly fast. Some reach supertyphoon intensity and remain there for days as with Supertyphoon Elsie (Fig. 5.1) while others only briefly touch on such intensities before weakening (note Supertyphoon Kim in Fig. 5.2). In order to describe these trends and isolate the various patterns, we will break down the life cycle into distinct stages.

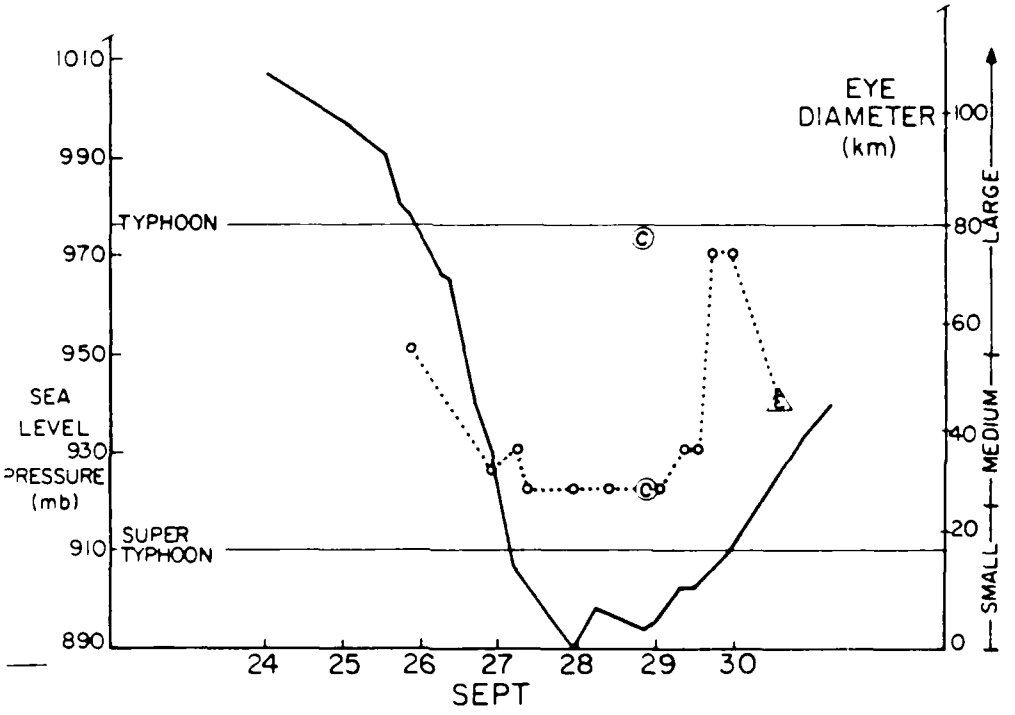

Figure 5.1: The evolution of the central pressure in Supertyphoon Elsie.

5.1 Stage of Intensity

Tropical cyclones that achieved considerable intensity and resided over water throughout their lifetime exhibit all the major life cycle features common to tropical cyclones. Therefore, 29 typhoons were chosen which intensified below 930 mb and displayed similar life cycle patterns. Particular attention was made to sort out those cyclones making landfall so that the momentum-destroying effects of the increased friction would not alter

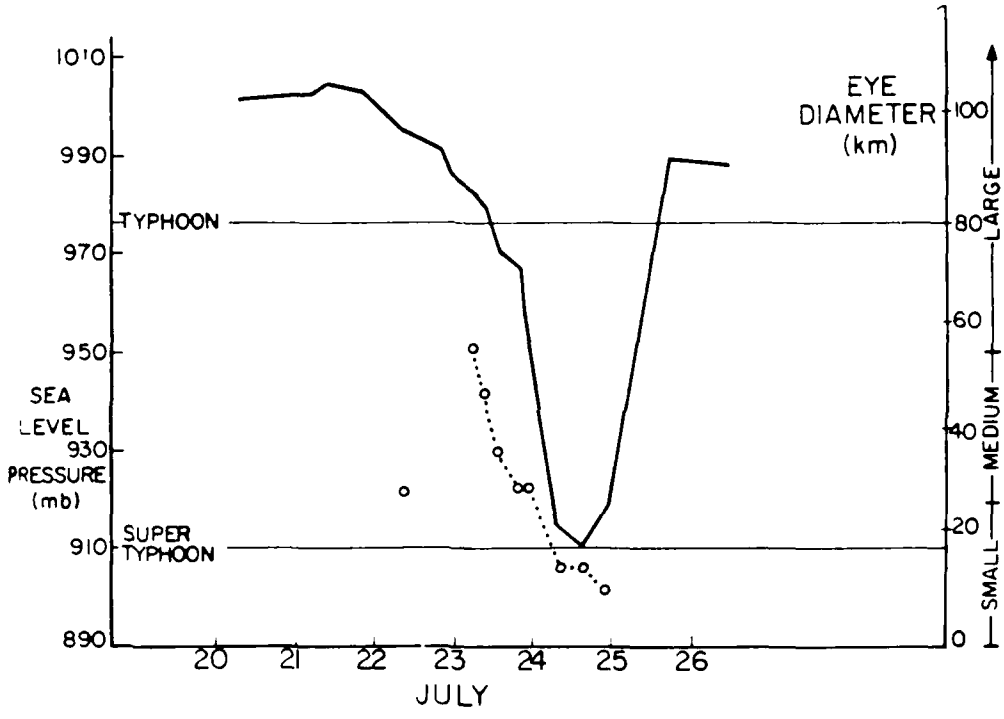

Figure 5.2: The evolution of the central pressure in Supertyphoon Kim.

the wind field results. Five typical life cycle stages (depicted in Fig. 5.3) were classified as follows:

STAGE	MSLP RANGE	NO. OF MISSIONS
1 - INTENSIFYING TROPICAL STORM	998 - 976 mb	102
2 - INTENSIFYING LEAST TYPHOON	976 - 930 mb	97
3 - INTENSIFYING INTENSE TYPHOON	930 - 870 mb	49
4 - FILLING INTENSE TYPHOON	870 - 930 mb	57
5 - FILLING LEAST TYPHOON	930 - 976 mb	68

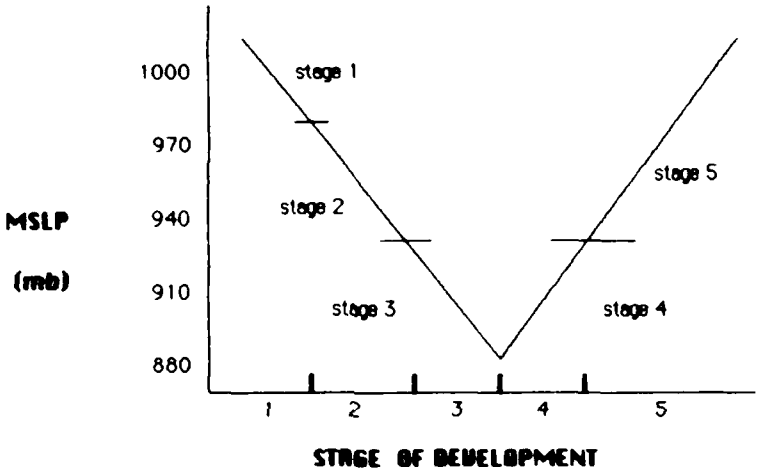

Figure 5.3: Schematic of the division of cyclones into their five life cycle stages. Intensification rates are not drawn to scale.

5.1.1 Azimuthally-averaged properties

Typical patterns of change occur as the tropical cyclone intensifies. As would be expected from the information in Table 5.1, the tropical cyclone generally moves northwestward as it intensifies, recurves to the east and fills. Notice how these intense typhoons achieve this intensity rather quickly but fill much more slowly (barring landfall). Without the destructive effects of landfall, it is observed that a cyclone spins up more rapidly in its inner core than it decays. Notice that the typhoons in stage 3 were, on average, rapidly deepening at a rate of 42 mb/d while in stage 4, filling occurred at a rate of about 14 mb/d, a third less. The Appendix depicts the MSLP, 700 mb OCS, eye temperature, and radar eye diameters during the life cycles of 47 cyclones. One can see for these traces that

those which exceeded 930 mb attained this intensity in a rapid fashion reinforcing the observations of Holliday and Thompson, 1979. Gradual deepening to extreme intensities is rare. Analysis of the cyclones which did not reach 930 mb and were thus not included in this subset typically intensify at much slower rates during the typhoon stage. Therefore, because it was determined that the cyclones in this subset must attain MSLP's of 930 mb, the classification of stages 1 through 5 is biased toward rapid deepeners. It is because changes occurred so rapidly in this sample that the MSLP change of Table 5.1 was given in 12 hour instead of full day increments. This served the purpose of better associating the MSLP changes with the Outer Core Wind Strength (OCS).

The greatest OCS occurs during the filling stages (4 or 5) and not the stage of greatest intensity (Stage 3). Notice how much higher the intensity is in Stage 5 (MSLP 959 mb) than for Stage 3 (MSLP 914 mb) for the same Outer Core Wind Strength. The ratio of maximum wind to OCS is 2.4 in stage 3 but only 1.6 in stage 5. This implies that the inner core maximum winds increase at a faster rate than the winds in the outer core during intensification.

Table 5.1: Averages of latitude, longitude, cyclone heading and speed of motion, MSLP and its change, and OCS for each stage of intensity change.

STAGE	LAT.	LONG.	HEAD	SPEED	MSLP	MSLP CHANGE	MAX WIND	OCS
				ms^{-1}	mb	mb/12 hr	ms^{-1}	ms^{-1}
1	13°	143°	290°	5	989	- 5	22	14
2	16°	137°	305°	5	955	-11	41	20
3	17°	134°	310°	5	914	-23	56	23
4	21°	132°	335°	5	922	+ 7	52	27
5	24°	132°	345°	6	959	+10	39	23

The tangential wind field clearly changes from the center out to 3° as the cyclone passes through its various life cycle stages (Fig. 5.4). Although cyclones begin their intensification in stage 1 with a flat wind field, their inner core winds pick up more quickly than the outer core winds, as they intensify through stages 2 and 3. However, during the filling stage 4 the inner core winds decrease rapidly while the outer core continues to

strengthen. Finally, in stage 5, the entire wind field decreases with the inner core doing so more rapidly than the outer core. This results in a return to a more flat wind profile, albeit at a much higher strength. These observations show that the radius of gale force winds will be much greater in the filling stage than in the deepening stage for cyclones with same MSLP.

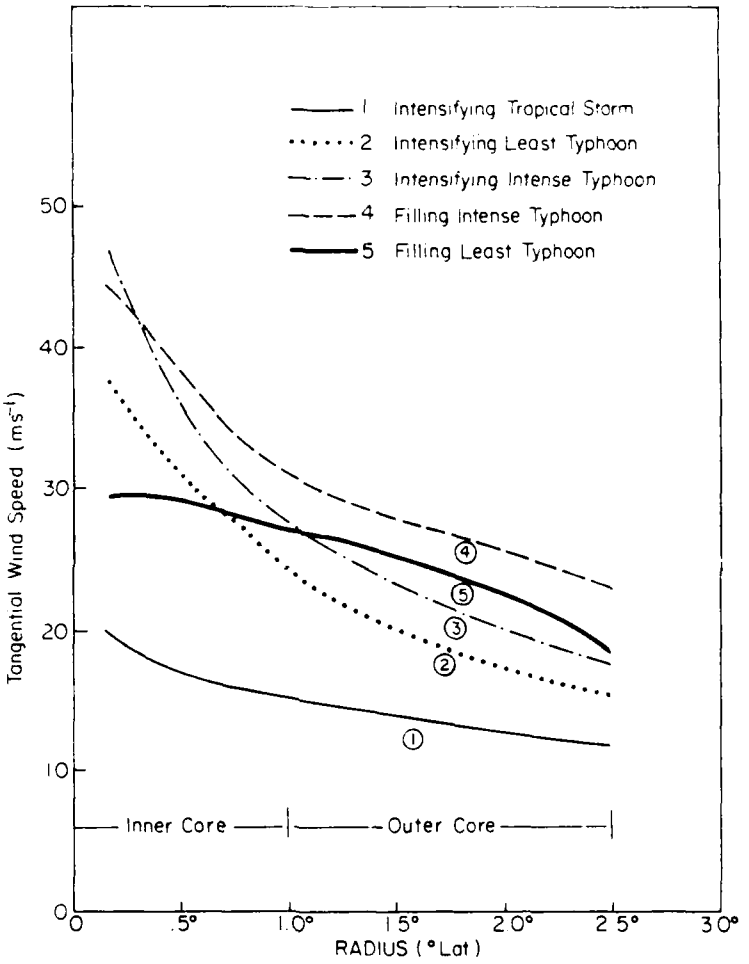

Figure 5.4: Average tangential wind fields for the five life cycle stages.

Figure 5.5 shows that despite the large variation in OCS with cyclone stage, vorticity is still very much concentrated near the center in all cases. Nevertheless, in the 1 to 2° radius region vorticity in stage 5 is nearly double that of the more intense stage 3. Notice how nearly equal the outer-core vorticity fields are for all intensifying stages (1, 2, and 3) but much larger for the filling stages (4 and 5). Because the vorticity provides

such a dominant contribution to the inertial stability, the outer core was only slightly stiffer to radial motions in the intense stage 3 than in the intensifying tropical storm stage 1. However, the inertial stability is generally twice as great in stage 4 as in stage 3 even though MSLP and maximum winds were only slightly weaker in stage 4. Following inertial stability arguments one could assume that radial inflow would be less able to penetrate into the cyclone's inner core in stage 4 than in stage 3 with the cyclone in stage 4 becoming consequently less intense. Inflow would thus be forced upward at larger radii in the decaying state.

To test this theory that higher inertial stability would force inflowing air upward at larger radii, the moisture fields were examined. As these outer core winds increase the outer core convection should increase as well, resulting in greater moistening of the 700 mb outer-core. Relative humidity values were also higher. Figure 5.6 shows that this is indeed the case. Stage 4 exhibits the highest outer core moisture and outer core wind field even though the central pressures are filling.

5.1.2 *Residual Core Wind Field by Cyclone Stage*

A cyclone undergoing rapid changes in intensity distorted the residual wind field far more than the relatively steady state cases shown in the previous chapters. Figures 5.7a-e depict the interior background wind field after cyclone motion and the mean vortex have been subtracted from all winds. Apparently, the cyclone forms from the inside out, interacting with its environment as it does. The residual wind field shows progressively greater distortion with stage. In stage 1, Fig. 5.7a, the environment is seen to flow from the front-left to the right- back relatively undistorted by the vortex except for the fact that less of the 700 mb current exits than enters the storm area, evidently retained in the intensifying inner. But, as the stage increases, less of the environmental flow through was detectable.

5.2 Wind Profile Change Patterns

As implied in the previous section and depicted in Fig. 5.8, the tangential wind field of a tropical cyclone generally follows three basic patterns of change (see Table 5.2). In

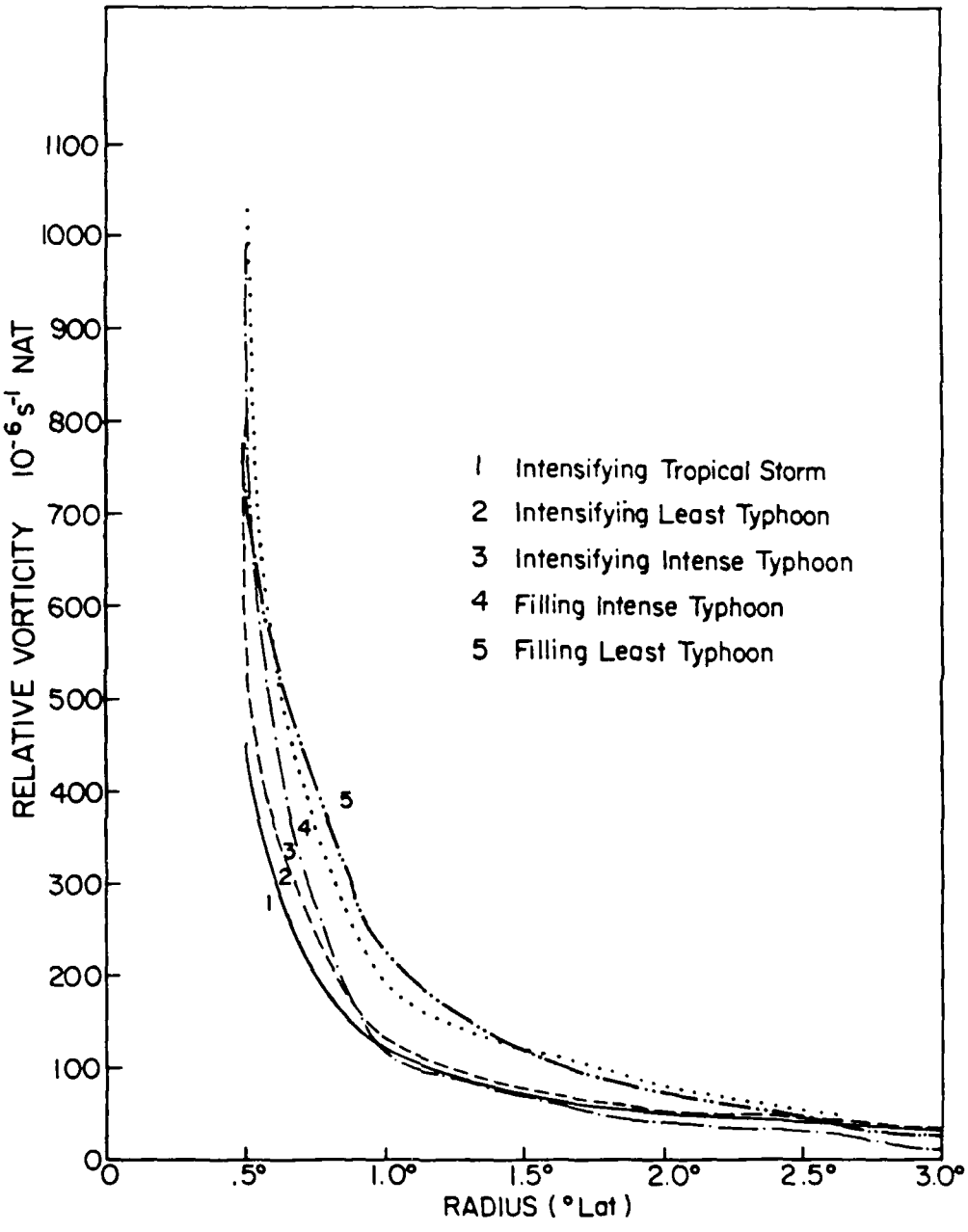

Figure 5.5: Vorticity fields for the five life cycle stages.

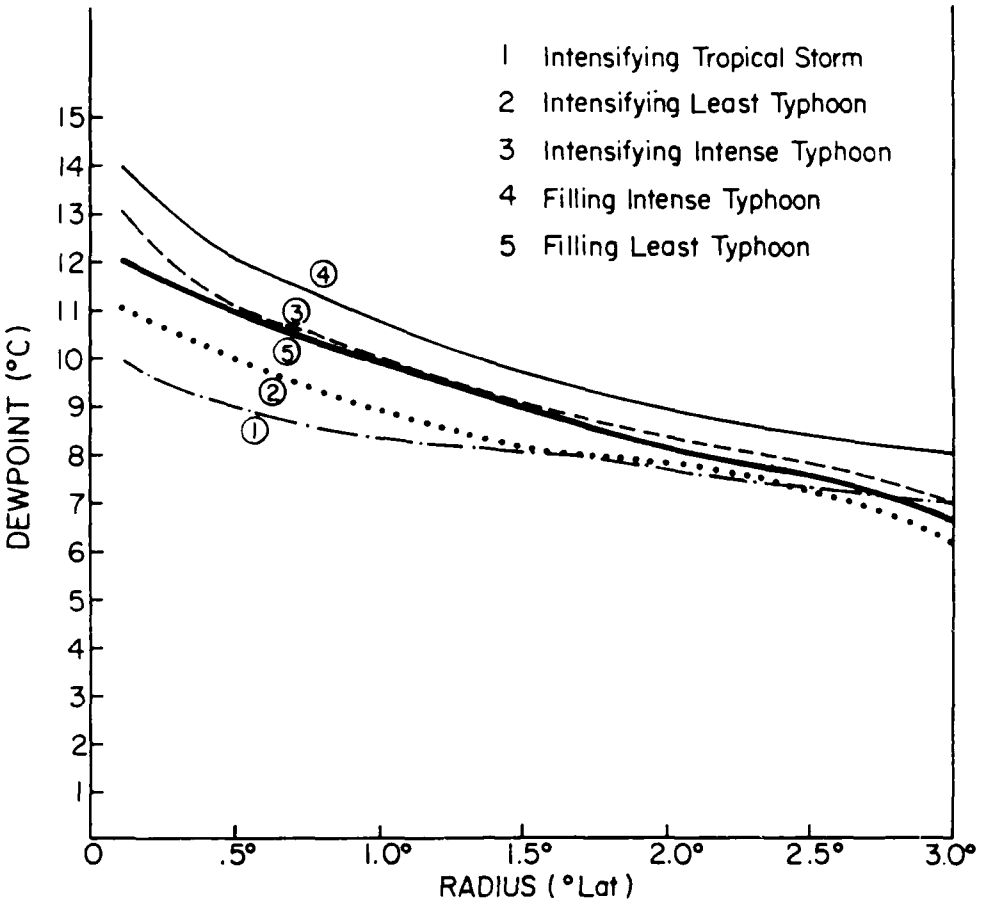

Figure 5.6: Dewpoint temperature fields for the five life cycle stages.

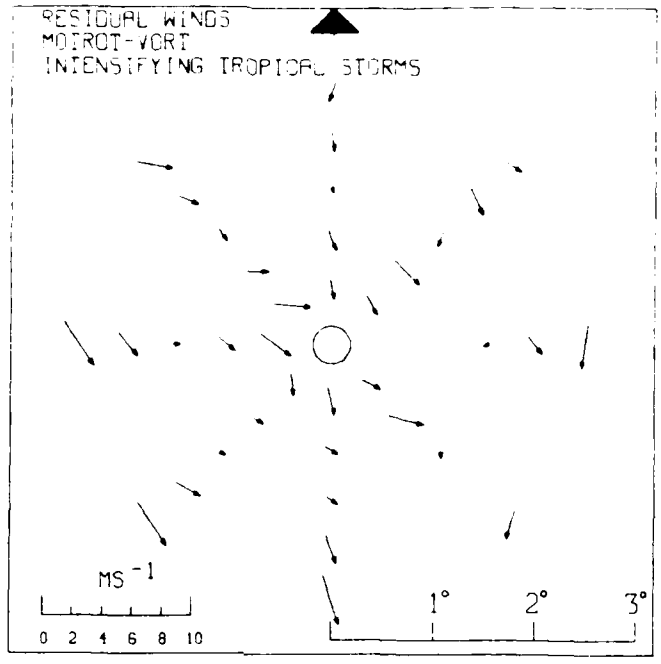

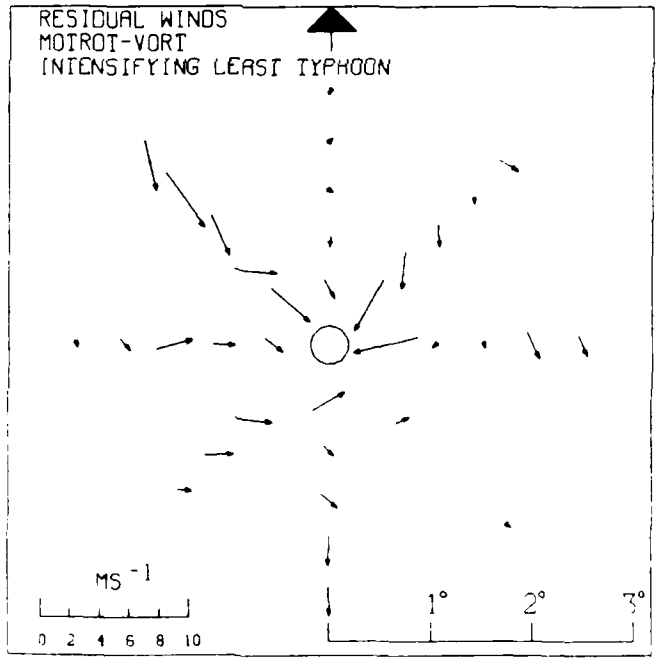

Figure 5.7: a-e. Plan-view depictions of the 700 mb residual wind field in MOTROT-VORT with the arrow on the rim denoting the cyclone heading of motion. Values are in ms^{-1} with arrow length implying speed as shown in the lower left corner.

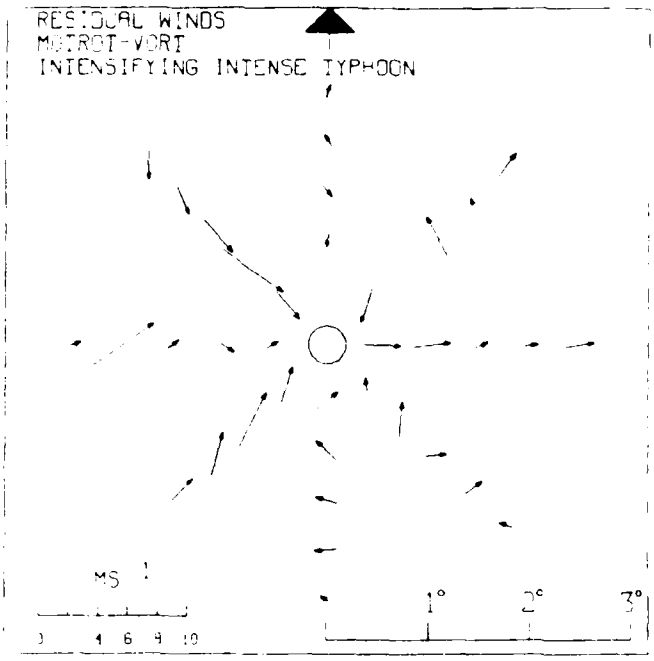

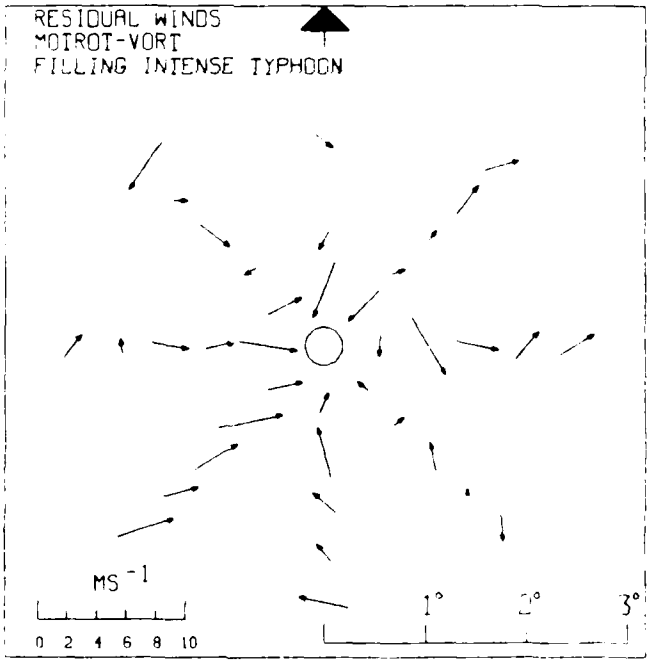

Figure 5.7: a-e. Continued.

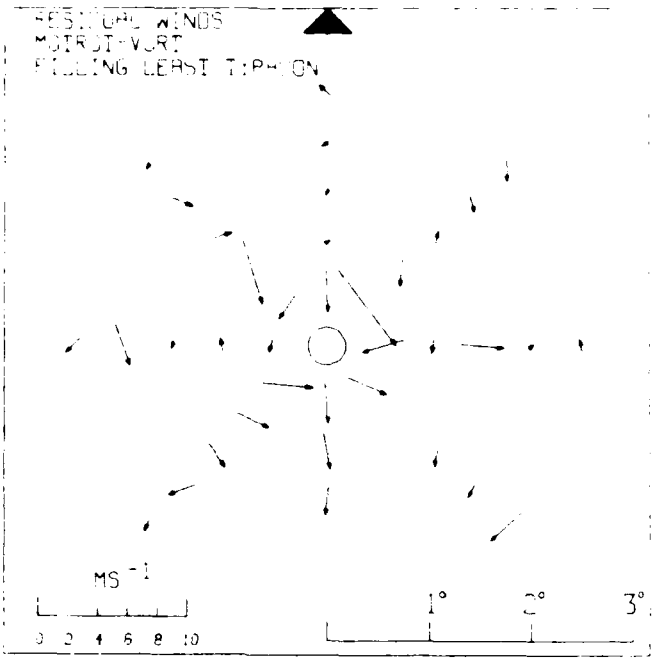

Figure 5.7: a-e. Continued.

the development phase, the entire wind field increases thus intensifying the inner core and strengthening the outer core. But after maximum intensity, the outer core does not necessarily weaken as the central pressure fills.

Table 5.2: Average positions, cyclone headings and speeds, MSLP and 24-hour changes, maximum wind speeds and outer core strengths for each phase; 1 = intensifying and strengthening, 2 = filling and strengthening, 3 = filling and weakening

PHASE	LAT.	LONG.	HEAD	SPEED	MSLP	MSLP CHANGE	MAX WIND	OCS
				ms^{-1}	mb	mb/12 hr	ms^{-1}	ms^{-1}
1	17°	136°	310°	5	953	-23	40	20
2	20°	135°	335°	5	939	+14	44	25
3	21°	133°	330°	5	967	+17	34	19

Phase 1 is the cyclone's intensification period in which the winds in both its inner and outer cores gather momentum. It may deepen slowly or rapidly, as will be covered in the next section, but its outer core strengthens as well. It is observed that on average, the

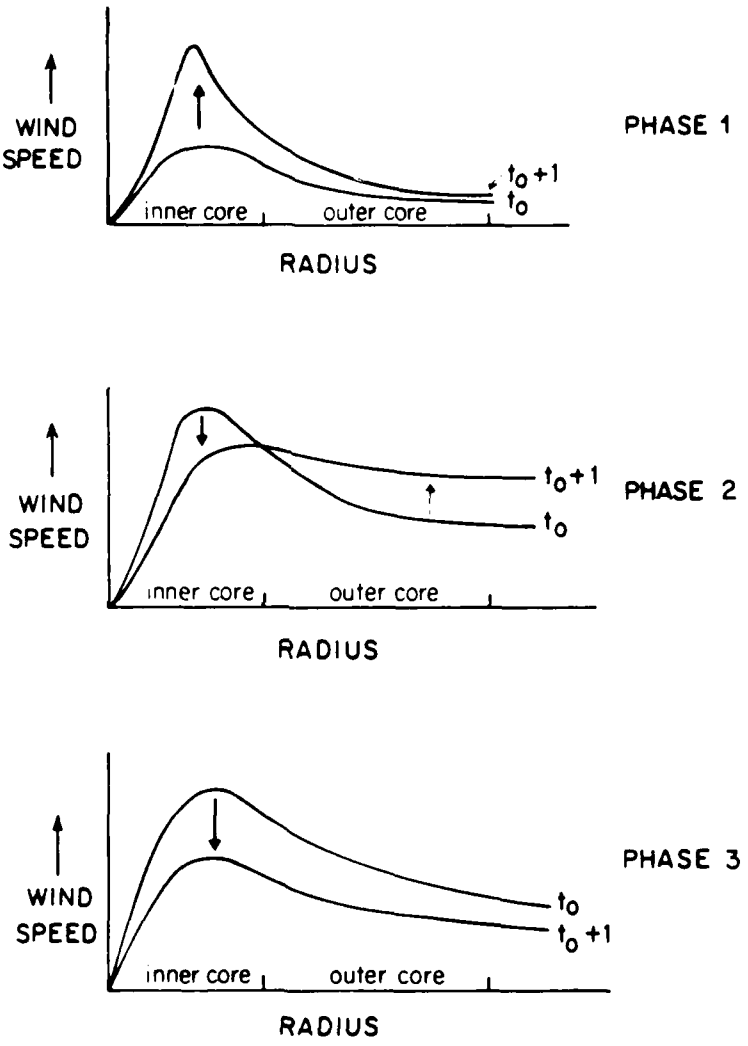

Figure 5.8: Schematic of the three possible wind profile phases where in phase 1 the inner core intensifies as the outer core strengthens, phase 2 depicts inner core filling and outer core strengthening, and in phase 3 the inner core fills as the outer core weakens.

inner core develops more rapidly (generally increasing maximum winds at 7.5 ms^{-1}/d as opposed to the outer core which increased at 2.5 ms^{-1}/d).

Evidently, the vortex concentrates its momentum close into the center in the intensifying phase. It is important to understand that these changes are occurring over a smoothed time period of days (4 days on average). Within this long time period small-scale changes can be quite variable as was noted in Weatherford and Gray, 1987b. They noted that in a period of 12 hours the outer core winds may remain unchanged while the inner core winds rapidly increased. These small-scale fluctuations are to be expected but when the same cyclones were studied throughout their deepening period, the outer core was observed to follow in kind by strengthening as well.

Once a cyclone passes its maximum intensity and fills, it converts its change patterns into either phase 2 or 3. (Cyclones can reach multiple maxima in MSLP as displayed by Supertyphoon Abby of 1983 and shown in the Appendix but the rule still applies.) If in phase 2, the outer core continues to strengthen at the same rate of 2.5 ms^{-1} as it does in phase 1. If in phase 3, the outer core weakens in conjunction with the inner core.

What then determines which phase the cyclone will follow as it fills? There appears to be an MSLP cutoff of 955 mb which determined whether a cyclone would weaken or continue to strengthen. The faster it fills the lower the MSLP at which the outer core weakens. As will be covered in the next chapter, this correlates well with the disappearance of the eye. Generally, a cyclone spent an average period of 4 days in phase 1, 1 day in phase 2 and 2 days in phase 3. Notice from Fig. 5.9 that the later the phase the farther from the center the inflow penetrated.

There is a fourth theoretically possible phase in which the inner core intensified at the expense of the outer core; thus, intensifying and weakening. Of the data set used here, no cases were found to match this type of change except those whose outer cores were over land and thus, due to increased friction, weakened while their center momentarily intensified (Supertyphoon Kim exhibited this effect while its center intensified to 909 mb but while its outer core was over land in Luzon island, Philippines). Thus, this fourth type of change has been discounted for the developed cyclone. Be reminded that the cases

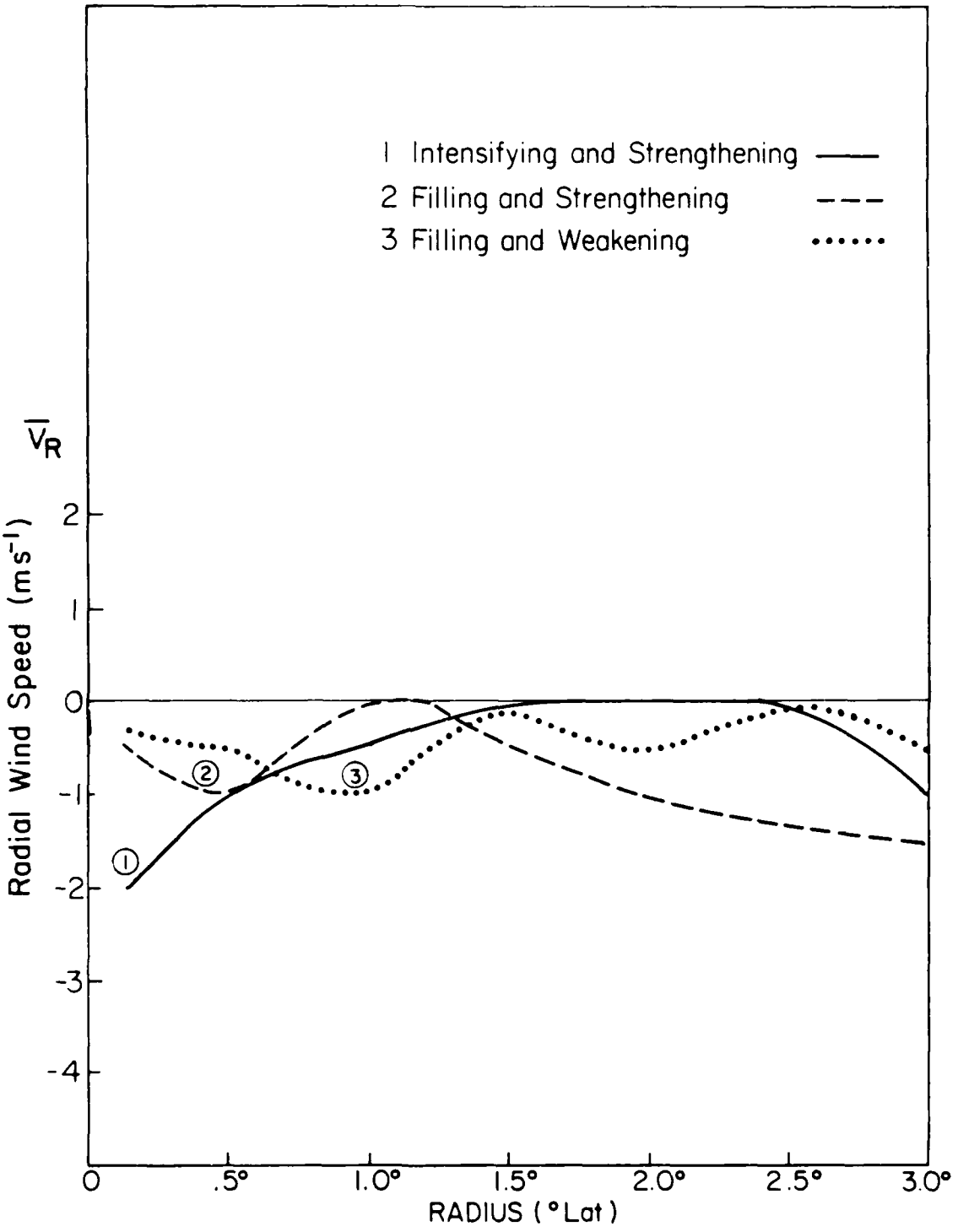

Figure 5.9: Azimuthally-averaged radial wind profiles for the three phases as defined in the figure.

studied here did not address the question of genesis for which this fourth type of change may be a possibility.

5.3 Deepening vs. Filling Cyclones of the Same Intensity

What then are the differences in the 700 mb wind field for cyclones of the same central pressures but in different phases (deepening vs. filling)? In order to isolate the differences between deepeners and fillers, two subsets were chosen, each with 235 missions, which bore the same MSLP so that the observed feature differences would not be due to MSLP differences. Table 5.3 lists various averages for each case. The most notable difference is the stronger OCS of the filling systems. This was not due to an expansion of the radius of maximum wind since the average eyewall diameters of each class was 40 km. Figure 5.10 shows this OCS increase from near the center to 3°. Note that the wind curves cross close to the center with the intensifying systems having the higher maximum winds. The outer core of the filling systems is thus a region of higher vorticity (Fig. 5.11). Notice that there is about 50% more vorticity at 2° radius with the filling system in comparison with the intensifying systems. Following inertial stability arguments, there should thus be more inflow for deepening cyclones due to their weaker outer core structure. This is indeed the case as seen in Fig. 5.12. The stronger outer core of the filling cyclones exerted twice the inertial stiffness as the deepeners given the same central pressure. Very likely, this is a factor in preventing low- level momentum from reaching the inner core of the filling systems. Apparently the inner radius to which inflow can penetrate is thus restricted for cyclones with a stronger outer-core circulation. Additionally, there is up to 50% less Kinetic Energy in the outer core of the intensifying system as shown in Fig. 5.13. This implies less momentum loss due to friction and less outer-core damage potential of intensifying vs. filling cyclones with the same MSLP.

There is also likely more rain in the outer core of a cyclone that is past its maximum intensity. It appears that an intensifying tropical cyclone sows seeds for its own subsequent weakening by its gradual build up of its outer core circulation which effectively reduces inflow from reaching the region of highest inner-core convective efficiency. Notice from

Table 5.3: Averages of position, cyclone motion, intensity and change, and OCS for cases *before* and *after* maximum intensity.

± MAX INT.	LAT.	LONG.	HEAD	SPEED	MSLP	MSLP CHANGE	MAX WIND	OCS
				ms^{-1}	mb	mb/d	ms^{-1}	ms^{-1}
Before Max	16°	137°	310°	5	956	-21	42	19
After Max	22°	133°	340°	5	956	+ 12	41	23

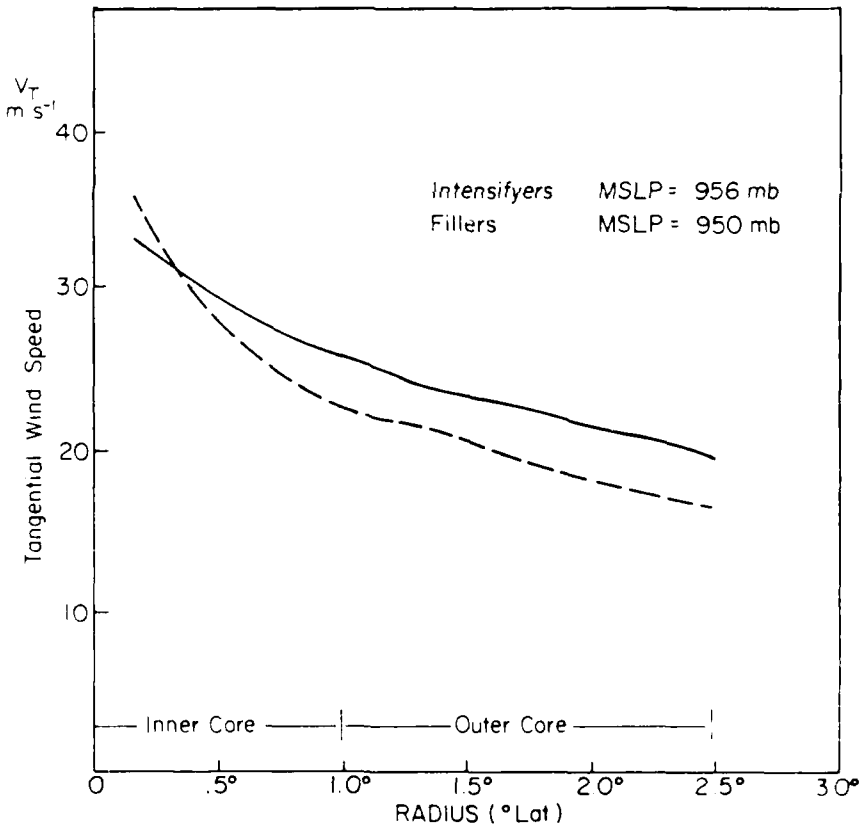

Figure 5.10: Azimuthally-averaged tangential wind profiles for intensifiers and fillers of the same MSLP.

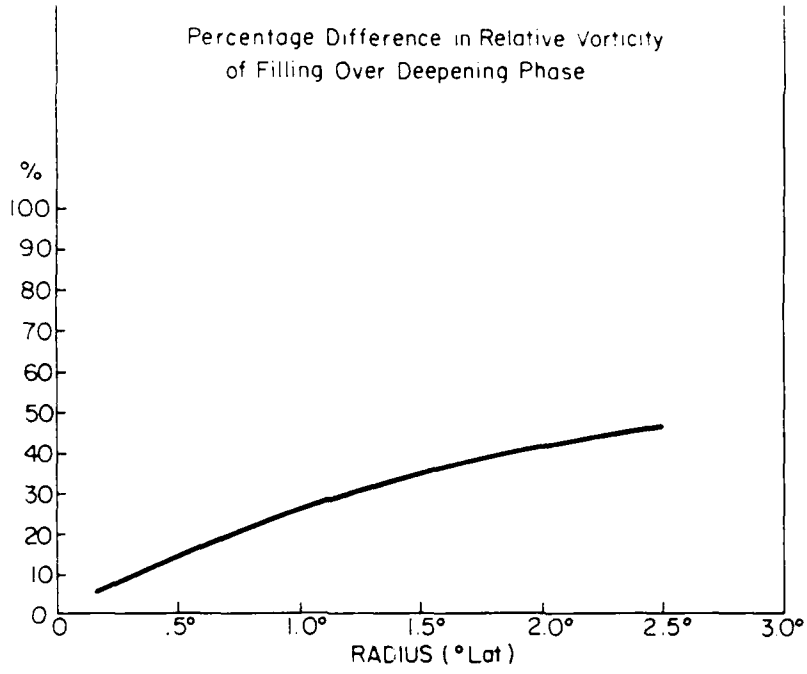

Figure 5.11: Difference (in percent) between the vorticity fields in fillers minus intensifiers given the same MSLP of 956 mb.

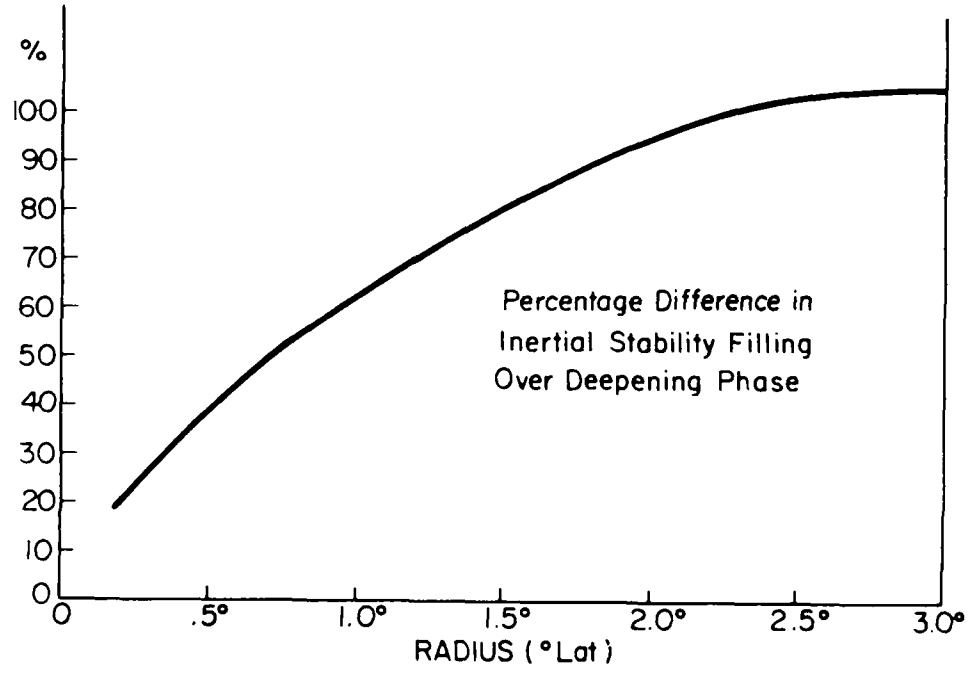

Figure 5.12: Difference (in percent) between the inertial stability fields of fillers minus intensifiers given the same MSLP of 956 mb.

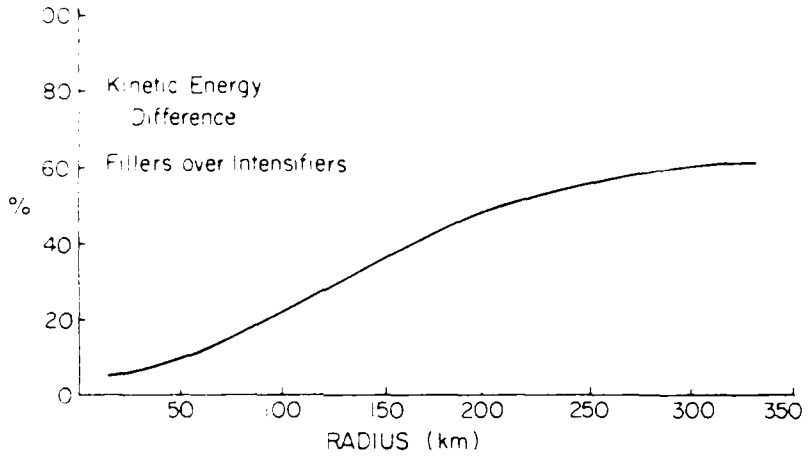

Figure 5.13: Difference (in percent) between the Kinetic Energy fields of fillers minus intensifiers given the same MSLP of 956 mb.

Fig. 5.14 that once past a certain OCS threshold, the stronger the OCS the less likely rapid inner core pressure drop will occur. We do not see typhoons attain intensities much below 870 mb nor would we expect to.

These advective processes act in a non-linear fashion and it is presumed that the faster they occur the deeper the cyclone can become. The rate at which a cyclone can intensify varies significantly from cyclone to cyclone and is the focus of the next section.

5.4 Rapid vs. Slow Deepeners

Rapid deepeners were defined by Holliday and Thompson (1979) as cyclones undergoing a period of intensification equalling or exceeding 42 mb in a day. This exceptional rate of change was observed in the northwestern Pacific in roughly one in seven cyclones. The circumstances that preceded this phenomenal rate of change are quite important for the forecaster to recognize because these cyclones can increase their maximum winds by values of up to 50 ms^{-1} in a day. Supertyphoon Forrest of 1983 was a tropical storm one day and a supertyphoon the next, nearly tripling the intensity of its maximum winds. By contrast, there are the slow deepeners which are defined here as those cyclones deepening at less than 9 mb per day. Differences in these two deepening rate classes can be significant.

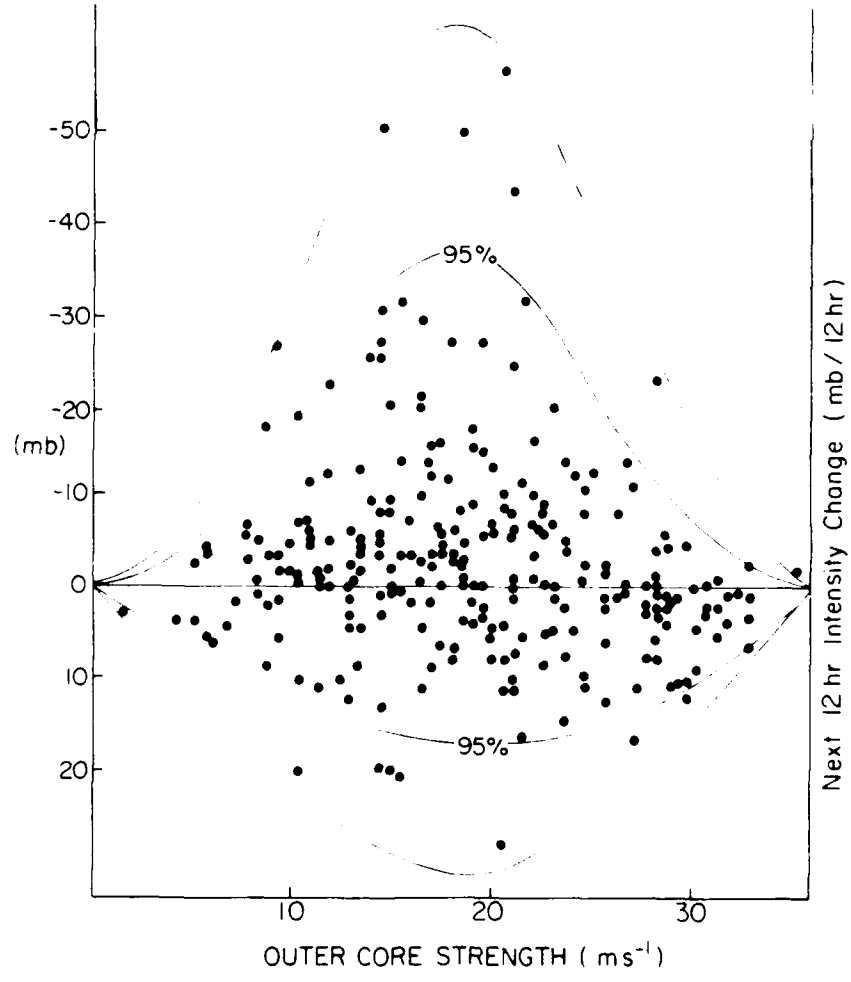

Figure 5.14: Scatter diagram showing the relationship between OCS and future intensity change.

Table 5.4 lists the averages of position, motion, intensity, and OCS for each deepening class. There were 20 cyclones in this data set that rapidly deepened providing 81 missions with which to analyze. Slow deepeners were naturally more abundant affording 200 missions. Rapid deepeners were located farther south and headed more to the west than their slowly deepening counterparts. Significant to note is the large difference in MSLP give the same OCS.

Table 5.4: Averages of position, heading and speed of the cyclone center, MSLP, maximum wind and OCS for rapid and slow deepeners.

RATE OF INCREASE	LAT.	LONG.	HEAD	SPEED ms^{-1}	MSLP mb	MAX WIND ms^{-1}	OCS ms^{-1}
RAPID DEEPENING	15°	136°	303°	5	945	44	18
SLOW DEEPENING	19°	137°	320°	5	971	31	18

The difference in OCS seems to be the key in distinguishing between the two cases. Rapid deepeners' OCS was 40% of the maximum wind speed as opposed to slow deepeners with OCS/maximum wind ratios equalling 58%. The wind field of the rapid deepener is observed to increase more rapidly toward the center than that of the slow deepeners, while the outer cores of both cases strengthen at generally the same rate. Apparently, the inner core of the rapid deepener concentrates more momentum in its inner core than slow deepeners. This can be seen from Fig. 5.15. Note how much more intense the rapid deepener is for the same outer core strength. One of the big clues in detecting the rapid deepener during its tropical storm stage lies with the appearance of its eye. This will be covered in detail in the next chapter.

5.5 Discussion

The wind profile of the tropical cyclone typically follows three patterns of change throughout its life cycle. Phase 1 is the intensification phase in which the wind field gathers

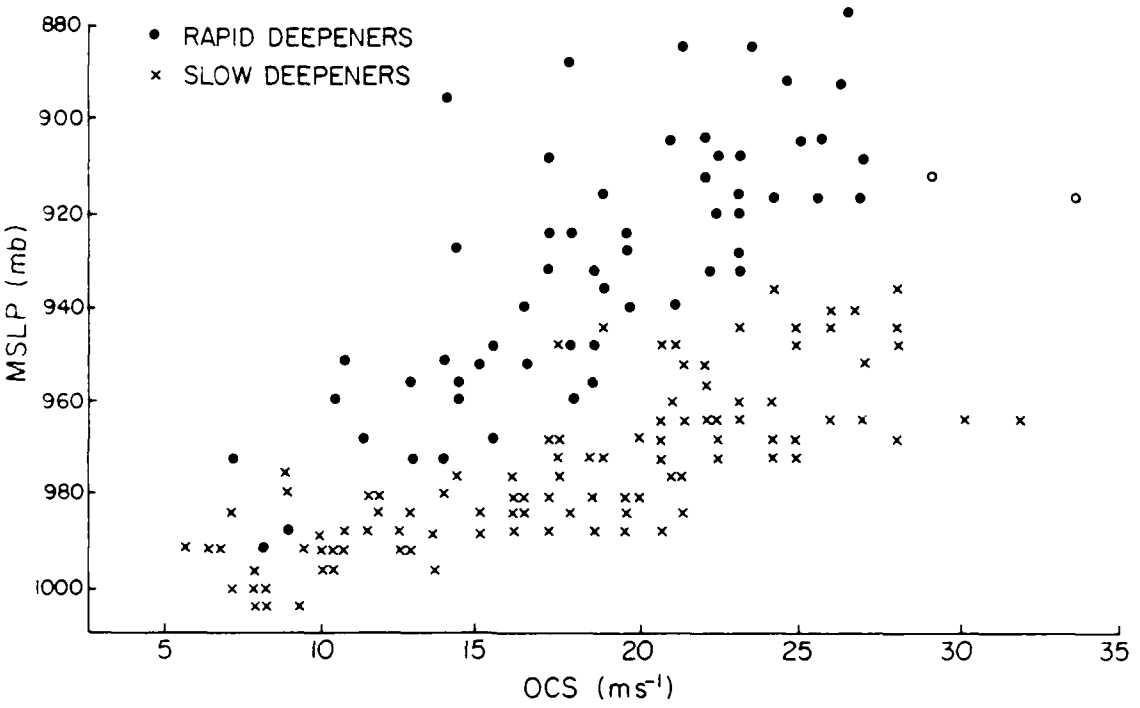

Figure 5.15: Scatter diagram of intensity (MSLP) versus OCS for rapid deepeners (denoted by circles and defined as an MSLP drop of 42 mb/d) and slow deepeners (denoted by X's and defined as an MSLP drop of less than 10 mb/d).

momentum and increases from the center to 3° radius. The inner core is observed to increase at a more rapid rate than the outer core as the cyclone concentrates its momentum near the center. What is not observed to occur is an outer core weakening while the inner core intensifies. Once past maximum intensity, the cyclone's center fills while the outer core winds either continue to increase, generally for typhoons of MSLP lower than 955 mb (Phase 2), or decrease for cyclones with MSLP higher than 955 mb (Phase 3).

There is cause to suspect that the strength of the outer core may have a restraining effect on the possible internal changes of the inner core of the cyclone. Willoughby (1979), Schubert and Hack (1982), and Shapiro and Willoughby (1982) have applied Elliasen's (1952) balanced vortex model to the hurricane in order to relate the effect that inertial stability has on its intensity change. Holland and Merrill (1984) applied these results to observations of Australian region cyclones suggesting that the strength of the low-level wind flow has a definite constraining effect on further intensity changes. Since it is inner core convection that must be energized in order to efficiently convert latent heat energy into kinetic energy, (Hack and Schubert, 1986) and is expressed in intensity changes, this outer core constraint on the inner core is observed. Typhoons that were filling generally exhibited twice the inertial stability in their outer cores than deepening typhoons of the same central pressures. This likely greatly inhibits momentum from reaching the region of greatest energy efficiency which lies near the center. Filling then commences. Since the behavior of the eyewall is a key factor in the intensification process, it is the focus of the next chapter.

Chapter 6

THE EYE AND THE WIND FIELD

The eye of the tropical cyclone is one of the most dramatic features seen by satellite, radar or direct observation. What makes the eye appear striking is the fact that a great many convective cells are tightly packed together into a ring and delineated by a sharp clear region in the center. It is no wonder that the eye of the storm grabs the attention of tropical forecasters for in addition to appearing so vivid, it is within the eyewall itself that the typhoon's strongest winds are located (as much as 90 ms^{-1} at the surface). This is where the energetics are most powerful, and where the author encountered the worst turbulence while flying through the typhoon region. Very little has been done to describe the basic features of the eye and its changes as the typhoon develops and decays. Thus, the focus of this chapter is to describe the natural progression of the eye size throughout the life cycle of the tropical cyclone and to relate the characteristics of the eye to other cyclone structural features.

6.1 Measurements of the Eye

During the five typhoon seasons of 1980-84 into which 101 cyclones were flown, 668 eyes were reported and measured during the flight missions. These spot measurements were generally taken 2 to 3 hours apart per mission with missions flown every 12 hours. Thus a 9 to 10 hour data void period would usually precede the next sighting of an eye which prevented an analysis of small time-scale fluctuations in its appearance. Data did, however, allow general eye size trends to be examined. Therefore, if a typhoon exhibited a continuous eye, it would normally be reported 4 times a day.

An eyewall was reported when it encompassed the center by at least 50% and was distinctly separate from a spiralling band of convection (feeder band). All measurements

were taken by the mission director on board who viewed the eye on the APN-59 3-cm radar from the flight level. (In this study, this usually meant at the 700 mb level, roughly 3000 m, but occasionally, while in an early-stage tropical storm, from 300 m. Throughout this study, measurements of the wind field were taken exclusively at the 700 mb level and will be in this chapter as well. But in order to adequately study the life cycle of the appearance of the eye, those rare low-level missions which noted an eye will be used.) Objective measurements were taken of the diameter of the eye as depicted in Fig. 6.1 (if circular; one diameter, if concentric; two diameters, and if elliptical; the diameters across both the long and short axes and their orientation), resulting in 668 reports.

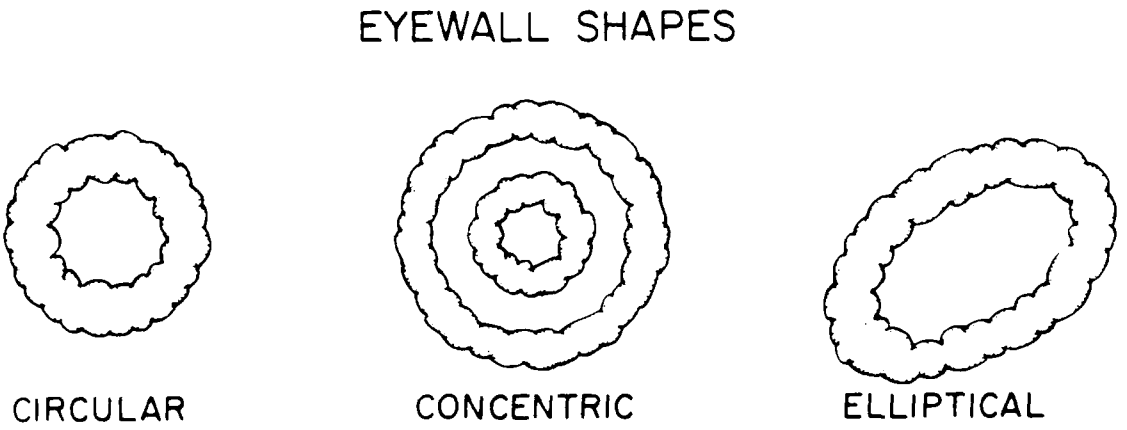

Figure 6.1: Schematic depiction of the three types of eyewalls observed; circular, concentric, and elliptical.

In addition to recording the size of the eye, subjective descriptions were included to answer questions such as; how much of the eye was encompassed by an eyewall, did the wall cloud appear diffuse or dense, how thick was the wall, and what was its general appearance, whether it produced the effect of a stadium, implying the wall expanded with height, or the effect of a fishbowl, denoting that the uppermost portion was filling over with cirrostratus, as shown in the schematic of Fig. 6.2. These latter subjective descriptions were provided in only the most intense cases in which the inner region was cloud-free from the boundary layer to the top due to powerful subsidence. However, in less intense cyclones, the area within the eye was often scattered with clouds too diffuse to be picked up on radar but visible to the eye and extending from the surface to the

tropopause, thus rendering an obscured visual depiction of the eye. The more intense the cyclone the fewer clouds remaining in the eye. Yet, even in the most intense typhoons, in which the eye was often clear from 1,500 meters to the top, there were always clouds which nearly covered the surface indicating that the subsidence did not penetrate boundary layer convergence thereby allowing positive vertical forcing on the moistened near surface air. After all reports of the eye were compiled, life cycle patterns of the eye were examined and compared with other structural features.

The size of the eye varied from 7 to 220 km in diameter for the typhoons of 1980-84 as depicted in Fig. 6.3 and averaged 42 km. In order to contrast differences, these have been classified by size into four bins- -small eyes (0 to 28 km), medium eyes (28 to 55 km), large eyes (greater than 55 km) and cyclones exhibiting no eye. Cyclones exhibit an eye nearly as often as not during their natural over water lifetimes with greater probability of an eye associated with higher intensities. Of those that display an eye, medium eyes were the most common. The medium eye class was determined so that it equally bounded the average diameter seen and comprised the class with the greatest number of sightings. Although most eyes fell into the medium class, those that fell significantly smaller or larger than this were classified separately in such a manner that small eyes were really tiny in comparison to the average while large eyes were quite immense. Notice from Fig. 6.3 how variable the size of the eye is with intensity. There have been small eyes observed in both tropical storms and supertyphoons.

Clearly, the intensity of a cyclone does not determine the size of its eye. (Cyclone eye size correlates with MSLP at -.09.)

6.2 The General Behavior of the Eye

The eye followed a general pattern of contracting while it intensified and expanding as it filled. This has been alluded to before by Jordan (1961) and will be shown in greater detail here. Yet this was not observed to be a hard and fast rule. Fluctuations in size on the time scale of 3 to 12 hours could be quite significant, however, if the size of the eye were smoothed in time, this general pattern was followed. Therefore the caveat that must

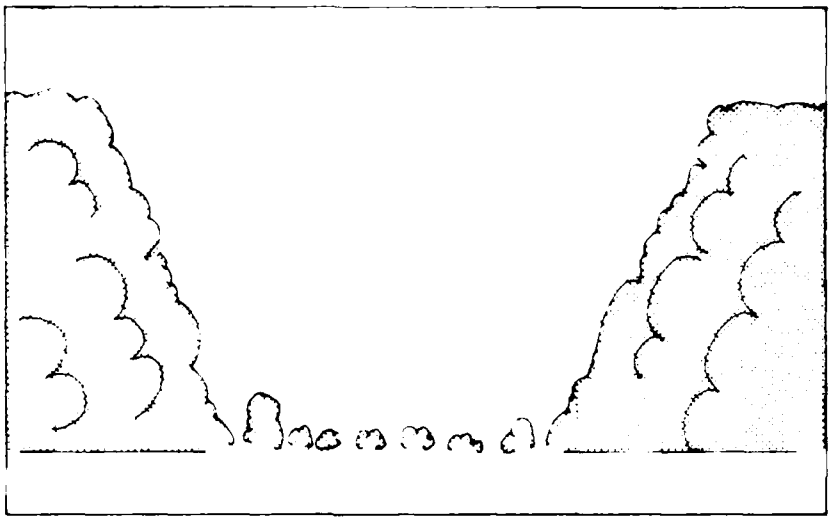

Stadium Effect

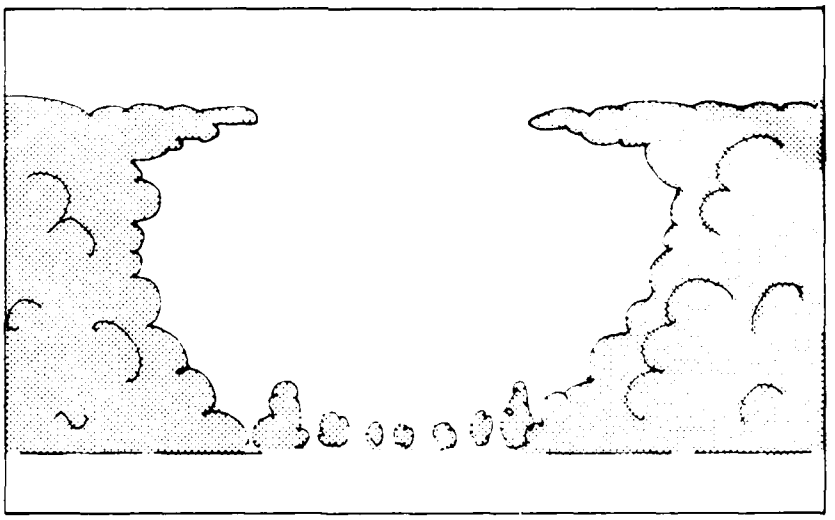

Fishbowl Effect

Figure 6.2: Schematic depiction of the eyewall viewed from the WC- 130 aircraft of the stadium and fishbowl effects.

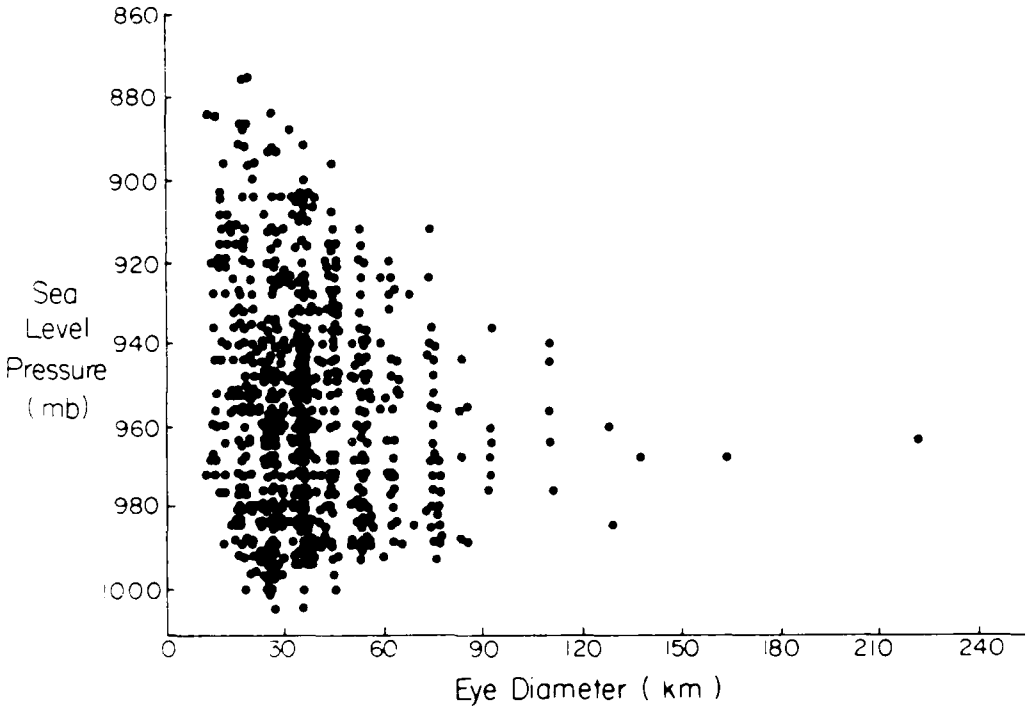

Figure 6.3: Scatter diagram of MSLP versus eye diameter.

accompany this observation is that if the eye has expanded in 3 hours, one cannot say with certainty that the central pressure has risen. Small-scale fluctuations are to be expected. Furthermore, there is a period of time, common to the most intense cyclones, in which the eye reaches a certain minimum size and remains locked into place even though the central pressure continues to fall. Thus, eye size and MSLP changes did not necessarily occur simultaneously.

Diurnal changes in the diameter of the eye at the 700 mb level as seen by aircraft radar were not observed. Zehr, 1987, showed significant diurnal variations in the area of coldest cloud tops in the inner core of a few of the same cyclones used in this data set. This implies changes in the strength of the convection occur independently of changes in the 700 mb diameter of the eyewall in a diurnal sense.

6.3 The Initial Appearance of the Eye

What has not been addresed in the literature is the initial appearance of the eye. It has been assumed to materialize when the cyclone reaches typhoon proportions but is this

indeed the case? Do cyclones that later become rapid deepeners show different eye characteristics prior to rapid intensification? When do concentric, circular, or elliptical eyes appear? Finally, when does the cyclone's eye disappear and under what circumstances?

Three-fourths of the cyclones studied produce an eyewall. When they do, the initial appearance of an eye corresponds to the cyclones' approach to typhoon intensity at 982 mb, ± 10 mb. Typhoons in the northwestern Pacific are designated as typhoons when their MSLP reaches 976 mb. (This was determined by Atkinson and Holliday to correspond to 64 kt of surface wind (33 ms^{-1}) and is widely used operationally.) However, there were cases which significantly deviated from the average.

Typhoon Ellen of 1983 exhibited an eye at the earliest intensity of 1000 mb, while Typhoon Betty of 1980 did not obtain an eye until its MSLP reached 951 mb. It is interesting to note that Ellen's initial eye was small while Betty's was large. This dependence of an initial eye's size on its MSLP seemed to be a common feature in all cases.

Table 6.1: Average, standard deviation and number of cyclones whose initial appearance of an eye corresponded to a small, medium, or large eye as defined above.

EYE CLASS	MSLP	STANDARD DEVIATION	NO. OF CYCLONES
SMALL	988 mb	± 10 mb	17
MEDIUM	982 mb	± 10 mb	45
LARGE	979 mb	± 9 mb	15

6.3.1 Elliptical Eyes

The initial eye was often elliptical and became more circular with intensity. It seemed to be a characteristic feature that elliptical eyes reflected a disorganization to the eye. Furthermore, large changes in elliptical size are typical. Elliptical eyes changed in diameter an average 9 km every twelve hours as opposed to circular eyes which expanded or contracted an average 2 km/12 hr. Elliptical eyes generally appeared in the early stages or late, filling stages of the cyclone. Far fewer elliptical eyes were found in intense stages. Evidently, the cyclone in transforming its central cloud fields into an eyewall only gradually forms a circular eye. In the early, less intense stages, the cyclone exhibits large changes in size

and odd shapes. One might wonder if the cyclone which is concentrating its convection into an eye is in search of a position of maximum efficiency in this initial stage.

6.3.2 Rapid Deepeners

Cyclones which later became rapid deepeners (42 mb/d MSLP drop) exhibited an eye at an earlier stage of development (985 mb) than other cyclones (980 mb for all but rapid deepeners). Rapid deepeners not only tended to form an eye earlier in their development than slow deepeners but develop a smaller eye as well. This was likely due to non-linear advective processes which act to concentrate energy into the core of the cyclone at a quicker rate for the rapid deepeners than for the others. Recall that the outer core strengthened at a relatively constant rate of 2.5 ms^{-1}/d throughout the intensification period. Therefore, the earlier an eye could form, the weaker and less inertially stable the outer core through which the needed momentum must pass through and the easier a cyclone could concentrate this momentum near its center. It is important to note that rapid deepeners usually began their rapid deepening period as soon as the eye appeared with an initial eye diameter of 40 km, as opposed to 50 km for all but rapid deepeners, and ended the rapid deepening phase with a considerably reduced eye, on average, of 20 km in diameter. Thus, rapid deepeners had a head start in their intensification process and could often be identified while tropical storms by their early eye appearance.

For the great majority of cyclones, this initial appearance of the eye occurred in the tropical storm stage which, following Atkinson and Holliday's technique, corresponded to a maximum wind of 27 ms^{-1} (53 knots) for rapid deepeners and 30 ms^{-1} for all but rapid deepeners. The OCS was generally 10 ms^{-1}, thus a period of time in which the cyclone's inertial stability was quite low. This allowed the tropical cyclone to more readily import moisture through inflow processes. These differences in the wind field help to explain the processes by which rapid deepeners form at a quicker rate than slow deepeners but are unlikely to be easily detected by the forecaster. What can be observed is the earlier appearance of the eyewall assuming reliable eye and central pressure information can be obtained.

6.3.3 Early vs. Late Initial Eye Appearance

In order to further isolate the appearance of the eye, a study was done contrasting early vs late eye appearance. These were chosen such that at the same average MSLP of 987 mb, cyclones which already had an eye could be contrasted against cyclones which had not yet attained an eye. Rapid deepeners and cyclones forming an eye at higher MSLP's than the average fell into the early class, while those whose eye formed after the average MSLP fell into the late class. Table 6.2 lists various averages for each. Note that cyclones showing an eye early in their development were generally farther southeast than the others. Maximum wind speeds were the same but their OCS' were less. Although small ($3\ ms^{-1}$), this difference appears to be significant and may support a type of inertial stability argument. Notice from Fig. 6.4, the relative vorticity is 50% higher for late eye-appearing cyclones corresponding to double the inertial stability thus effectively putting a stronger constraint on the radial inflow. The ease with which a cyclone can import momentum through the outer core and near the center is vital to its further capacity to intensify.

Table 6.2: Averages of position, cyclone motion, intensity, intensity change, and OCS (Outer Core Strength) for cyclones in which the eye appeared early vs. those whose eye appeared late in their development.

EYE APPEAR-ANCE	LAT.	LONG.	HEAD	SPEED	MAX WIND	MSLP	MSLP CHANGE	OCS
				ms^{-1}	ms^{-1}	mb	mb/d	ms^{-1}
EARLY	14°	141°	290°	6	24	987	- 10	11
LATE	17°	138°	315°	5	24	987	-7	14

The inflow processes, so vital to a cyclones development, delineate the differences between the early and late developing eyes more clearly. Figure 6.5 depicts the azimuthally-averaged radial winds after the cyclone's motion has been removed. Cyclones forming eyes early had significantly greater inflow inside 150 km from the center. Notice from the plan-view depictions of Figs. 6.6a and b how much the near environment was drawn

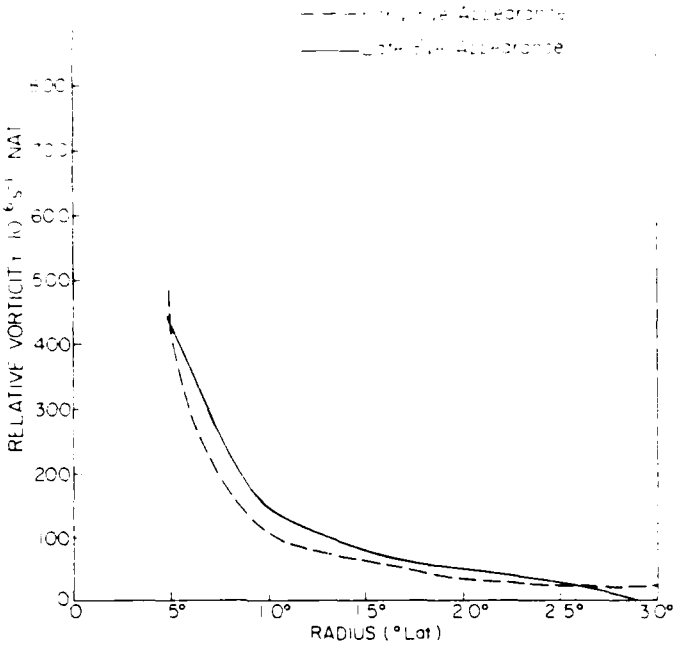

Figure 6.4: Azimuthally-averaged vorticity fields for early versus late eye forming cyclones.

into the cyclones which developed an eye earlier than other cyclones. The divergence patterns (Fig. 6.7) reflect this concentration of flow close to the center in this early stage of intensification.

6.4 The Eye During Intensification

After the eye appears, the cyclone speeds up its intensification rate no matter what the initial size. Prior to the initial appearance of the eye, the cyclone generally intensifies at 8 mb/d. Once the eye forms, however, this rate then increases to, on average, 20 mb/d, for cases still in the tropical storm stage. This 250% increase in MSLP drop clearly enhances the intensity of the cyclone. Recall that rapid deepeners were generally the first to obtain an eye thereby gaining the initial advantage in concentrating energy quickly into the inner core while the outer core was still weak. The average deepening rate throughout the entire deepening period for cyclones with eyes is 24 mb/d. Apparently the eye reflects the cyclones ability to concentrate energy into the core.

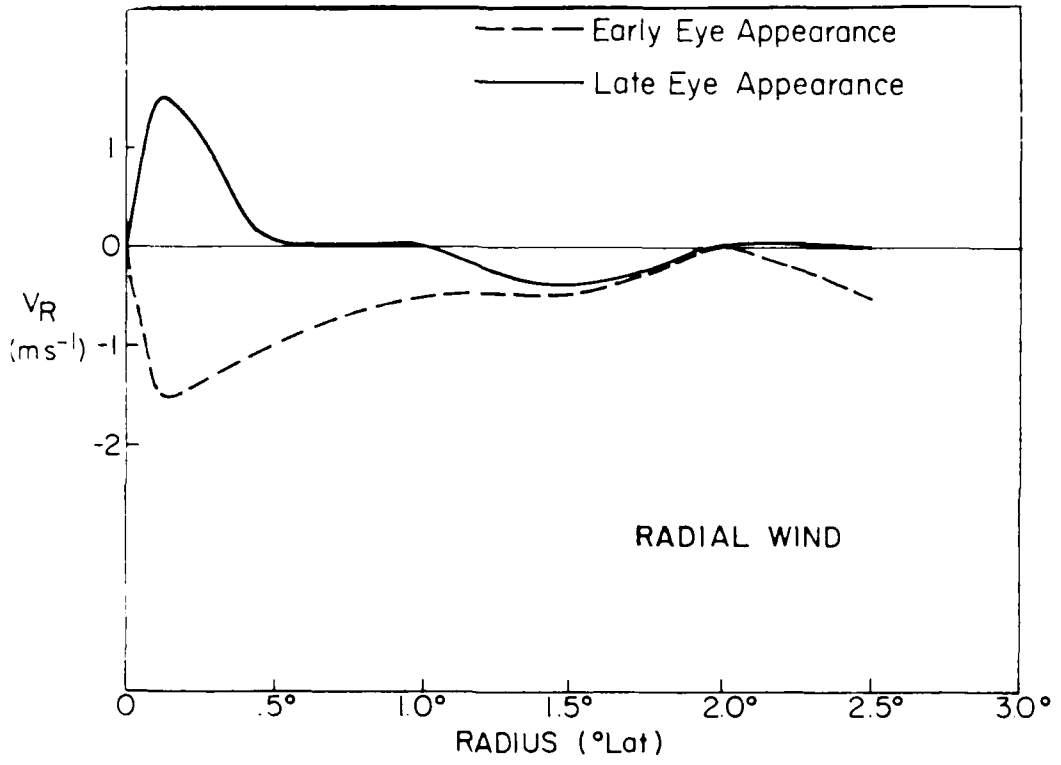

Figure 6.5: Azimuthally-averaged radial wind fields for early versus late eye forming cyclones.

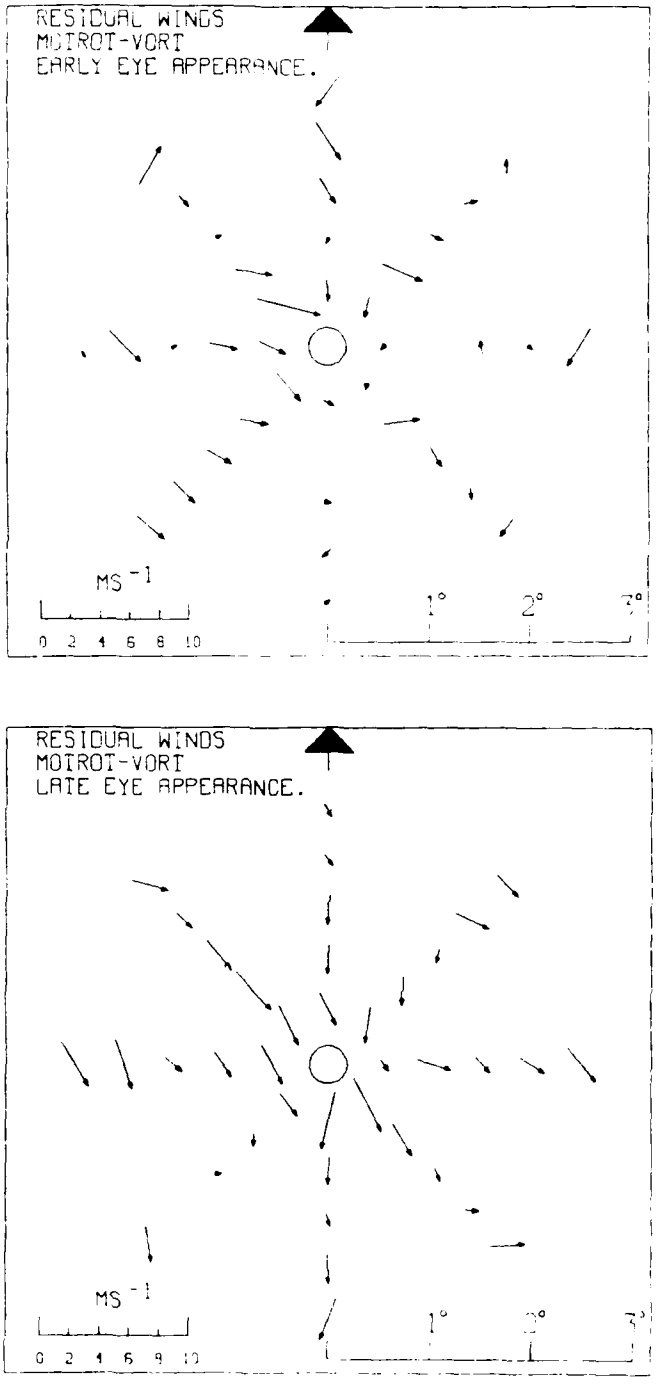

Figure 6.6: a-b. Plan-view depictions of the 700 mb residual wind field in MOTROT-VORT with the arrow on the rim denoting the cyclone heading of motion. Values are in ms^{-1} with arrow length implying speed as shown in the lower left corner. The classes are for a) early versus b) late eye forming cyclones.

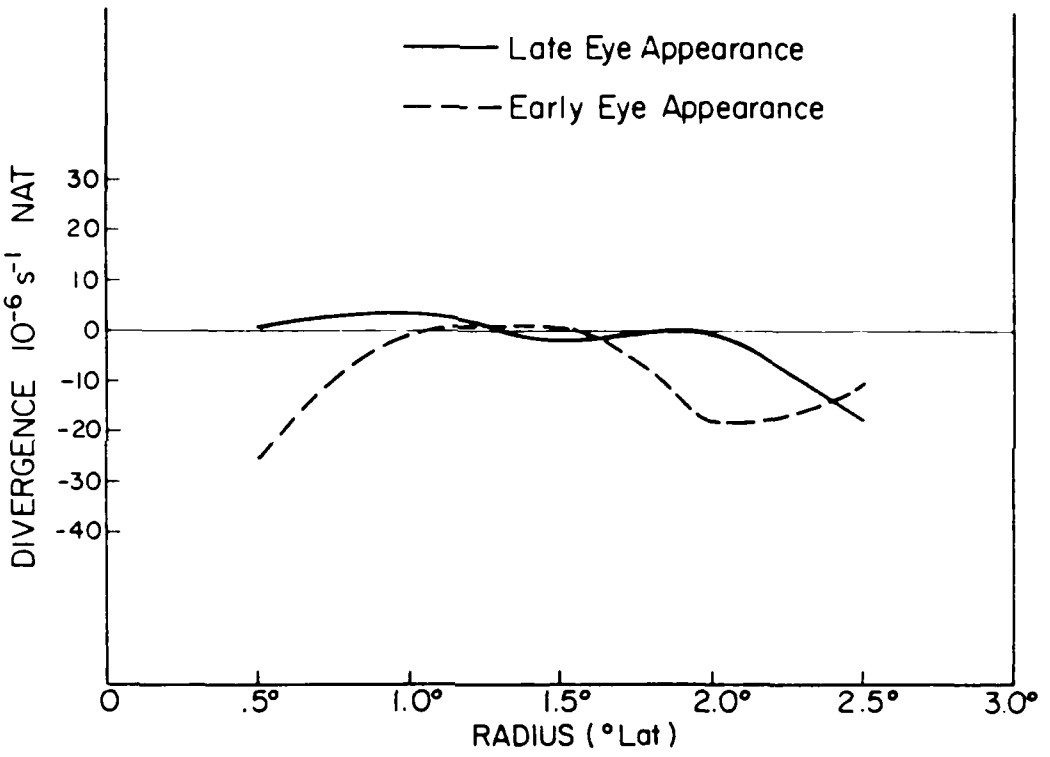

Figure 6.7: Divergence fields by radius for early versus late eye forming cyclones.

It was also characteristic of the eye to contract while deepening, no matter the rate of deepening or the initial size of the eye. The Appendix provides many examples of the change in the eye's size as the MSLP drops intensity. Some cyclones form an initially large eye and show sizable contractions while those with small initial eyes, with much less room to contract, show slight changes in size. There is evidently a minimum size which an eye could attain which varied for each case. However, once a cyclone attains its maximum intensity, it usually exhibits its smallest eye. The smallest eyes observed were 7 km across for Typhoons Dinah of 1980 and Gay of 1981. So, while the eye contracts with intensity, it reaches at least this minimum size. This further intensification at which no contraction is evident may, in some cases, last a few days as in the case of Supertyphoon Forrest of 1983. It was often at this steady state period of the eye's size when concentric eyes appeared.

6.5 Concentric Eyes

Concentric eyes, when they appeared, occurred only for those cyclones which had MSLP pressures lower than 945 mb. Observations of concentric eyes were relatively rare, occurring for 4% of all individual period eye sightings but in 16% of all cyclones. Generally, if a cyclone exhibited concentric eyes, it occurred an average 3 days after the initial eye sighting and was seen in most cases only once in its lifetime. Recall that there was generally a 9-10 hour data void period between missions in which no reports of an eye were provided, therefore the changes that preceded or followed the observation of a concentric eye on timescales shorter than this are unknown. A few typhoons exhibited concentric eyes for two consecutive missions. But in no case did this extend beyond 15 hours. Consecutive eyes are thus observed to last only a fraction of a day. Note the cases of Supertyphoons Wynne (1980) and Vanessa (1984) in the Appendix. Concentric eye diameters were on average, 20 km for the inner eye and 55 km for the outer eye (recall that the average eye regardless of shape or MSLP is 42 km across).

The average MSLP at concentric sighting was 925 mb located at 17° N with the highest MSLP of 946 mb and lowest of 886 mb. It seems this occurrence corresponded to the time in which an intense typhoon was in the process of switching over from a deepening

to a filling stage. When concentric eyes were observed, 30% were in deepening typhoons, 20% at the period in which the MSLP had bottomed out and was steady, and 50% of the time while filling. All were circular, both inner and outer eyewalls. Willoughby,

6.6 Eye Characteristics During Cyclone Filling

While filling, the eyewall generally expands until it was so diffuse as to no longer be recognized as an eye. The faster the filling rate, the quicker the eye disappears. Supertyphoon Wynne (1980) lost its eye while over water at the most intense stage of 927 mb without reappearing over the next few days in which it filled. This is the lowest pressure for eye disappearance of this data set. This is in notable contrast to the MSLP at which the eye first appears (980 mb). On average, a cyclone filling over water lost its eye near 954 mb.

Cyclones lose their eyes at same time that they stop strengthening which is independently observed, on average, to be at 955 mb. Figure 6.8 depicts the height field for Supertyphoon Abby every 0.5° from the center in order to pinpoint these effects more clearly. Notice how the height field in the outer core continued to lower six days after the height at the center began its rise. The outer core ($\sim$ 2.0° radius) heights started rising when Abby lost its eye (Fig. 6.9). Therefore, even though a cyclone's central pressure fills, as long as an eye exists, momentum continues to be advected through the outer core towards the eyewall thereby strengthening the outer core. Once the eye disappears, however, the outer core begins to weaken as well, marking the beginning of the decay of the entire vortex.

6.7 Eye Characteristics Related to Core Winds

The eyes, classified by size, showed greater concentration of core region (< 2.5°) air the smaller they were. These classifications along with the number of sightings in each class are defined as follows:

EYE CLASS	RANGE OF DIAMETERS	NO. OF SIGHTINGS
SMALL EYE	< 28 km	164
MEDIUM EYE	28 to 55 km	411
LARGE EYE	> 55 km	91
NO EYE	—	755

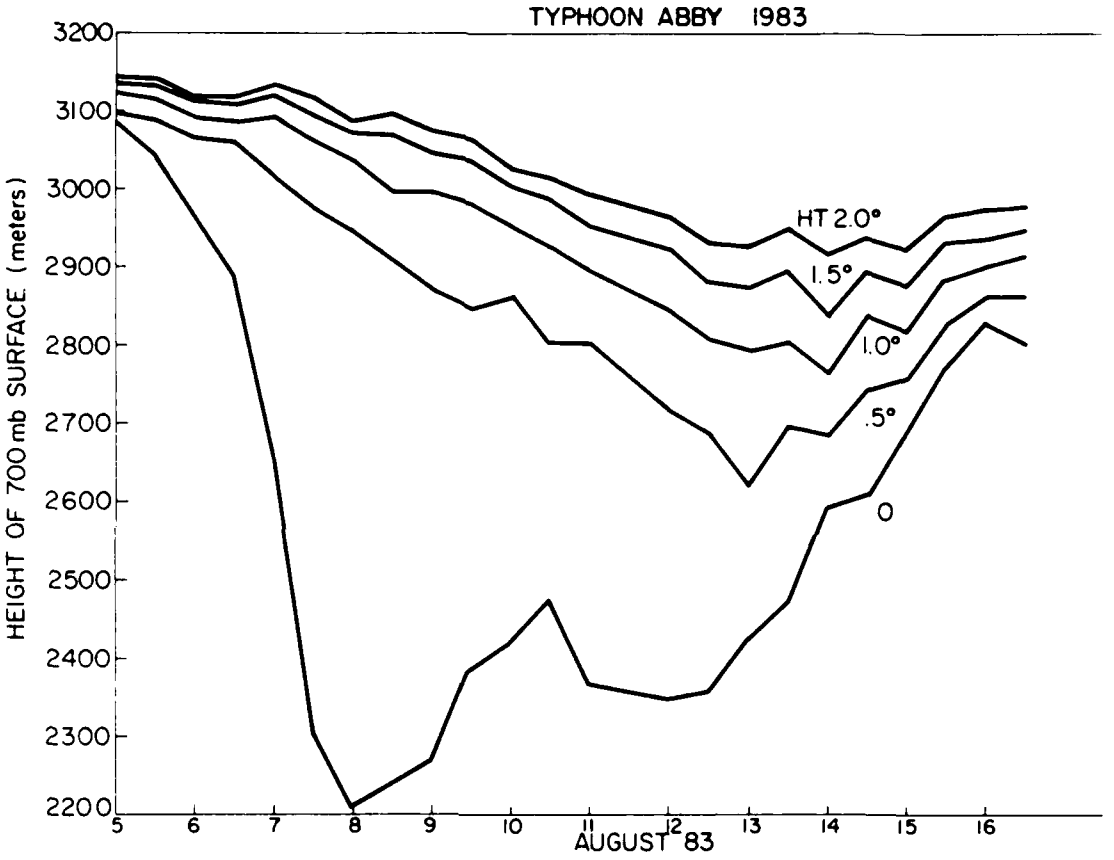

Figure 6.8: 700 mb height versus time profiles at the center (0°), .5°, 1.0°, 1.5° and 2.0° for Supertyphoon Abby.

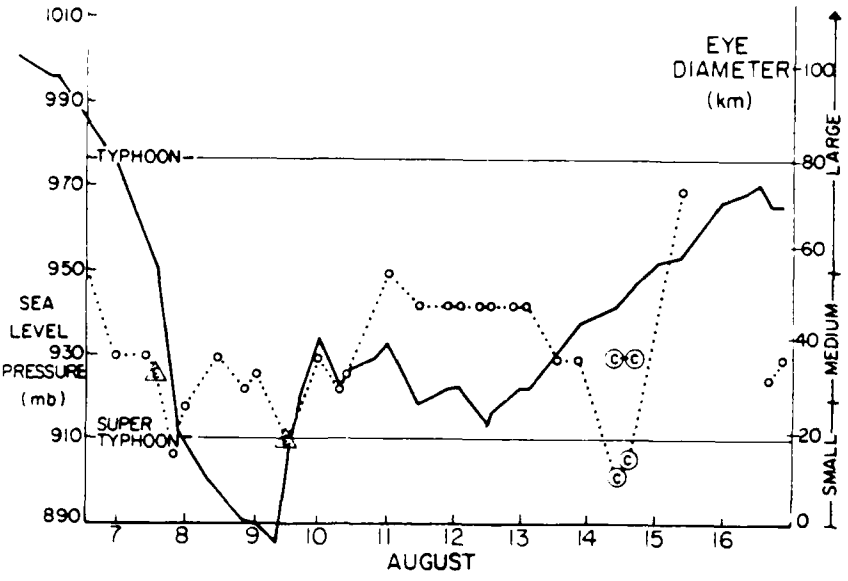

Figure 6.9: Evolution of MSLP and eye diameter versus time for Supertyphoon Abby.

Table 6.3 depicts the averages of various parameters for each eye class. All eye classes lie in the same geographical region, have the same forward speed, and direction. Even the intensities were very close to being the same. Therefore the differences lay elsewhere than with position, motion or intensity. Notice, however, the difference in the OCS. From Table 6.3 it can be seen that the smaller the eye the higher the intensity and, yet, the weaker the outer core. This likely contributes to the greater concentration of momentum into the inner core. For instance, at 100 km, the inertial stability of the large eye was double that of the small eye. Thus, subtle differences in the magnitude of the wind could provide significantly different forcings on radial motions.

The height fields provide further support to the contention that the smaller the eye, the more focused the energy and momentum near the center. In Fig. 6.10, the 700 mb height profile was scaled to the central pressure and environmental values. A scaled height of 100% equalled the height of the environment following the equation:

$$ht_r - ht_c / ht_\infty - ht_c \tag{6.1}$$

Table 6.3: Averages of position, cyclone motion, intensity and its change, and OCS for each eye-size class.

EYE CLASS	LAT.	LONG.	HEAD	SPEED	MAX WIND	MSLP	MSLP CHANGE	OCS
				ms^{-1}	ms^{-1}	mb	mb/d	ms^{-1}
SMALL	17°	137°	315°	5	42	951	- 16	19
MEDIUM	18°	135°	317°	5	42	955	-10	20
LARGE	19°	137°	318°	5	41	961	-2	22
NO	19°	137°	320°	6	27	985	-1	16

where ht_r = the height at radius r, ht_c = the height at the center, and ht_∞ = the height well away from the storm (3130 m). Thus, in the figure one can see how the height gradient is more concentrated in the center for the smaller eyes. This is to be expected.

6.7.1 Eye Size Related to Interior Wind Fields

Figures 6.11a-d portray 700 mb radial wind fields in the NAT coordinate system which are associated with the various eye sizes. Little asymmetric differences are found. Generally the cyclone is embedded in a similar 700 mb steering current regardless of eye size. This also is the case when viewed in the cyclone relative coordinate system as shown in Figs. 6.12a-d. Radial winds are observed to flow through the cyclone at 700 mb from the left front to right back. Differences are found, however, in the residual wind field shown when both radial and tangential components are combined as in Figs. 6.13a-d. This residual wind shows distinct inner core concentration on the small and medium eye classes contrasting with general flowthrough for the cyclones without eyes. Notice in Fig. 6.13d that cyclones without an eye generally reflect the 700 mb steering current but once an eye exists more of this steering current is drawn into the center with less passing through to the other side.

6.8 The Temperature of the Eye

The temperature inside the eye is indirectly an indication of the force of the vertical motions in the eyewall convection which, in turn, induces subsidence warming in the center.

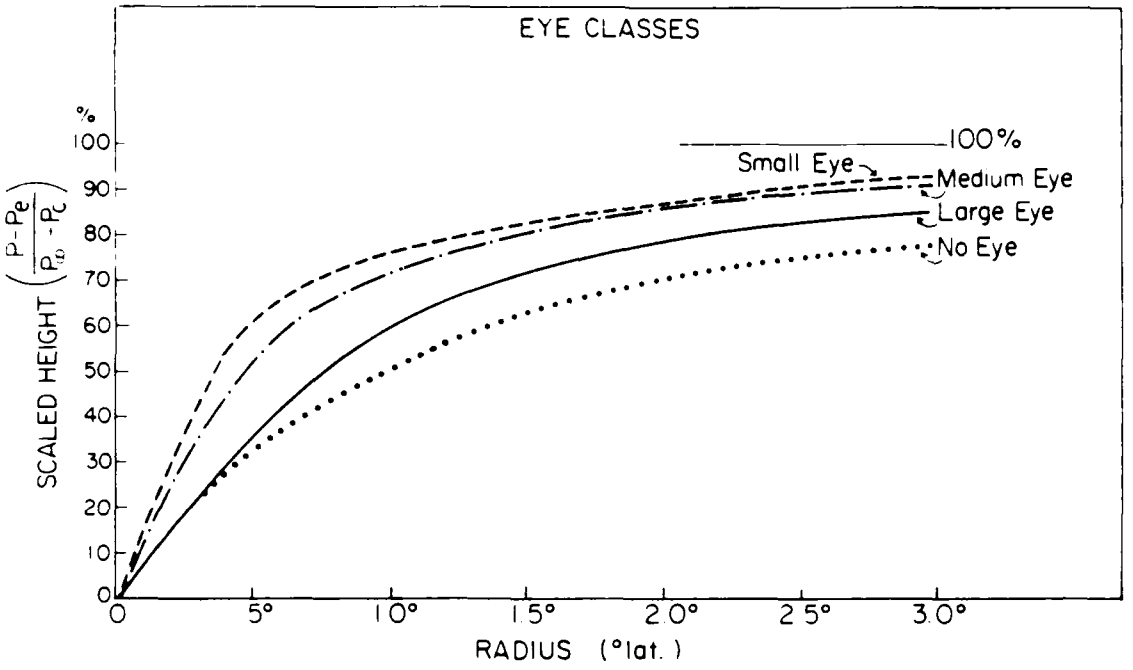

Figure 6.10: 700 mb height field for the four cases of eye size, scaled by the equation: $h_r - h_c/h_\infty - h_c$.

The stronger the eye-wall convection, the warmer one would expect the eye temperatures to be. Generally, the average temperature in the Tropics at the 700 mb level is 10° C. The highest temperature measured at 700 mb in this data set was 31° C in Supertyphoon Vanessa of 1984. No where else on earth have temperatures this extreme at 700 mb been found than in the eyes of intense tropical cyclones. Therefore, analysis of the cyclone's inner temperature can provide clues to the intensity of the cyclone.

As Fig. 6.14 reveals, not only does eye temperature generally increase with lower MSLP, but also note that eye temperature is related to the shape and structure of the eye. The temperature inside concentric eyes was cooler for the same intensity than either circular or elliptical eyes. Presumably this is due to the eye cycle which Willoughby, et al., discussed, i.e. when the inner eye contracted and eventually vanished in the center, the evaporative cooling which resulted from the added moisture would cause a lowering of temperatures.

The eye's temperature is not strictly a function of its intensity and character but also the intensity change. The maximum temperatures were found to occur while the cyclone

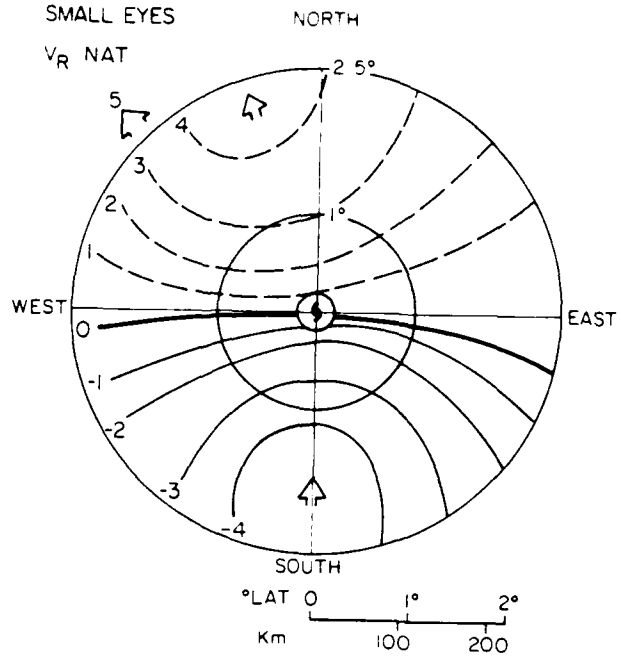

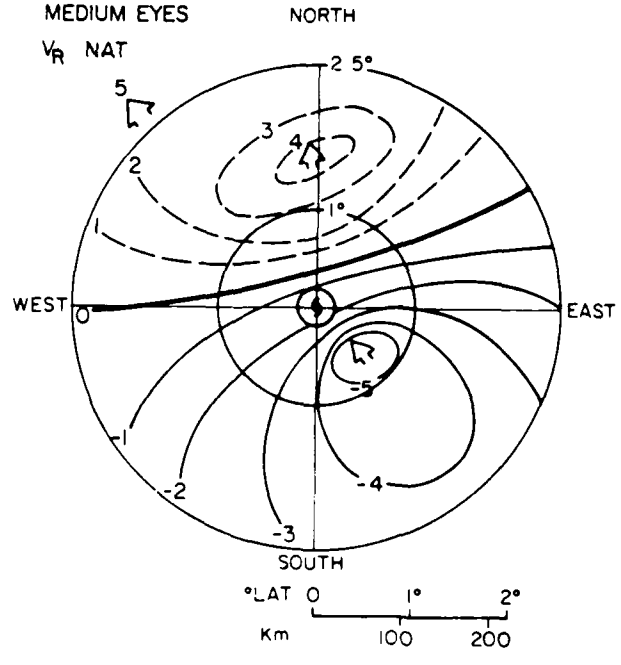

Figure 6.11: a-d. Plan-view depictions of the radial wind field (V_r) in ms^{-1} and in earth-relative coordinates (NAT) for the four eye size classes of a) small eye, b) medium eye, c) large eye and, d) no eye.

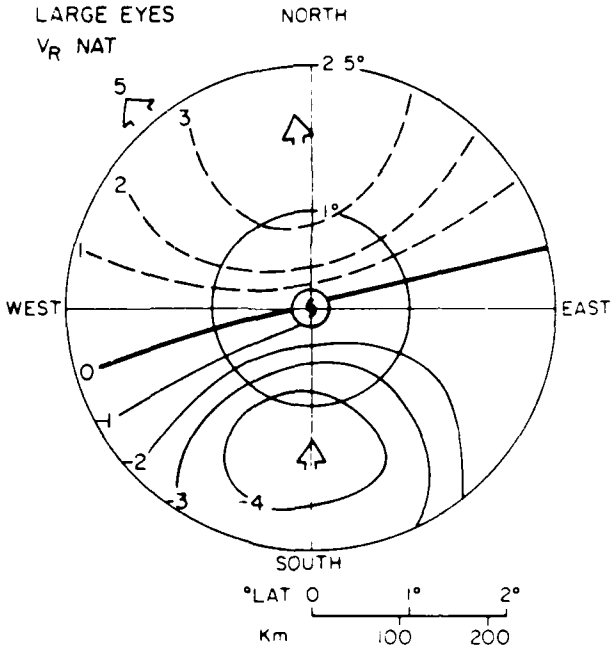

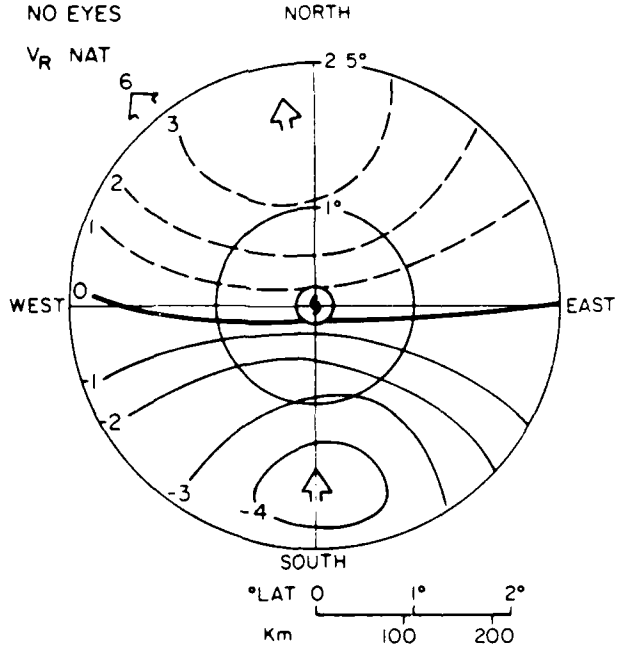

Figure 6.11: a-d. Continued.

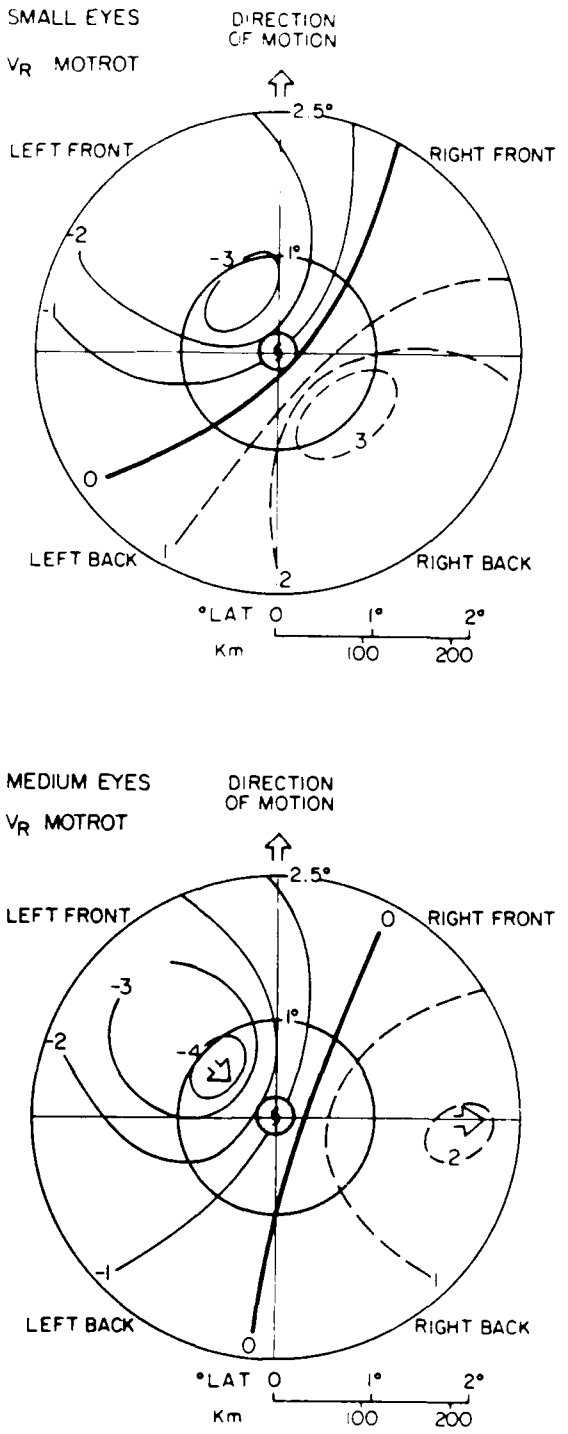

Figure 6.12: a-d. Plan-view depictions of the radial wind field (V_r) in ms^{-1} and in cyclone-relative coordinates (MOTROT) for the four eye size classes of a) small eye, b) medium eye, c) large eye and, d) no eye.

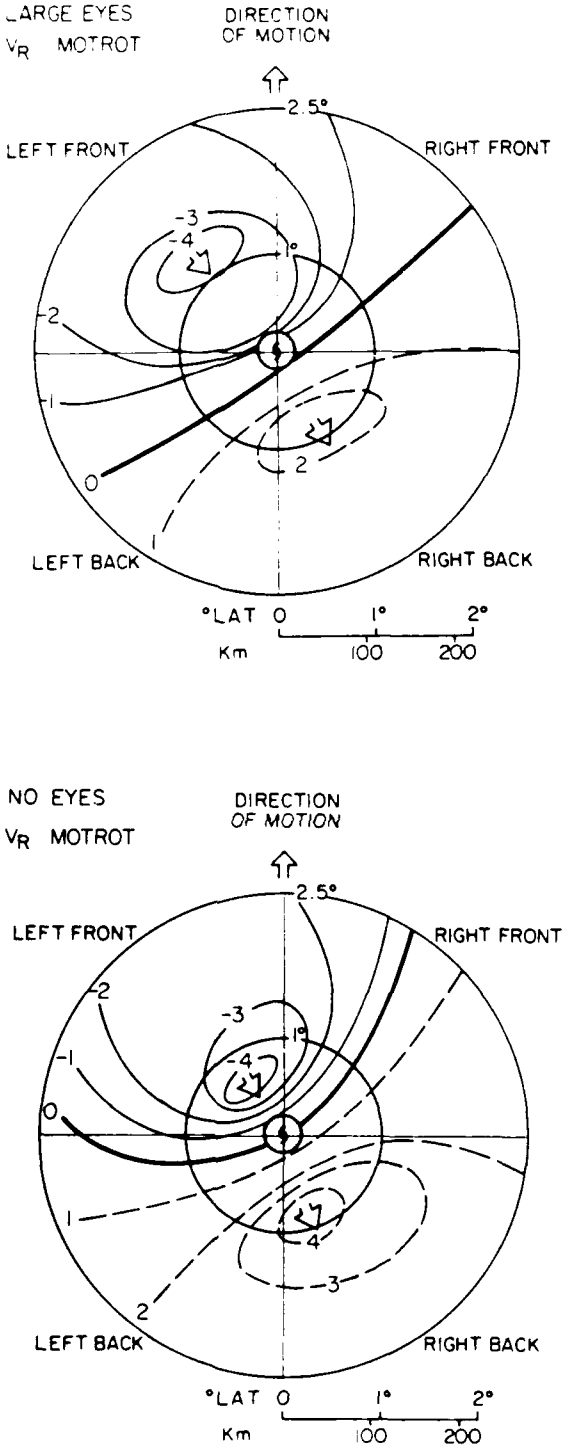

Figure 6.12: a-d. Continued.

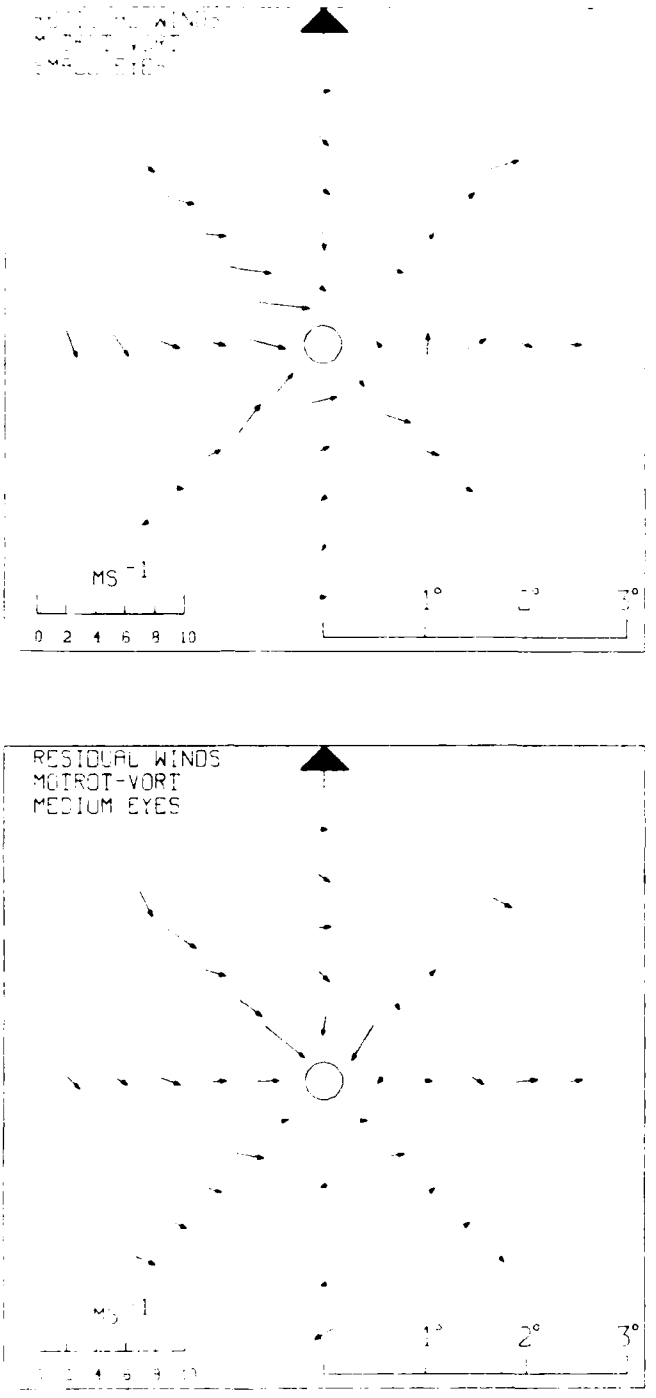

Figure 6.13: a-d. Plan-view depictions of the 700 mb residual wind field in MOTROT-VORT with the arrow on the rim denoting the cyclone's heading. Values are in ms^{-1} with arrow length implying speed as shown in the lower left corner. The classes are for the four eye size classes of a) small eye, b) medium eye, c) large eye and, d) no eye.

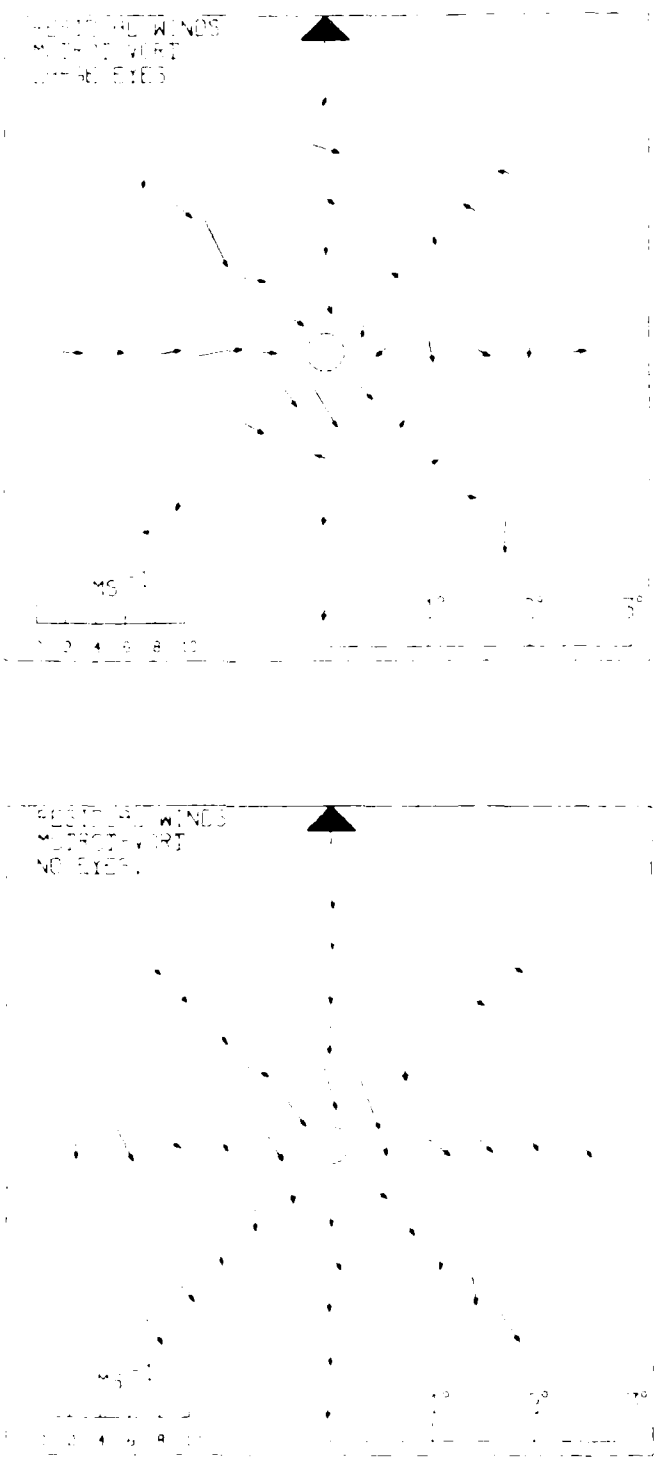

Figure 6.13: a-d. Continued.

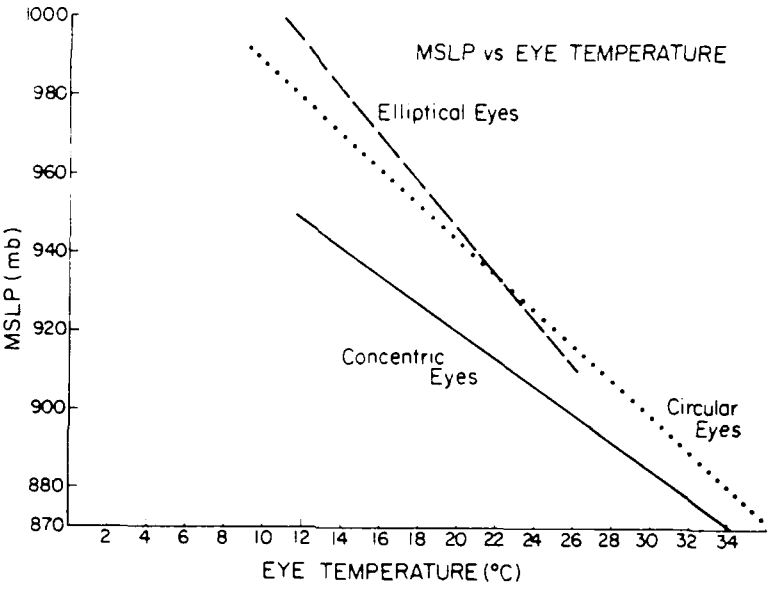

Figure 6.14: MSLP versus 700 mb inner eye temperature for elliptical, circular, and concentric eyewalls.

was intensifying, not at its maximum intensity which corresponded to a plateau of change, nor while filling. It is likely that the eyewall convection is most vigorous while intensifying and that when the convective processes slow down, the intensification rate slows with it resulting in lessened subsidence- forced warming and cooler central temperatures.

6.8.1 Equivalent Potential temperature (θ_e)

Equivalent potential temperature has been used at JTWC on Guam for the past few years as a predictive measure of a cyclones intensity. Dunnavan (1981) devised a predictive scheme which attempted to specify those cyclones which would become intense from those which would not. His study indicated that when a cyclone's MSLP and θ_e curves intersected, as plotted according to Dunnavan's specifications for the θ_e and MSLP scaling shown in Fig. 6.15, a cyclone would do one of two things; it would either rapidly deepen or would reach a MSLP of at least 925 mb. Those curves which did not cross would be forecast as slower deepeners.

In order to test Dunnavan's theory, all 101 cyclones of this 5-year data set were used. Of these, 48 typhoons' MSLP intersected with their θ_e. All of these cyclones reached

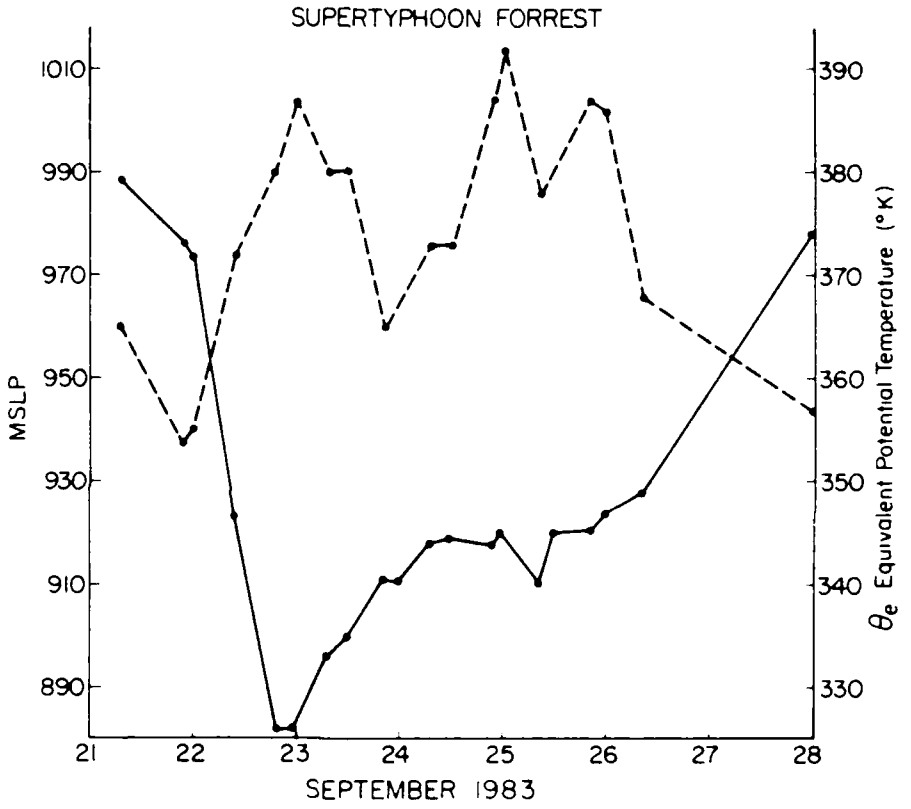

Figure 6.15: Evolution of MSLP and 700 mb equivalent potential temperature for Supertyphoon Forrest.

maximum intensities below 950 mb. This is a given due to the design of the MSLP/θ_e grid.) Of those that crossed MSLP with their θ_e on this scaling, 10% made landfall within a day, thus future intensity could not be verified. Less than half (40%) actually followed Dunnavan's prediction of either rapidly deepening or reaching 925 mb while providing any lead time. Since this is a predictive scheme, lead time is an important factor in judging its usefulness. Thirteen percent crossed curves without providing such lead time. For the example of Supertyphoon Elsie, Fig. 6.16, it wasn't until Elsie hit 902 mb that the crossing was evident. Indeed, Elsie was rapidly deepening before the curves crossed. Not all typhoons exhibiting this curve intersection reached 925 mb or deepened rapidly. A full 38% gave false alarms (see the example of Typhoon Pamela in Fig. 6.17). The only common feature to all cyclones that intersected MSLP and θ_e curves was that they reached at least 950 mb, barring landfall within 12 hours, thus developed into intermediate typhoons at least.

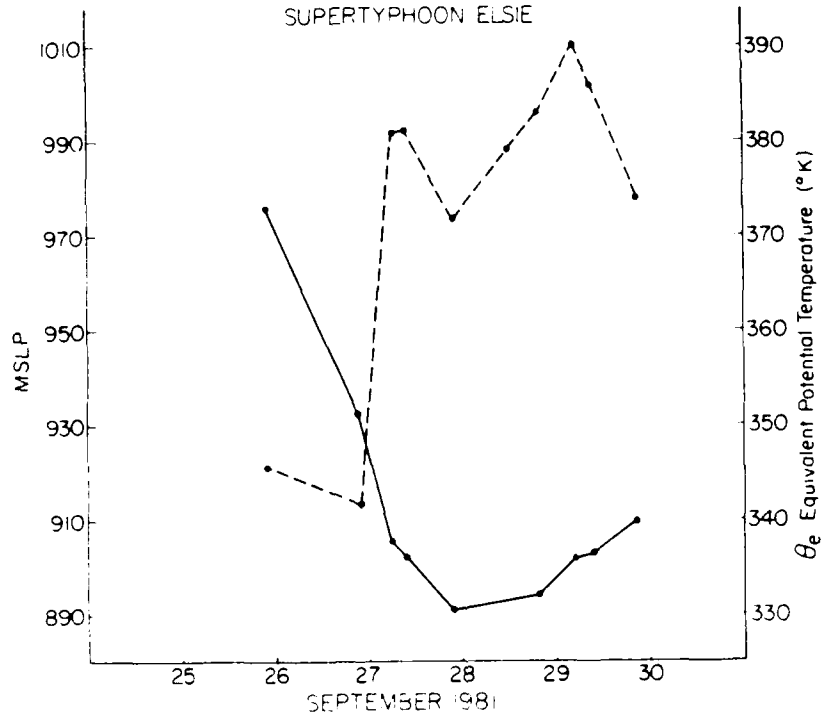

Figure 6.16: Evolution of MSLP and 700 mb equivalent potential temperature for Supertyphoon Elsie.

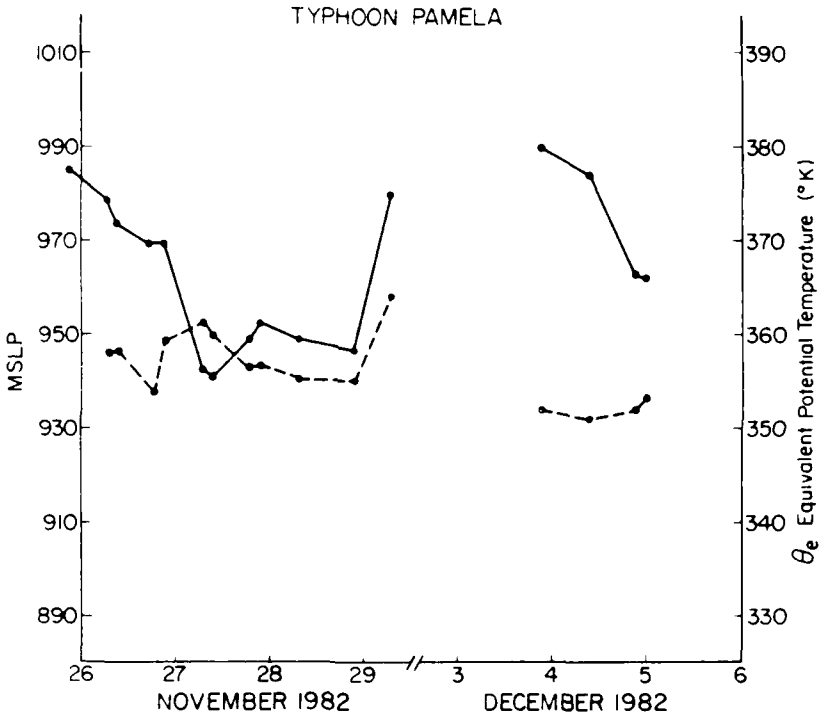

Figure 6.17: Evolution of MSLP and 700 mb equivalent potential temperature for Typhoon Pamela.

None of the cyclones whose curves did not cross ever exceeded 955 mb, thus developing in to minimal typhoons at best. However, this finding may be due entirely to the design of the $\theta_e/MSLP$ grid. The critical crossing point lay on average at 950 mb and 360° K, thus cyclones would have to reach 950 mb at least. Evidently, some cyclones reached 950 mb and intensified no further. Unfortunately for the value of this predictive scheme, less than half of the cyclones studied did intensify to 925 mb or deepen at a rate of 42 mb/d with lead time. All that can really be said about this forecasting tool is that cyclones will reach at least 950 mb, but only after reaching 950 mb.

Evidently, Dunnavan's predictive scheme does not appear to be a very useful tool when applied to a large data sample.

Chapter 7

SUMMARY AND DISCUSSION

7.1 The Life Cycle of the Tropical Cyclone

This substantial data set has provided a broader understanding into the manner in which intensity change occurs in the tropical cyclone. The typhoon is observed in most cases to form from its center outward. Although inner core convection drives the intensity changes, this process is constrained, in part, by the strength of the adjoining outer core. A weak outer core provides easier access into the eyewall, while a strong outer core places an increasingly effective brake on inflowing momentum thereby depleting the inner core's momentum supply. These effects follow a typical lifecycle as depicted in Fig. 7.1.

In the tropical cyclone's intensification period, phase 1, the momentum gathers and builds up the winds in its inner and outer cores at the 700 mb level. Although the entire 700 mb wind field builds, the inner core intensifies at 2 to 20 times the rate of the outer core. This concentration of momentum close to the cyclone center is much more efficient for intensification (surface pressure drop and maximum wind increase). This process also causes an eyewall cloud to form, the appearance of which is a key to the rate of further intensification.

Before the eye appears, the process of concentrating momentum into the inner core is slow. In this tropical storm stage, intensification occurs at an average rate of 8 mb/d. This is equivalent to a maximum wind increase of about 5 ms^{-1} and a strengthening of the outer core (1-2.5° radius) an average of 2.5 ms^{-1} per day. Once the eye appears, usually at 980 mb, however, the rate of intensity change increases an average 250% to 20 mb/d. Evidently, the eye acts to effectively concentrate energy close to the center where energy conversions are most efficient. Rapid deepening cyclones exhibit an earlier

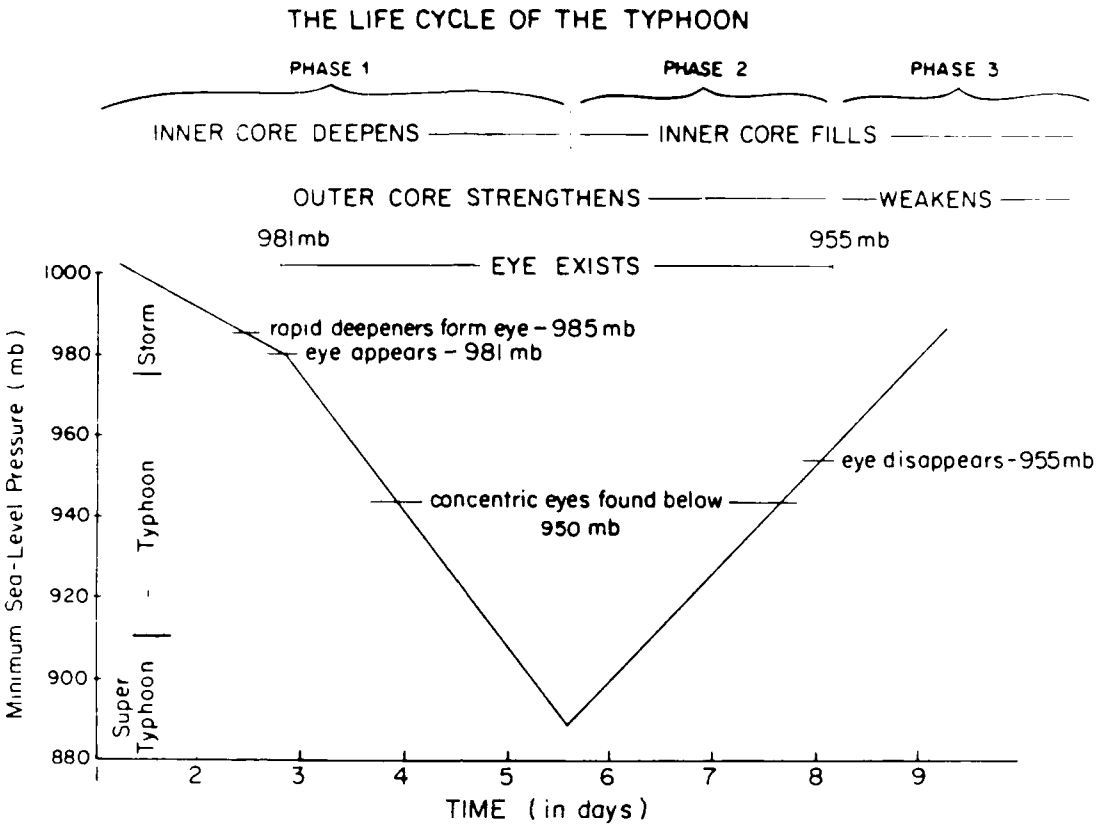

Figure 7.1: Main events in the typical life cycle of the tropical cyclone.

eye formation, at 985 mb and immediately begin deepening at 42 mb/d or more. The most phenomenal rate of change for the five years studied was 92 mb/d in Supertyphoon Forrest of 1983 which first developed an eyewall at 988 mb. Therefore, the earlier in the cyclone's development the eye appears the more rapid the intensity increase.

This may result from reasoning derived from inertial stability theory. Since momentum must be advected into the eyewall which is located in the inner core of the cyclone, it must pass through the outer core region to get there. (Observations reveal that inner core winds do not intensify at the expense of the outer core winds since the outer core is observed to strengthen as well.) Thus, the sooner the eye forms, the less the outer core has strengthened, providing much easier access of inflowing low-level air into the eyewall. Cyclones whose eyes form late do not reach intensities much below 930 mb. This is perhaps due to the inertial stiffness of their outer core. Recall that in the Pacific, typhoons have

reached intensities of 870 mb, and that a full third of the cyclones that became typhoons reached intensities below 930 mb. Therefore, late-forming eyes suggest the cyclone will not rapidly deepen, nor will it intensify into an extreme typhoon.

The filling process in which the central pressure starts rising, does not necessarily imply the cyclone's outer-core wind field is decaying. Indeed, this may characterize the cyclone's period of greatest gale- force extent and strength of outer core winds. As long as an eye exists in the filling phase (generally at MSLP's lower than 955 mb) typhoons will continue to draw momentum through the outer-core and continue to strengthen the winds in their outer cores. This is the period in which the inner core winds are diminishing while the outer core winds are increasing and is classified as Phase 2. The eye expands during this time. Inner core filling continues as the inflowing air penetrates less close to the cyclone center. Recall how for the same central pressure, the inertial stability is twice as large in the filling stage as in the deepening stage thereby effectively stiffening the outer core to radial inflow. The expanding eye thus becomes less and less efficient and the central core fills.

This knowledge may avert the disastrous surprise that arises when one expects gale-force winds to contract if maximum winds are diminished. It is important to realize that even though the center is filling in Phase 2, the radius of damaging winds are still expanding as long as an eye exists. Therefore, if one has information on whether the central pressure is filling and whether an eye exists, forecasts of outer-wind strength are likely to be far more accurate. In the case of Supertyphoon Abby this expansion occurred for 6 days after the MSLP started filling! This suggests that the cyclone reaches its largest areal proportions while filling. Forecasters should expect larger gale- force wind radii in the filling versus intensifying phase given the same MSLP. Eyewalls are maintained for cyclones with MSLP's below 955 mb. The longer the cyclone spends in phase 2, the generally stronger will be the outer-radius winds.

The eye is observed to disappear about the time that the outer core begins to weaken. This is characteristic of the beginning of Phase 3. Therefore, once the eye vanishes, gone apparently also is the import of angular momentum that built up the outer core and the

entire outer radius low-level wind field begins to decay. These effects are, once again, for cyclones which did not encounter landfall. No doubt landfall would erode the wind field regardless of the appearance of an eye. Steady state periods may exist anywhere along the life cycle, however. The more intense the cyclone, the less likely it will encounter a period of no substantial intensity change.

Life cycle changes were described by Dvorak (1975) in terms of cloud field features and their changes as the cyclone's maximum winds progressed in time. Without wind information in the cyclone's outer core region, the wind field away from the maximum wind zone was not analyzed with respect to cloud field changes. Since these outer winds are important as well, satellite and wind field comparisons are needed.

7.2 The 700 mb Interior Background Wind Field

Deeper insight into the physical processes of cyclone motion is revealed when the cyclone's motion and its mean vortex are removed. This residual wind field most clearly reflects the interaction between background winds and the vortex. Therefore, MOTROT-VORT was defined in this paper to be the resulting wind field after the cyclone's motion and mean vortex have been removed from all winds and the direction of motion of the cyclone is rotated to a common heading.

First and foremost the cyclone's interior wind field shows a distinct 700 mb steering current passing through it. Apparently the inner-core vortex is not fully shielded from the outer-core environment. The concept of a 'spinning top' embedded in a stream that impinges on only its outer edges cannot completely describe the motion of the cyclone. It is observed that the cyclone allows a continual flow from its outer- core to pass directly through the vortex. Tropical cyclones of the northwestern Pacific basin are observed to move faster and to the left of their 700 mb environment. Evidently the reason they move faster is due to the fact that the steering current is more heavily weighted to the stronger winds that lie in the upper troposphere. Cyclones are likely deflected westward by the Beta-effect. It is also observed that the stronger the winds in the outer core the more the cyclone is deflected leftward. This is in agreement with some recent numerical modeling of cyclone motion with different magnitudes of outer circulations employing the Beta-effect.

The effect of this faster and leftward drift of the cyclone is to induce an environmental flow-through from left-front to right-back in cyclone- relative coordinates. Thus, a natural, flowthrough-induced asymmetry is superimposed on the cyclone's 700 mb wind field with strongest tangential winds on the left quadrant. The greater the intensity of the cyclone the more nearly symmetric the tangential wind field. An unusual, two-wave asymmetry pattern appears for cyclones which are approaching the westerlies and a strongly sheared environment.

This normally-observed environmental flow through from left-front to right-back yields clues to the future intensity changes of the cyclone. This implies that the cyclone is being fed at its lower levels by the new environment to which it moves. Since it is in the low-levels that the cyclone must obtain its moisture supply, what lies ahead of the cyclone's path is what will enhance or retard future development.

7.3 Future Research

Northwestern Pacific flight data have revealed a wealth of new information on the changing structure of the tropical cyclone. The success of removing the mean vortex and cyclone motion vectors to reveal the 700 mb interior background wind field is especially pertinent to the motion question. The possibilities of learning more from this flight data are very promising.

Much has been learned from this flight data about the evolution of the tropical cyclone. Yet, the more we learn the more questions are raised. What interactions occur between the vortex and its environment beyond 2.5°? What changes do the cloud fields reveal during the cyclone's life cycle? In order to answer these question, the tropical project, headed by Professor William Gray, is already in the process of gathering and compiling the accompanying satellite pictures that match this 1980-84 data set. Additionally, the synoptic fields at many levels shall be studied in order to better pin down answers to the motion question. Plans are already in the works to expand the present 5-year data set to 7 years with the addition of 1985 and 1986 Pacific reconnaissance data. This will make 150 named tropical cyclones available for analysis. Recall that the reconnaissance will terminate in October 1987. This continuing study of the evolution of the

tropical cyclone's wind field should greatly enhance our understanding of this extremely hazardous phenomenon, thereby enabling us to improve our tropical cyclone forecasts.

Chapter 8

GENERAL FORECASTING RULES, OBSERVATIONS, AND SCIENTIFIC HIGHLIGHTS

Some of the findings of this study may be applied to aid the forecaster in predicting intensity change and the researcher to further understand the process by which tropical cyclones develop and move. Therefore, the highlights of this research have been generalized into three categories; forecasting rules, general observations and scientific measurements. It is important to realize that these are only general statements and that individual case variability from these statements can sometimes occur.

8.1 General Forecasting Rules

1. An intensifying cyclone expands its gale-force wind radii on average at 40 km/d. A filling cyclone will continue to expand at this same rate as long as the eye exists.

2. The strength of the Outer Core (1-2.5° radius) Wind Strength (OCS) is, on average, half the value of the maximum wind speed.

    - a. For an intensifying cyclone, when the OCS is less than half the maximum wind, expect more rapid deepening than normal.
    - b. For an intensifying cyclone, when the OCS is more than half the maximum wind speed expect slower than normal deepening.

3. The outer core generally strengthens at a rate of 2.5 ms^{-1}/d regardless of whether the cyclone fills or deepens, as long as an eye exists.

4. A developing cyclone intensifies an average 8 mb/d before it obtains an eye and an average 20 mb/d just after the eye appears.

5. The eye typically appears at an MSLP of 980 mb and disappears at 955 mb.

6. For cyclones that had achieved MSLP's below 955 mb, the outer core does not begin to weaken until the eye disappears.

7. The sooner the eye appears, the more rapid the deepening rate, and the more likely the cyclone will become intense (MSLP $\leq$ 930 mb).

8. Cyclones which are going to become rapid deepeners ($\geq$ 42 mb/d) will usually form an eye by the time they reach a MSLP of 985 mb. This eye will characteristically be smaller in size than the average eye (40 km vs. 50 km diameter).

9. The later the eye appears, the slower the deepening and less likely the cyclone will become intense.

10. The more intense the cyclone, the more closely the 700 mb level approximates the steering current speed.

8.2 General Observations

1. In the northwestern Pacific, cyclones moves faster and drift left of their low-level environment.

2. The greater the OCS, the more leftward drift the cyclone experiences from its 700 mb 0-2.5° steering current.

3. There is a maximum tangential wind speed on the left-back quadrant and minimum on the right-front of the cyclone after cyclone motion is removed.

4. The more intense the cyclone, the smaller the RMW.

5. The more intense the cyclone, the more symmetric the tangential wind field.

6. The higher the OCS, the higher 700 mb moisture content out to 4° radius.

7. Cyclones that move southwestward are unlikely to intensify and typically do not intensify much past tropical storm stage. These cyclones move slower and drift more to the left than the average cyclone.

8. Cyclones moving eastward are likely to fill and exhibit a two- wave asymmetry pattern in their tangential wind field.

9. The more intense the cyclone, the less likely the central pressure will plateau; i.e., undergo a steady state period.

10. For cyclones which intensified below 955 mb, the filling portion of their life cycle is characteristic of lower maximum wind speed but higher OCS values than its deepening phase at the same central pressure.

11. The eye generally contracts with deepening and expands while the cyclone fills. Small time scale fluctuations to this rule are common, however. A change in size does not necessarily imply a change in the intensity.

12. Circular eyes are more conservative in size than elliptical eyes. Elliptical eyes fluctuate in size at 4 to 5 times the rate of circular eyes.

13. Elliptical eyes are commonly seen when the cyclone is first forming an eye and the eye begins to disappear.

14. Concentric eyes occur, on average at 925 mb, but were not found above 950 mb.

8.3 Scientific Highlights

1. Cyclones were observed to develop from the inner core outward and decay from the inner core outward.

2. The more intense the cyclone, the more subgradient the inner-core wind field outside the RMW at 700 mb implying a greater role of cumulus friction.

3. The more intense the cyclone, the more the 700 mb residual wind current is seen to draw into the inner core.

4. The higher the inertial stability of the outer core the stiffer the outer core to inflow, thereby placing an increasing brake on the transport of momentum to the inner core.

5. The higher the MSLP at which the eye appears, the less resistant the outer core is to radial inflow, and the more the angular momentum concentrates into the inner core enhancing the deepening process. The longer it takes a cyclone to form an eye, the more resistant the outer core to radial inflow thus repressing the deepening process.

6. The greater the OCS, the more the cyclone drifts leftward of the 700 mb current.

7. The more intense the cyclone, the more symmetric the tangential wind field.

8. The sooner the eye appears, the more rapid the deepening rate, and the more likely the cyclone will become intense, if embedded in a moist environment.

9. Cyclone deepening and filling is much more rapid with an eye than without an eye.

REFERENCES

Adem, J., 1956: A series solution for the barotropic vorticity equation and its application in the study of atmospheric vortices. *Tellus*, 8, 364-372.

Anthes, R. A., 1974: The dynamics and energetics of mature tropical cyclones. *Rev. Geoph. and Space Physics*, 12, 495-521.

Anthes, R. A., 1982: Tropical cyclones, their evolution, structure and effects. *Meteor. Monographs*, Vol. *19*, AMS, 45 Beacon Street, Boston, MA, 02108, 208 pp.

Atkinson, G. D. and C. R. Holliday, 1977: Tropical cyclone minimum sea level pressure maximum sustained wind relationship for the western North Pacific. *Mon. Wea. Rev.*, 105, 421-427.

Barnes, G. M., E. J. Zipser, D. Jorgensen, and F. Marks, 1983: Mesoscale and convective structure of a hurricane rainband. *J. Atmos. Sci.*, 40, 2125-2137.

Barnes, G. M., and G. J. Stossmeister, 1987: The structure and decay of a rainband in Hurricane Irene. Submitted to *Mon. Wea. Rev.*.

Brown, K. M., and J. E. Dennis, 1972: Derivative free analogues of the Levenberg-Marquardt and Gauss algorithms for nonlinear least squares approximations. *Numerische Mathematik*, 18, 289-297.

Chan, J. C. and W. M. Gray, 1982: Tropical cyclone movement and surrounding flow relationships. *Mon. Wea. Rev.*, 110, 1354-1374.

Chan, J. C. and W. M. Gray, 1984: An observational study of the physical processes responsible for tropical cyclone motion. *J. Atmos. Sci.*, Vol. 41, 6,1036-1048.

Chan, J. C., and R. T. Williams, 1987: Analytical and numerical studies of the Beta-effect in tropical cyclone motion. Part 1: Zero mean flow. *J. Atmos. Sci.*, in press.

Colon, J. A. and Staff, NHRP, 1961: On the structure of Hurricane Daisy (1958). NHRP Report No. 48, 102 pp.

Colon, J. A. and Staff, NHRP, 1963: On the evolution of the wind field during the life cyclone of tropical cyclones. NHRP Report No. 65, 36 pp.

Colon, J. A. and Staff, NHRP, 1964: On the structure of Hurricane Helene (1958). NHRP Report No. 72, 50 pp.

Depperman, C. E., 1947: Notes on the Origin and Structure of Philippine Typhoons. *Bull. Amer. Meteor. Soc.*, 9, 399-404.

DeMaria, M., 1985: Tropical cyclone motion in a nondivergent barotropic model. *Mon. Wea. Rev.*, 113, 1199-1210.

Dunnavan, G. M., 1963: An evaluation of 700 mb aircraft reconnaissance data for selected northwest Pacific tropical cyclones. MS thesis Naval Postgraduate School, Monterey, CA, 92 pp.

Dvorak, V. F., 1975: Tropical cyclone intensity analysis and fore- casting from satellite imagery. *Mon. Wea. Rev.*, 103, 420-430.

Elliassen, A., 1951: Slow thermally or frictionally controlled motions in a circular vortex. *Astrophys. Norv.*, 5, 19-60.

Frank, W. M., 1977: The structure and energetics of the tropical cyclone I. Storm structure. *Mon. Wea. Rev.*, 105, 1119-1135.

Frank, W. M., and W. M. Gray, 1980: Radius and frequency of 15 m/s (30 kt) winds around tropical cyclones. *J. Appl. Meteor.*, 19 219-223.

Frank, W. M., 1984: Composite analysis of the core of Hurricane Frederick 1979. *Mon. Wea. Rev.*, 112, 2401-2420.

George, J. E. 1975: Tropical cyclone motion and surrounding parameter relationships. Dept. Atmos. Sci. Paper No. 241, Colo. State Univ., Fort Collins, CO, 105 pp.

George, J. E., and W. M. Gray, 1976: Tropical cyclone motion and surrounding parameter relationships. *J. Appl. Meteor.*, 15, 1252-1264.

Gray, W. M., and D. J. Shea, 1973: The hurricane's inner core region. II. Thermal stability and dynamic characteristics. *J. Atmos. Sci.*, 30, 1565-1576.

Gray, W. M, and W. M. Frank, 1977: Tropical cyclone research by data compositing. US Navy Environmental Prediction Research Facility Report. Tech Paper No. 77-01.

Gray, W. M., 1979: Hurricanes: their formation, structure, and likely role in the tropical cyclone. Meteorology over the Tropical Oceans. D. B. Shaw, Ed., *Roy. Meteor. Soc.*, 155-218.

Gray, W. M., 1981: Recent advances in tropical cyclone research from rawinsonde composite analysis. WMO Programme on Research in Tropical Meteorology. This report was prepared at the request of the WMO Commission for Atmospheric Science, Geneva, Switzerland, 407 pp.

Hack, J. J., and W. H. Schubert, 1986: On the nonlinear response of atmopheric vortices to heating by organized cumulus convection. *J. Atmos. Sci.*, 43, 1559-1573.

Hawkins, H. F., 1962: Vertical wind profiles in hurricanes. NHRP Report No. 55, 16 pp.

Hawkins, H. F. and D. T. Rubsam, 1968a: Hurricane Hilda, 1964. I: Genesis, as revealed by satellite photographs conventional and aircraft data. *Mon. Wea. Rev.*, 96, 428-452.

Hawkins, H. F. and D. T. Rubsam, 1968b: Hurricane Hilda, 1964. II: Structure and budgets of the hurricane on October 1, 1964. *Mon. Wea. Rev.*, 96, 617-636.

Hawkins, H. F., 1971: Comparison of results of the Hurricane Debbie (1969) modification experiments with those from Rosenthal's numerical model simulation experiments. *Mon. Wea. Rev.*, 99, 427-434.

Hawkins, H. F. and S. M. Imbembo, 1976: The structure of a small intense hurricane—Inez 1966. *Mon. Wea. Rev.*, 104, 418-442.

Henderson, R. S., 1978: USAF Aerial Weather Reconnaissance using the Lockheed WC-130 Aircraft. *Bull. Amer. Meteor. Soc.*, 59, 1136- 1143.

Holland, G. J., 1980: An analytical model of the wind and pressure profiles in hurricanes. *Mon. Wea. Rev.*, 108, 8, 1212-1218.

Holland, G. J.,1983: Tropical cyclone motion: environmental interaction plus a beta effect. *J. Atmos. Sci.*, 40, 328-342.

Holland, G. J., and R. T. Merrill, 1984: On the dynamics of tropical cyclone structure changes. *Quart. J. Meteor. Soc.*, 110, 723-745.

Holliday, C. R., and A. H. Thompson, 1979: Climatological characteristics of rapidly intensifying typhoons. *Mon. Wea. Rev.*, 107, 1022-1034.

Hughes, L. A., 1952: On the low level wind structure of tropical cyclones. *J. Meteor.*, 9, 422-428.

Jilesnianski, C., 1973: A preliminary view of storm surges before and after storm modifications. NOAA Tech. Memo, ERL WMPO-3, 33 pp.

Jordan, C. L., 1961: Marked changes in the characteristics of the eye of intense typhoons between the deepening and filling stages. *J. Meteor.*, 15, 779-789.

Jordan, C. L., D. A. Hurt and C. A. Lowry, 1960: On the structure of Hurricane Daisy of 27 August 1958. *J. Meteor.*, 17, 337-348.

Jorgensen, D. P., 1984a: Mesoscale and convective scale characteristics of mature hurricanes. I. General observations by research aircraft. *J. Atmos. Sci.*, 41, 1268-1285.

Jorgensen, D. P., 1984b: Mesoscale and convective scale characteristics of mature hurricanes II. Inner core structure of hurricane Allen (1980). *J. Atmos. Sci.*, 41, 1287-1311.

LaSeur, N. E., and H. F. Hawkins, 1963: An analysis of Hurricane Cleo (1958) based on data from research reconnaissance aircraft. *Mon. Wea. Rev.*, 91, 694-709.

Lee, C.-S., 1984: The bulk effects of cumulus momentum transports in tropical cyclones. *J. Atmos. Sci.*, 41, 4, 590-603.

Lee, C.-S., 1986a: An observational study of tropical cloud cluster evolution and cyclogenesis in the western North Pacific: I: Background and evolution of non-genesis cloud clusters. Being submitted to *J. Atmos. Sci.*

Lee, C.-S., 1986b: An observational study of tropical cloud cluster evolution and cyclogenesis in the western North Pacific: II: Evolution of genesis cloud clusters and comparison to non-genesis cases. Being submitted to *J. Atmos. Sci.*

Lee, C.-S., 1986c: An observational study of tropical cloud cluster evolution and cyclogenesis in the western North Pacific: III: Moisture, energy, and angular momentum budget analysis. Being submitted to *J. Atmos. Sci.*

Lee, C.-S., 1986d: Some large scale characteristics associated with tropical cyclone development in the western North Pacific. Being submitted to *Mon. Wea. Rev.*

Levenberg, K., 1944: A Method for the solution of certain non-linear problems in least squares. *Quart. Appl. Math.*, 2, 164-168.

Marks, F. D., and R. A. Houze, 1987: Inner core structure of Hurricane Alicia from airborne Doppler radar observations. Submitted to *J. Atmos. Sci.*

Marquardt, D. W., 1963: An algorithm for least-squares estimation of nonlinear parameters. *J. Siam.*, 11.

Matsumoto, C. L., and W. M. Gray, 1986: A statistical method for one- to three-day tropical cyclone track prediction. Being submitted to *Mon. Wea. Rev.*

Merrill, R. T., 1984: A comparison of large and small tropical cyclones. *Mon. Wea. Rev.*, 112, 1408-1418.

Merrill, R. T., 1986a: Characteristics of the upper-tropospheric environmental flow around hurricanes. Submitted to *J. Atmos. Sci.*

Merrill, R. T., 1986b: Environmental influences on hurricane intensification. Submitted to *J. Atmos. Sci.*

Miller, B. I., 1957: On the maximum intensity of hurricanes. NHRP Report No. 14, 19 pp.

Miller, B. I., 1958: The three dimensional wind structure around a tropical cyclone. NHRP Report No. 15, 41 pp.

Miller, B. I., 1962: On the momentum and energy balance of Hurricane Helene (1958). NHRP Report No. 53, 19 pp.

Powell, M. D., 1982: The transition of the Hurricane Frederick boundary-layer wind field from the open Gulf of Mexico to landfall. *Mon. Wea. Rev.*, 110, 1912-1932.

Ooyama, K., 1969: Numerical simulation of the life cycle of tropical cyclones. *J. Atmos. Sci.*, 26, 3-39.

Ooyama, K., 1982: Conceptual evolution of the theory and modeling of the tropical cyclone. *J. Meteor. Soc. Japan*, 60, 369-379.

Riehl, H., and J. Malkus, 1961: Some aspects of Hurricane Daisy, 1958. *Tellus*, 13, 181-213.

Schubert, W. H., and J. Hack, 1982: Inertial stability and tropical cyclone development. *J. Atmos. Sci.*, 39, 1687-1697.

Shapiro, L. J., and H. E. Willoughby: The response of balanced hurricanes to local sources of heat and momentum. *J. Atmos. Sci.*, 39, 378-394.

Shea, D. J., and W. M. Gray, 1973: The hurricane's inner core region. I. Symmetric and asymmetric structure. *J. Atmos. Sci.*, 30, 1544-1564.

Shea, D. J., and W. M. Gray, 1976: Data summary of NOAA's hurricane inner-core radial leg flight penetrations 1957-1967, and 1969. Dept. of Atmos. Sci. Paper No. 257, Colo. State Univ., Fort Collins, CO, 220 pp.

Sheets, R. C., 1967a: On the structure of Hurricane Janice (1958). NHRL Report No. 76, 38 pp.

Sheets, R. C., 1967b: On the structure of Hurricane Ella (1962). NHRL Report No. 77, 33 pp.

Sheets, R. C., 1968: On the structure of Hurricane Dora (1964). NHRL Report No. 83, 64 pp.

Weatherford, C., and W. M. Gray, 1987: Typhoon structure as revealed by aircraft reconnaissance: Part I: Data analysis and climatology. Submitted to *Mon. Wea. Rev.*

Weatherford, C., and W. M. Gray, 1987: Typhoon structure as revealed by aircraft reconnaissance: Part II: Structural variability. Submitted to *Mon. Wea. Rev.*

Willoughby, H. E., 1978: A possible mechanism for the formation of hurricane rainbands. *J. Atmos. Sci.*, 35, 838-858.

Willoughby, H. E., 1979: Forced secondary circulations in hurricanes. *J. Geophys. Res.*, 84, 3173-3183.

Willoughby, H. E., J. A. Clos and M. G. Shoreibah, 1982: Concentric eye walls, secondary wind maxima, and the evolution of the hurricane vortex.

J. Atmos. Sci., 39, 395-411.

Willoughby, H. E., F. D. Marks, and R. J. Feinberg, 1984: Stationary and moving convective bands in hurricanes. *J. Atmos. Sci.*, 41, 3189-3211.

Appendix A

INDIVIDUAL CASE LIFE CYCLE PATTERNS

The life cycle patterns portrayed in the text of this paper were derived from the compositing of a large number of individual cases. In order to better understand the variations typical of individual cases, the following typhoons have been depicted throughout the time in which aircraft reconnaissance observed their major features. Four fields are portrayed in each case; the eye temperature, OCS, MSLP, and eye diameter. The temperature of the eye (dashed curve) was taken at the warmest position at 700 mb. The largest value can be seen for Supertyphoon Vanessa who obtained 31°C. The OCS (upper solid curve) was an area-weighted average wind speed at 700 mb from 1° to 2.5° radius. The solid lower curve depicts the MSLP. Finally, the dotted curve portrays the diameter of the eyewall with the following shape codes superimposed on the plot: "E" enclosed by a triangle denotes an elliptical eye, "O" marks a circular eye, and "C" enclosed by a circle denotes concentric eyes with both diameters depicted.

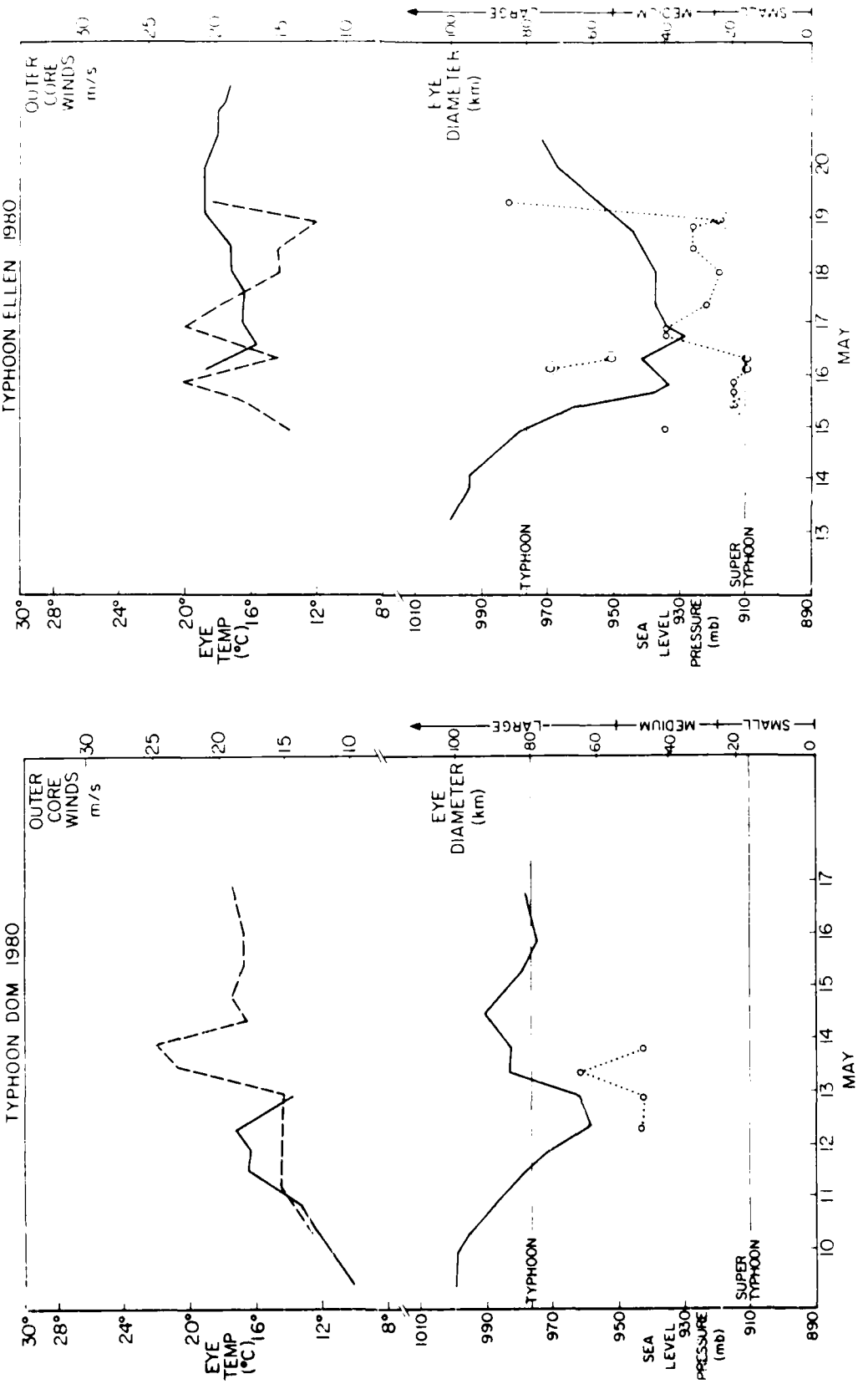
TYPHOON ELLEN 1980
TYPHOON DOM 1980
OUTER CORE WINDS m/s
EYE DIAMETER (km)
SMALL
MEDIUM
LARGE
EYE TEMP (°C)
SEA LEVEL PRESSURE (mb)
TYPHOON
SUPER TYPHOON
MAY

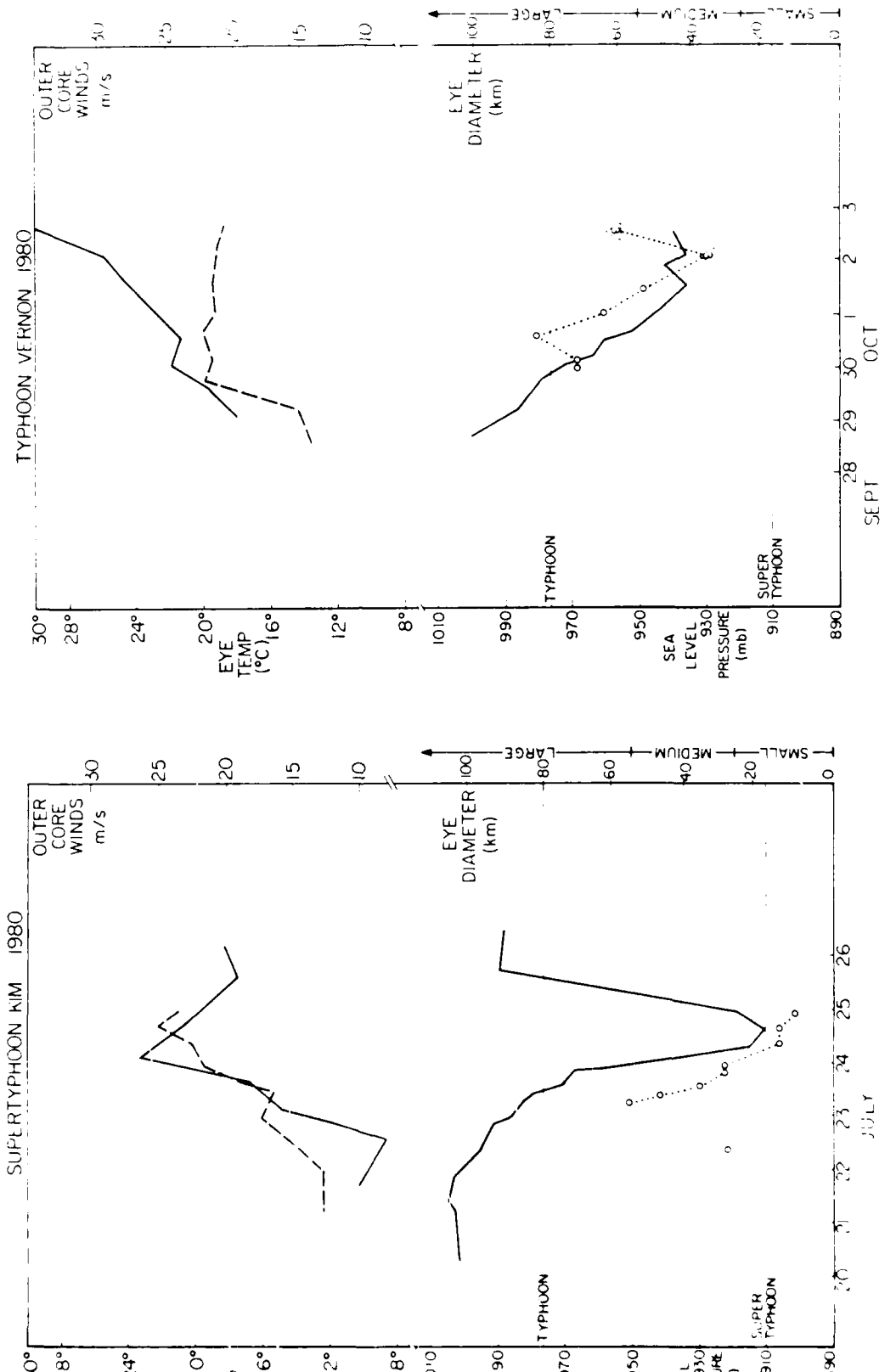
TYPHOON VERNON 1980
OUTER CORE WINDS m/s
EYE DIAMETER (km)
EYE TEMP (°C)
SEA LEVEL PRESSURE (mb)
TYPHOON
SUPER TYPHOON
SMALL
MEDIUM
LARGE
SEPT
OCT
SUPERTYPHOON KIM 1980
JULY

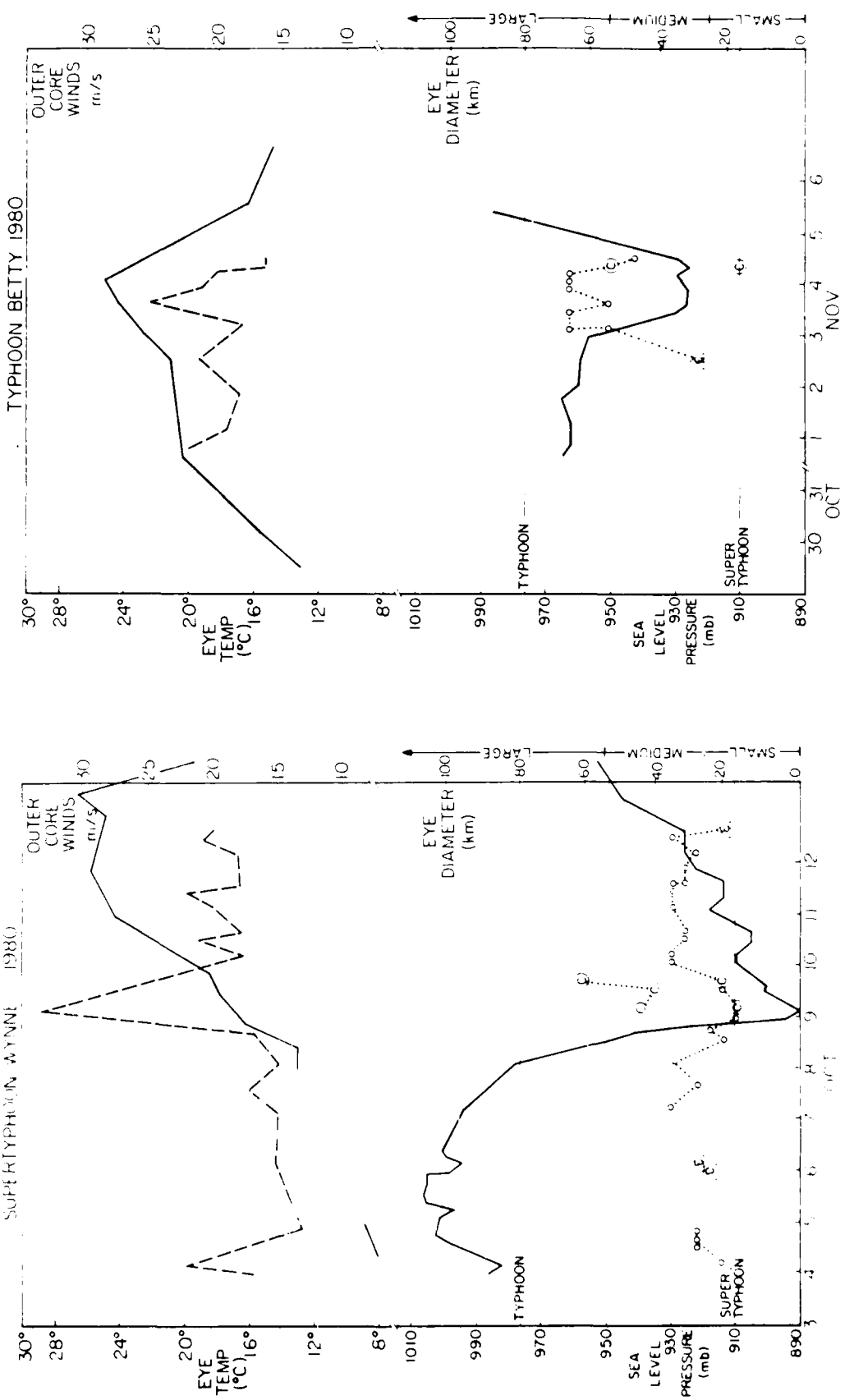
TYPHOON BETTY 1980
OUTER CORE WINDS m/s
EYE DIAMETER (km)
EYE TEMP (°C)
SEA LEVEL PRESSURE (mb)
TYPHOON
SUPER TYPHOON
SMALL
MEDIUM
LARGE
OCT
NOV

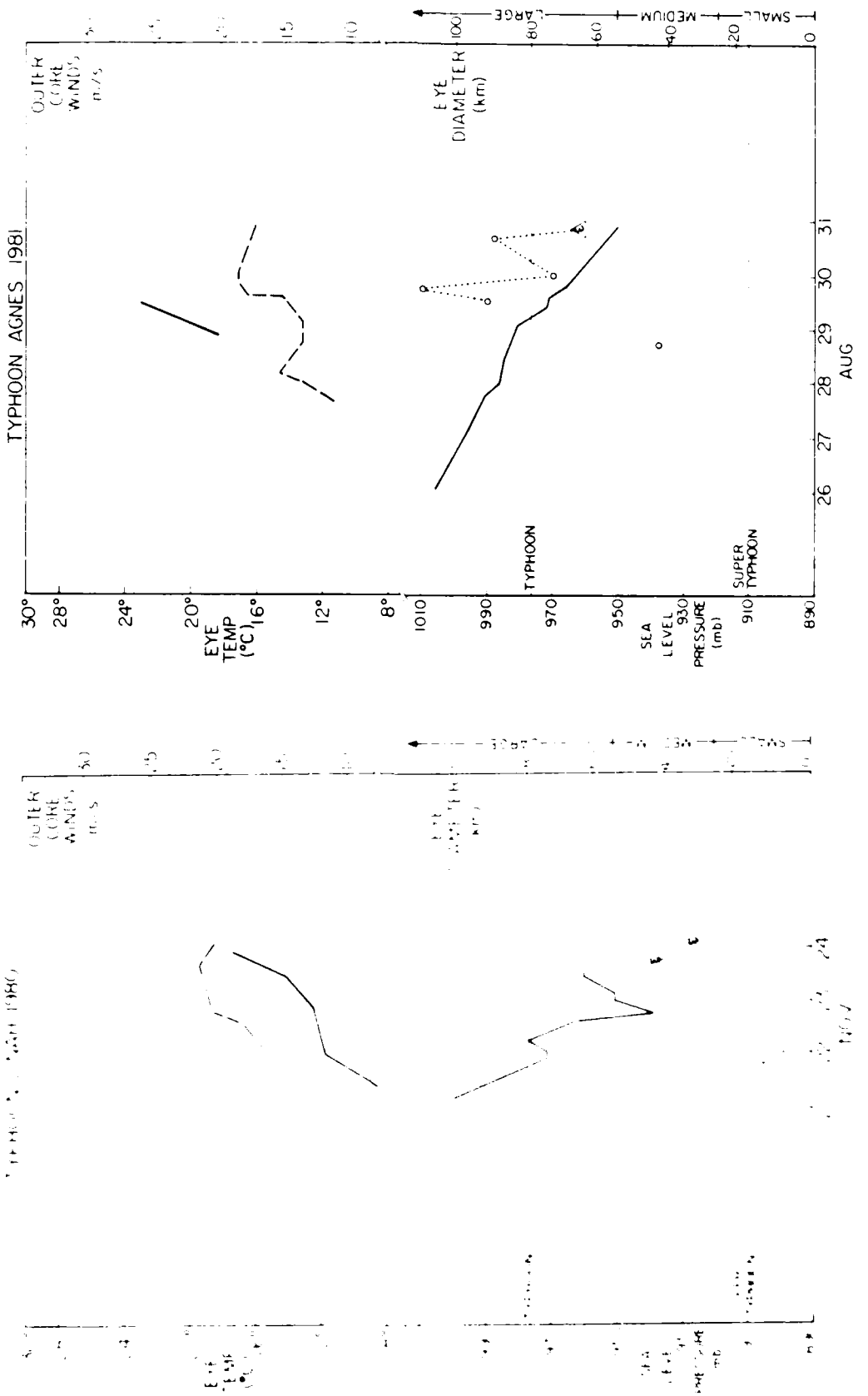
TYPHOON AGNES 1981
OUTER CORE WINDS m/s
EYE DIAMETER (km)
LARGE
MEDIUM
SMALL
EYE TEMP (°C)
SEA LEVEL PRESSURE (mb)
TYPHOON
SUPER TYPHOON
AUG

AD-A186 090 TYPHOON STRUCTURAL EVOLUTION(U) AIR FORCE INST OF TECH 1/1
WRIGHT-PATTERSON AFB OH C L WEATHERFORD 1987
AFIT/CI/NR-87-125D

UNCLASSIFIED F/G 4/2 NL

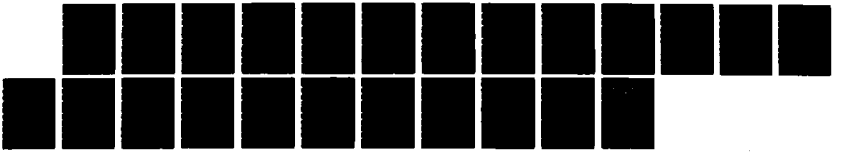

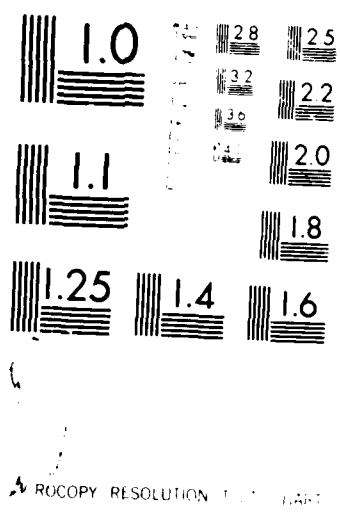

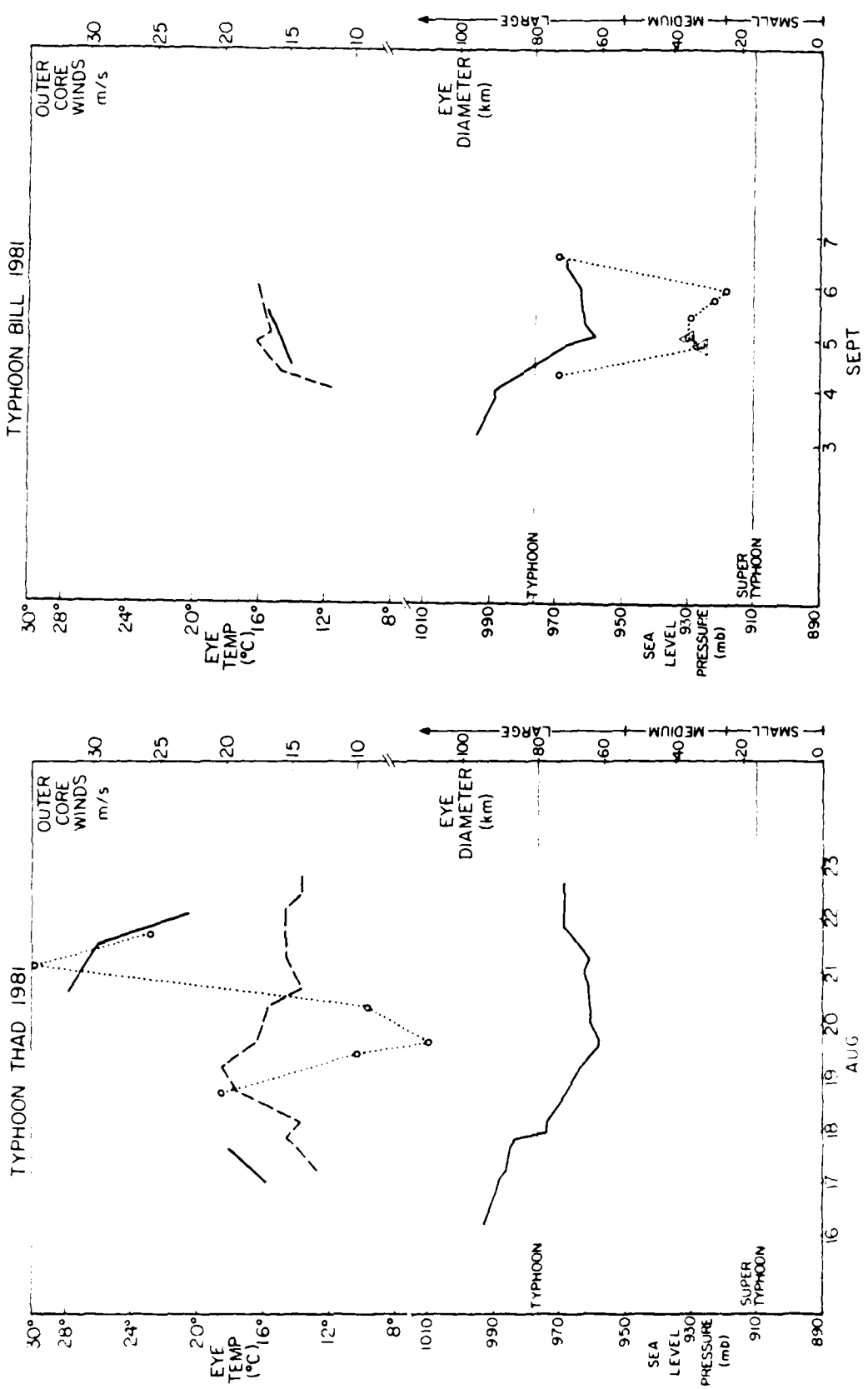
TYPHOON BILL 1981
OUTER CORE WINDS m/s
EYE DIAMETER (km)
SMALL
MEDIUM
LARGE
EYE TEMP (°C)
SEA LEVEL PRESSURE (mb)
TYPHOON
SUPER TYPHOON
SEPT
TYPHOON THAD 1981
AUG

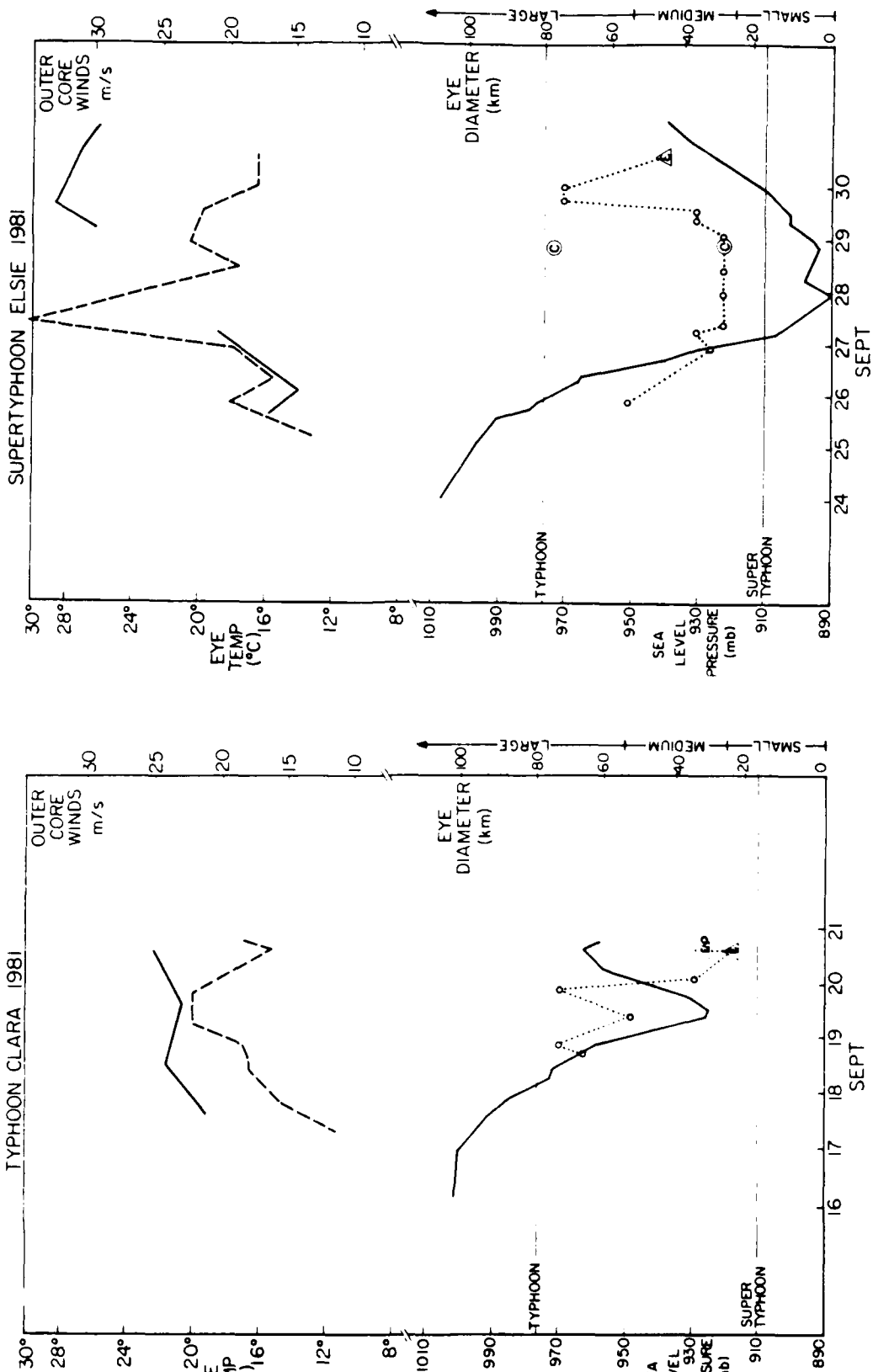
SUPERTYPHOON ELSIE 1981
OUTER CORE WINDS m/s
EYE DIAMETER (km)
SMALL
MEDIUM
LARGE
EYE TEMP (°C)
SEA LEVEL PRESSURE (mb)
TYPHOON
SUPER TYPHOON
SEPT
TYPHOON CLARA 1981
OUTER CORE WINDS m/s
EYE DIAMETER (km)
EYE TEMP (°C)
SEA LEVEL PRESSURE (mb)
TYPHOON
SUPER TYPHOON
SEPT

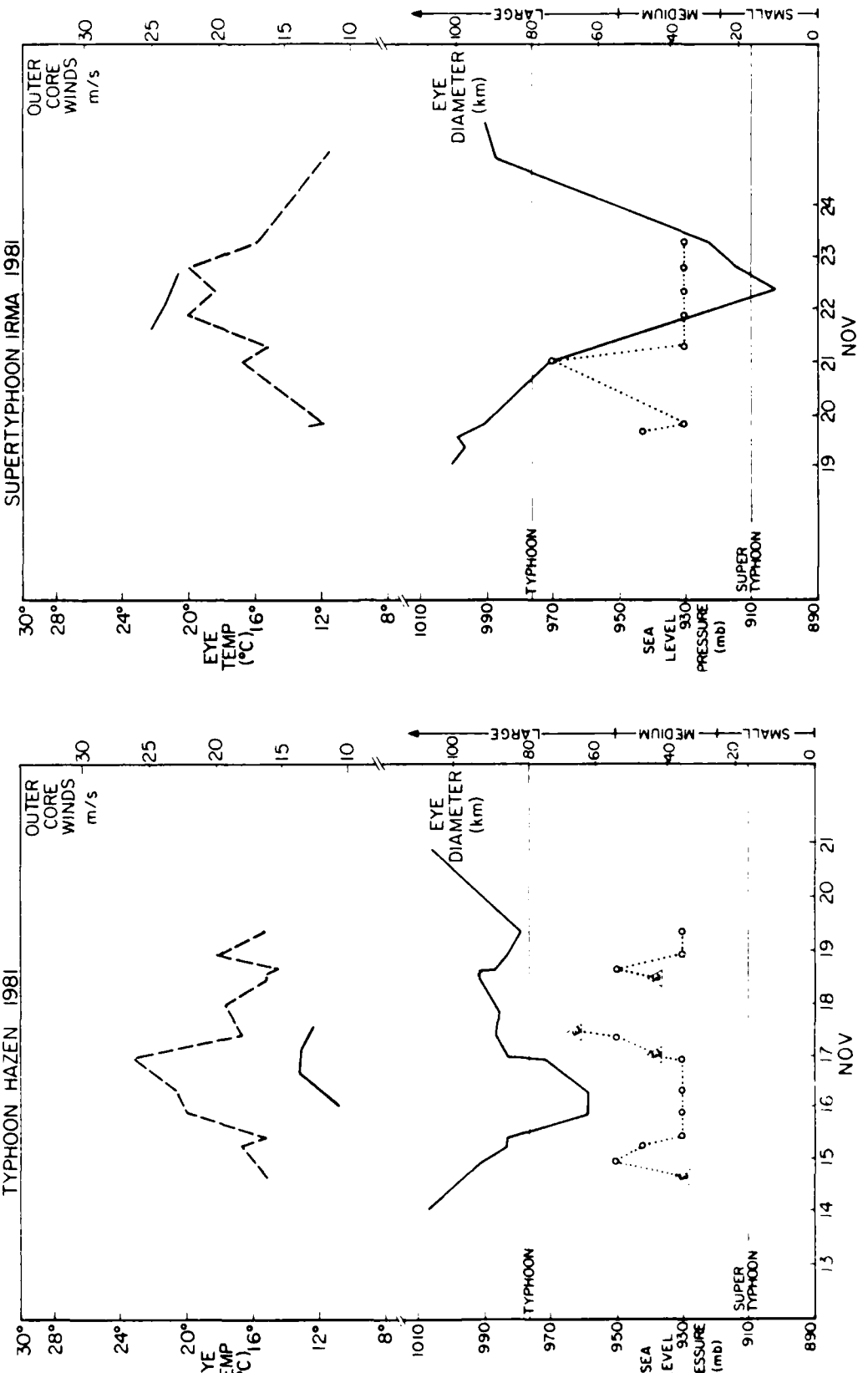
SUPERTYPHOON IRMA 1981
OUTER CORE WINDS m/s
EYE DIAMETER (km)
SMALL
MEDIUM
LARGE
EYE TEMP (°C)
SEA LEVEL PRESSURE (mb)
TYPHOON
SUPER TYPHOON
NOV
TYPHOON HAZEN 1981
OUTER CORE WINDS m/s
EYE DIAMETER (km)
SMALL
MEDIUM
LARGE
EYE TEMP (°C)
SEA LEVEL PRESSURE (mb)
TYPHOON
SUPER TYPHOON
NOV

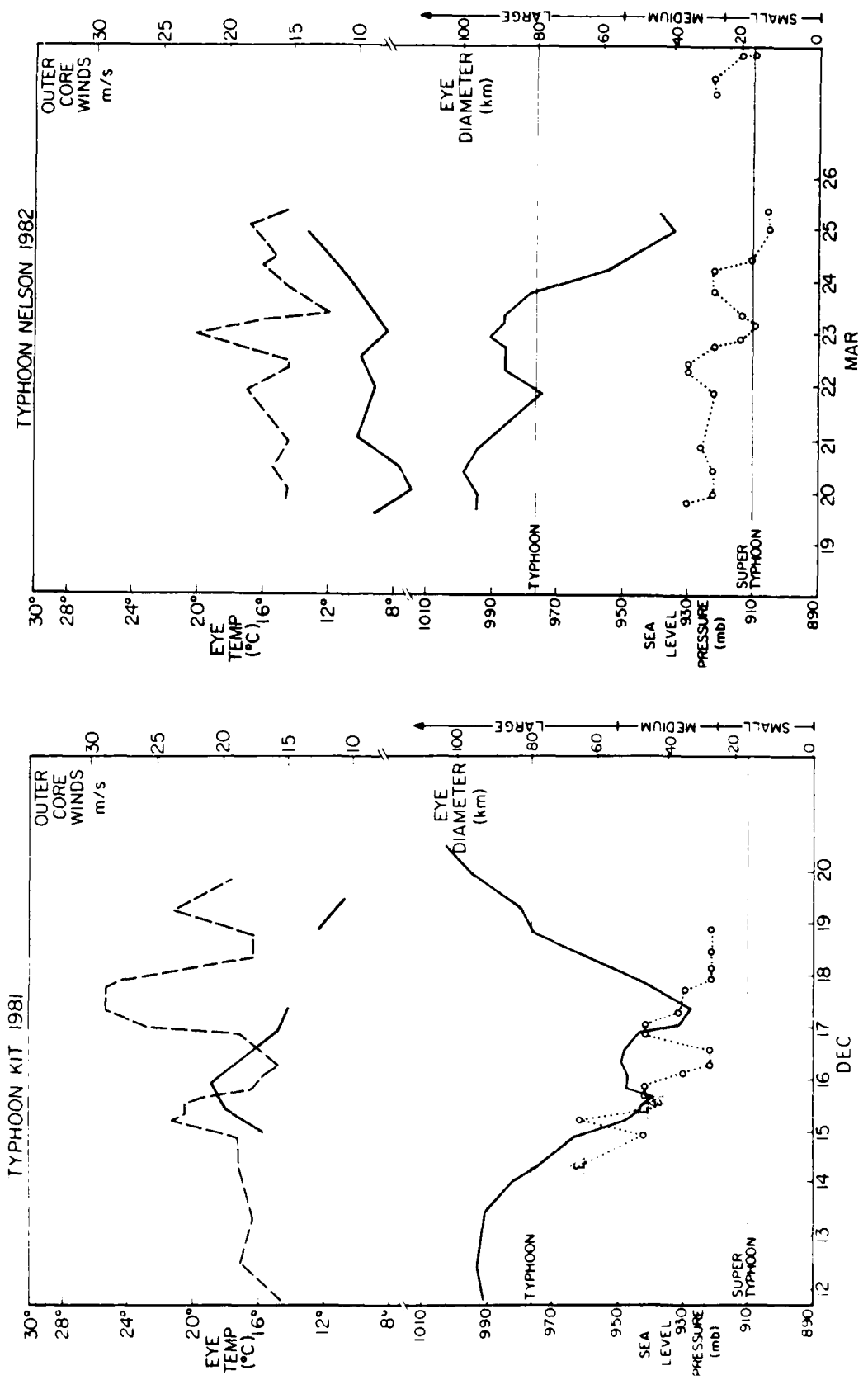
TYPHOON NELSON 1982
OUTER CORE WINDS m/s
EYE DIAMETER (km)
SMALL
MEDIUM
LARGE
EYE TEMP (°C)
SEA LEVEL PRESSURE (mb)
TYPHOON
SUPER TYPHOON
MAR
TYPHOON KIT 1981
DEC

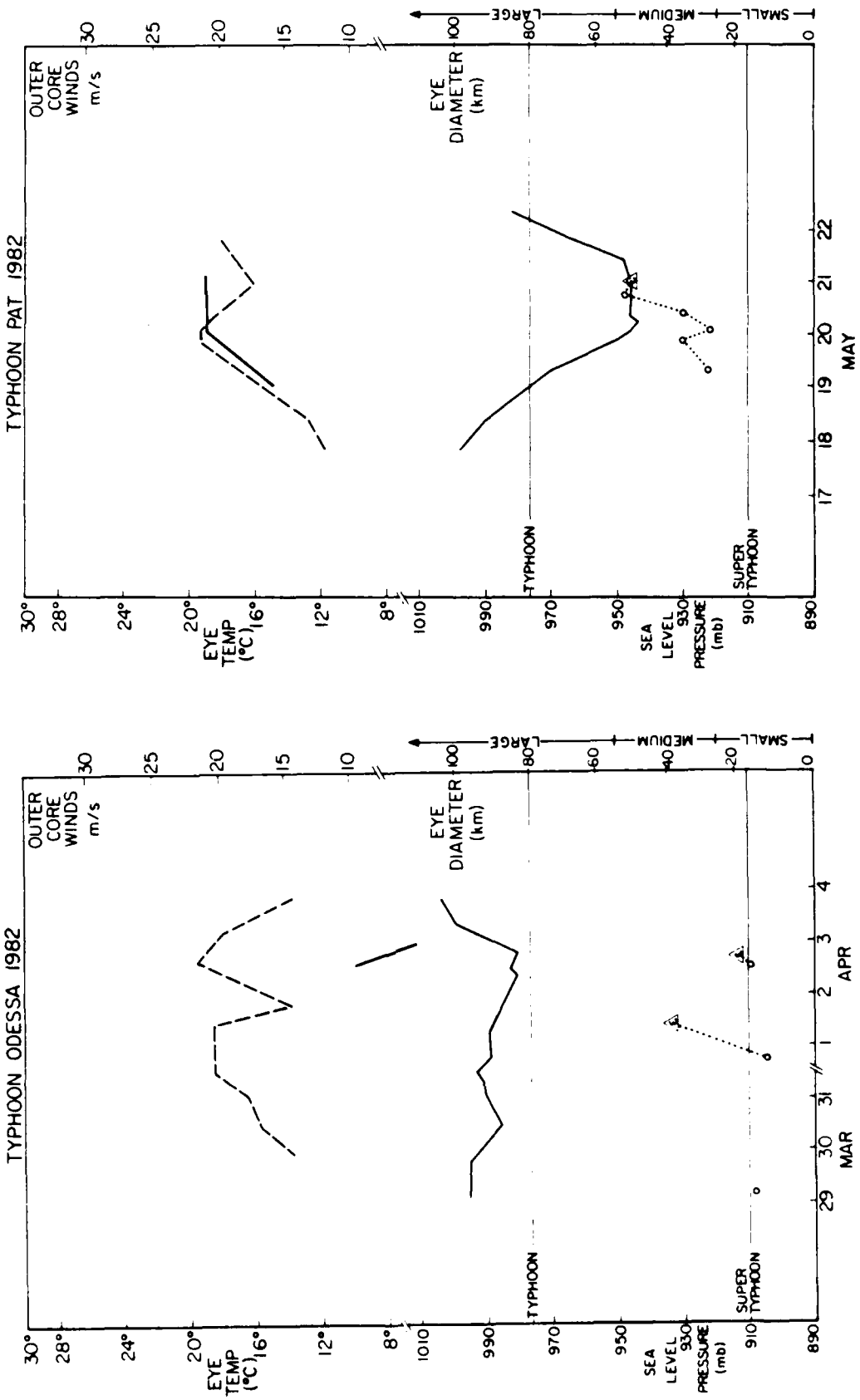
TYPHOON PAT 1982
OUTER CORE WINDS m/s
EYE DIAMETER (km)
SMALL
MEDIUM
LARGE
EYE TEMP (°C)
SEA LEVEL PRESSURE (mb)
TYPHOON
SUPER TYPHOON
MAY
TYPHOON ODESSA 1982
MAR
APR

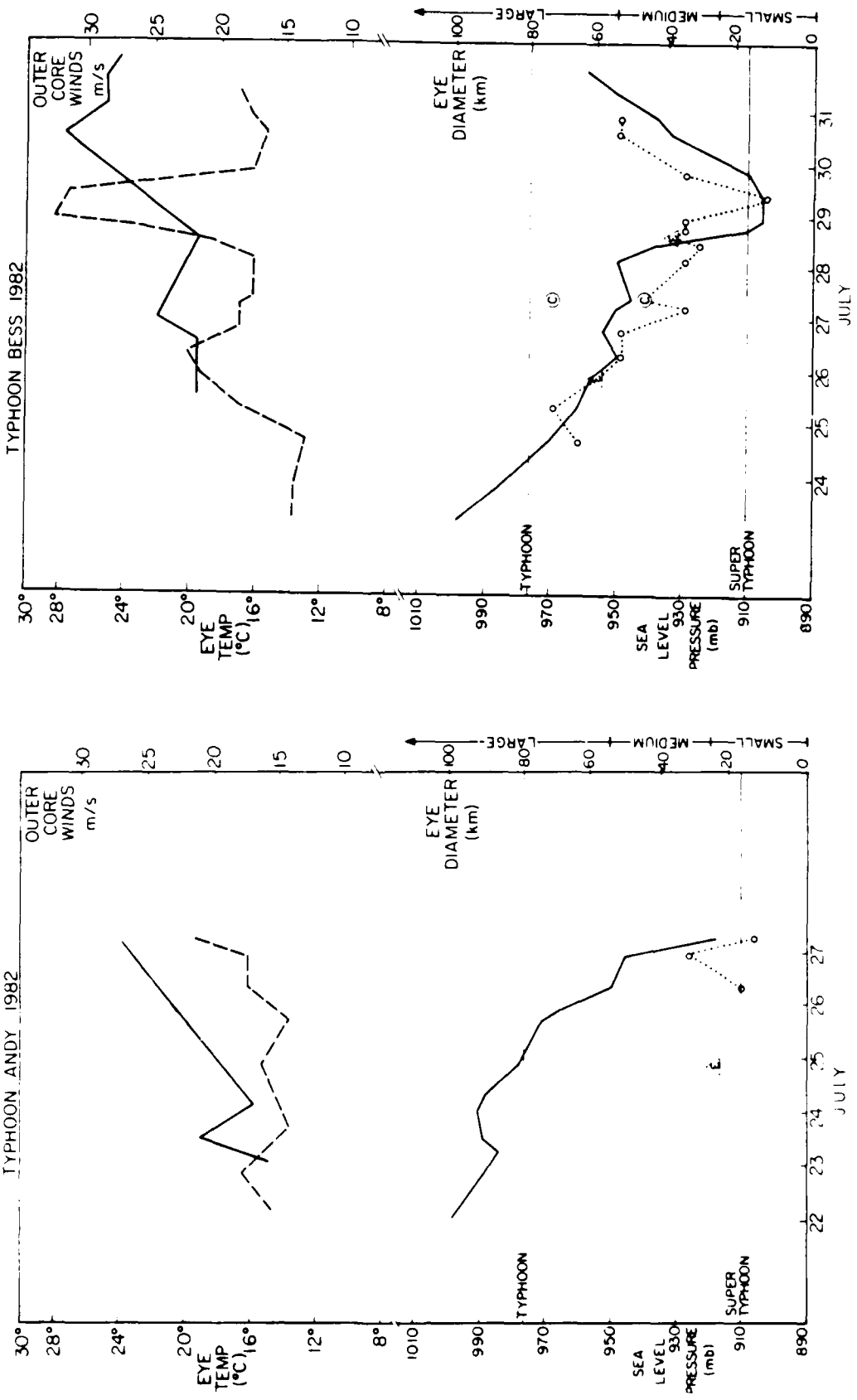
TYPHOON BESS 1982
OUTER CORE WINDS m/s
EYE DIAMETER (km)
SMALL
MEDIUM
LARGE
EYE TEMP (°C)
SEA LEVEL PRESSURE (mb)
TYPHOON
SUPER TYPHOON
JULY
TYPHOON ANDY 1982
OUTER CORE WINDS m/s
EYE DIAMETER (km)
EYE TEMP (°C)
SEA LEVEL PRESSURE (mb)
TYPHOON
SUPER TYPHOON
JULY

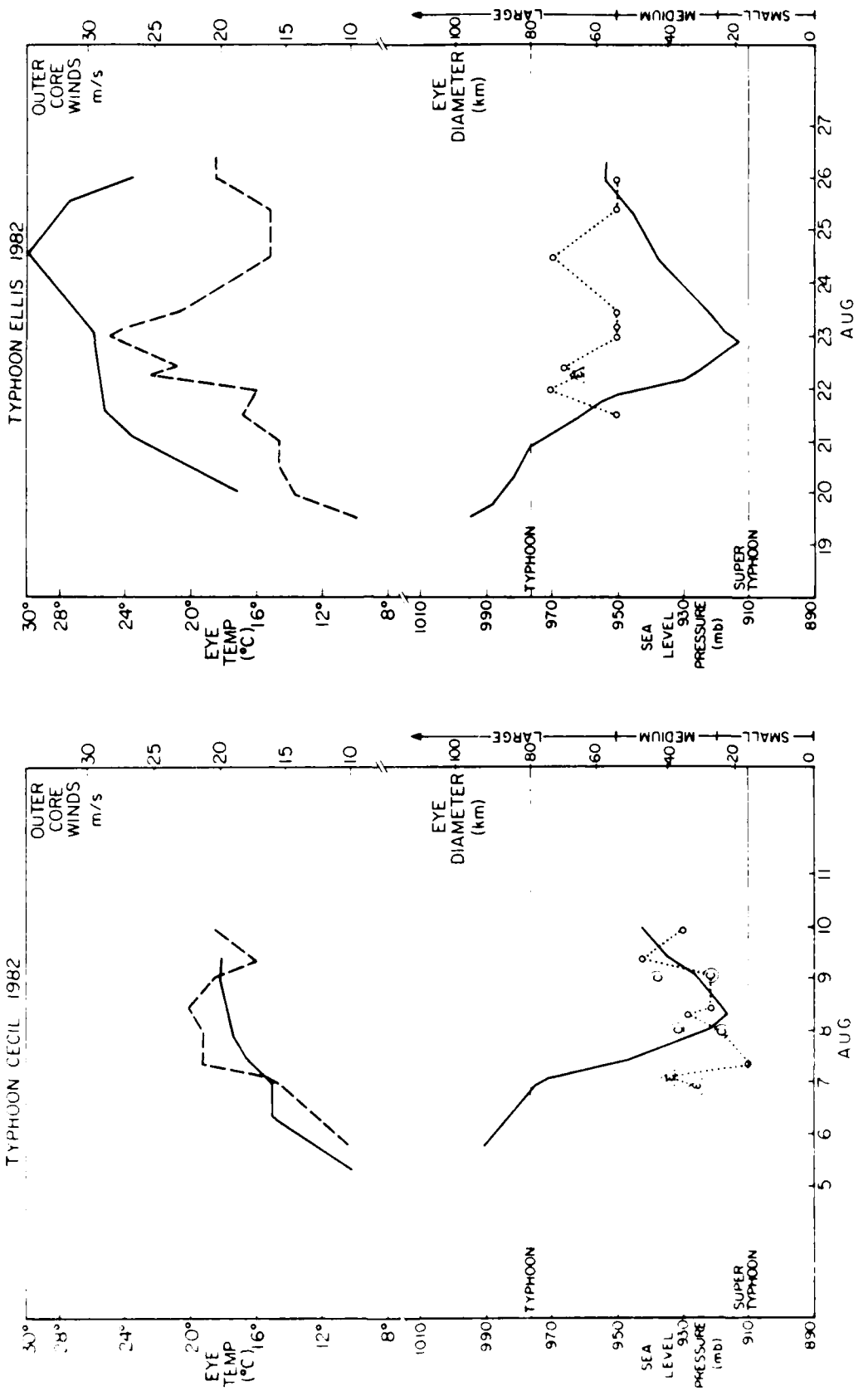
TYPHOON ELLIS 1982
TYPHOON CECIL 1982
OUTER CORE WINDS m/s
EYE DIAMETER (km)
SMALL
MEDIUM
LARGE
EYE TEMP (°C)
SEA LEVEL PRESSURE (mb)
TYPHOON
SUPER TYPHOON
AUG

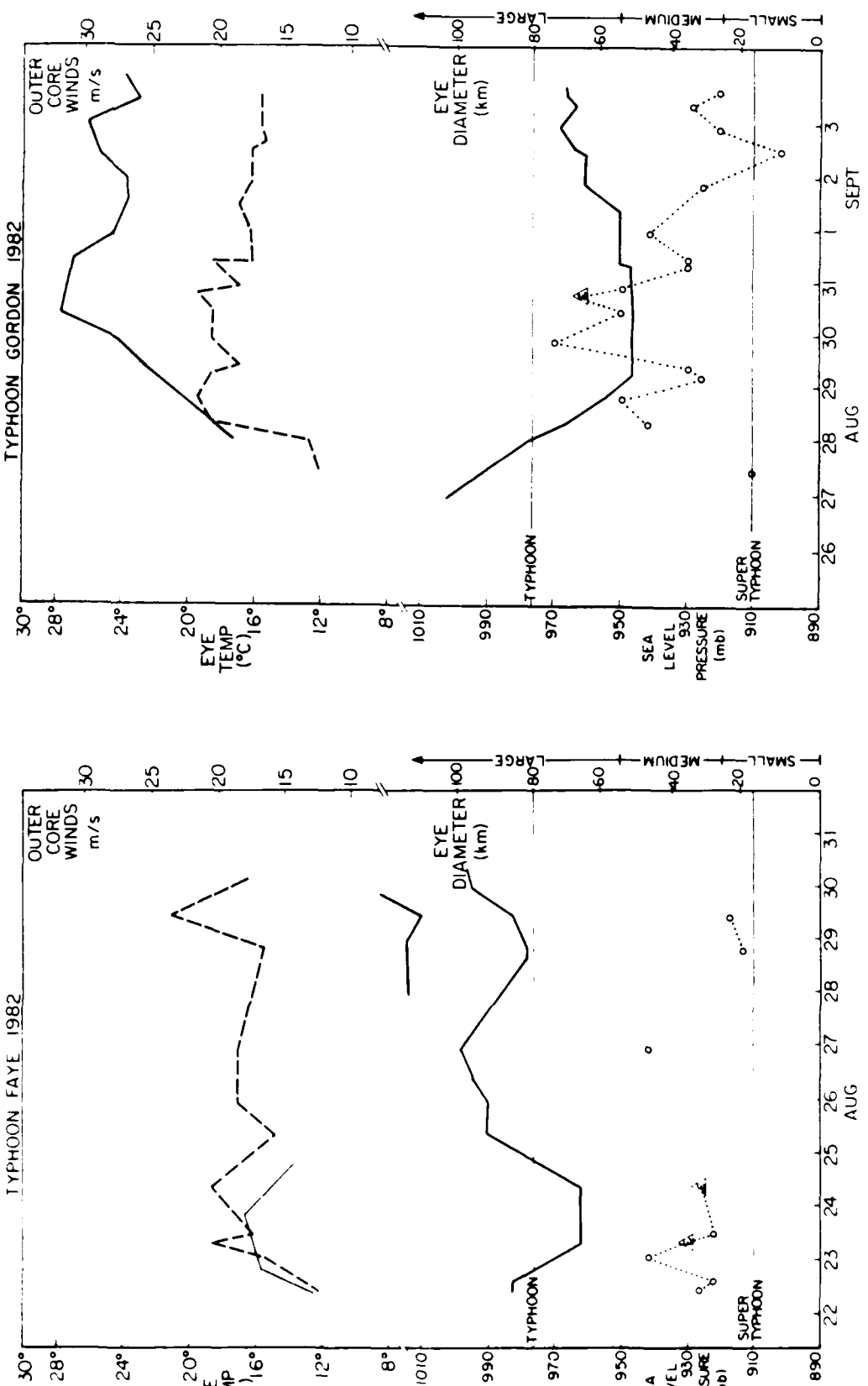
TYPHOON GORDON 1982
OUTER CORE WINDS m/s
EYE DIAMETER (km)
SMALL
MEDIUM
LARGE
EYE TEMP (°C)
SEA LEVEL PRESSURE (mb)
TYPHOON
SUPER TYPHOON
AUG
SEPT
TYPHOON FAYE 1982
OUTER CORE WINDS m/s
EYE DIAMETER (km)
SMALL
MEDIUM
LARGE
EYE TEMP (°C)
SEA LEVEL PRESSURE (mb)
TYPHOON
SUPER TYPHOON
AUG

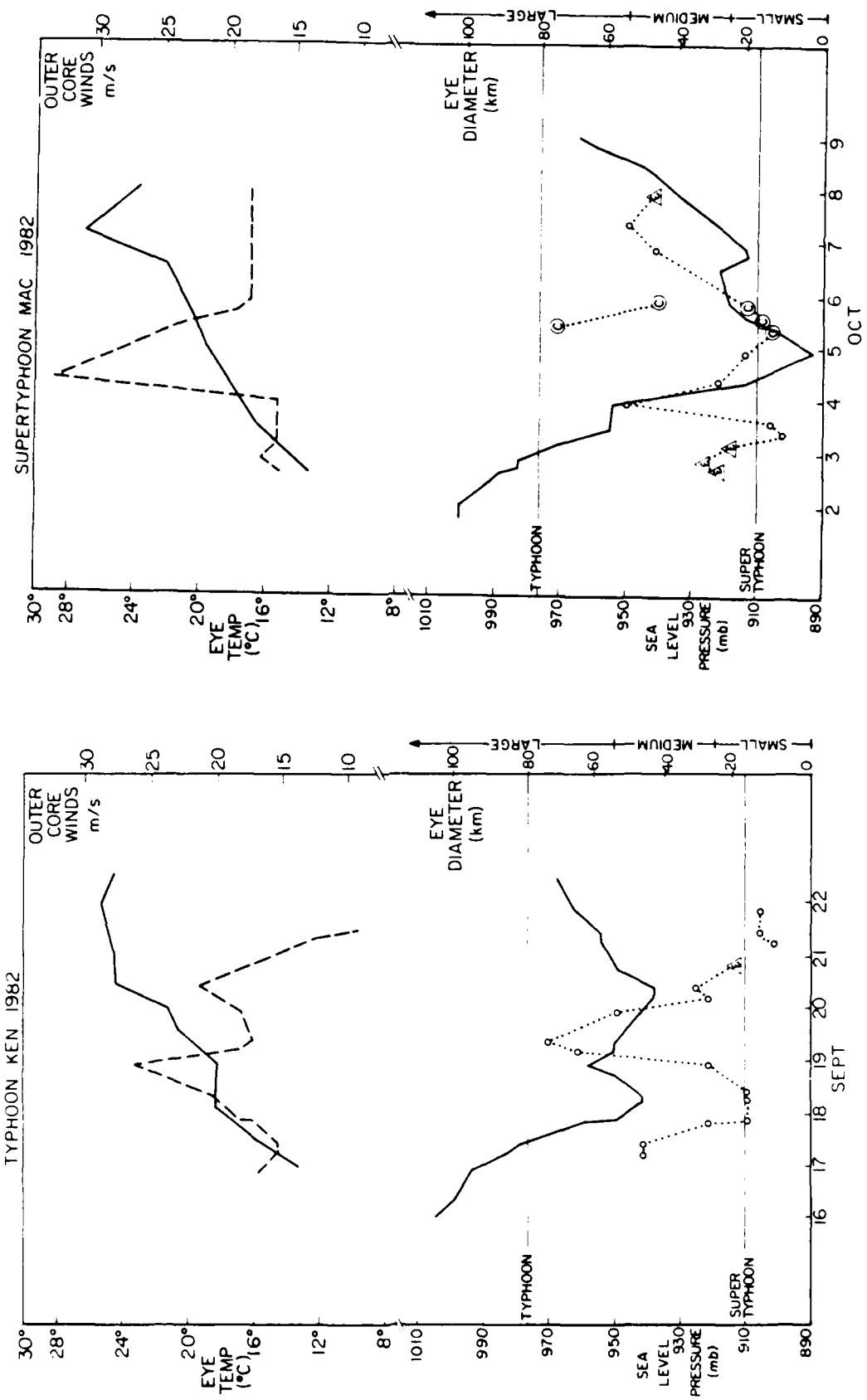
SUPERTYPHOON MAC 1982
OUTER CORE WINDS m/s
EYE DIAMETER (km)
EYE TEMP (°C)
SEA LEVEL PRESSURE (mb)
TYPHOON
SUPER TYPHOON
SMALL
MEDIUM
LARGE
OCT
TYPHOON KEN 1982
SEPT

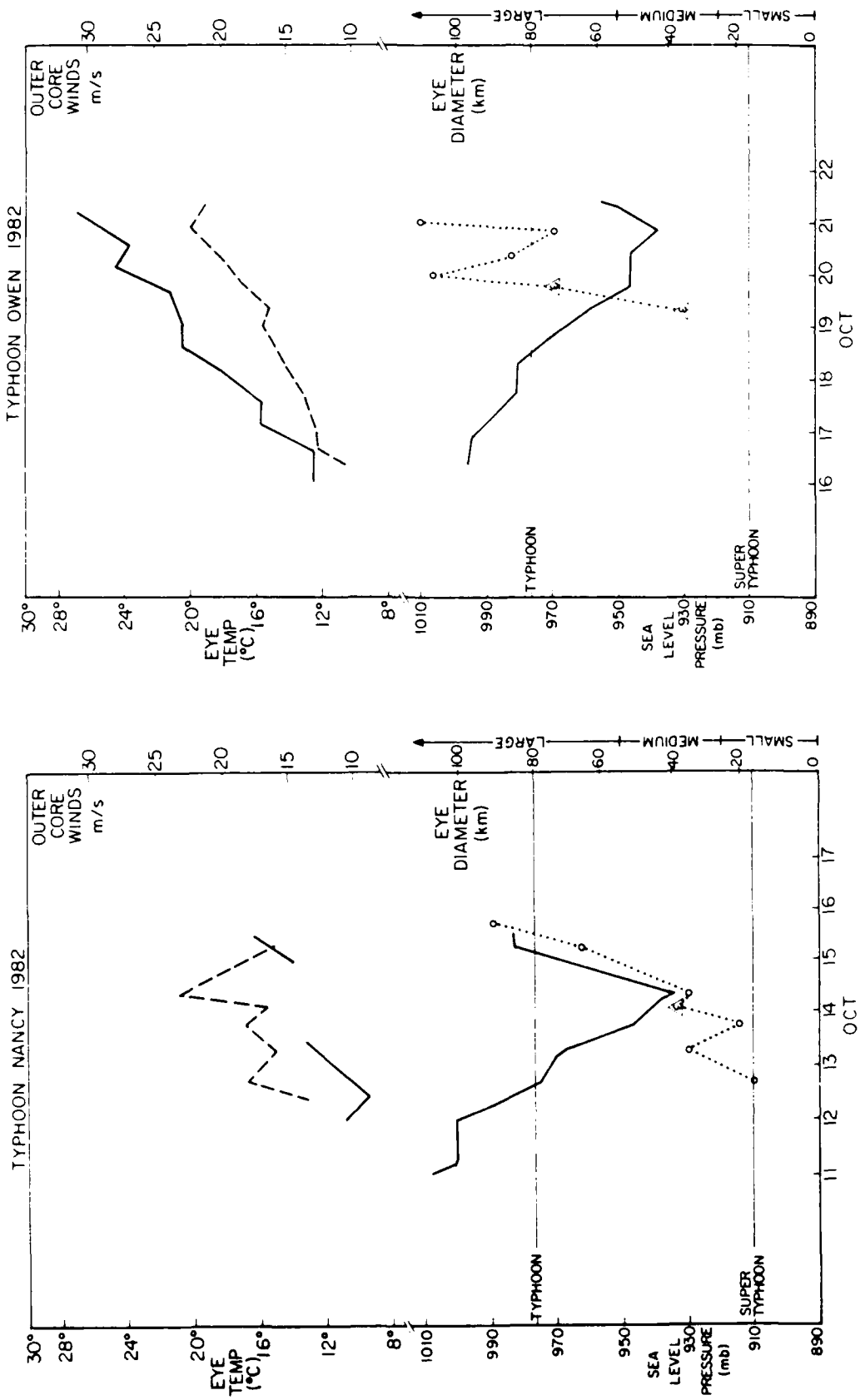
TYPHOON OWEN 1982
TYPHOON NANCY 1982
OUTER CORE WINDS m/s
EYE DIAMETER (km)
SMALL
MEDIUM
LARGE
EYE TEMP (°C)
SEA LEVEL PRESSURE (mb)
TYPHOON
SUPER TYPHOON
OCT

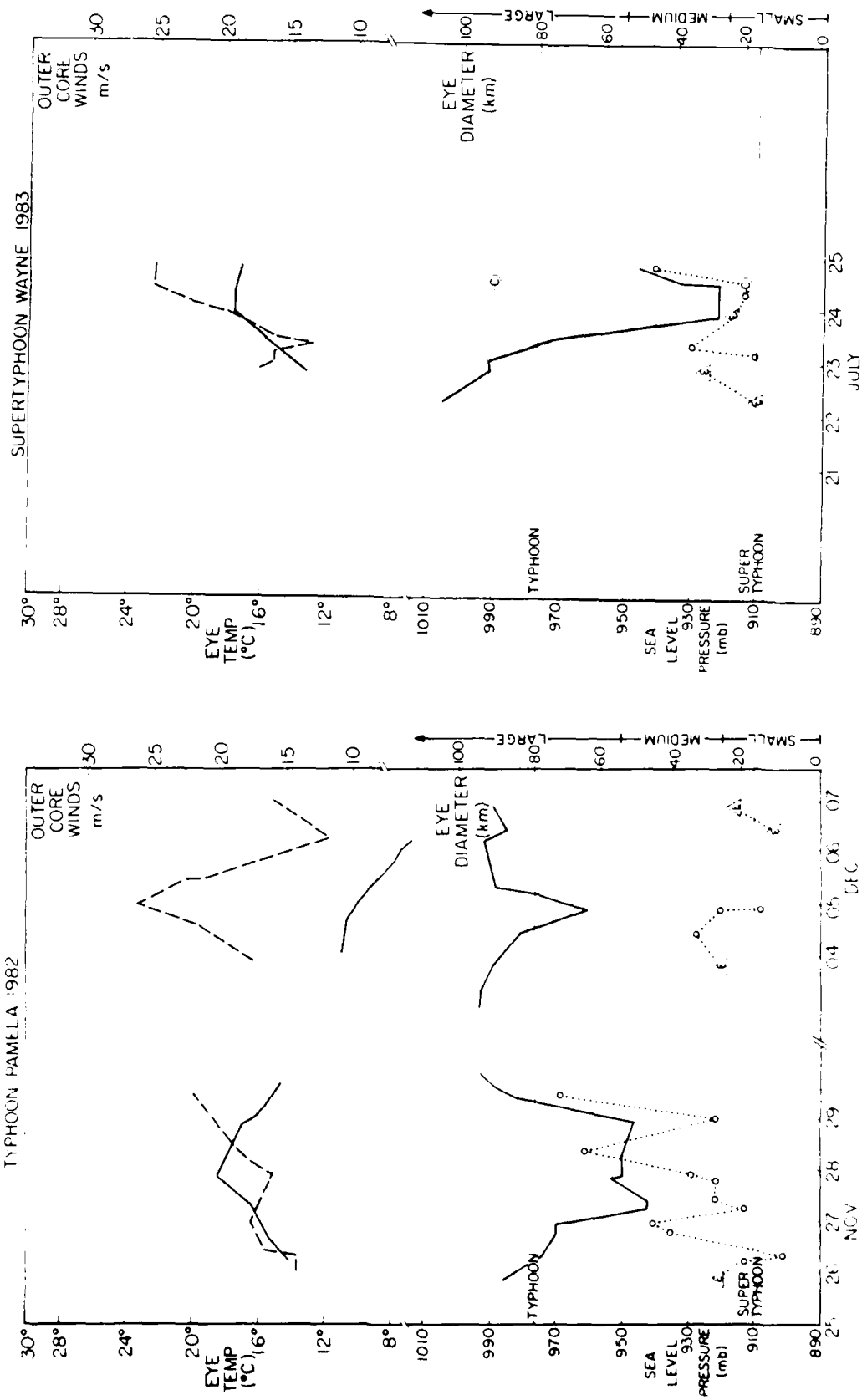
SUPERTYPHOON WAYNE 1983
OUTER CORE WINDS m/s
EYE DIAMETER (km)
SMALL
MEDIUM
LARGE
EYE TEMP (°C)
SEA LEVEL PRESSURE (mb)
TYPHOON
SUPER TYPHOON
JULY
TYPHOON PAMELA 1982
NOV
DEC

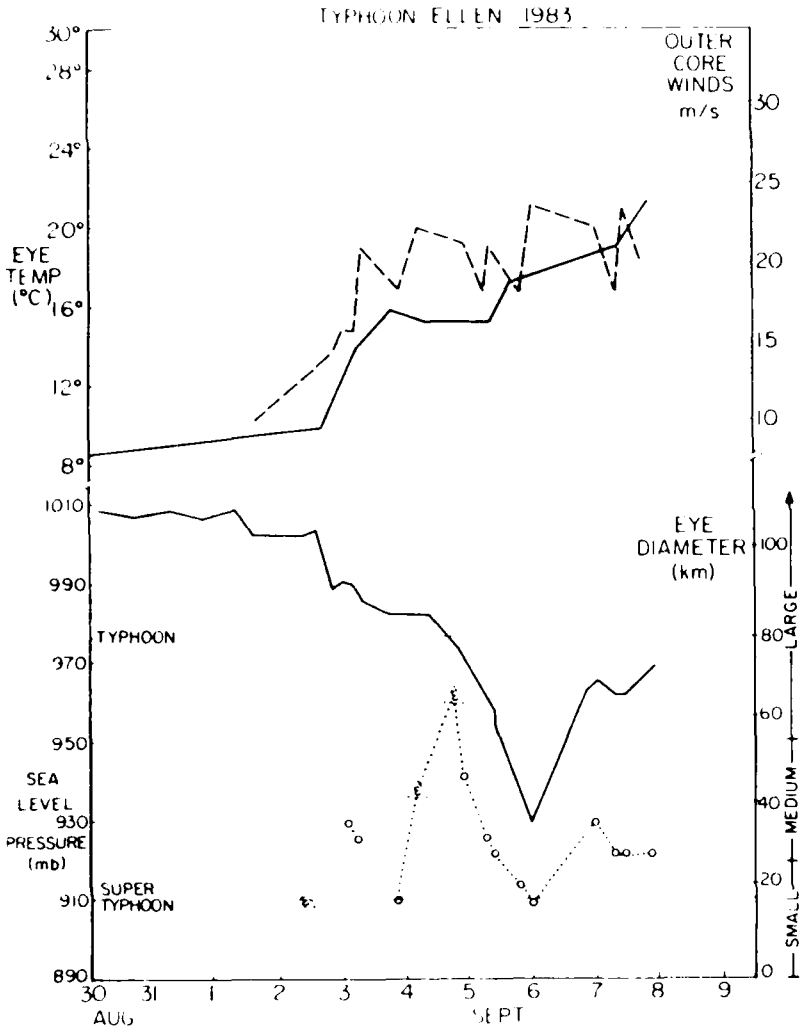
TYPHOON ELLEN 1983
OUTER CORE WINDS m/s
EYE TEMP (°C)
EYE DIAMETER (km)
TYPHOON
SUPER TYPHOON
SEA LEVEL PRESSURE (mb)
SMALL
MEDIUM
LARGE
AUG
SEPT

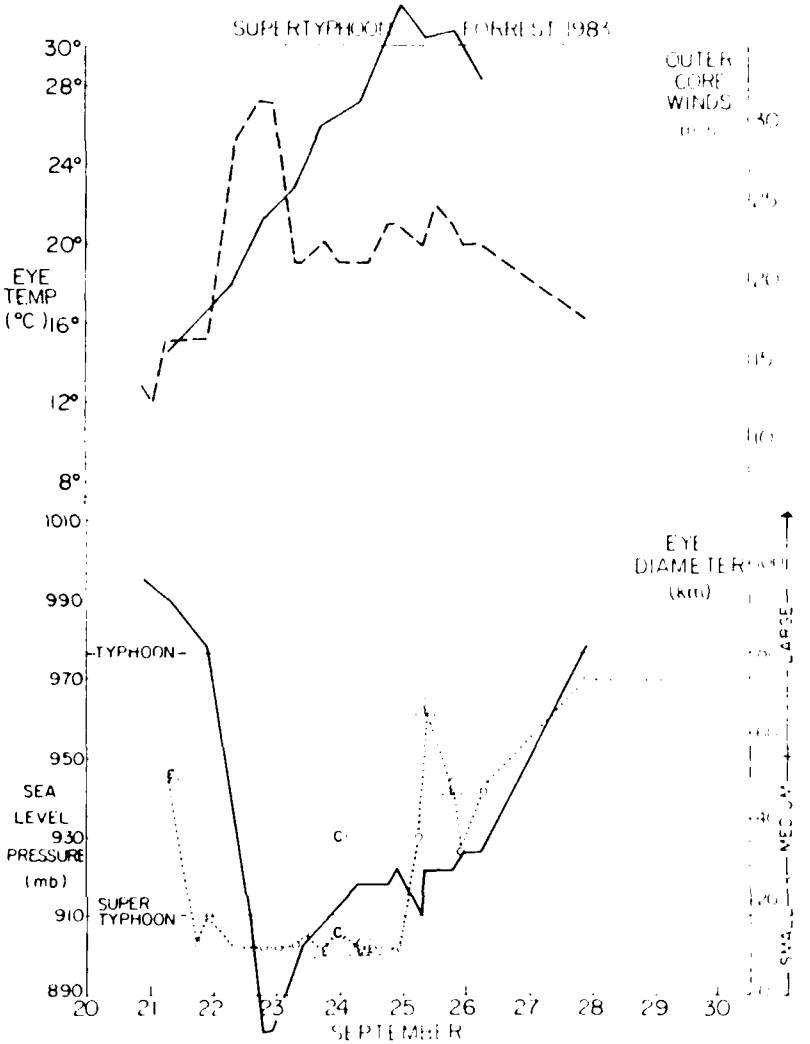
SUPERTYPHOON FORREST 1983
OUTER CORE WINDS
EYE TEMP (°C)
EYE DIAMETER (km)
TYPHOON
SUPER TYPHOON
SEA LEVEL PRESSURE (mb)
SEPTEMBER

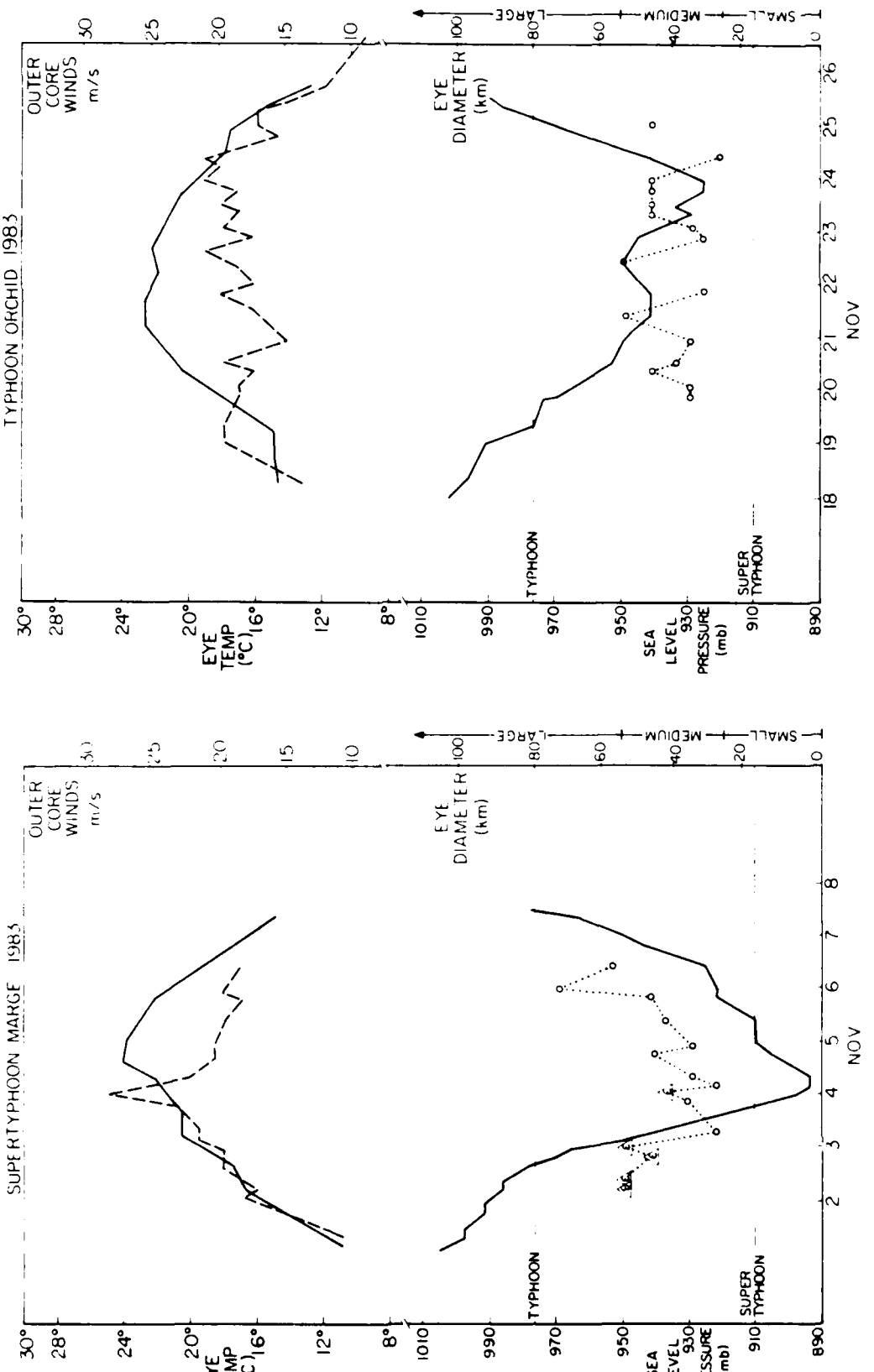
TYPHOON ORCHID 1983
OUTER CORE WINDS m/s
EYE DIAMETER (km)
EYE TEMP (°C)
SEA LEVEL PRESSURE (mb)
TYPHOON
SUPER TYPHOON
SMALL
MEDIUM
LARGE
NOV
SUPERTYPHOON MARGE 1983
OUTER CORE WINDS m/s
EYE DIAMETER (km)
EYE TEMP (°C)
SEA LEVEL PRESSURE (mb)
TYPHOON
SUPER TYPHOON
SMALL
MEDIUM
LARGE
NOV

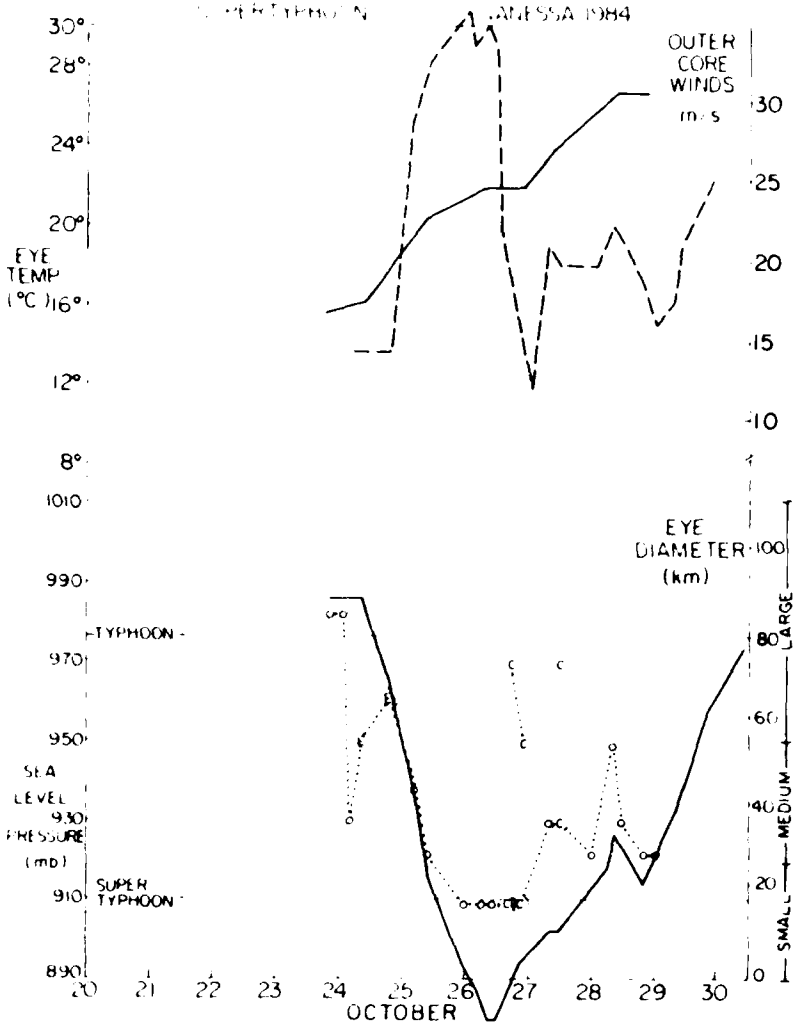
VANESSA 1984
OUTER CORE WINDS m/s
EYE TEMP (°C)
EYE DIAMETER (km)
TYPHOON
SUPER TYPHOON
SEA LEVEL PRESSURE (mb)
SMALL
MEDIUM
LARGE
OCTOBER

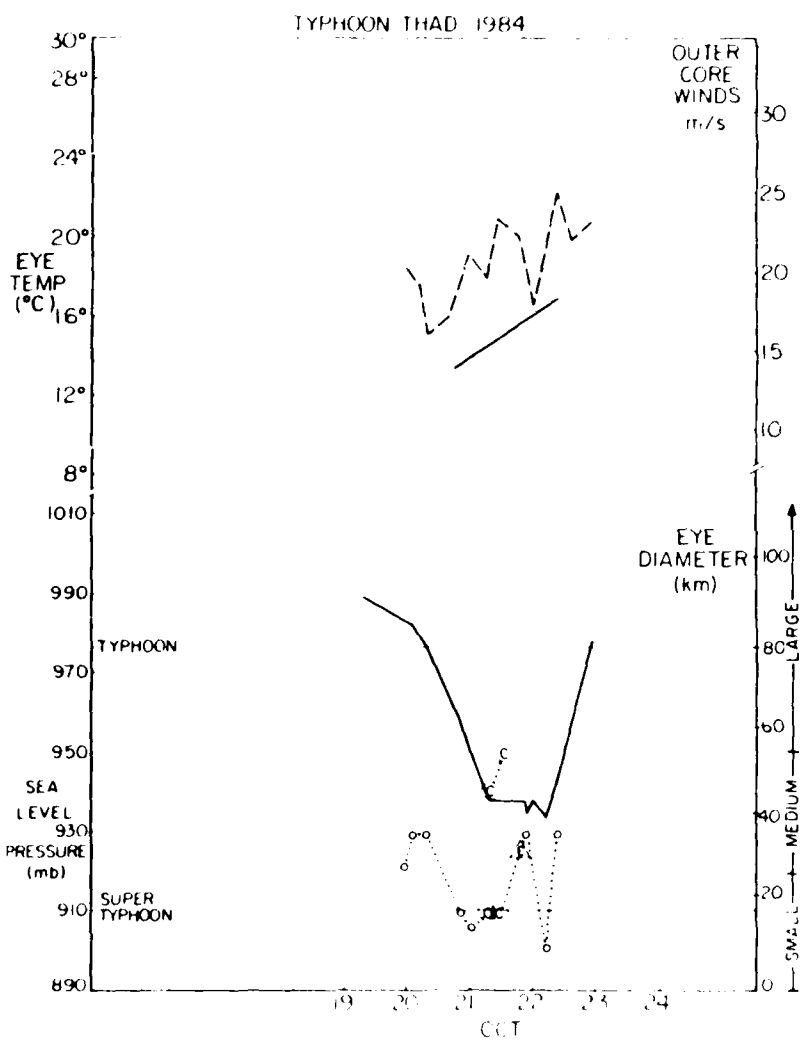
TYPHOON THAD 1984
OUTER CORE WINDS m/s
EYE TEMP (°C)
EYE DIAMETER (km)
TYPHOON
SUPER TYPHOON
SEA LEVEL PRESSURE (mb)
SMALL
MEDIUM
LARGE
OCT

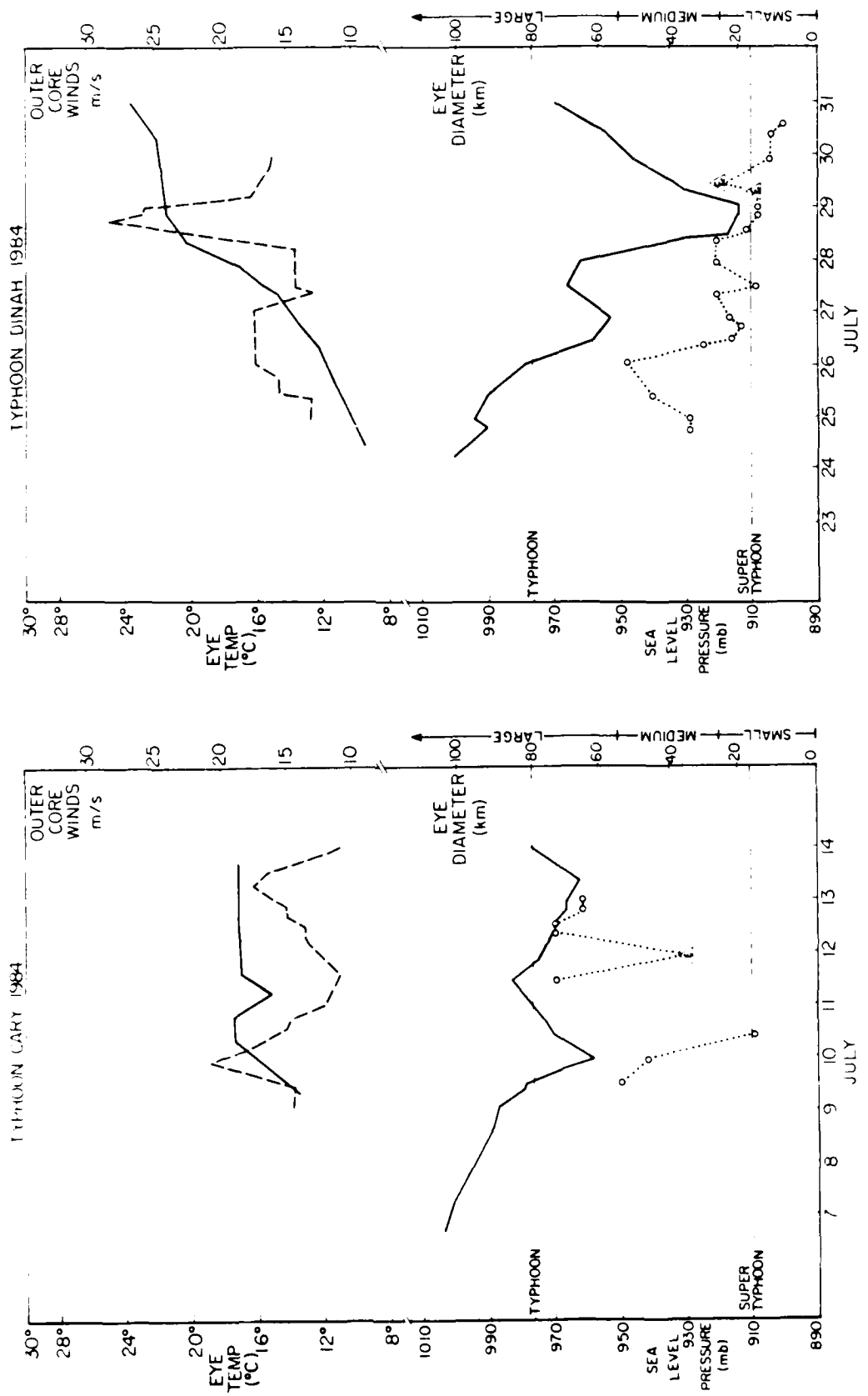
TYPHOON DINAH 1984
OUTER CORE WINDS m/s
EYE DIAMETER (km)
SMALL
MEDIUM
LARGE
EYE TEMP (°C)
SEA LEVEL PRESSURE (mb)
TYPHOON
SUPER TYPHOON
JULY

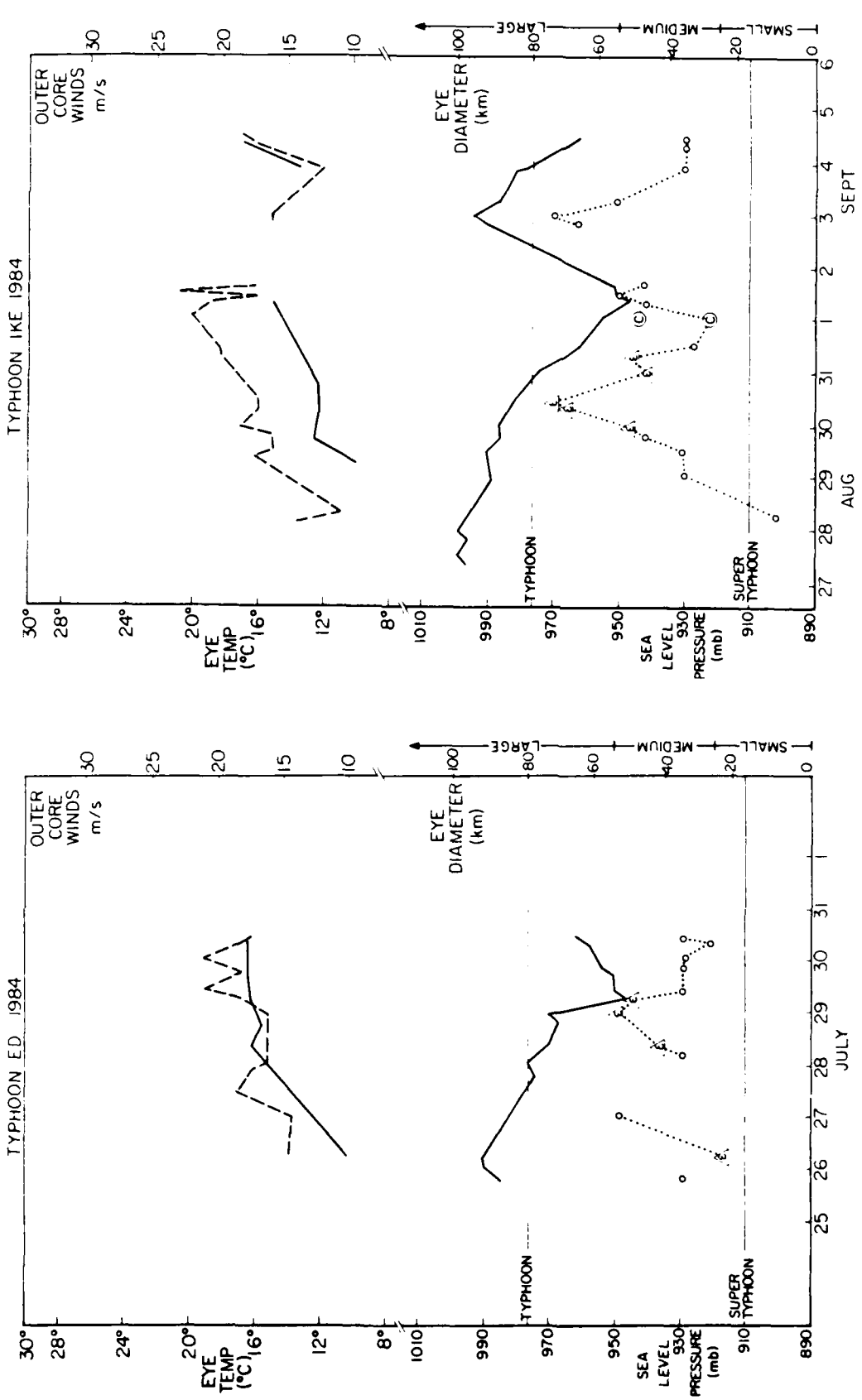
TYPHOON IKE 1984
TYPHOON ED 1984
OUTER CORE WINDS m/s
EYE DIAMETER (km)
SMALL
MEDIUM
LARGE
EYE TEMP (°C)
SEA LEVEL PRESSURE (mb)
TYPHOON
SUPER TYPHOON
AUG
SEPT
JULY

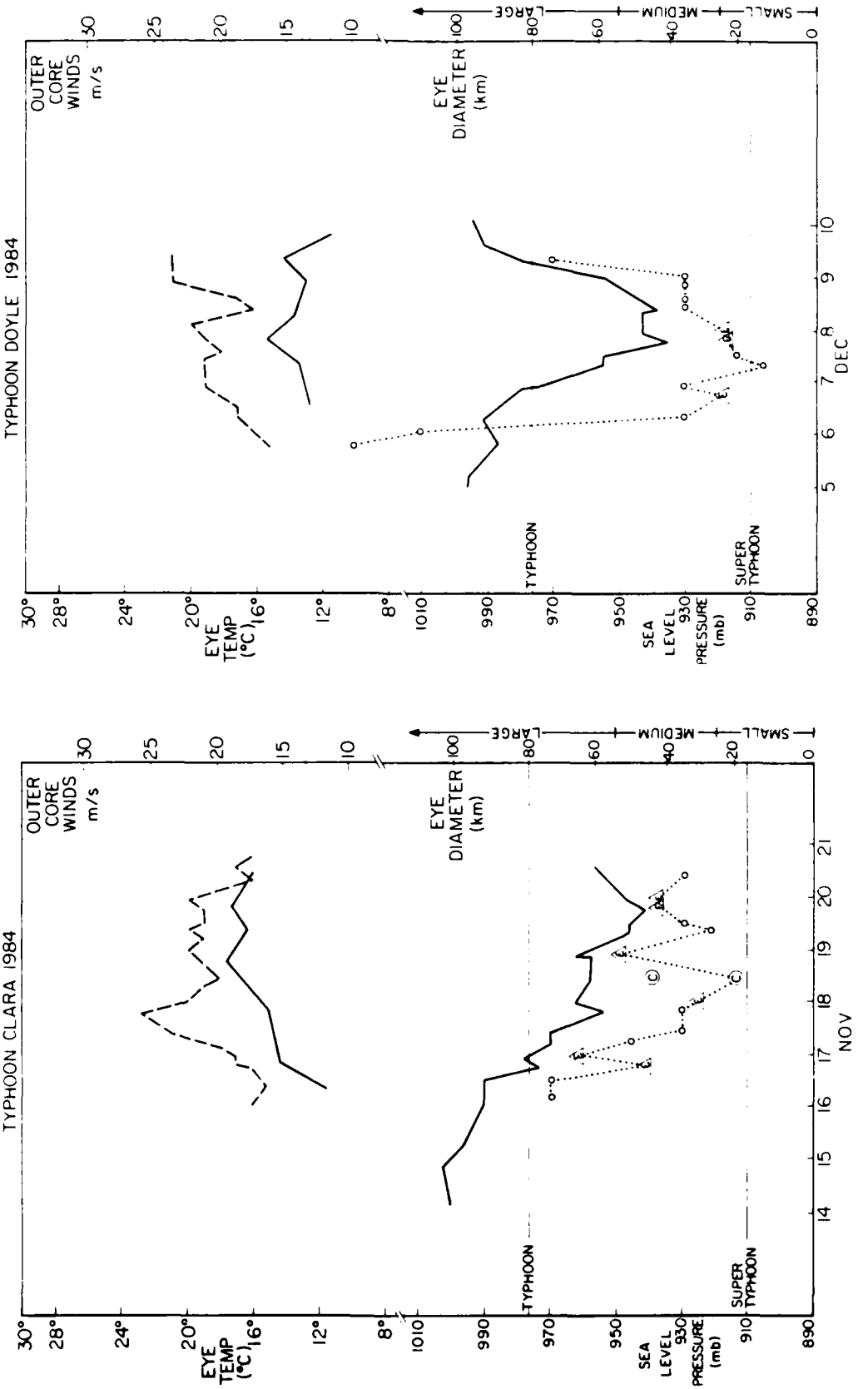
TYPHOON DOYLE 1984
OUTER CORE WINDS m/s
EYE DIAMETER (km)
EYE TEMP (°C)
SEA LEVEL PRESSURE (mb)
TYPHOON
SUPER TYPHOON
SMALL
MEDIUM
LARGE
DEC
TYPHOON CLARA 1984
NOV

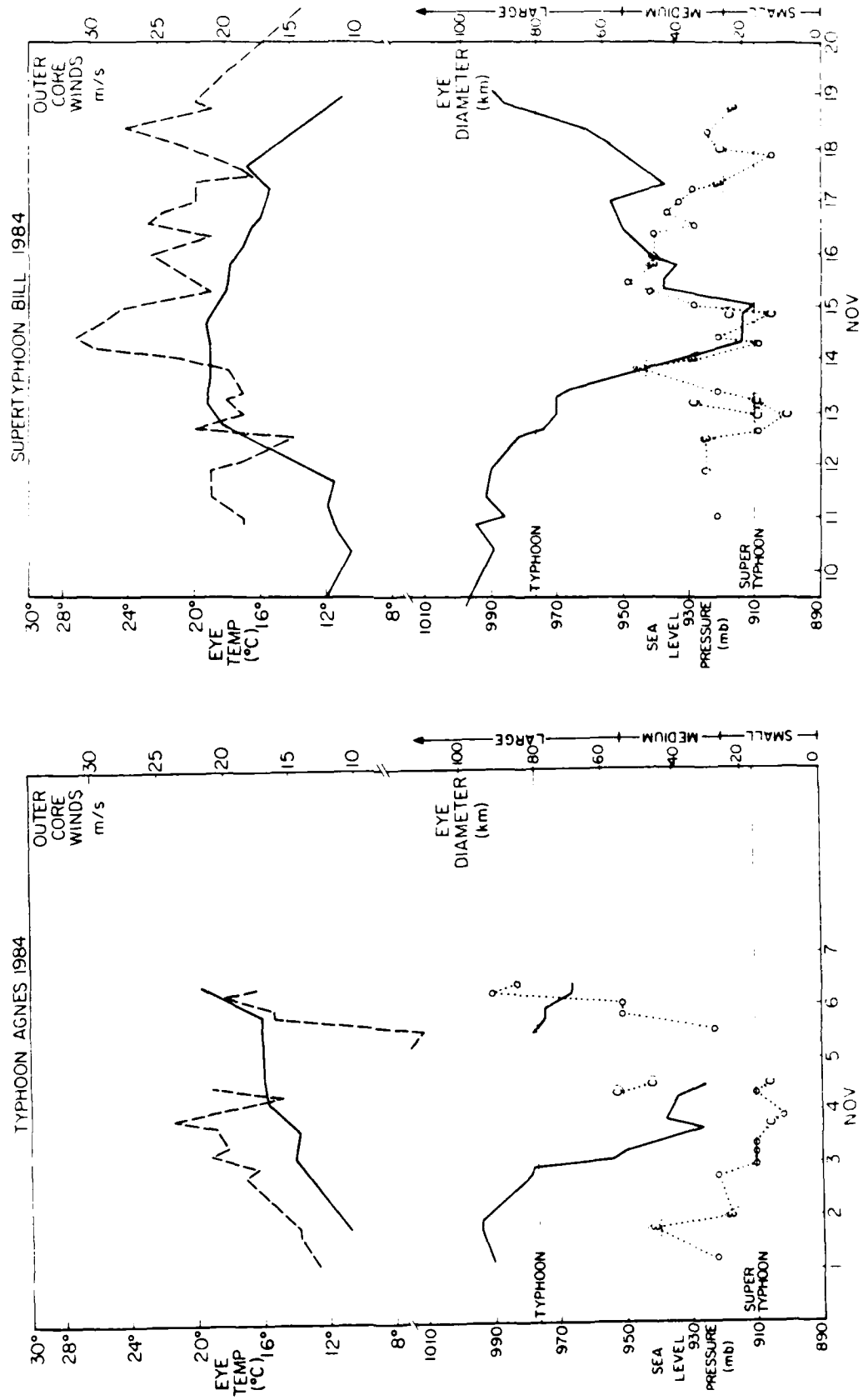
SUPERTYPHOON BILL 1984
OUTER CORE WINDS m/s
EYE DIAMETER (km)
EYE TEMP (°C)
SEA LEVEL PRESSURE (mb)
TYPHOON
SUPER TYPHOON
SMALL
MEDIUM
LARGE
NOV
TYPHOON AGNES 1984
OUTER CORE WINDS m/s
EYE DIAMETER (km)
EYE TEMP (°C)
SEA LEVEL PRESSURE (mb)
TYPHOON
SUPER TYPHOON
SMALL
MEDIUM
LARGE
NOV

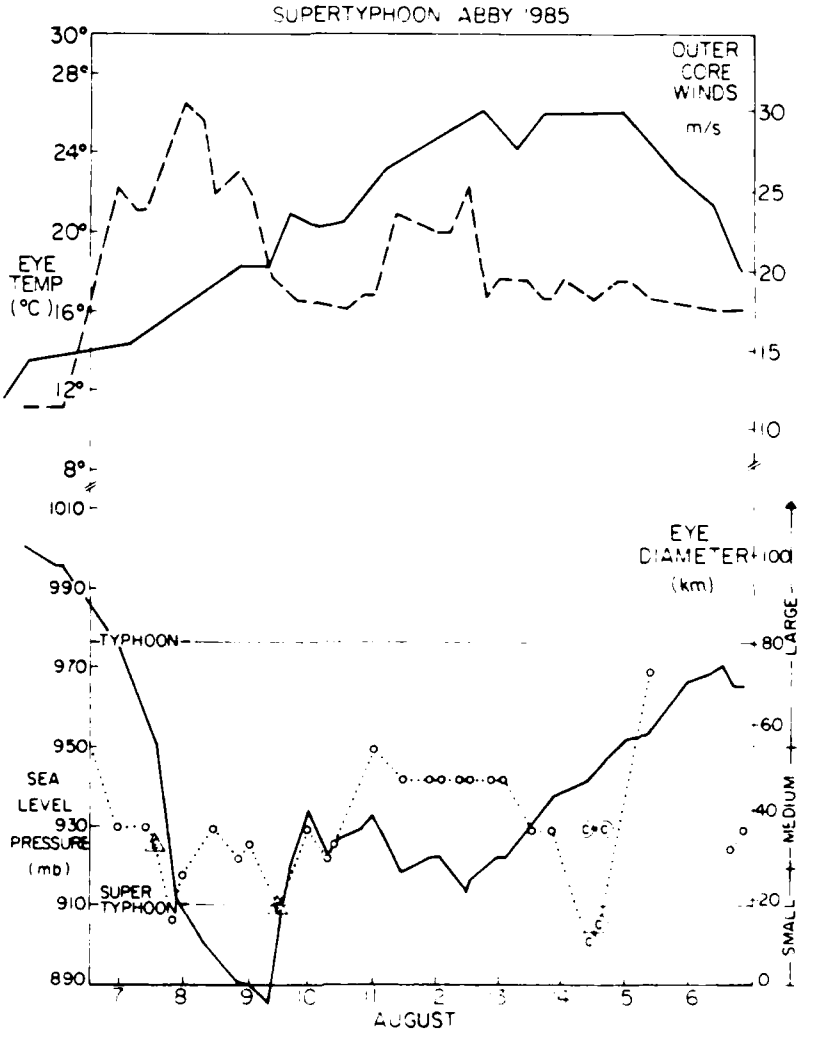
SUPERTYPHOON ABBY '985
OUTER CORE WINDS
m/s
EYE TEMP (°C)
EYE DIAMETER (km)
TYPHOON
SUPER TYPHOON
SEA LEVEL PRESSURE (mb)
LARGE
MEDIUM
SMALL
AUGUST

Appendix B

DATA PROCESSING

This study is based on five years of flight data of the northwestern Pacific Ocean basin. Many years went into the processing of this data set which involved a number of steps to complete.

The first step consisted of gathering the data. This involved a trip to the NOAA's National Climate Data Center at Asheville, NC, where the original forms are stored. Locating, sorting and copying the forms took two weeks. In this and all steps it was vital that someone who had worked with these forms before, take a direct role in overseeing the entire process. This precluded non-cyclone data from being incorporated into a strictly tropical cyclone study.

Preparing the forms for key punching involved highlighting only that information which was needed for the research. Dates were checked to ensure against observer error. This was critical since observations with the wrong date would be matched with the wrong center from which to navigate. All remarks which accompanied the form were checked in case equipment problems invalidated the reported observations. This step took three months.

Key-punching the information into the computer entailed a massive effort. Realize that all the information was handwritten onto seven different forms by dozens of different observers. Combine in-flight turbulence with an overloaded trainee and the difference between a "2" and a "7" often took a committee to decipher, one of which had to be someone knowledgeable with the code. It was at this step that all data which included

a code denoting equipment problems were sorted out. We were primarily concerned with the navigational and wind measuring equipment. If either of these were faulty, the entire mission was scrapped. Missions with other equipment problems, such as an inoperative dew-point hygrometer, were retained with the bad data entered as missing. Seven months of man-hours went into this step.

Once all the data were placed into the computer, it was the job of the programmer to decode all seven codes and their changes over the years into a common and usable format. Error checks were incorporated all along the way. Low-level missions which were labelled 'cyclone' and later developed into a named storm were traced back and named at the earliest possible stage. The coupling of an experienced programmer with someone intimately familiar with the codes got this step done in two man-years.

Aircraft usually spent 4 hours taking observations in the storm area but positioned the center only twice, therefore the next step entailed navigating all data to an appropriate moving center position. To accomplish this a supplemental data set was used. Cyclone center motion was most completely traced by JTWC forecasters and compiled in their 'Best Track' position archive. These were used to provide aircraft- measured centers with an appropriate heading and speed so that all observations could be appropriately navigated. This took four months of programming.

It wasn't until this point that an analysis of the data could commence. Particular attention was given this data set in these early stages with the realization that results which stand on a clean and carefully processed data sample will provide the best results. Considering the fact that typhoons are inherently quite variable to begin with, only a clean data set would allow results to stand out. Massive data sets have the potential of providing many answers but require such meticulous handling.

Overall, the task of processing 5 years of flight data involved an enormous effort. Three and a half years went into just the compiling of this data set. Evidently, it is easy to see why no one before has attempted such a task. It was vital to the completion of this

job that someone familiar with the code and the method of observing be at the helm of this job. This has always been a military person. Those military coming back from the assignment in Guam to go to school are typically given 21 months to complete a Master's degree and 3 years for a Ph.D. This often falls far short of the job required just to place the data into a semblance of order and well before any analysis can be done. The only way the author who did fly in Guam for nearly three years in the Air Force accomplished this task was due to the full support of Professor Gray who continually provided me with the support necessary to get the job done in as quick a manner as possible.

END

DATE

FILMED

DEC.

1987